ACCUMULATION, DISTRIBUTION AND CHEMICAL FORM OF ORGANIC MERCURY IN BRAIN TISSUE AND LARVAL ZEBRAFISH (DANIO RERIO)

A Thesis Submitted to the
College of Graduate and Postdoctoral Studies
In Partial Fulfillment of the Requirements
For the Degree of Doctor of Philosophy
In the Western College of Veterinary Medicine
University of Saskatchewan
Saskatoon, Saskatchewan, Canada

By

Ashley Katerine James

PERMISSION TO USE STATEMENT

In presenting this thesis in partial fulfillment of the requirements for a Postgraduate degree from the University of Saskatchewan, I agree that the Libraries of this University may make it freely available for inspection. I further agree that permission for copying of this thesis in any manner, in whole or in part, for scholarly purposes may be granted by the professor or professors who supervised my thesis work or, in their absence, by the Head of the Department or the Dean of the College in which my thesis work was done. It is understood that any copying or publication or use of this thesis or parts thereof for financial gain shall not be allowed without my written permission. It is also understood that due recognition shall be given to me and to the University of Saskatchewan in any scholarly use which may be made of any material in my thesis.

Requests for permission to copy or to make other uses of materials in this thesis in whole or part should be addressed to:

Head of the Toxicology Centre
University of Saskatchewan
44 Campus Drive
Saskatoon, Saskatchewan S7N 5B3 Canada

OR

Dean
College of Graduate and Postdoctoral Studies
University of Saskatchewan
116 Thorvaldson Building, 110 Science Place
Saskatoon, Saskatchewan S7N 5C9 Canada

ABSTRACT

Compounds of organometallic mercury have been recognized for their toxicity to humans since the mid-1800s. While mercury is a natural constituent of the Earth's crust, with natural processes resulting in its release into the larger environment, anthropogenic activities including coal combustion and gold mining have increased the global bioavailable mercury burden. Atmospheric mercury can be transported globally, and its transformations between different environmental compartments can result in the formation of toxic organometallic mercury species. These compounds are known to bioaccumulate and biomagnify through trophic levels to animal species which may be consumed by human populations, and which may result in toxicity and even death.

The mechanisms by which methylmercury (the most highly studied form of organometallic mercury) exerts its toxicity are many and varied. It is due to these complexities that methylmercury (and inorganic species of mercury) continue to be the focus of a great deal of research. The goal of this research was to advance the prevailing understanding of organometallic mercury through investigation of its toxicity as it relates to chemical speciation, as well as its accumulation and distribution in relation to transportation and defensive mechanisms. To that end, the chemical speciation of mercury in both feline and human cases of historical exposures to organometallic mercury species were studied using X-ray absorption spectroscopy (XAS) and high energy resolution fluorescence detection XAS (HERFD-XAS) to gain insight into the dynamics of mercury in unique samples which did not originate from a model organism. Cases of exposure which would be defined as acute were dominated by varying forms of inorganic mercury, with some remaining organometallic mercury present (in most cases). In contrast, mercury species present in chronic cases of exposure coming from residents of the Seychelles, where a lifetime of consuming fish species which may contain high levels of mercury is the norm, remained entirely organometallic. The implications of this finding are important as most of what is known about mercury poisoning in human populations comes from cases of acute exposure, even while most instances of exposure of humans to mercury occurs at chronic low-levels. Comparisons were also made using XAS between formalin-fixed and frozen brain tissue, as well as cryopreserved and methacrylate embedded zebrafish (*Danio rerio*) to determine whether samples which had undergone more extensive preservation may be relied upon in studies of chemical form, which has been shown to be highly important in toxicity. Mercury was not

observed to be affected by preservation method in terms of speciation in brain tissue or in accumulation and distribution in larval zebrafish. Other endogenous elements, however, were noted to be affected. Both the transportation of methylmercury as well as the mechanisms through which defense against the toxicity of methylmercury occurs are routinely studied. Transportation of methylmercury, currently assumed to occur via L-system transporters, was seen to be affected by compounds likely to compete for uptake. This was demonstrated by increased survival in toxicity studies and reduced concentrations of mercury in target organs using X-ray fluorescence imaging (XFI) of larval zebrafish which had been co-exposed to methylmercury-L-cysteine in the presence of various LAT competitors. Transportation is thought to be primarily stereoselective and indeed, zebrafish exposed to methylmercury-D-cysteine demonstrated increased survival. Differences in mercury concentrations in target organs between enantiomers were noted but did not prove to be statistically significant. Lastly, an unforeseen target of mercury accumulation was observed using XFI after exposures to various organic and inorganic mercury species: the epithelial layer of larval zebrafish, where mucosal production occurs. Subsequent titrations of organometallic mercury with harvested mucosa examined using XAS demonstrated the occurrence of demethylation which, to our knowledge, has never been seen. While many faceted, the research conducted in this thesis highlights the complexity of mercury and, with the discoveries made herein demonstrates the need for continuing research.

ACKNOWLEDGEMENTS

First I would like to thank my supervisors, Drs. Graham George, Ingrid Pickering and Pat Krone for their expertise, patience and friendship. I have valued their scientific and "real-life" advice tremendously. I would very much like to thank them also for their tireless support in my endeavour to obtain this degree while simultaneously being a mother to my three (nearly four) children. Their support and flexibility in this particular area has meant everything to me. I would like to thank my committee members, Drs. Phyllis Paterson, Ian Coulthard, Brian Eames and David Janz for their guidance and advice throughout the course of my degree.

I would like to acknowledge my numerous funding sources, including supervisor grants from the Canadian Institutes of Health Research (CIHR), Saskatchewan Health Research Foundation (SHRF) and Natural Sciences and Engineering Research Council (NSERC). I would also like to acknowledge the CIHR-THRUST (Training in Health Research using Synchrotron Techniques) program for providing me with the Fellowship scholarship.

I acknowledge the synchrotrons at which I collected my data: the Advanced Photon Source (APS; Argonne National Laboratory, accessed through the CLS@APS program) and the Stanford Synchrotron Radiation Lightsource (SSRL; SLAC National Accelerator Center); results chapters provide full acknowledgements. I would like to specifically thank Drs. Robert Gordon and Zou Finfrock (APS) and Dr. Sam Webb (SSRL) for their dedication and valuable assistance during my many beamtimes. I will remember the time spent at their respective synchrotrons very fondly.

I would very much like to thank the many members of the Molecular Environmental Sciences group, specifically Drs. Tracy MacDonald, Susan Nehzati, Kelly Summers and Natasha Dolgova for the many years of friendship and shared love of science. I can honestly say I would not have made it through this experience without the love and support that have come from all of you.

Lastly I have to thank my own family, including my husband Jon and my sweet daughters Mya, Jaedyn and Landry who have been a part of this adventure for so many years. Thank you all, Jon especially, for understanding why it meant so much for me to complete this degree. I also have to thank my massive extended family – Mom, Dad, Joel, Josie, Kaitlyn, Jason, Jordan, James, Moses, Shalyn, Mary, Hannah, Tim, Jeannine, Tammy, Travis, BJ and Jodi for cheering me on and for being my beautiful support system.

TABLE OF CONTENTS

LIST OF TABLES

LIST OF FIGURES

LIST OF ABBREVIATIONS

°C	degree Celsius
α-HgS	alpha mercuric sulfide, also known as cinnabar
β-HgS	beta mercuric sulfide, also known as metacinnabar
µg	microgram, 10^{-6} g
µg/cm^2	microgram per square centimetre
µm	micron or micrometer, 10^{-6} m
µM	micromolar, 10^{-6} M
Å	Ångströms, 10^{-10} m
APS	Advanced Photon Source
BBB	blood brain barrier
BCH	2-amino-2-norbornanecarboxylic acid
CCAC	Canadian Council of Animal Care
cm^2	square centimetre
CO_2	carbon dioxide
cryo-EM	cryogenic electron microscopy
DFT	density functional theory
DOE	Department of Energy
dpf	days post-fertilization
DTNB	5,5'-dithiobis (2-nitrobenzoic acid)
eV	electron volt, unit of energy
EXAFS	extended X-ray absorption fine structure
FTIR	Fourier-transform infrared spectroscopy
g	gram
GeV	10^9 eV
GSH	glutathione
HEPES	4-(2-Hydroxyethyl)piperazine-1-ethanesulfonic acid
HERFD-XAS	high energy resolution fluorescence detection X-ray absorption spectroscopy
Hg^0	zero-valent mercury
Hg^{1+}	univalent mercury
Hg^{2+}	mercuric mercury
I_0	signal from ion chamber, pre-sample
I_1	signal from ion chamber, post-sample
I_2	signal from ion chamber, post-standard foil
JB-4	plastic embedding kit
K	Kelvin (temperature)
KB mirrors	Kirkpatrick-Baez mirrors
keV	10^3 eV
K_{ow}	octanol-water partition coefficient
L	litre(s)
LASU	Lab Animal Services Unit
LAT	L-type neutral amino acid transporters
LINAC	linear accelerator
LOAEL	lowest-observed adverse effect level
M	molar

m^2	square metre
mA	10^{-3} Amperes
MeAIB	α-methylaminoisobutyric acid
MeHg	methylmercury
MeHg-D-Cys	methylmercury-D-cysteineate
MeHg-L-Cys	methylmercury-L-cysteineate
MeHgCl	methylmercury chloride
mL	10^{-3} litre
mM	10^{-3} molar
mRNA	messenger RNA
ms	10^{-3} second
n	number
N_2	dinitrogen
ng	10^{-9} gram
NIGMS	National Institute of General Medical Sciences
NIH	National Institutes of Health
nm	10^{-9} metre
NMR	nuclear magnetic resonance
NOAEL	no-observed adverse effect level
OCT	optimal cutting temperature
PBS	phosphate-buffered saline
PBST	phosphate-buffered saline with Tween 20
pH	measurement of acidity or basicity
PIXE	particle-induced X-ray emission
pmol	picomole
RF	radio frequency
RIXS	resonant inelastic X-ray scattering
SD	standard deviation
SLC	solute carrier (families)
SPEAR	Stanford Positron Electron Accelerating Ring
SSRL	Stanford Synchrotron Radiation Lightsource
TU	Tübingen strain of zebrafish
U.S. EPA	U.S. Environmental Protection Agency
WHO	World Health Organization
wt	weight
XANES	X-ray absorption near-edge structure
XAS	X-ray absorption spectroscopy
XFI	X-ray fluorescence imaging
Z	atomic number
ZFIN	Zebrafish Information Network

CHAPTER 1: GENERAL INTRODUCTION

1.1 Mercury

The compounds of mercury are known to be highly toxic to most forms of life including plants, animals and humans, and are particularly harmful because routes of exposure are surprisingly common for human populations. Mercury is a heavy metal having an atomic number of 80 in the periodic table and being denoted by the symbol Hg. Mercury is commonly classified under three categories having different toxicities including metallic mercury, or elemental mercury (Hg^0), inorganic mercury and organometallic mercury.[1] Organometallic mercury compounds, which encompass the most toxic forms of mercury, are defined as those having an Hg–C covalent bond and will be the primary focus of this thesis and introduction; inorganic mercury will also be discussed briefly.

This introductory chapter lays the groundwork for the research which follows, beginning with the sources and cycling of mercury in the environment. The toxicokinetics and toxicodynamics as well as safety concerns of methylmercury, which is the primary focus of this thesis, are then addressed. Historical poisonings of human populations by mercury species are also considered. This chapter concludes with some discussion on zebrafish (*Danio rerio*) as a model organism for heavy metal toxicology. A separate introduction is then presented in Chapter 2 which is focussed on relevant synchrotron methodologies utilized within this thesis.

1.1.1 Natural and anthropogenic sources of mercury

Mercury as an element is found naturally within the Earth's crust. Its concentration in the Earth's crust may vary considerably depending on location.[1] Mercury is released into the environment through natural processes and can cycle between environmental compartments including the atmosphere, soil and water. Mercury is often found in coal associated with its organic content or sulfides, as well as in geologic deposits as an ore such as cinnabar which is composed of α-mercuric sulfide (α-HgS).[2] Cinnabar was historically valued by the Romans due to its red pigmentation.[3] The world's largest known cinnabar deposit, the Almadén mine, was historically mined to utilize the beautiful pigmentation of cinnabar for paint and cosmetic use.[3] Mercury can also be released into the environment from additional natural sources including volcanic eruptions, oceanic emissions and forest fires.[1]

A most significant anthropogenic source of mercury is the burning of fossil fuels. This includes particularly large contributions from coal-fired power plants as well as contributions from artisanal and small scale gold-mining.[4] Additional sources include cement production, and waste from consumer goods and other industrial activities.[4] It has been estimated that approximately 5500 to 8900 tonnes of mercury is released or re-released annually into the atmosphere, with 10% of total emissions coming from natural sources, 30% resulting from anthropogenic activity and the remaining 60% of emissions coming from mercury which has been re-emitted into the atmosphere from previously deposited mercury in land or water compartments.[4] While controls are increasing on anthropogenic mercury emissions and utilization due to environmental and human health concerns, mercury still exists in numerous consumer products including: dental amalgams, batteries, switches, lighting bulbs and formulated products such as pharmaceuticals, preservatives, reagents and testing kits.[5]

1.2 Cycling of Mercury in the Environment

Mercury released into the atmosphere from the most significant source of anthropogenic mercury, coal-fired power plants, is in varying ratios of the chemical forms of Hg^0, Hg^{2+} and mercury bound to particulate matter, depending on the pollution controls in place.[6] Mercury that is released as Hg^0 can have an atmospheric lifetime of 0.5-2 years with the ability to be transported globally.[6] Here, what started as a point source of contamination can ultimately contaminate even the most remote, pristine locations. Mercury released from a point source such as a coal-fired power plant will in part be deposited locally in vegetation, soil or surface water. Local deposition will primarily consist of inorganic forms (Hg^{2+} and particulate bound Hg) rather than Hg^0 which will remain in the atmosphere for a longer period of time.[7]

1.2.1 Cycling between environmental compartments

Many factors may affect the cycling of mercury between environmental compartments. Within each compartment, there are numerous biotic and abiotic processes occurring that may affect the movement and speciation of mercury. Over time within the atmosphere, all available mercury species including Hg^0, Hg^{2+} (gas or aqueous) and Hg^{2+} (particulate-bound) will undergo redox reactions, cycling between chemical species until the inevitable deposition on land or in water (fresh or oceanic).[8] An important mechanism of deposition of atmospheric Hg^0 to soil and surface waters is via its oxidation to Hg^{2+9}. The soil compartment is the largest terrestrial mercury sink with estimates of 200-1000 megagrams of Hg existing within at any given time.[8]

Atmospheric depositions into soil are highly contained within upper sediment layers which are often highly biologically active and rich with organic content to which mercury species will likely associate.[8] Depositions of Hg^0 into soil (as Hg forms bound to solid matter, no longer in a gaseous phase) also undergo redox reactions, with mercury subsequently returning to the atmosphere if the organic material to which it is bound to is burned, or through volatilization.[10] Mercury within the soil compartment can be retained for very long periods of time before evasion back into the atmosphere.[10] However, movement can also occur through soil and groundwater to the aquatic compartments of either freshwater or ocean water.

Mercury present in the atmosphere including Hg^0, Hg^{2+}(gas), Hg^{2+}(aqueous) and Hg(particulate-bound) can be deposited into either freshwater or oceanic aquatic compartments.[8] Large bodies of water are commonly stratified into a surface layer, or epilimnion, which is characterized by warmer temperatures and oxic conditions with high levels of aerobic biological activity and a bottom layer, or hypolimnion, which is characterized by anoxic conditions with anaerobic biological activity and cooler temperatures.[11] After deposition into surface waters, Hg^{2+} species may become reduced to Hg^0 and subsequently re-volatilize into the atmosphere. Alternatively, they may sorb to dissolved organic material or other inorganic chemical species present in surface waters, or become deposited into sediment.[11] Photolysis may occur within the epilimnion, where chemical bonds of mercury perhaps bound to organic material become broken by light. The resulting divalent Hg may then be reduced to Hg^0 and evaded or it may bind once again to dissolved organic material.[11]

Mercury species in surface waters and sediments may undergo anaerobic biotransformations. For example, inorganic mercury species existing within the anoxic hypolimnion and sediment may become methylated by microbial actions.[12] It has been noted that communities of sulfate-reducing bacteria present in anaerobic environments are highly involved in the methylation of inorganic mercury species.[12] Methylated, or organic forms of mercury are of significant toxicological concern because of the risk of both organism-level bioaccumulation and trophic level biomagnification.[12] Methylmercury may accumulate in microorganisms through active transport or via diffusion, where it will become associated with cellular components which are taken up and retained by organisms in the next trophic level.[12] This differs from uptake of inorganic mercury species, which are also retained within the bacterium (as an example) but become associated with cellular components that tend to be excreted from the organism which

consumed the bacterium.[12] Bioaccumulation beginning at the lowest trophic levels may result in biomagnification into higher trophic levels to large, predatory organisms which can then contain very high methylmercury concentrations. Examples of top accumulators of methylmercury in aquatic environments include bass, walleye, pike, shark and swordfish, which may be consumed by human populations and result in acute or chronic toxicity.[13]

1.3 Methylmercury: Toxicokinetics

The chemical form of mercury which will be the focus of this thesis is methylmercury. Methylmercury is the most frequently studied form of organomercury. The following discussion relates primarily to acute methylmercury exposure scenarios, as less is known about the toxicokinetics and dynamics of chronic methylmercury exposures. Common symptoms related to organic mercury poisoning in adult exposures include paresthesia, ataxia, dysarthria, visual and auditory disturbances, tremor and muscle weakness.[14] Similar symptoms can be seen in a prenatal exposure, but can further include delayed achievement of developmental milestones and severe brain damage or cerebral palsy.[14,15] The most common route of exposure of humans to methylmercury is through the ingestion of mercury-containing fish, as discussed above. Upon ingestion, mercury is highly absorbed (approximately 95%) from the gastrointestinal tract to the bloodstream,[16] becoming bound to hemoglobin on red blood cells with very little existing in the blood plasma.[17] Early work observing methylmercury toxicokinetics in human subjects after ingestion of methylmercury-contaminated fish determined that peak absorption of mercury occurs in the first 20-30 hours after ingestion.[18] This is preceded by both an initially fast clearance rate representing distribution to tissues with an average half-life of 7.6 hours, followed by a subsequently slower clearance rate of total mercury from the body with an average half-life of 51.9 days.[18] The half-life within the blood has been measured to be approximately 50-70 days,[19] although the concentration rapidly decreases to approximately 5% of the absorbed dose within the initial fast clearance half-life given above.[20] Blood and hair concentrations of methylmercury are considered to be valid biomarkers for exposure. Generally, concentrations of methylmercury in hair are 250 times those of the concentration found in the blood compartment.[19] Hair concentrations of mercury are thought to be a sink primarily for organomercury compounds compared to inorganic mercury. Indeed, research has shown the chemical forms of mercury in hair of individuals consuming a high fish diet (which can be associated to higher risk of organomercury consumption) to be approximately 80%

methylmercury cysteine (or some closely related chemical species) and 20% inorganic mercury bound to thiolate species.[21] As the average growth rate of human hair is approximately 1 cm/month, methylmercury exposure can be measured in hair as a factor of time which can aid in giving a general outline of an exposure scenario.

Methylmercury will subsequently move from the blood compartment to organ tissues where it binds to thiol groups to form water-soluble compounds which are readily transported throughout the body. Transport of organic mercury at the cellular level has long been assumed to be via large neutral amino acid transporters (LAT1 and LAT2) although other transporters may also be involved. The complexity of transportation of methylmercury species is examined in more detail in Chapter 6. LAT transporters are essential for any tissue performing protein synthesis and requiring amino acids. Absorption in the gastrointestinal tract is thought to occur using LAT transport.[22] LAT transporters are found ubiquitously throughout the human body, including a presence at the blood-brain and blood-placental barriers,[23,24,25] both of which are known targets of methylmercury toxicity. It has been estimated that the ratio of methylmercury concentrations in the brain to blood compartments is approximately 5:1 while the concentration found within the fetal brain can be as high as fives time that found within the brain of the mother.[20] Methylmercury is also passed through breast milk to a suckling infant.[16] Other targets for deposition outside of the brain, fetus and hair include the liver and kidneys. Enterohepatic circulation can also occur, with methylmercury being transported into liver cells as complexes with cysteine and subsequently out of liver cells via complexes with reduced glutathione into bile. In this form it may be reabsorbed into the bloodstream through the gall bladder and the other areas of the intestinal tract.[16,26]

Metabolism of organic mercury to inorganic mercury within the body is an important defense mechanism. Methylmercury that is not reabsorbed may be metabolized to inorganic mercury through the breakdown of the mercury-carbon bond by microflora in the intestinal tract. Possible demethylation of organic mercury species in an unexpected medium is discussed in Chapter 7. Methylmercury is also largely demethylated in the liver, where it is excreted into bile as glutathione conjugates.[16] From here, mercury is largely eliminated (approximately 90%) through fecal excretion.[16,20,26] Within the brain, demethylation of organic mercury to inorganic species such as mercuric selenide (HgSe) which are non-toxic and bio-unavailable is another critical form of defense. A recent review which investigated both human and animal studies has

estimated the half-life of inorganic mercury in human brain to be on the order of years, or even decades.[27] As there is no clear mechanism for the uptake of inorganic mercury into the brain, the presence of inorganic mercury in these tissues is primarily explained by the demethylation of organic mercury. How this occurs, precisely, is still unknown and is discussed in more detail in Chapter 4.

1.4 Methylmercury: Toxicodynamics

The mechanisms through which methylmercury exerts its toxicity are many and varied. Methylmercury is primarily known as a neurotoxicant, having the ability to cause extensive damage to the nervous system. Methylmercury is known to induce oxidative stress through increased reactive oxygen species formation,[28] possibly due to damage to the mitochondria, a known target of methylmercury[29] which is responsible for some reactive oxygen species production.[30] Increased oxidative damage may also occur due to depletion of intracellular glutathione (GSH),[31] a known antioxidant and scavenger of available methylmercury. Other work has shown that methylmercury can reduce cellular levels of precursors for GSH production, including cysteine and cystine which are integral for GSH production, further enhancing oxidative stress.[28] Methylmercury is also known to disrupt intracellular calcium homeostasis[28,32] and to inhibit protein synthesis.[29] Methylmercury has also been shown to disrupt microtubule formation by impairing tubulin polymerization through binding of cysteine residues. This can ultimately impact the cellular cytostructure, especially in the developing brain.[33,34]

Within the adult human brain, methylmercury will cause degeneration of specific neuronal cell types including cerebellar granule cells (with adjacent Purkinje cells remaining relatively intact) as well as neuronal cells within the calcarine fissure present in the occipital lobe.[35] The calcarine fissure is located within the primary visual cortex. Damage to neuronal cells of this region is associated with symptomatic constriction of the visual field.[14,36] Some research has shown that methylmercury inhibits protein synthesis at granule cells such that this synthesis does not recover, while protein synthesis at Purkinje cells recovers and can even surpass the original rate of synthesis.[37] It has also been shown that that certain receptors on the extracellular surface of granule cells might be more sensitive to inhibition by methylmercury than those found on Purkinje cells.[38] Damage to the cerebellar granule cells is thought to be linked to symptoms of ataxia. Additional neuronal degeneration has also been noted in the auditory cortex of the temporal lobe as well as in precentral and postcentral areas of the cerebral cortex[36] which may be

linked to clinical symptoms of affected audition, paresthesia and dysarthria.[28,39] Neuropathological changes in neuronal cells in a prenatal exposure to methylmercury occur more diffusely throughout the cerebrum and cerebellum compared to the specific locations noted above in an adult exposure.[40] Here, rather than atrophy, neuronal cells demonstrate hypoplasia, or arrested development.[40] As well, the hallmark pathological change of atrophy of cerebellar granule cells is reduced in a fetus, compared with an adult exposure.[41]

One of the most curious remaining uncertainties regarding organic mercury toxicology is the latency period which exists between exposure and exhibition of clinical symptoms in adults. In the case of a 48-year old Dartmouth chemistry professor who accidently became exposed to a high concentration of dimethylmercury through dermal absorption, the latency period between exposure and becoming symptomatic was 5 months.[42] The absorbed dimethylmercury this individual was exposed to was thought to become metabolized to mono-methylmercury in approximately 6 days.[43] In the case of the Iraqi poisoning event of the 1970s, where wheat and barley treated with a methylmercury-based fungicide was accidently utilized for bread consumption, the latency period ranged from 16 to 38 days.[44] For the Dartmouth case, symptoms began with affected balance, gait and speech. These symptoms became increasingly severe within the next several weeks, at which point the patient was experiencing increasing difficulty walking, and with speech as well as constriction of the visual field.[42] The patient became fully unresponsive to stimuli 22 days after being admitted to the hospital. Death occurred within 5 months of becoming symptomatic, just over 10 months past the original exposure event.[42] For the Iraqi bread poisoning case, symptoms ranged in a dose-dependent fashion from paresthesia to deafness, blindness, or ultimately, fatality. When comparing these two exposure scenarios (and others) it appears that the concentration of the absorbed dose is unrelated to the length of time of the latency period, even while it is certainly related to the severity of the symptoms. The reason for this remains unclear.

1.5 Safety Recommendations

The World Health Organization (WHO), Health Canada and the U.S. EPA have all established safety guidelines regarding exposure risks to methylmercury. A Swedish expert group examined the data from the Japanese Minamata disease (see Section 1.7.1) and Iraqi bread consumption exposure event to make an early attempt at a lowest-observed adverse effect level (LOAEL) guideline of 50 µg Hg/g in scalp hair and 200 µg Hg/L in whole blood.[45] A WHO

expert group took these guidelines further by applying safety factors of 10 to each value, establishing NOAELs (no-observed adverse effect levels) for blood and hair to be 20 µg Hg/L and 5 µg Hg/g.[16] From the Iraqi exposure data, the same WHO expert group determined that a maternal scalp hair concentrations of mercury above 70 µg/g were associated with an approximate 30% risk of the infant exhibiting abnormal neurological and developmental characteristics. They also noted that a lower concentration of 10-20 µg/g is associated with a lower risk of approximately 5%.[16] Health Canada has derived a tolerable daily intake value to be <8 µg/L Hg in blood for pregnant women, girls and women aged 0-49 years, and males aged 18 years and younger. They equated this to 0.2 µg/kg body weight per day, with a slightly less restrictive value of <20 µg/L blood Hg for males older than 18 years of age.[46]

The most recent U.S. EPA guidelines regarding methylmercury exposure risks were based off values derived from one of the three most prominent, large-scale human studies conducted evaluating long-term methylmercury consumption in humans. These studies were based off human populations from New Zealand, the Faroe Islands and the Seychelles. Chronic mercury exposures in both New Zealand and the Seychelles are discussed in sections 1.7.2 and 1.7.3. The U.S. EPA values were ultimately based off the research conducted on natives of the Faroe Islands, where periodic consumption of whale meat and blubber occurs regularly throughout life. The data from this study has been looked at time and again, using different forms of statistics, or examining different endpoints. The original study published in 1992[47] included a total of 1023 infants with subsequent publications including data collected from infancy to the time the children were 14 years old. This work aimed to determine whether relationships existed between a variety of developmental milestones, neurological, and neuropsychological tests with mercury concentrations in the hair of the mother as well as in cord blood.[48,49] The authors determined there to be a negative effect of chronic methylmercury consumption when using cord blood as the primary indicator of children aged 7 years-old based off of hand-eye coordination exams as well as learning-based exams.[48] Some indicators of differences in audition were noted in children 14 years of age using both cord blood and maternal hair mercury concentrations. From this body of work, the U.S. EPA determined the adult oral reference dose for methylmercury, which by definition is the acceptable daily dose of a substance, to be 0.1 µg/kg/day.[50]

1.6 Inorganic Species of Mercury

This brief discussion will focus on mercuric mercury (Hg^{2+}), rather than other inorganic forms as mercuric mercury was the only form utilized in this thesis. Many sources of inorganic mercury are now be considered historical sources, having been essentially phased out. These include the use of inorganic mercury compounds as fungicides in latex paints and in various pharmaceutical and agricultural products as well as in laxatives and teething remedies.[51] Inorganic mercury compounds can still be found in skin-lightening creams in varying concentrations today.[52] A recent report has described the poisoning of a toddler due to ingestion of a skin-lightening cream produced in Mexico containing high levels of mercury.[53] An exposure to inorganic mercury can also occur through ingestion of fish or seafood which may contain inorganic mercury compounds,[47] as well as organic mercury species which become metabolized to inorganic mercury within the body.

Exposure to inorganic mercury may occur dermally through the use of lightening creams as mentioned above or in an occupational context if in close contact with products which incorporate such forms of mercury. Inorganic mercury is less well absorbed in the gastrointestinal tract than organic mercury, about 7-15% compared to the 95% absorption of methylmercury.[26] Mercuric mercury is likely transported throughout the body as conjugates of thiol-containing amino acids or glutathione with primary targets being the kidneys and the liver. Half-life of the absorbed dose is estimated between 1-2 months. Inorganic mercury is not hypothesized to cross the blood-brain barrier and has historically been assumed to not cross the blood-placental barrier. However, some research has shown that some movement across the placental barrier may occur although the transport mechanism is not fully elucidated.[54]

Inorganic mercury will initially be excreted through feces. This may happen in the first few days after exposure as the burden of unabsorbed mercury is eliminated.[20] Subsequent elimination will occur largely in the urine, as the kidneys are the primary location for accumulation of inorganic mercury.[20] Inorganic mercury will also be eliminated via breastmilk.[26] Accumulation in the kidneys occurs primarily in the proximal tubules, potentially leading to kidney damage and failure.[54] Inorganic mercury in the form of mercury salts will cause damage to the gastrointestinal tract.[55] Toxicity of inorganic mercury species is highly related to the solubility of the chemical species. For example, $HgCl_2$ is more soluble and more toxic compared

to other chemical forms such as HgS or HgSe whose solubility is so low as to be considered essentially non-toxic.[56]

1.6.1 Elemental mercury

Elemental mercury is not discussed in detail in this thesis. Briefly however, elemental mercury is commonly referred to as "quicksilver" due to its liquid nature (at room temperature) and silver colouring.[1] Sources of human exposure to elemental mercury include thermometers, fluorescent bulbs, dental amalgams and mercury switches.[1] The primary risk to humans from elemental mercury comes from the inhalation of mercury vapours, which occur most often in occupational settings.

1.7 Historical Incidents of Mercury Poisoning in Human Populations

Mercury has been known to humans since antiquity. Metallic mercury was well-known in the time of Aristotle, who coined the term "quicksilver."[56] However, it was not until the mid-nineteenth century that the first alkylmercury compounds were synthesized.[56] Their use increased dramatically upon discovery of their anti-bacterial and anti-fungal properties with these compounds becoming widely used in the early 1900s and beyond due to these properties. The toxic effects on human populations remained largely unexplored until the early documentation of four human poisoning cases of individuals who worked at a facility where methylmercury compounds were being manufactured as anti-fungal seed dressings.[57] These individuals were noted to have symptoms rooted in neurological distress, with all surviving but with varying remaining abilities of mobility, vision and speech.[57] Years later, an autopsy on one of these previously exposed individuals was performed, with significant contributions made to the former lack of knowledge on neuropathological alterations caused by methylmercury intoxication.[39]

1.7.1 Acute exposure to organometallic mercury: Minamata disease

Only a few years following this latest publication on the neuropathology of organic mercury was the official discovery of Minamata disease (May 1, 1956), one of the most infamous, historical organic mercury poisoning events of human populations. Minamata disease was the result of organic mercury contaminated effluent being released from a local factory into Minamata Bay, from which was harvested the fish and seafood relied upon by local populations. Organic mercury was not determined to be the cause until numerous years after the official discovery of the strange, neurological disease. The research done by Hunter et al.[39,57] provided crucial evidence which aided in identifying the cause as organic mercury. Shortly after organic

mercury was identified as the causal agent, experiments testing the toxicity of the waste effluent on local felines were conducted but not transparently reported until many years later.[58] Recent work (Chapter 3) re-analyzing these historical feline experiments has confirmed the presence of organic mercury within brain tissue and further suggested the possibility of an alternative mercury species, α-mercuri-acetaldehyde, as the chemical form being released as a waste product from the factory.[59]

Total mercury concentrations in scalp hair of affected individuals ranged from non-detectable to highs of 920 μg/g.[60] Substantial mercury concentrations were found in target organs of individuals who died; brains containing 2.6-24.8 μg/g, livers having 22-70.5 μg/g and kidneys ranging from 21.2-140 μg/g.[61] Approximately 2900 individuals have been officially certified as having Minamata disease.[62] The unofficial count is likely far greater, having been estimated to have affected approximately 200,000 individuals.[60] The environmental clean-up of Minamata Bay and surrounding area was a huge operation, taking almost 10 years and requiring 1.5 million m^2 of mud to be dredged and 71 000 m^2 of sludge to be enclosed in soil.[61]

1.7.2 Chronic exposures to organometallic mercury: Faroe Islands and New Zealand

Additional acute organic mercury exposure events including the mass 1970s Iraqi bread consumption event[44] and the individual intoxication of the Dartmouth chemistry professor in 1996[42] were discussed previously and can also be reviewed in Chapter 4. More cases of organic mercury poisoning exist but will not be discussed in detail here. Acute organic mercury poisoning has been a heavily researched topic in all aspects, from examinations of autopsy materials from poisoning events, to *in vivo* and *in vitro* experiments regarding mechanisms of uptake, transport, toxicity and more. However, chronic organic mercury poisoning is somewhat more difficult to study, and the effects of long-term exposure to low concentrations of methylmercury are very much under debate. Interesting differences in mercury speciation in acute and chronic cases of human exposure can be read about in Chapter 4.

Three large, longitudinal studies examining chronic exposure of human populations to methylmercury have been under-taken with the aim of understanding subclinical effects of exposure, with conflicting results. The Faroe Islands research was briefly summarized above; with ultimate conclusions of a negative effect of chronic organomercury exposure on various neurological and neurobehavioral endpoints of individuals followed from infancy to 14 years of age.[47,48,49] A similar set of studies was conducted in New Zealand where shark, a large predator

fish likely to contain high concentrations of methylmercury, is periodically consumed as "fish and chips" meals. A small group of 38 children aged 4 years were designated as a "high" Hg consumption group and compared against 36 children of the same age designated to be the reference, or "low" Hg consumption group.[20] Abnormal or questionable results were recorded in 52% of the high consumption group vs. 17% of the low consumption group, as determined by a common developmental screening tool.[20] A follow-up study was conducted on 237 children aged 6 years old and included numerous examinations focussed on fine and gross motor skills, language development and social and general intelligence.[20] The results of these examinations were regressed against maternal hair mercury levels, with numerous end points being negatively associated with mean mercury measurements.[20]

1.7.3. Chronic exposures to organometallic mercury: Seychelles

A third major epidemiological study was conducted on human populations residing in the Seychelles where daily consumption of marine fish is the norm, albeit at concentrations estimated at approximately 10 times lower than the other populations discussed above. An initial pilot study was conducted using 789 infants ranging in age from 5 weeks to just over 2 years of age who were examined for endpoints of muscle tone, deep tendon reflex as well as an overall neurological exam.[63] Results were regressed against maternal hair mercury concentrations during pregnancy with no associations seen between mercury concentrations and abnormal results. A main cohort study followed the pilot study with a total of 740 infant-mother pairs selected with infants aged 6.5 months old, and having the same examinations performed as the pilot study.[64] Once again, no associations were seen between abnormal or questionable results and maternal hair mercury concentrations during pregnancy. Another study was conducted when 738 of the same infants were 19 months old.[65] Here, numerous developmental milestones were examined, again with no associations to maternal hair mercury. Additional analysis of 711 infants from the main cohort was performed at approximate ages of 5.5 years of age, with neurodevelopmental assessments of reading, mathematical ability, language development, and other social and cognitive endpoints.[66] No adverse associations were seen with maternal hair, and interestingly, one positive correlation was seen with an examination of language expression and increasing maternal hair mercury.

The Seychelles study where no negative associations were seen differs from both the Faroe Islands and the New Zealand studies, which identified negative effects on individuals in a

prenatal exposure to methylmercury as determined using both cord blood and maternal hair mercury concentrations. With such conflicting results, it is clear that the effects of chronic exposure to organic mercury compounds requires continuing research.

1.8 Zebrafish (*Danio rerio*) as a Model Organism for Heavy Metal Toxicology

Zebrafish (*Danio rerio*) are a highly versatile model organism for vertebrate development and are commonly utilized to study the impacts of exposure to a variety of metals including mercury, cadmium, copper, nickel and zinc, among others.[67,68] Ideal model organism characteristics include their small size and short reproductive cycle as well as their high fecundity and rapid development of larvae.[67] Zebrafish larvae develop outside of the mother and their developmental stages are very well characterized. However, this could also make zebrafish an inaccurate model organism for researchers wishing to examine maternal or placental transfer during gestation. The embryos produced are transparent[67] which is useful for visualizing and characterizing internal abnormalities resulting from experimental exposures. However, caution is warranted as agents used to effect the transparency have been seen to interfere with the action of metals.[69] Administering food is unnecessary for the first seven days of life as larvae will utilize the nutrients contained within the yolk sac during that time period.[70] As well, the conditions and procedures for maintenance and optimal breeding of zebrafish is very well described.[71]

Zebrafish have been seen to be sensitive to methylmercury exposure.[72,73] Uptake and accumulation of inorganic and organic mercury species have been seen in larval zebrafish in organs which are established target organs in human exposures.[74,75,76] L-type amino acid transporters (LAT) transport is currently assumed to be the primary method of transport of methylmercury within the human body, specifically at the blood-brain barrier.[77] This has been hypothesized in zebrafish as well[75] with the blood-brain barrier estimated to fully mature between 3 and 10 days post fertilization[78,79] and transporters orthologous to human LAT shown to be present.[80]

The importance of chemical form in toxicity has been demonstrated using larval zebrafish.[76] Methylmercury is known to cause damage to the primary visual cortex of the brain, which has been linked to affected vision in individuals poisoned by organic mercury.[35] However, mercury has recently been shown to directly accumulate in the exterior layer of the lens of the eye as well as the retinal pigmented epithelia following methylmercury-L-cysteine exposure.[74,75] Mercury accumulation has been further specified to exist within the outer segments of

photoreceptor cells within the retina following exposure to methylmercury chloride in zebrafish larvae.[81] Dynamics of organic mercury and selenium,[82,83] as well as impacts on sensory systems due to inorganic mercury have been studied using larval zebrafish.[84]

1.9 Statement of Purpose, Objectives, and Hypotheses

Methylmercury is recognized as a global pollutant with the ability to cause devastating effects on both human health and the environment. Despite the long history of adverse effects of mercury to human populations, there is much that is not known about its mechanisms regarding transportation within the human body, its exertion of toxicity, and the defensive mechanisms which are in place. The primary goals of this thesis were to better understand the toxicity of organometallic mercury through the investigation of rare autopsy materials from acute and chronic organomercury poisoning cases for the presence of mercury and chemical form of mercury and selenium species. It also aimed to complement the autopsy studies by using the well-described zebrafish vertebrate model organism to better understand LAT transport of methylmercury in the human body and, given the brain tissue samples worked with, to highlight the need for caution when determining methods of sample preservation. From work with zebrafish, an unexpected observation led to the exploration of a potential defensive mechanism of teleost fish against organometallic mercury. The specific objectives and hypotheses for each individual experimental chapter of this thesis were as follows:

1.9.1 Chapter 3 objectives and hypotheses

Chapter 3 examined brain tissue from the historic Cat 717 experiment which occurred during the time of Minamata disease in Minamata, Japan. These unique historical samples originated from the Minamata Institute of Japan and became available for examination through a fortuitous collaboration.

Objective of chapter:

Use high energy resolution fluorescence detection X-ray absorption spectroscopy (HERFD-XAS) to determine chemical forms of mercury and selenium in a historical brain tissue sample from Cat 717. As well, density functional theory (DFT) was used to test the validity of the commonly held theory of methylmercury being released as a by-product of the chemical processes occurring within the industrial plant which was responsible for the effluent release into Minamata Bay.

Hypothesis:

The effluent waste to which Cat 717 was exposed contained mercury which was organic in nature.

Experimental Predictions:

1. Mercury will remain detectable within the feline brain tissue, however, organomercury may not still exist within this tissue.

Hypothesis:

The chemical processes occurring at the industrial plant did not result in methylmercury production.

Experimental Prediction:

1. An alternative organomercury species, in addition to, or in place of methylmercury was produced as an unintentional by-product.

1.9.2 Chapter 4 objectives and hypotheses

Chapter 4 was aimed at characterizing the chemical forms of mercury and selenium in human brain tissue from individuals who experienced both acute and chronic exposures to organomercury species. Brain tissue samples from poisoning events are typically rare and well-protected; due to this fact a large portion of what has been discerned about the dynamics of mercury in the brain comes from *in vitro* and *in vivo* research. The opportunity to examine human brain tissue for mercury, post-exposure, was exceedingly unique.

Objectives of chapter:

Use HERFD-XAS to identify similarities and differences in speciation of mercury and selenium in brain tissue samples from victims who had been either acutely or chronically exposed to organometallic mercury to better understand the nature of mercury in human brain tissue. Additionally, to determine whether preservation method (formalin-fixation vs. fresh-frozen) affected the speciation of mercury and selenium in brain tissue samples.

Hypothesis:

The mechanisms of toxicity of acute and chronic organomercury exposures are the same.

Experimental Predictions:

1. No major differences in chemical speciation of mercury exist between acute and chronic low-level exposures in human brain tissue samples examined.
2. Differences will be limited to concentrations of mercury between exposure scenarios, with higher quantities of mercury being seen in brain tissue having had acute exposures.

Hypothesis:

Formalin fixation preserves the level and form of mercury and selenium in tissue.

Experimental Prediction:

1. No differences in mercury or selenium speciation or level exist between formalin-fixed and fresh-frozen brain tissue.

1.9.3 Chapter 5 objectives and hypotheses

Chapter 5 utilized larval zebrafish to further explore the potential consequences of preservation method on mercury and various endogenous elements after working with formalin-preserved tissues in both Chapters 3 and 4. Past research within this group has utilized a methacrylate embedding protocol (which includes fixative steps) on mercury-exposed zebrafish for the examination of mercury accumulation and distribution throughout various target tissues.

Objectives:

Use X-ray fluorescence imaging (XFI) to examine the effects of cryopreservation and methacrylate embedding protocol on quantity and distribution of mercury and endogenous elements in zebrafish larvae following exposure to organometallic mercury.

Hypothesis:

Methacrylate embedding protocol preserves the accumulation and distribution of mercury in exposed larval zebrafish but disrupts the same in endogenous elements.

Experimental Predictions:

1. Qualitative and quantitative examination of mercury will yield no differences in the vertebrate model organism, zebrafish (*Danio rerio*) which had been exposed to methylmercury and subsequently cryopreserved or preserved using the methacrylate protocol.
2. Endogenous elements which are inherently more mobile than mercury will be affected by preservation method.

1.9.4 Chapter 6 objectives and hypotheses

The work accomplished in both Chapters 3 and 4 led to the consideration of the mechanism by which methylmercury is transported across the blood-brain barrier. Scientific literature commonly cites L-system transport as the mechanism (LAT) by which methylmercury is transported at the blood-brain barrier, blood-placental barrier, and ubiquitously throughout the body.

Objectives:

Use toxicity studies with larval zebrafish to determine whether the toxicity of methylmercury-L-cysteine could be ameliorated through co-exposure with various LAT substrates and a LAT inhibitor, and further, to use XFI to determine whether co-exposure would result in reduced uptake of mercury into target organs and tissues. As well, to determine whether the (presumed) stereoselectivity of LAT transport would apply to methylmercury-D-cysteine by testing the same endpoints with the same methods.

Hypothesis:

LAT is responsible for the transport of methylmercury in larval zebrafish. This transport is stereoselective.

Experimental Predictions:

1. Co-exposure of larval zebrafish to methylmercury-L-cysteine and LAT substrates or inhibitor results in increased survival of larval zebrafish as well as reduced uptake of mercury into target organs compared to those exposed exclusively to methylmercury-L-cysteine.
2. Survival is increased and mercury concentrations in target organs are decreased following exposure to methylmercury-D-cysteine in larval zebrafish compared to those exposed to methylmercury-L-cysteine.

1.9.5 Chapter 7 objectives and hypotheses

Similar to Chapter 6, the research in Chapter 7 was the result of the exploration of an idea stemming from the research in Chapters 3 and 4. Defensive mechanisms against mercury became a topic of interest after observing the demethylation of organic mercury occurring in the aforementioned brain tissue samples. As well, demethylation of organometallic mercury is known to occur in the mucosal-lined gastrointestinal tract of the human body. Previous work completed within this research group with larval zebrafish and inorganic mercury demonstrated a slight accumulation of mercury in the exterior layer of sectioned zebrafish, the region in which mucosal production would occur.

Objectives:

Use XFI to determine whether accumulation of mercury in the exterior epithelial layer of larval zebrafish occurs after exposures to various organometallic and inorganic forms of mercury. Further, to use XAS to examine what compounds of sulfur exist in harvested steelhead trout

(*Oncorhynchus mykiss*) mucosa, and what compounds of mercury form after titration of organometallic or inorganic mercury with such mucosa.

Hypothesis:

Exterior epithelial layer of larval zebrafish and teleost mucosa are both targets for various forms of inorganic and organomercury.

Experimental Predictions:

1. The exterior epithelial layer of zebrafish, where mucosa is produced accumulates both organic and inorganic mercury.
2. Harvested mucosa of the steelhead trout forms complexes with both organometallic and inorganic mercury when titrated together.

1.10 References

(1) Agency for Toxic Substances and Disease Registry (ASTDR). *Toxicological profile for mercury*. U.S. Department of Health and Human Services, Atlanta, GA, 1999.

(2) Pavlish, J.H., Sondreal, E.A., Mann, M.D., Olson, E.S., Galbreath, K.C., Laudal, D.L., Benson, S.A. Status review of mercury control options for coal-fired power plants. *Fuel Process. Technol.* **2003**, *82*, 89-165.

(3) Barnett, J.R., Miller, S., Pearce, E. Colour and art: A brief history of pigments. *Opt. Laser Technol.* **2006**, *38*, 445-453.

(4) United Nations Environment Programme (UNEP). *Global mercury assessment: Sources, emissions, releases and environmental transport.* UNEP Chemicals Branch, Geneva, Switzerland, 2013.

(5) U.S. Environmental Protection Agency (U.S. EPA). *Inventory of mercury supply, use, and trade in the United States 2020 report.* Office of Chemical Safety and Pollution Prevention. Reporting year 2018, Washington, DC.

(6) Carpi, A. Mercury from combustion sources: A review of the chemical species emitted and their transport in the atmosphere. *Water Air Soil Pollut.* **1997**, *98*, 241-254.

(7) Driscoll, C.T., Mason, R.P., Chan, H.M., Jacob, D.J., Pirrone, N. Mercury as a global pollutant: Sources, pathways and effects. *Environ. Sci. Technol.* **2013**, *47*, 4967-4983.

(8) Obrist, D., Kirk, J.L., Zhang, L., Sunderland, E.M., Jiskra, M., Selin, N.E. A review of global environmental mercury processes in response to human and natural perturbations: Changes of emissions, climate and land use. *Ambio* **2018**, *47*, 116-140.

(9) Si, L., Ariya, P.A. Recent advances in atmospheric chemistry of mercury. *Atmosphere* **2018**, *9*, article number 76

(10) Selin, N.E. Global biogeochemical cycling of mercury: A review. *Annu. Rev. Environ. Resour.* **2009**, *34*, 43-63.

(11) Hemond, H.F., Fechner-Levy, E.J. *Chemical fate and transport in the environment*. San Diego, CA: Academic Press, 2000.

(12) Morel, F.M.M., Kraepiel, A.M.L., Amyot, M. The chemical cycle and bioaccumulation of mercury. *Annu. Rev. Ecol. Syst.* **1998**, *29*, 543-566.

(13) Government of Canada. *Mercury in the food chain*. Retrieved from: https://www.canada.ca/en/environment-climate-change/services/pollutants/mercury-environment/health-concerns/food-chain.html#MethylF

(14) Eto, K. Pathology of Minamata Disease. *Toxicol. Pathol.* **1997**, *25*, 614-623.

(15) Risher, J.F., Murray, H.E., Prince, G.R. Organic mercury compounds: human exposure and its relevance to public health. *Toxicol. Ind. Health* **2002**, *18*, 109-160.

(16) World Health Organization (WHO). *Environmental Health Criteria 101: Methylmercury*. International Programme on Chemical Safety, Geneva, Switzerland, 1990.

(17) Clarkson, T.W., Vyas, J.B., Ballatori, N. Mechanisms of mercury disposition in the body. *Am. J. Ind. Med.* **2007**, *50*, 757-764.

(18) Kershaw, T.G., Dhahir, P.H., Clarkson, T.W. The relationship between blood levels and dose of methylmercury in man. *Arch. Environ. Health* **1980**, *35*, 28-36.

(19) Mergler, D., Anderson, H.A., Chan, L.H.M., Mahaffey, K.R., Murray, M., Sakamoto, M., Stern, A.H. Methylmercury exposure and health effects in humans: A worldwide concern. *Ambio* **2007**, *36*, 3-11.

(20) Clarkson, T.W., Magos, L. The toxicology of mercury and its chemical compounds. *Crit. Rev. Toxicol.* **2006**, *36*, 609-662.

(21) George, G.N., Singh, S.P., Myers, G.J., Watson, G.E., Pickering, I.J. The chemical forms of mercury in human hair: a study using X-ray absorption spectroscopy. *J. Biol. Inorg. Chem.* **2010**, *15*, 709-715.

(22) Simmons-Willis, T.A., Koh, A.S., Clarkson, T.W., Ballatori, N. Transport of a neurotoxicant by molecular mimicry: the methylmercury-L-cysteine complex is a substrate for human L-type large neutral amino acid transporter (LAT) 1 and LAT2. *Biochem. J.* **2002**, *367*, 239-246.

(23) Kerper, L.E., Ballatori, N., Clarkson, T.W. Methylmercury transport across the blood-brain barrier by an amino acid carrier. *Am. J. Physiol.* **1992**, *262*, 761-765.

(24) Mokrzan, E.M., Kerper, L.E., Ballatori, N., Clarkson, T.W. Methylmercury-thiol uptake into cultured brain capillary endothelial cells on amino acid system L. *J. Pharmacol. Exp. Ther.* **1995**, *272*, 1277-1284.

(25) Kajiwara, Y., Yasutake, A., Adachi, T., Hirayama, K. Methylmercury transport across the placenta via neutral amino acid carrier. *Arch. Toxicol.* **1996**, *70*, 310-314.

(26) World Health Organization (WHO). *Environmental Health Criteria 1: Mercury*. International Programme on Chemical Safety, Geneva, Switzerland, 1976.

(27) Rooney, J.P.K. The retention time of inorganic mercury in the brain – A systematic review of the evidence. *Toxicol. Appl. Pharmacol.* **2014**, *274*, 425-435.

(28) Sanfeliu, C., Sebastià, J., Cristofòl, R., Rodriguez-Farré, E. Neurotoxicity of organomercurial compounds. *Neurotox. Res.* **2003**, *5*, 283-306.

(29) Yoshino, Y., Mozai, T., Nakao, K. Distribution of mercury in the brain and its subcellular units in experimental organic mercury poisoning. *J. Neurochem.* **1966**, *13*, 397-406.

(30) Polunas, M., Halladay, A., Tjalkens, R.B., Philbert, M.A., Lowndes, H., Reuhl, K. Role of oxidative stress and the mitochondrial permeability transition in methylmercury cytotoxicity. *Neurotoxicology* **2011**, *32*, 526-534.

(31) Farina, M., Aschner, M., Rocha, J.B.T. Oxidative stress in MeHg-induced neurotoxicity. *Toxicol. Appl. Pharmacol.* **2011**, *256*, 405-417.

(32) Atchison, W.D., Hare, M.F. Mechanisms of methylmercury-induced neurotoxicity. *FASEB J.* **1994**, *8*, 622-629.

(33) Han, K.K., Delacourte, A., Hemon, B. Chemical modification of thiol group(s) in protein: Application to the study of anti-microtubular drugs binding. *Comp. Biochem. Physiol.* **1987**, *88B*, 1057-1065.

(34) Castoldi, A.F., Barni, S., Turin, I., Gandini, C., Manzo, L. Early acute necrosis, delayed apoptosis and cytoskeletal breakdown in cultured cerebellar granule neurons exposed to methylmercury. *J. Neurosci. Res.* **2000**, *59*, 775-787.

(35) Philbert, M.A., Billingsley, M.L., Reuhl, K.R. Mechanisms of injury in the central nervous system. *Toxicol. Pathol.* **2000**, *28*, 43-53.

(36) Takeuchi, T., Morikawa, N., Matsumoto, H., Shiraishi, Y. A pathological study of Minamata Disease in Japan. *Acta Neuropathol.* **1962**, *2*, 40-57.

(37) Syversen, T.L.M. Effects of repeated dosing of methyl mercury on in vivo protein-synthesis in isolated neurons. *Acta Pharmacol. Toxicol.* **1982**, *50*, 391-397.

(38) Yuan, Y., Atchison, W.D. Methylmercury differentially affects $GABA_A$ receptor-mediated spontaneous IPSCs in Purkinje and granule cells of rat cerebellar slices. *J Physiol.* **2003**, *550.1*, 191-204.

(39) Hunter, D., Russell, D.S. Focal cerebral and cerebellar atrophy in a human subject due to organic mercury compounds. *J. Neurol. Neurosurg. Psychiat.* **1954**, *17*, 235-241.

(40) Eto, K. Minamata disease. *Neuropathology* **2000**, *20*, 14-19.

(41) Eto, K., Marumoto, M., Takeya, M. The pathology of methylmercury poisoning (Minamata disease). *Neuropathology* **2010**, *30*, 471-479.

(42) Nierenberg, D.W., Nordgren, R.E., Chang, M.B., Siegler, R.W., Blayney, M.B., Hochberg, F., Toribara, T.Y., Cernichiari, E., Clarkson, T.W. Delayed cerebellar disease and death after accidental exposure to dimethylmercury. *N. Engl. J. Med.* **1998**, *338*, 1672-1676.

(43) Weiss, B., Clarkson, T.W., Simon, W. Silent latency periods in methylmercury poisoning and in neurodegenerative disease. *Environ. Health Perspect.* **2002**, *110*, 851-854.

(44) Bakir, F., Damluji, S.F., Amin-Zaki, L., Murtadha, M., Khalidi, A., Al-Rawi, N.Y., Tikriti, S., Dhahir, H.I., Clarkson, T.W., Smith, J.C., Doherty, R.A. Methylmercury poisoning in Iraq. *Science* **1973**, *181*, 230-241.

(45) Swedish Expert Group. Methylmercury in fish. A toxicological-epidemiological evaluation of risks. *Nord. Hyg. Tidskr.* **1971**, *4*, 19-364.

(46) Legrand, M., Feeley, M., Tikhonov, C., Schoen, D., Li-Muller, A. Methylmercury blood guidance values for Canada. *Can. J. Public Health* **2010**, *101*, 28-31.

(47) Grandjean, P., Weihe, P., Jørgensen, P.J., Clarkson, T., Cernichiari, E., Viderø, T. Impact of maternal seafood diet on fetal exposure to mercury, selenium and lead. *Arch. Environ. Health* **1992**, *47*, 185-195.

(48) Grandjean, P., Weihe, P., White, R.F., Debes, F., Araki, S., Yokoyama, K., Murata, K., Sørensen, N., Dahl, R., Jørgensen, P.J. Cognitive deficit in 7-year-old children with prenatal exposure to methylmercury. *Neurol. Teratol.* **1997**, *19*, 417-428.

(49) Grandjean, P., Weihe, P., White, R.F., Debes, F. Cognitive performance of children prenatally exposed to "safe" levels of methylmercury. *Environ. Res.* **1998**, *77*, 165-172.

(50) U.S. Environmental Protection Agency (U.S. EPA). *IRIS assessment plan for methylmercury (scoping and problem formulation materials)*. U.S. EPA Office of Research and Development, Washington, DC, EPA/635/R-18/292, 2019.

(51) U.S. Environmental Protection Agency (U.S. EPA). *Mercury compounds*. Retrieved from https://www.epa.gov/sites/production/files/2016-09/documents/mercury-compounds.pdf

(52) Ho, Y.B., Abdullah, N.H., Hamsan, H., Tan, E.S.S. Mercury contamination in facial skin lightening creams and its health risks to user. *Regul. Toxicol. Pharmacol.* **2017**, *88*, 72-76.

(53) Ori, M.R., Larsen, J.B., Shirazi, F.M. Mercury poisoning in a toddler from home contamination due to skin-lightening cream. *J. Pediatr.* **2018**, *196*, 314-317.

(54) Bridges, C.C., Zalups, R.K. Mechanisms involved in the transport of mercuric ions in target tissues. *Arch. Toxicol.* **2017**, *91*, 63-81.

(55) World Health Organization (WHO). *Elemental mercury and inorganic mercury compounds: Human health aspects*. Concise international chemical assessment document (CICAD) 50. Geneva, Switzerland, 2003.

(56) Clarkson, T.W. The toxicology of mercury. *Crit. Rev. Clin. Lab. Sci.* **1997**, *34*, 369-403.

(57) Hunter, D., Bomford, R.R., Russell, D.S. Poisoning by methyl mercury compounds. *Q. J. Med.* **1940**, *9*, 193-213.

(58) Eto, K.; Yasutake, A.; Nakano, A.; Akagi, H.; Tokunaga, H.; Kojima, T. Reappraisal of the historic 1959 cat experiment in Minamata by the Chisso factory. *Tohoku J. Exp. Med*. **2001**, *194*, 197–203.

(59) James, A.K., Nehzati, S., Dolgova, N.V., Sokaras, D., Kroll, T., Eto, K., O'Donoghue, J.L., Watson, G.E., Myers, G.J., Krone, P.H., Pickering, I.J., George, G.N. Rethinking the Minamata tragedy: What mercury species was really responsible? *Environ. Sci. Technol.* **2020**, *54*, 2726-2733.

(60) Ninomiya, T., Imamura, K., Kuwahata, M., Kindaichi, M., Susa, M., Ekino, S. Reappraisal of somatosensory disorders in methylmercury poisoning. *Neurotoxicol. Teratol.* **2005**, *27*, 643-653.

(61) Harada, M. Minamata disease: Methylmercury poisoning in Japan caused by environmental pollution. *Crit. Rev. Toxicol.* **1995**, *25*, 1-24.

(62) Takizawa, Y. Understanding Minamata disease and strategies to prevent further environmental contamination by methylmercury. *Water Sci. Technol.* **2000**, *42*, 139-146.

(63) Myers, G.J., Marsh, D.O., Cox, C., Davidson, P.W., Shamlaye, C.F., Tanner, M.A., Choi, A., Cernichiari, E., Choisy, O., Clarkson, T.W. A pilot neurodevelopmental study of Seychellois children following *in utero* exposure to methylmercury from a maternal fish diet. *Neurotoxicology* **1995**, *16*, 629-638.

(64) Myers, G.J., Marsh, D.O., Davidson, P.W., Cox, C., Shamlaye, C.F., Tanner, M.A., Choi, A., Cernichiari, E., Choisy, O., Clarkson, T.W. Main neurodevelopmental study of Seychellois children following *in utero* exposure to methylmercury from a maternal fish diet: Outcome at six months. *Neurotoxicology* **1995**, *16*, 653-664.

(65) Myers, G.J., Davidson, P.W., Shamlaye, C.F., Axtell, C.D., Cernichiari, E., Choisy, O., Choi, A., Cox, C., Clarkson, T.W. Effects of prenatal methylmercury exposure from a high fish diet on developmental milestones in the Seychelles child development study. *Neurotoxicology* **1997**, *18*, 819-830.

(66) Davidson, P.W., Myers, G.J., Cox, C., Axtell, C., Shamlaye, C., Sloane-Reeves, J., Cernichiari, E., Needham, L., Choi, A., Wang, Y., Berlin, M., Clarkson, T.W. Effects of prenatal and postnatal methylmercury exposure from fish consumption on neurodevelopment. Outcomes at 66 months of age in the Seychelles child development study. *JAMA* **1998**, *280*, 701-707.

(67) Hill, A.J., Teraoka, H., Heideman, W., Peterson, R.E. Zebrafish as a model vertebrate for investigating chemical toxicity. *Toxicol. Sci*. **2005**, *86*, 6-19.

(68) Dai, Y.J., Jia, Y.F., Chen, N., Bian, W.P., Li, Q.K., Ma, Y.B., Chien, Y.L., Pei, D.S. Zebrafish as a model system to study toxicology. *Environ. Toxicol. Chem*. **2014**, *33*, 11-17.

(69) MacDonald, T.C., Nehzati, S., Sylvain, N.J., James, A.K., Korbas, M., Caine, S., Pickering, I.J., George, G.N., Krone, P.H. Phenylthiourea alters toxicity of mercury compounds in zebrafish larvae. *J. Inorg. Biochem*. **2015**, *151*, 10-17.

(70) McGrath, P., Li, C.Q. Zebrafish: a predictive model for assessing drug-induced toxicity. *Drug Discov. Today* **2008**, *13*, 394-401.

(71) Westerfield, M. The zebrafish book: A guide for the laboratory use of zebrafish (Danio rerio). Eugene, OR: University of Oregon Press, 1995.

(72) Samson, J.C., Goodridge, R., Olobatuyi, F., Weis, J.S. Delayed effects of embryonic exposure of zebrafish (Danio rerio) to methylmercury (MeHg). *Aquat. Toxicol*. **2001**, *51*, 369-376.

(73) Hassan, S.A., Moussa, E.A., Abbott, L.C. The effect of methylmercury exposure on early central nervous system development in the zebrafish (Danio rerio) embryo. *J. Appl. Toxicol*. **2012**, *32*, 707-713.

(74) Korbas, M., Blechinger, S.R., Krone, P.H., Pickering, I.J., George, G.N. Localizing organomercury uptake and accumulation in zebrafish larvae at the tissue and cellular level. *Proc. Natl. Acad. Sci. USA*. **2008**, *105*, 12108–12112.

(75) Korbas, M., Krone, P.H., Pickering, I.J., George, G.N. Dynamic accumulation and redistribution of methylmercury in the lens of developing zebrafish embryos and larvae. *J. Biol. Inorg. Chem*. **2010**, *15*, 1137-1145.

(76) Korbas, M., MacDonald, T.C., Pickering, I.J., George, G.N., Krone, P.H. Chemical form matters: Differential accumulation of mercury following inorganic and organic mercury exposures in zebrafish larvae. *ACS Chem. Biol*. **2012**, *7*, 411-420.

(77) Kerper, L.E., Ballatori, N., Clarkson, T.W. Methylmercury transport across the blood-brain barrier by an amino acid carrier. *Am. J. Physiol-Reg*. **1992**, *262*, 761-76.

(78) Jeong, J.Y., Kwon, H.B., Ahn, J.C., Kang, D., Kwon, S.H., Park, J.A., Kim, K.W. Functional and developmental analysis of the blood-brain barrier in zebrafish. *Brain Res. Bull*. **2008**, *75*, 619-628.

(79) Fleming, A., Diekmann, H., Goldsmith, P. Functional characterisation of the maturation of the blood-brain barrier in larval zebrafish. *PLOS One* **2013**, *8*, article number e77548.

(80) Takayama, K., Akihiko, M., Yutaka, K. Leucine/glutamine and v-ATPase/lysosomal acidification via mTORC1 activation are required for position-dependent regeneration. *Sci. Rep*. **2018**, *8*, article number 8278.

(81) Korbas, M., Lai, B., Vogt, S., Gleber, S.C., Karunakaran, C., Pickering, I.J., Krone, P.H., George, G.N. *ACS Chem. Biol*. **2013**, *8*, 2256-2263.

(82) MacDonald, T.C., Korbas, M., James, A.K., Sylvain, N.J., Hackett, M.J., Nehzati, S., Krone, P.H., George, G.N., Pickering, I.J. Interaction of mercury and selenium in the larval stage zebrafish vertebrate model. *Metallomics* **2015**, *7*, 1247-1255.

(83) Dolgova, N.V., Hackett, M.J., MacDonald, T.C., Nehzati, S., James, A.K., Krone, P.H., George, G.N., Pickering, I.J. Distribution of selenium in zebrafish larvae after exposure to organic and inorganic selenium forms. *Metallomics* **2016**, *8*, 305-312.

(84) MacDonald, T.C., Sylvain, N.J., James, A.K., Pickering, I.J., Krone, P.H., George, G.N. Effects of inorganic mercury on the olfactory pits of zebrafish larvae. *Metallomics* **2016**, *8*, 514-517.

CHAPTER 2: SYNCHROTRON BASED TECHNIQUES: INTRODUCTION AND EXPERIMENTAL ASPECTS

2.1 Synchrotron Introduction

A major portion of the studies of toxicology of mercury presented in this thesis rely on two techniques – X-ray fluorescence imaging and X-ray absorption spectroscopy – which are conducted using synchrotron light. This chapter serves to provide an overview of the principles and experimental aspects of these techniques. The first section of this chapter provides a high level overview of the synchrotron including a brief discussion on relevant optics (Sections 2.1 – 2.3). The second half of this chapter builds on this introduction by providing additional background on the techniques. It will explore some relevant theory behind X-ray spectroscopy as well as provide an examination of the experimental data collection and analysis approaches utilized for the techniques in this thesis (Section 2.4). This is not intended to be an in-depth discussion covering the mathematics or physics behind the theory; however, relevant equations will be noted with citations for material containing such detailed discussions. This introduction will focus on pertinent elements of the synchrotron as is relevant to the experiments conducted as part of this thesis with the intention of keeping the discussion high-level and yet accessible to a wider audience. Table A.2.1 (Appendix A) contains definitions for symbols found in all equations.

2.1.1 Synchrotrons: The basics

A synchrotron is a closed-path particle accelerator that produces electromagnetic radiation (photons, including X-rays) through the acceleration of electrons at speeds nearing the speed of light and uses radio frequency to synchronize the electron pulses. The synchrotron radiation produced is highly bright and tunable.[1] This beam of light is often referred to as a "white beam," meaning it is comprised of a continuous spectrum, with photon energies ranging from the infra-red to highly energetic X-rays, from which specific energies can be selected in an experimental set-up. A synchrotron is designed as a large ring-like structure, from which synchrotron radiation is emitted tangentially as changes in direction of the electron beam occur, as influenced by magnetic components. Beamlines organized around the diameter of the ring focus, tune and shape the synchrotron light to individual experimental enclosures for a variety of experiments.

Components within each individual beamline will determine the specific capabilities of each beamline.

2.1.2 Source, LINAC and booster ring

An electron gun is the typical source of electrons in a synchrotron. Here, a cathode is heated using an electrical current to approximately 1000 degrees resulting in the release of electrons which are pulled into the linear accelerator, the first step of acceleration. The linear accelerator is comprised a series of radio frequency (RF) cavities which boost the energy of the electrons while simultaneously synchronizing the electrons into bunches. These electron bunches are transferred into the booster ring, also called a booster synchrotron which is responsible for further accelerating electrons to relativistic speeds (those nearing the speed of light, and the speed at which they are required to be at to enter the storage ring). These electrons will be synchronously introduced into the storage ring for circulation. Synchrotrons which run in "top-up mode" continuously add synchronized bunches of electrons into the storage ring to replace the electrons and to maintain the circulating electron current over time.

2.1.3 Storage ring

The storage ring is the ring which contains circulating electrons that are accelerated to their highest speed. The ring can be considered to be a many-sided polygon with bend magnets at the corners, which serve to accelerate and deflect the electrons between one straight section (polygon edge) and the next, accelerating the electron beam towards the centre of each bend, causing them to curve around each bend in the ring. In first, second, third and some (but not all) fourth generation synchrotron sources, many beamlines exist having simply a bend magnet as the photon source.

Synchrotrons are commonly described based off the electron beam energy in GeV (where 1 Giga electron volt = 10^9 eV, with an electron volt being energy gained by accelerating an electron through a potential of 1 volt). It is important to note that the velocity of the circulating electrons is relativistic even for relatively low-energy synchrotron sources (e.g. 1.2 GeV for the Thai synchrotron) just as with higher electron beam energy synchrotron sources (e.g. 7 GeV for the Advanced Photon Source). However, the angular distribution of the beam is inversely related to the beam energy of the synchrotron, where a synchrotron with a higher energy beam is capable of producing a beam with less angular divergence (or is more tightly collimated). Another important synchrotron characteristic is the emittance of the beam, which can be described in

layman's terms as the "electron beam fuzziness" and can be envisioned as the opposite of a beam which is tightly collimated. This characteristic is commonly associated with the physical size of the storage ring itself, whereby a smaller synchrotron source requiring stronger bend magnets will produce an electron beam with higher emittance compared to a larger facility with fewer bend magnets. Here, a smaller emittance results in a brighter beam, which is preferable.

Insertion devices, either wigglers or undulators are commonly placed in the straight sections of the storage ring and serve to increase the photon flux of its designated beamline. Both wigglers and undulators by design are a paired series of magnets which are separated by a gap through which the electron beam passes, forcing the beam to "wiggle" from side to side, releasing fans of synchrotron radiation (photons) as it does. In the case of a wiggler, the result of the electron beam passing through is the production of fans of photons throughout which do not align, resulting in a beam which is more intense than a bend magnet but with a broader fan and a more continuously varying intensity as a function of energy. In the case of an undulator, the deviations of the electron beam from side to side are minimal, resulting in an intense beam at defined energies whose angular divergence is small.

2.2 Beamline 7-3 (SSRL): X-ray Absorption Spectroscopy (XAS)

The technique of XAS involves the collection of spectra which are used for determining the chemical form of a particular element, specifically including information on the immediate ligands including ligand bond length and numbers of atoms bound to the element of interest in a defined spot on the sample being investigated.[1] These XAS spectra can also give information on chemical forms present in mixtures which may occur in complex biological materials.[2,3,4] This technique was utilized herein to investigate the chemical forms of mercury and selenium present in brain tissue (Chapters 3, 4) and epidermal mucosa collected from local Saskatchewan steelhead trout, *Oncorhynchus mykiss* (Chapter 7).

All XAS data collected in this thesis were measured at the Stanford Synchrotron Radiation Lightsource (SSRL), Menlo Park, CA. The majority of this data, specifically XAS of mercury and selenium, were measuring using SSRL beamline 7-3, which is described in the following sections. High energy resolution X-ray fluorescence detection XAS (HERFD-XAS) of mercury and selenium were collected on SSRL beamline 6-2, and is described briefly later in the chapter. The sulfur K-edge data were collected at SSRL beamline 4-3, which is described in Chapter 7.

2.2.1 Source – to – experimental hutch (7-3)

The source at SSRL beamline 7-3 is a permanent 2T wiggler producing an intense beam containing a broad spectrum of energies. The following discussion highlights important characteristics and roles of key optics present at this beamline.

One of the key optical components of the beamline is the monochromator. This is the most important piece of equipment in selecting the energy that will be used in the experiment in question. An important quality of the monochromator is good energy resolution, meaning the outgoing photon beam contains a narrow spread of energies which have been selected from the radiation received from the wiggler, which contains many energies. Ideally, the outgoing beam also has a high photon flux (meaning it contains many photons).

Beamline 7-3 employs a double crystal monochromator which is comprised of two individual single crystals of silicon containing highly ordered crystal lattice planes which serve to diffract the photon beam with a specific angle corresponding to a specific energy. The incoming beam is diffracted off the first crystal and onto the second crystal. Diffraction is dependent upon the Bragg equation which is defined as $n\lambda = 2d\sin\theta$ where θ is the angle between the lattice planes and both the incident and diffracted beam, d is a fixed value defined as the separation of the crystal lattice planes, and λ is the wavelength which is inversely related to energy. Hence, adjustment of θ results in a change to the desired energy, essentially allowing a tunable incident energy for the experiment. Diffraction off one crystal deflects the beam and diffraction off the second returns the outgoing monochromatic X-ray beam to be close to the horizontal plane. It is important to note that while the incoming beam can be diffracted forwards at the specific energy selected, secondary diffraction in a different direction at a specific energy can cause a crystal "glitch" resulting in a loss of beam intensity at that particular energy. It is important to be aware of where the crystal glitches exist in order to avoid them.

The Bragg equation includes the integer n, meaning that more than one energy can be diffracted for a given angle. In general, $n=1$ is the fundamental, desired energy, and $n>1$ are undesirable harmonics. If adjustable optics are part of the beamline, then rejection of harmonics (unwanted energies) can be accomplished by setting the incident angle of the X-ray mirror to reflect the fundamental but not the harmonics. Alternatively, a process called "detuning" the monochromator may be used. Here the one crystal of the double crystal monochromator is offset from the other in angle. Because the rocking curve – the variation in intensity with angle – is

steeper for the harmonics than for the fundamental – detuning in this way by approximately 60% of peak intensity will preferentially rid the beam of harmonics. Beamline 7-3 allows for a wide energy range of experiments including the energies of absorption edges for the mercury L_{III}-edge and selenium K-edge XAS experiments requiring incident energies in the hard X-ray regime of 12 284 and 12 658 eV, respectively (see Section 2.4.1).

Mirrors which may exist at both upstream and downstream locations in reference to the monochromator are essential for numerous things including distribution of the power of the beam (so as to not cause damage to downstream elements), harmonic rejection of unwanted energies (discussed above), as well as shaping of the beam. Shaping the beam includes vertical collimation whereby a vertically diverging beam is made effectively parallel, as well as focussing where the now vertically parallel beam is reflected in such a way that it becomes focussed into a small point. 7-3 has a vertically collimating mirror which can be optionally inserted or dropped from the beam path.

2.2.2 Experimental hutch (7-3)

As the incident beam enters the hutch it encounters the first component involved in detection, an ion chamber. The ion chamber located directly upstream of the sample is commonly referred to as I_0. The ion chambers used in these experiments were N_2 gas-filled chambers which contain two parallel metal plates to which a high voltage is applied resulting in the separation of positive and negative charges as the X-rays pass through. This creates a current which is proportional to the intensity of beam which will be attenuated after passing through and being absorbed by the sample. This change in intensity is measured by another ion chamber located directly downstream of the sample, called I_1. This setup is called transmission detection which can be understood as the result of defining the absorption of X-rays by a material. This method of detection is typically utilized for concentrated samples, as well as when measuring a calibration foil as an energy standard. In this work, an internal calibration using a calibration foil is present downstream of the sample between ion chambers I_1 and I_2. This data is utilized for calibrating each sweep of the experimental data collected as well as for calibrating the monochromator to the correct energy prior to data collection.

When measuring samples which contain dilute levels of the element of interest, a fluorescence detection setup is often utilized whereby the fluorescence given off the sample is collected using an energy dispersive fluorescence detector located at a 90° angle to the incident

beam in the horizontal plane, to minimize scatter. The sample typically is situated at a 45° angle to the incident beam within a helium gas-filled cryostat kept cool at 10K to reduce thermal vibrations and for prevention of beam damage to the sample. The detector utilized at beamline 7-3 in the experiments described within this thesis was a 30-element germanium solid-state detector. An advantage of this type of detector is that it allows for the electronic "windowing" of the fluorescence coming from the element of interest, meaning only the photons found within this specific energy range are counted. These counts as a function of incident energy are translated into the resulting XAS spectra. A disadvantage of solid-state detectors is they are limited by high count rates. Count rates which are very high result in non-linearity of the detector. This means the electronic processing capabilities of the detector become overwhelmed with photons resulting in some photons being essentially lost from the experiment (not counted). The reason for this is that each photon takes a short but defined amount of time to register. If a second photon arrives before that time is completed, the second photon will not be counted, and moreover this "dead time" period starts over upon arrival of the second photon. A related consequence of the high count rates is that the energy resolution of the detector becomes degraded, resulting in a higher degree of overlap of elements. An additional problem which can occur with very concentrated samples (related to high count rates) is detector pile-up. This occurs when the distinct energies of two photons arriving at the detector aren't counted individually (e.g. 6 KeV and 6 KeV), but instead are counted as a single photon of higher energy (e.g. 12 Kev).

High count rates at the detector can be reduced by using various materials which aid in filtering out unwanted photons, of which the majority for dilute biological systems is scattered radiation. The components include X-ray filters and Soller slits, which are placed between the sample and the detector. X-ray filters incorporate an element with an absorption edge of the filter material which is lower than the absorption edge of the element of interest, but higher in energy than the fluorescence energy of the energy of interest. For lower atomic number (Z) elements of interest including selenium, X-ray filter materials are commonly based of the simple formula Z-1 and aid in absorbing X-ray scatter while leaving the fluorescence of the element of interest unchanged. Here, arsenic filters were used for selenium XAS. For higher Z elements this formula doesn't apply; gallium filters were used for mercury XAS. Since additional fluorescence is also given off by the filter itself, Soller slits are then placed between the X-ray filter and the detector

to minimize additional undesirable fluorescence including given off by the X-ray filters, while maximizing fluorescence coming from the sample itself.

It is important to note that X-ray fluorescence, which is the result of attenuation of X-rays by matter and the resulting emittance of X-ray photons, differs from visual fluorescence. Fluorescence microscopy, for example, relies on the illumination of matter with light of a certain wavelength which becomes absorbed by the fluorophores present in the fluorescent dye to which a sample may have been treated. The fluorophores emit light at wavelength distinct from the absorbed wavelength.

2.3 Beamline 20-ID-B (APS): X-ray Fluorescence Imaging (XFI)

The technique of XFI involves the re-creation of the sample being investigated as a digital image coloured specifically to reflect accumulations of individual elements in every part of the sample. This technique was utilized in this thesis to investigate mercury and essential metals in complex biological samples including human brain tissue (Chapter 4) and the model organism larval zebrafish, Danio rerio (Chapters 5, 6, 7).

2.3.1 Source – to – experimental hutch (20-ID-B)

Beamline 20-ID-B (Advanced Photon Source (APS), Argonne National Laboratory, Argonne, IL) is where all imaging data was collected aside from one single image which was collected at the nano-imaging beamline 2-ID-D, also located at APS. The following discussion will not reiterate what has been discussed above but will simply add relevant details regarding the setup of this beamline.

The source of beamline 20-ID-B is an undulator, creating a very intense beam of a narrow energy spread. This beamline employs a Si(111) double crystal monochromator with an upstream Rh-coated silicon mirror. Micro-focus optics are responsible for the very small spot sizes achieved at most XFI beamlines. The micro-focus optics used on 20-ID-B are a Kirkpatrick-Baez mirror pair (KB mirrors) which serve to focus the beam in both the horizontal and vertical direction to the spot size of 5 µm × 5 µm. The nano-imaging beamline 2-ID-D employs Fresnel zone plates in place of KB mirrors which produces a micro-focussed beam with a minimal spot size of approximately 250 nm.

2.3.2 Experimental hutch (20-ID-B)

Similar to the XAS fluorescence detection setup, the sample at 20-ID-B is oriented at a 45° angle to the incoming beam with a silicon drift Vortex® detector located at a 90° angle to the

incident beam. Ion chambers are present directly upstream and downstream of the sample for measuring both the incident beam and the absorption occurring at the sample. An additional optical microscope is situated at a 90° angle to the sample to monitor the sample throughout data collection as well as to position the sample within the beam.

2.4 Principles of X-ray Absorption Spectroscopy and X-ray Fluorescence Imaging Theory

2.4.1 X-ray fluorescence imaging (XFI)

The theory of X-ray absorption spectroscopy centres on the concept of how X-rays interact with matter. An incoming X-ray beam with a given energy incident upon some form of matter (solid, liquid, gas) may interact in a number of possible ways. The incident photon may be transmitted through the matter with the X-ray remaining unchanged in energy or direction, it may interact with said matter in such a way which results in no change in energy but a change in direction of the energy (elastic scatter), it may result in a change in both energy and direction (inelastic scatter), or it may become absorbed by that matter.[5] The absorbance of X-rays into matter as a function of incident energy can be measured by transmittance or by fluorescence, which are defined by the equations:

$$A_t = \mu x = \ln\frac{I_0}{I_1} \tag{2.1}$$

and

$$A_f \propto \frac{I_f}{I_0} \tag{2.2}$$

where A_x is the absorbance measured by directly via transmittance or indirectly via fluorescence, μ is the X-ray absorption coefficient, x is the sample depth, I_0 is the incident energy prior to the sample, I_1 is the beam intensity post-sample, and I_f is the intensity of the fluorescence. Measuring the absorbance by way of fluorescence is commonly done with dilute samples which are either dilute or thin whereas transmittance is utilized for samples which have a high elemental concentration (e.g. standard foils).[1]

X-ray absorption spectroscopy depends on absorption of X-rays by matter. The threshold energy (E_0) of an element, also known as the electron binding energy, is defined as the specific

energy required to excite a core-level electron beyond its normal bound state into unfilled bound states, unbound and quasi-bound states (called XANES, discussed below).[5] Electrons are excited fully into the continuum as the incident energy becomes sufficiently higher than this threshold energy (called EXAFS, discussed below).[5] Absorption of X-rays at specific energies results in excitations of electrons from different atomic shells (e.g. 1s, 2s, 2p, etc.) which correspond to different X-ray absorption edges, referred to as *K*-, *L*-, *M*- edges,[6] etc. This thesis focussed primarily on data collected at the mercury L_{III}-edge and selenium K-edge. The mercury L_{III}-edge has an assumed electron binding energy of 12 284 eV which corresponds to the excitation of $2p_{3/2}$ electrons while the selenium K-edge electron binding energy is assumed to be 12 658 eV which corresponds to the excitation of 1s core-level electrons.[6] As an electron is excited by the incident photon as a photoelectron, there is concomitant decay of an outer shell electron into the vacancy created.[5] An outer shell electron may decay by releasing a fluorescent photon, a concept which is utilized in both X-ray absorption spectroscopy and X-ray fluorescence imaging through translation into XAS spectra or an XFI image.

As discussed previously, the excitation of a core-level electron with the concomitant decay of an outer shell electron to fill such an unstable core-hole is accompanied by the release of a fluorescent photon.[5] To summarize it simply, the XFI technique is centred on the detection of fluorescent photons as a function of the incident beam's location on the sample, with the data being translated into a digital reconstruction of the sample which is elementally specific. Photons are emitted at characteristic emission lines for each element which are a function of the absorption edge energy and can be found in the X-ray data booklet.[6] The energy of these emission lines are lower in energy compared to the excitation energy of the element being measured. Absorption at the mercury L_{III}-edge results in $L\alpha_1$ and $L\alpha_2$ emission lines which are present at 9988.8 and 9897.6 eV, respectively, with $L\alpha_1$ having the highest relative intensity while absorption at the selenium K-edge results in $K\alpha_1$ and $K\alpha_2$ emission lines present at 11 222.4 and 11 181.4, with $K\alpha_1$ having the highest relative intensity.[6] Absorption at the sulfur K-edge results in $K\alpha_1$ and $K\alpha_2$ emission lines very close in energy, at 2307.8 and 2306.6 eV, with $K\alpha_1$ having the highest intensity.[6] XFI and conventional XAS detectors do not separate these emission lines; fluorescence is measured as the combined $\alpha_{1,2}$.

The XFI technique is different from the XAS technique where an energy range is chosen and swept through, exciting the absorption edge and the region beyond. In XFI, a discrete energy

is selected which is high enough to encompass the energies of all emission lines of interest. In the XFI experiments conducted in this thesis, an incident energy of 13 450 eV was consistently chosen for the collection of mercury fluorescence as well as the fluorescence of a variety of biologically relevant elements including selenium, sulfur, calcium, copper and zinc.[7,8]This also provided an excitation energy below the bromine K-edge which occurs at 13 474 eV, to avoid exciting fluorescence from bromine which is a contaminant of many plastics which may be present in the experimental set-up.[7,8]

2.4.2 XFI data collection

At beamline 20-ID-D (Advanced Photon Source, Argonne, IL), the sample stage within the experimental hutch is located at a 45° angle to the incoming X-ray beam while the detector is positioned at a 90° angle, which is similar to an XAS collection arrangement.[9] Here, a collimator was attached to the end of the X-ray pipe to minimize stray scatter and fluorescence of non-sample origin from reaching the detector. Fluorescent photons were collected by a 4-element silicon drift Vortex® detector. Here the detector diodes are silicon-based rather than germanium-based as is the case with the XAS detector. An optical microscope was present at a 90° angle to the sample for the purpose of monitoring the sample during collection.[9] An on-line optical microscope is a useful tool for monitoring the physical sample when a collimator is employed, which can be placed very close to the sample but not so close that it encounters the sample.

Key XFI parameters which are adjustable at the beamline include the step size (a measurement of how large each pixel is) and the dwell time (how long the X-ray beam interrogates each pixel of the sample).[9] In this thesis, all data collected at 20-ID-D was defined by a 5 µm step size and a 600-millisecond dwell time (Chapters 5, 6, 7). Data were collected in "fly scan" mode, meaning data collection is continuous. In this way, XFI images are slowly "built" from the bottom left-hand corner of the sample to the top right-hand corner, with each pixel containing spectra from numerous elements. A typical zebrafish head section is somewhat smaller than 1 mm by 1 mm and yet takes approximately 3-4 hours to collect a fluorescence map. Standards with known concentrations are collected in the same run, in the same environment and using the same specifications as the experimental data.[9]

2.4.3 XFI analysis

Most of the XFI images collected in this thesis were analyzed using the "binning" technique, whereby a low and high boundary are placed on either side of an electronic window

which has been centered on the fluorescence emission line of each element of interest. The area under the peak, in reference to the concentration standards, determines the quantity of each element present in each pixel of the experimental sample.[9] This is a relatively simple method of analysis which is considered to be quite accurate, however, one must be aware of the potential for unintendedly overlapping windowed elements whose fluorescence lines are in close energy proximity.[9] This would result in a false signal and could lead to misinterpretation of results. An alternate method of analysis which is becoming increasingly common is peak-fitting, where the peak produced at each elemental emission line is baseline corrected and fit accordingly. Numerous programs exist which accommodate this technique, including PyMCA,[10] MAPS[11] and M-BLANK.[12] PyMCA was utilized in this thesis for control (non-mercury treated) samples only.

Once all images have been acquired, they are collectively normalized by dividing the image pixels by the value of I_0 (the fluorescence of the incoming X-ray beam). A small region of the background in each image then is selected for and subtracted from each pixel in the image, to account for non-element background counts from scatter or other sources.[7,13,14] Finally, images are quantified into units of areal density ($\mu g/cm^2$) using the calibration standards collected.[7,13,14] All elements are calibrated using a standard of the same element with the exception of mercury, which is calibrated using both thallium (Tl) and gold (Au) standards. The values from both of these standards, which fall on either side of mercury on the periodic table (Z+1 and Z-1), are used to interpolate the mercury value, as it has been noted that mercury standards decrease in concentration over time, probably through loss of vapor phase Hg, making them unreliable for quantification.[14]

2.4.4 X-ray absorption spectroscopy (XAS)

At excitation energies just below that needed for complete ejection into the continuum, photoelectrons may be excited into bound states in vacant outer shells.[15] The pattern of absorbance as a function of energy encompassing these bound-state transitions and the absorption edge itself are referred to as the near-edge spectrum, or XANES (X-ray absorption near-edge structure) and can provide valuable information on the electronic state and even the geometric coordination and nature of the ligands around the absorbing atom.[15] The near-edge spectrum essentially provides a “fingerprint” of the unknown chemical species within a mixture, which can be analyzed through linear combination fitting with a library of standards which were analyzed for the same absorber atom (e.g. Hg near-edge experimental data compared to a library of Hg

near-edge compounds) under similar conditions.[15] In this thesis, mercury, selenium, and sulfur near-edges were compared against a library of biologically relevant standards which contained 25, 12, and 19 standard compounds, respectively. The strength of this type of near-edge analysis relies on the number and importantly, on the relevance of the standard spectra which are available for comparison. This thesis has the benefit of drawing on comprehensive libraries of previously collected spectra compiled over time from within the current research group for the elements examined.

An X-ray absorption spectrum is conventionally divided into two energy regions (Fig. 2.1) which can be analyzed to provide complementary information about the central, absorbing atom. The first such component is the near-edge which comprises the initial 50-100 eV of the spectrum occurring beyond the absorption edge[16] and has been discussed above. The EXAFS (extended X-ray absorption fine structure) component highlighted in Fig. 2.1 is the second component and is comprised of the oscillating extended high energy side of the spectrum.

Here we return to the concept of the photoelectric effect. At the energies of the EXAFS, the photoelectron has been ejected into the continuum. In the case of a molecular compound, the photoelectron will interact with atoms surrounding the absorbing atom which are referred to as backscattering atoms.[5] These are the atoms to which the absorbing atom (e.g. mercury) is bound as ligands or other atoms in close proximity. Here it may be useful to envision the outgoing photoelectron as a de Broglie wave, which, in its interactions with backscattering atoms may experience both constructive and destructive interference when the wave is in and out of phase, respectively, with the backscattered wave from said backscattering atoms.[15] As the energy increases past the absorption threshold energy (E_0), the photoelectron wavelength decreases. These interactions give rise to the oscillatory part of the XAS spectrum which are referred to as EXAFS.

The EXAFS (χ), equation can be simplified into:

$$\chi(E) = \frac{\mu(E) - \mu_0(E)}{\mu_0(E)} \qquad (2.3)$$

which in its simplest explanation is the oscillatory part of the absorption coefficient, $\mu(E)$, subtracted by the theoretical, non-oscillatory part of the absorption coefficient, $\mu_0(E)$ with the

energies expressed in eV. The expanded EXAFS equation[17] which can be sub-divided into three parts (amplitude, frequency and phase, and the Debye-Waller term) becomes

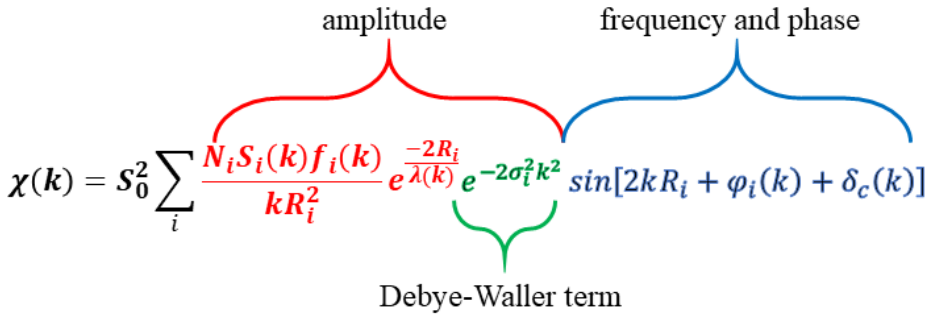

(2.4)

where firstly, lowercase "i" indicates that the following values are specific to a single backscattering atom type, and the sum is over all backscattering atoms types being considered. Important terms for the purposes of curve-fitting the EXAFS include N_i as the coordination number (the number of atoms coordinating the absorber atom) for atom type i (e.g. 4 sulfur atoms bound to mercury), R_i is the pathlength between the absorbing atom and backscattering atom type i (e.g. Hg-S bond length of 2.35 Å) and σ_i^2 being the Debye-Waller term, which is defined as the mean square deviation in R_i.

2.4.5 XAS data collection

No single discrete energy point is used in an XAS experiment, as is the case with X-ray fluorescence imaging. Rather, an energy range specific to the element of interest is swept, with the absorbance being measured as a function of energy. The so-called "sweep" moves from a low to high energy and is set to encompass three distinct regions of the XAS spectrum which are a function of energy (eV) including the pre-edge, the absorption edge with the near-edge region, and the EXAFS region (Fig. 2.1). The pre-edge, corresponding to energies at which the incident photon is not quite sufficient to excite an electron is typically collected from about 200 eV below the absorption edge for background subtraction purposes. The collection of data at the absorption edge will typically utilize small "steps" in energy with each step having a relatively small dwell time. This is to achieve good resolution at the edge which contains many features which can be used to provide additional spectral information as was discussed previously. The EXAFS region is collected with slightly larger step sizes, but also longer dwell times for achieving good signal-

to-noise on the oscillations present in this region. The product of this sweep in its entirety will be an XAS spectrum, with this process being repeated many times over to ensure reproducibility and to improve signal-to-noise. Samples which contain dilute elemental concentrations will be swept more times than those which are concentrated. In this thesis, samples such as brain tissue containing dilute concentrations of mercury or selenium were scanned an average of 13 times over, which results not only in many consecutive hours of data collection, but also produces many individual spectra per sample.

2.4.6 XAS analysis

Upon collection, XAS spectra are analyzed using the EXAFSPAK suite of programs (https://www-ssrl.slac.stanford.edu/exafspak.html).[18] Initial steps include data reduction, data calibration, and data averaging. Data reduction includes the removal of dead detector channels (channels which display no experimental data) and the removal of abnormal spectra (those which have been photo-oxidized or photo-reduced, data with ice diffraction effects, etc.). Following this, every spectrum is then calibrated to the first inflection point (in energy) of a calibration foil which is collected internally and simultaneous to data collection. In this thesis an Hg-Sn amalgam standard foil was used for Hg L_{III} edge and a gray hexagonal elemental Se standard foil was used for Se K-edge with the lowest-energy inflection points assumed to be 12284 and 12658 eV, respectively. All spectra are then averaged together to produce a single representative spectrum which utilized for all following analyses.

The averaged spectrum is then background-subtracted by fitting against the pre-edge region. Subsequent to this, a polynomial function called a spline is fit to the data beginning just above the absorption edge and passing through the middle of the EXAFS oscillations. The purpose of this is to normalize the edge jump to unity as well as to extract the EXAFS. The EXAFS are k^3-weighted with the purpose of enhancing the EXAFS amplitudes occurring at the high end of the *k*-range, which are rapidly highly damped as a function of *k*. A Fourier transform of the EXAFS provides an intuitive representation which is easier to visually interpret compared to the EXAFS oscillations themselves (Fig. 2.1). A phase-correction for the primary backscatterer is defined here (e.g. when analyzing Hg EXAFS of mercuric selenide, the primary backscattering atom is defined as selenium). While the EXAFS are plotted in *k*-space, the Fourier transform are plotted in *R* space, with peaks centred at distances in *R* (when phase-corrected), which are

indicative of bond lengths between the absorbing atom (e.g. mercury) and the backscattering atom (e.g. sulfur) and are articulated in units of Å (angstroms).

The final stage of EXAFS analysis is performed using the OPT program in EXAFSPAK. This program allows for the refinement of three key parameters in the experimental data from the perspective of the absorbing atom: the bond length (*R*) between absorber and backscatterer, the number of backscattering atoms (*N*) and the Debye-Waller factor (σ^2) in order to minimize the differences between the experimental EXAFS data and the theoretical calculated scattering paths. In this thesis, theoretical phase and amplitude functions were calculated using the program FEFF (version 8.25). One of the primary strengths of the technique is the accuracy with which interatomic distances (*R*) between absorbing atom and backscattering atoms can be determined, commonly within 0.02 Å.[1] The Debye-Waller factor is an important component which accounts for the innate vibrational and static contributions of individual atoms. All atoms have an innate vibrational behavior which can be dampened at lower temperatures; it is for this purpose that EXAFS samples are kept cool at a temperature of 10 K during data collection. The number of backscattering atoms (*N*) is usually changed in a stepwise manner as correlations are high if it is refined simultaneously with σ^2. The program FEFF, which is a standalone program but which can be run within EXAFSPAK, provides *ab initio* theoretical pathway calculations of the local structure surrounding the absorbing atom, which can be compared with the experimental data to further refine the model of the ligand environment.[19] The accuracy of the fit can be measured throughout, using a goodness-of-fit parameter with the goal of minimizing this value as much as possible.

It should be noted that bond length resolution or discrimination of two similar distances for similar ligands is not a particular strength of the EXAFS technique.[1] The resolution is limited by the *k*-range collected, given by the formula:

$$\Delta R \approx \frac{\pi}{2k} \qquad (2.5)$$

In this thesis, mercury EXAFS were collected to a maximum *k*-range of 12 $Å^{-1}$ which in turn calculates into a bond length resolution of 0.13 Å while selenium EXAFS were collected to a slightly larger *k*-range of 14 $Å^{-1}$, resulting in a bond length resolution of 0.11 Å. This rule generally applies to ligands which are close in atomic number. For example, Hg EXAFS ligands

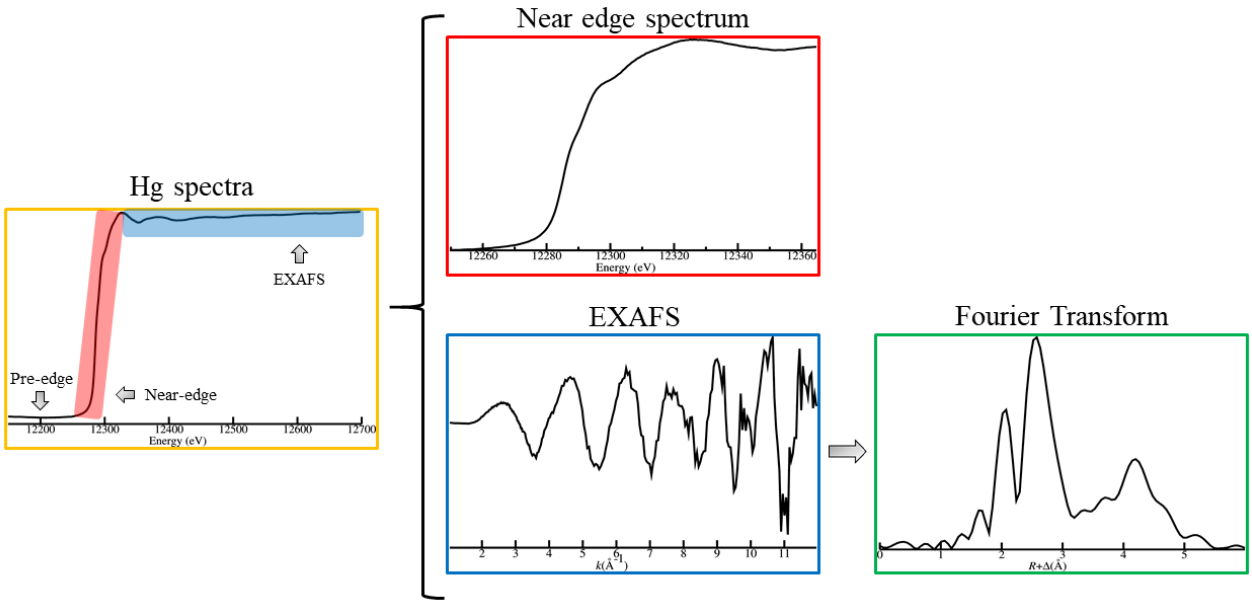

Figure 2.1: Hg spectrum featuring highlighted sections. Individual tiles depicting each region alone, including the near-edge spectrum, k^3-weighted EXAFS oscillations and the corresponding Fourier transform. Figure modified from the work of G.N. George and I.J. Pickering.[15]

which are closer in distance than 0.13 Å cannot be resolved. Thus, two Hg-O having bond lengths of 2.1 and 2.2 cannot be individually resolved, but rather contribute to the static Debye-Waller factor.

Ultimately, refinement of EXAFS data can become a model building exercise which must be executed carefully and thoughtfully, keeping in mind what chemical compounds are plausible and which are not. Success in applying EXAFS to questions in the toxicology of heavy metals involves broad interdisciplinary skills, often incorporating knowledge of chemistry and physics which may be best accomplished through collaboration. Assuming this can be achieved, EXAFS as a technique has many strengths. As mentioned previously, bond lengths can be determined with accuracy which is essential in defining chemical compounds. Samples can be analyzed regardless of phase (solid, liquid, gas), or heterogeneity (such as biological tissues or sediments) with little to no pre-treatment aside from loading into sample cuvettes.[1] This technique is highly compatible with other techniques including density functional theory (DFT); refinements from EXAFS can be compared with DFT calculations for confirmation of chemical compounds and for production of three-dimensional representations of such compounds, as well as for consideration of chemical processes (see Chapter 3).

2.5 High Energy Resolution Fluorescence Detection X-ray Absorption Spectroscopy (HERFD-XAS)

HERFD-XAS is a relatively new technique which produces spectra which have significantly enhanced sensitivity to speciation compared to those produced by conventional XAS. The enhanced resolution is a result of the partial elimination of core-hole lifetime broadening effects. The core-hole lifetime produced in the initial photoexcitation event on a timescale is incredibly small (fractions of a femtosecond) and increasingly so with increasing atomic number.[20] Specifically, this event includes the excitation and subsequent ejection of a core-level electron. Broader spectral resolutions are associated with smaller core-hole lifetimes.[20] When using conventional XAS the broadening effect on the spectra of some elements can create difficulties in distinguishing specific chemical environments of the element, especially when present in a mixture. Mercury is indeed, such an element with broad spectra that can be hard to speciate with confidence (see Figure S3.2, Figure 4.1).[21] In HERFD-XAS, the exceptionally high energy resolution detection of the X-ray fluorescence is related to the core-hole lifetime of that which was created through the decaying of an outer shell electron into the initial core-hole and

release of the fluorescent photon rather than the initial photoexcitation event.[22] This allows for the selection of a sliver of the emission line of an element which produces increasingly sharp features on the resultant spectra (Chapters 3, 4).[22] While the major source of degradation of spectral resolution is core-hole lifetime broadening, optical broadening effects also contribute, and with the HERFD-XAS experiment, broadening contributions will come from both the analyzer optics and the monochromator. At the X-ray energies of Hg Lα1 and Se Kα1 and with analyzer Bragg angles of 82° and 85°, respectively, we estimate an analyzer resolution of approximately 0.9 eV. In addition, there will be a broadening contribution from the monochromator which at the Hg L_{III} and Se K-edge energy will be approximately 0.3 eV for a Si(311) monochromator. We note that the monochromator resolution is an inherent function of the crystal cut; for example, this resolution would be poorer if a Si(220) were used and substantially improved with a Si(511).

Experimental set-up at SSRL beamline 6-2 includes a Johann-arrangement of multiple crystal analyzers which are elementally specific as well as the precise placement of the sample and a single-element silicon drift detector.[23] In this thesis, Si(555) crystals mounted onto the Johann-spectrometer were used to capture Hg $L\alpha_1$ fluorescence emission and Si(844) crystals were used to capture Se $K\alpha_1$ emission (Chapters 3, 4). All three of these experimental elements (sample, Johann crystal spectrometer and detector) exist together in a geometrical arrangement called Rowland circles. Briefly, the incident beam interrogates the sample, which produces fluorescence at an emission line of known energy. This fluorescence encounters the arrangement of crystal analyzers which is then directed towards the silicon drift Vortex® detector (Hitachi High-Tech Science America, Schaumburg, Illinois, USA).

Although the experimental set-up is unique from what is seen at a conventional XAS beamline, the data collection is similar. Fluorescence at a specific emission line is collected as the energy is scanned through a discrete range. Energy calibration is achieved using standard foils as on 7-3. Once HERFD spectra are collected, they are analyzed in a manner which is very similar to XAS data. HERFD data are reduced, calibrated, and averaged followed by background subtraction and normalization. EXAFSPAK is then utilized as a fitting program.

2.6 Acknowledgements

This thesis used data collected from two synchrotron facilities. Use of the Stanford Synchrotron Radiation Lightsource (SSRL), SLAC National Accelerator Laboratory, is supported by the U.S. Department of Energy, Office of Science, Office of Basic Energy Sciences under Contract No. DE-AC02-76SF00515. The SSRL Structural Molecular Biology Program is supported by the DOE Office of Biological and Environmental Research, and by the National Institutes of Health, National Institute of General Medical Sciences (P30GM133894). The contents of this publication are solely the responsibility of the authors and do not necessarily represent the official views of the NIGMS or NIH. This research also used resources of the Advanced Photon Source (APS), an Office of Science User Facility operated for the U.S. Department of Energy (DOE) Office of Science by Argonne National Laboratory, and was supported by the U.S. DOE under Contract No. DE-AC02-06CH11357, and the Canadian Light Source and its funding partners.

In addition, some of the material presented here was based on the University of Saskatchewan GEOL 851.3 course which was created by and materials from which were provided by G.N. George and I.J. Pickering.

2.7 References

(1) George, G.N., Pickering, I.J. X-ray Absorption Spectroscopy in Biology and Chemistry. In Brilliant Light in Life and Material Sciences; Tsakanov, V., Wiedemann, H., Eds.; NATO Security through Science series. Springer, Dordrecht: 2007.

(2) Harris, H.H., Pickering, I.J., George, G.N. The chemical form of mercury in fish. *Science* **2003**, *301*, 1203.

(3) George, G.N., MacDonald, T.C., Korbas, M., Singh, S.P., Myers, G.J., Watson, G.E., O'Donoghue, J.L., Pickering, I.J. The chemical forms of mercury and selenium in whale skeletal muscle. *Metallomics* **2011**, *3*, 1232-1237.

(4) Hackett, M.J., Smith, S.E, Paterson, P.G., Nichol, H., Pickering, I.J., George, G.N. X-ray absorption spectroscopy at the sulfur K-edge: A new tool to investigate the biochemical mechanisms of neurodegeneration. *ACS Chem. Neurosci*. **2012**, *3*, 178-185.

(5) Teo, B.K. EXAFS: Basic principles and data analysis. Springer-Verlag: Berlin, Germany, 1986. Vol.9.

(6) Thompson, A., Attwood, D., Gullikson, E., Howells, M., Kim, K.-J., Kirtz, J., Kortright, J., Lindau, I., Liu, Y., Pianetta, P., Robinson, A., Scofield, J., Underwood, J., Williams, G., and Winick, H. X-ray data booklet, Center for X-ray Optics and Advanced Light Source, Lawrence Berkeley Laboratory, Berkeley, California, 2009.

(7) Korbas, M., MacDonald, T.C., Pickering, I.J., George, G.N., Krone, P.H. Chemical form matters: Differential accumulation of mercury following inorganic and organic mercury exposures in zebrafish larvae. *ACS Chem. Biol*. **2012**, *7*, 411-420.

(8) MacDonald, T.C., Korbas, M., James, A.K., Sylvain, N.J., Hackett, M.J., Nehzati, S., Krone, P.H., George, G.N., Pickering, I.J. Interaction of mercury and selenium in the larval stage zebrafish vertebrate model. *Metallomics* **2015**, *7*, 1247-1255.

(9) Pushie, M.J., Pickering, I.J., Korbas, M., Hackett, M.J., George, G.N. Elemental and chemically specific X-ray fluorescence imaging of biological systems. *Chem. Rev*. **2014**, *114*, 8499-8541.

(10) Sole, V. A., Papillon, E., Cotte, M., Walter, P., and Susini, J. A multiplatform code for the analysis of energy-dispersive X-ray fluorescence spectra. *Spectrochim. Acta, Part B* **2007**, *62*, 63-68.

(11) Vogt, S. MAPS: A set of software tools for analysis and visualization of 3D X-ray fluorescence data sets, *J. Phys. IV* **2003**, *104*, 635-638.

(12) Crawford, A.M., Deb, A., Penner-Hahn, J.E. M-BLANK: a program for the fitting of X-ray fluorescence spectra. *J. Synch. Rad*. **2019**, *26*, 497-503.

(13) Korbas, M., Krone, P.H., Pickering, I.J., George, G.N. Dynamic accumulation and redistribution of methylmercury in the lens of developing zebrafish embryos and larvae. *J. Biol. Inorg. Chem*. **2010**, *15*, 1137-1145.

(14) Korbas, M., Blechinger, S., Krone, P.H., Pickering, I.J., George, G.N. Localizing organomercury uptake and accumulation in zebrafish larvae at the tissue and cellular level. *Proc. Natl. Acad. Sci. USA*. **2008**, *105*, 12108–12112.

(15) George, G.N., Pickering, I.J. X-ray Absorption Spectroscopy of Metals in Biology. In Encyclopedia of Biophysics; Roberts, G.C. Ed.; Springer: Berlin, Heidelberg, 2013.

(16) Aksenov, V.L., Koval'chuck, M.V., Kuz'min, A.Y., Purans, Y., Tyutyunnikov, S.I. Development of methods of EXAFS spectroscopy on synchrotron radiation beams: review. *Crystallogr. Rep*. **2006**, *51*, 908-935.

(17) Stern, E.A. Theory of the extended X-ray absorption fine structure. *Phys. Rev. B: Condens. Matter* **1974**, *10*, 3027-3037.

(18) George, G.N. EXAFSPAK. https://www-ssrl.slac.stanford.edu/exafspak.html (2001).

(19) Rehr, J.J., Leon, J.M., Zabinsky, S.I., Albers, R.C. Theoretical X-ray absorption fine structure standards. *J. Am. Chem. Soc*. **1991**, *113*, 5135-5140.

(20) Hämäläinen, K., Siddons, D.P., Hastings, J.B., Berman, L.E. Elimination of the inner-shell lifetime broadening in X-ray absorption spectroscopy. *Phys. Rev. Lett*. **1991**, *67*, 2850-2853.

(21) James, A.K., Nehzati, S., Dolgova, N.V., Sokaras, D., Kroll, T., Eto, K., O'Donoghue, J.L., Watson, G.E., Myers, G.J., Krone, P.H., Pickering, I.J., George, G.N. Rethinking the Minamata tragedy: What mercury species was really responsible? *Environ. Sci. Technol*. **2020**, *54*, 2726-2733.

(22) Nehzati, S., Dolgova, N.V., James, A.K., Cotelesage, J.J.H., Sokaras, D., Kroll, T., George, G.N., Pickering, I.J. High energy resolution fluorescence detected X-ray absorption spectroscopy: An analytical method for selenium speciation. Submitted: *Anal. Chem*.

(23) Sokaras, D., Weng, T.C., Nordlund, D., Alonso-Mori, R., Velikov, P., Wenger, D., Garachtchenko, A., George, M., Borzenets, V., Johnson, B., Rabedeau, T., Bergmann, U. A seven-crystal Johann-type hard x-ray spectrometer at the Stanford Synchrotron Radiation Lightsource. *Rev. Sci. Instrum*. **2013**, *84*, article number 053102.

CHAPTER 3: RETHINKING THE MINAMATA TRAGEDY: WHAT MERCURY SPECIES WAS REALLY RESPONSIBLE?

3.1 Preface

Minamata disease, which occurred during the 1950s and 1960s in Minamata, Japan is among the most devastating examples of organometallic mercury poisoning of human populations. Here, an industrial factory was releasing mercury-contaminated effluent into Minamata Bay from which local human and wildlife populations consumed fish and seafood products. The result was thousands of cases of organometallic mercury exposure, with symptoms ranging from mild to severe with many deaths including those from congenital exposures.

The etiology of this disease, which took 3 years to expose, was aided by experiments performed in the late 1950s on a small number of felines which were directly exposed to contaminated effluent from the factory. Only one such animal was preserved after euthanization, the so-called Cat 717. This exploratory research using a brain tissue sample from Cat 717 was the centre of this chapter, and indeed, the cornerstone of the thesis in its entirety. X-ray absorption spectroscopy (XAS), as well as high-energy resolution fluorescence detection-XAS (HERFD-XAS) were utilized to investigate the forms of mercury and selenium remaining within this extraordinarily unique tissue sample. Further to that, considerations of the chemical processes occurring within the factory resulting in the presumed production of methylmercury were investigated using density functional theory (DFT). The results of this study demonstrated that Cat 717 was exposed to organometallic mercury directly, given the large amount of organomercury present within its preserved brain tissue. As well, DFT calculations surprisingly suggested that an alternative organomercury species, α-mercuri-acetaldehyde, not methylmercury, was the most likely by-product of the chemistry occurring within the factory.

This research was published in *Environmental Science and Technology* and was reformatted to comply with the university manuscript style thesis guidelines.

James, A. K.,¶ Nehzati, S., ¶ Dolgova, N. V., Sokaras, D., Kroll, T., Eto, K., O'Donoghue, J. L., Watson, G., Myers, G. J., Krone, P. H., Pickering, I. J., George, G. N. Rethinking the Minamata

tragedy: What mercury species was really responsible? *Environ. Sci. Technol*. **2020**, *54*, 2726–2733. ¶ These authors contributed equally to this work.

A.K. James analyzed XAS data and HERFD-XAS data and drafted the manuscript.

S. Nehzati collected analyzed HERFD-XAS data and assisted in drafting the manuscript.

N.V. Dolgova analyzed HERFD-XAS data and assisted in drafting the manuscript.

D. Sokaras and T. Kroll provided beamline assistance.

K. Eto provided experimental samples.

J.L. O'Donoghue, G. Watson, and G.J. Myers assisted with obtaining experimental samples and provided historic and scientific input to the manuscript.

P.H. Krone, I.J. Pickering and G.N. George contributed scientific input and guidance and provided funding for the research. I.J. Pickering and G.N. George assisted in drafting the manuscript. G.N. George conducted DFT analysis.

3.2 Abstract

Industrial release of mercury into the local Minamata environment with consequent poisoning of local communities through contaminated fish and shellfish consumption is considered the classic case of environmental mercury poisoning. However, the mercury species in the factory effluent has proved controversial, originally suggested as inorganic, and more recently as methylmercury species. We used newly-available methods to re-examine the cerebellum of historic Cat 717, which was fed factory effluent mixed with food to confirm the source. Synchrotron high energy resolution fluorescence detection-X-ray absorption spectroscopy (HERFD-XAS) revealed sulfur-bound organometallic mercury with a minor β-HgS phase. Density functional theory (DFT) indicated energetic preference for α-mercuri-acetaldehyde as a waste product of aldehyde production. The consequences of this alternative species in the "classic" mercury poisoning should be re-evaluated.

3.3 Introduction

The potentially deadly effects of organomercury compounds have been defined by tragic mass-poisonings of human populations. The most infamous is the Minamata tragedy,[1–3] for which organomercury poisoning is named Minamata disease.[3] Release of mercury-contaminated industrial waste from a chemical plant resulted in local marine pollution, leading to contamination of fish and other seafood that was ingested by local villagers. Those poisoned experienced varying signs and symptoms now assumed to be typically associated with methylmercury poisoning (paresthesia, dysarthria, visual and auditory disturbances, ataxia, seizures and ultimately death).[1,4] Over 50 congenital cases were also diagnosed,[5] resulting in the first recognition that prenatal methylmercury (MeHg) exposure might harm the fetus at levels not particularly harmful to mothers. Integral to diagnosing the etiology of Minamata disease was the identification of disease-related signs in local feline populations, which locals called the "dancing cat syndrome".[6] In 1959, three years after the official discovery of Minamata disease, its cause was still unknown. To test whether industrial waste from the nearby Chisso acetaldehyde manufacturing plant might be responsible, a company physician fed ten cats on a daily basis food that had been combined with effluent taken directly from the chemical plant. At 4–11 weeks into the experiment eight of the cats exhibited signs similar to the human symptoms. Two cats were autopsied and biological materials preserved. One was Cat 717[6] which is analyzed and discussed herein.

The Minamata poisoning (Minamata disease) is frequently taught in undergraduate toxicology as the prototypical example of biomethylation of inorganic mercury with magnification through trophic levels, leading to human methylmercury exposure.[7] Recently Eto et al.[3] have challenged this scenario, suggesting that the Minamata poisonings were due to direct release of methylmercury, rather than inorganic mercury, from the Chisso factory into Minamata bay.[3] They studied brain tissue of Cat 717 using conventional chemical analysis methods which suggested that methylmercury was only a minority fraction of total mercury.[6] They attributed this to the prolonged preservation. Here we re-examine the chemical forms of mercury and selenium from the same Cat 717 using state-of-the-art synchrotron techniques only recently developed to show that the predominant form of mercury in Cat 717 brain tissue is sulfur-bound organometallic. We complement these results with density functional theory (DFT) calculations relevant to the chemical process and plausible biotransformation to show that the most probable

dominant neurotoxic chemical form of mercury was neither methylmercury nor inorganic mercury, but rather α-mercuri-acetaldehyde or a chemically related species.

3.4 Materials and Methods

3.4.1 Sample preparation

Reagents were purchased from Sigma-Aldrich (Oakville, Ontario, Canada) and were of the highest quality available. Methylmercury L-cysteinate was prepared as previously described.[8] Methylmercury L-selenocysteinate was prepared following the method of Carty et al.[9] except employing L-selenocystine rather than the racemate. Briefly, synthesis was carried out anaerobically under an atmosphere of nitrogen using degassed solutions. Solid L-selenocystine was dissolved in deionized water by adding NaOH to a final pH of 12, and was reacted with a slight molar excess of aqueous $NaBH_4$ to give a final Se concentration of 0.1 M. The yellow L-selenocystine solution turned colorless after about 5 min. following addition of $NaBH_4$ at which point the pH was adjusted to 4 by adding HCl to remove any excess $NaBH_4$. Equimolar aqueous CH_3HgOH was then added, with the solution being filtered and reduced in volume by evaporation until white crystals of methylmercury L-selenocysteinate formed. β–HgS was prepared as a black precipitate by mixing aqueous solutions of Na_2S and $HgCl_2$, which was filtered, washed with de-ionized water, and then dried. Other selenium compounds were prepared according to Pickering et al.[10] Solutions and tissue samples were loaded or packed into 2 mm thick poly-acetal cuvettes closed with a polyimide adhesive tape window, and then frozen by immersion into a partly-frozen isopentane slurry with a temperature of approximately 120 K. Solids were finely powdered, mixed with a boron nitride diluent and packed into 1 mm thick aluminum plates sealed on either side with polyimide adhesive tape. Samples were transported and stored at liquid nitrogen temperatures until data acquisition.

3.4.2 Historical Cat 717

Historical Cat 717 was part of a landmark set of observations 55 years ago. The disease that was observed in the local cat population was reproduced by feeding cats fish and shellfish caught in the local bay. Initially the etiology and source of the etiologic agent of Minamata disease was unknown, but suspected to be connected to a chemical manufacturing plant. In 1959, in order to test whether the plant effluent might be responsible, a company physician from the chemical manufacturing plant and his staff conducted an experiment.[6] They intentionally fed ten cats food mixed with industrial waste from the acetaldehyde plant daily.[6] The waste material was

collected at three different times spanning a period of 14 months. At 4-11 weeks following the start of the experiment eight of the cats exhibited signs most commonly of tremor, ataxia, and paralysis. One of these animals, Cat 717, received 20 ml per day of the effluent, exhibited onset of disease at day 40, and was characterized as showing severe tremor, moderate ataxia and severe paralysis with decrease in body weight from 2.2 to 1.4 kg. Cat 717 was sacrificed five days after the onset of symptoms.[6] As Eto et al. recount,[6] preserved specimens of Cat 717 were rediscovered after more than 40 years in a storage area at the Kumamoto University School of Medicine. Cat 717 not only showed signs of neurotoxicity,[6] but had histological lesions in the cerebellum and other regions of the brain that were similar to human cases of Minamata disease when the cat brain was examined 40 years after the initial experiment.[6] The cerebellar tissue of Cat 717 for the current investigation was received as a formalin-fixed specimen that was trimmed to include all of the cellular layers of a cerebellar folium. It was loaded into poly-acetal cuvettes as described above.

3.4.3 X-ray spectroscopy (XAS)

Standard X-ray absorption spectroscopy (XAS), including Extended X-ray absorption fine structure (EXAFS) and high energy resolution fluorescence detected (HERFD) XAS were both carried out at the Stanford Synchrotron Radiation Lightsource (SSRL) using beamlines 7-3 and 6-2, respectively with the SPEAR3 storage ring containing 500 mA at 3.0 GeV. On both beamlines in-hutch photon shutters were employed to prevent exposure of the sample to the X-ray beam when data were not being actively recorded. Samples were maintained at a temperature of 10 K using a helium flow cryostat (Oxford instruments, Abingdon, UK) with cuvettes inclined at an angle of 45° to the incident X-ray beam to facilitate measurement of X-ray fluorescence, giving an incident X-ray path length of 2.8 mm. On both 7-3 and 6-2 the incident beam energy calibration was relative to the lowest-energy inflection of Hg-Sn amalgam foil for the Hg L_{III} edge, or a grey hexagonal selenium foil for the Se K-edge, values for which were assumed to be 12284.0 eV and 12658.0 eV, respectively.

On 7-3 a Si(220) double crystal monochromator was used for the incident beam, with harmonic rejection accomplished by detuning the monochromator to 60% of peak intensity. Incident and transmitted X-rays were monitored using nitrogen-filled gas ionization chambers, while X-ray absorption was measured as the Hg $L\alpha_{12}$ or Se $K\alpha_{12}$ fluorescence excitation spectrum using an array of 30 germanium detectors (Canberra Ltd. Meriden, Connecticut, USA).[11] In order

to maintain detector count-rates in the pseudo-linear regime, Ga_2O_3 and elemental arsenic X-ray filters were employed for Hg L_{III} and Se K-edge XAS respectively, to preferentially absorb scattered radiation, together with silver Soller slits (EXAFS Co., Pioche, Nevada, USA) to reject filter fluorescence. Data were collected using the XAS Collect data acquisition software.[12]

On 6-2 a Si(311) double crystal monochromator was used for the incident beam with harmonic rejection achieved through the cut-off energy (*ca*. 18 keV) of upstream Rh-coated specular optics. Incident and transmitted X-rays were monitored using gas ionization chambers filled with helium and nitrogen, respectively. High resolution X-ray fluorescence was measured by means of a 6-element array of spherically bent crystal analyzers, using Si(555) and Si(844) crystals[13] to select a narrow energy band of the Hg $L\alpha_1$ or Se $K\alpha_1$ emission, respectively. The emission intensity was measured using a single-element silicon drift detector with aluminum filters upstream of the incident ion chamber used to adjust X-ray exposures and to maintain the detector count-rates in the pseudo-linear regime. Data were collected using the SPEC data acquisition software (Certified Scientific Software, Cambridge, Massachusetts, USA).

Data reduction and analysis were carried out as previously described[14] using the EXAFSPAK suite of computer programs (https://www-ssrl.slac.stanford.edu/exafspak.html). Extended X-ray absorption fine structure (EXAFS) phase and amplitude functions were calculated using the program FEFF.[15,16] Data normalization was carried out using the EXAFSPAK program BACKSUB which employs tabulated X-ray cross sections (see supplementary material Figure S3.1).[17]

3.4.4 Density functional theory (DFT) calculations

DFT geometry optimizations and energy calculations were carried out using DMol^3 and Biovia Materials Studio Version 2018 R1[18,19] using the meta-GGA approximation employing the M11-L functional both for the potential during the self-consistent field procedure, and for the energy.[20] DMol^3 double numerical basis sets included polarization functions for all atoms with all-electron relativistic core treatments. Transition state search and optimization used the linear synchronous transit/quadratic synchronous transit/conjugate gradient (LST/QST/CG) method implemented within DMol^3.

3.5 Results and Discussion

3.5.1 Sulfur-bound organometallic mercury species predominant in Cat 717 brain tissue

Fig. 3.1 shows the HERFD-XAS Hg L_{III} spectrum of cerebellar brain tissue from Cat 717. HERFD-XAS uses enhanced energy resolution (supplementary material Fig. S3.2) to probe the local atomic and electronic environment and hence speciation of a target element, here mercury, and can do so in complex materials such as biological tissues.[21] The HERFD-XAS Hg L_{III} spectrum of Cat 717 cerebellar brain tissue was fit to binary linear combinations[22] of a library of HERFD spectra of standard compounds. The best match (Fig. 3.1) is with organometallic and inorganic mercury standard compounds, 78±4% sulfur-bound organometallic mercury in a C–Hg–S linear two-coordinate environment and 22±4% inorganic as β-mercuric sulfide (β–HgS). The ten best binary combinations, listed in Table 3.1 (see caption for method), all included sulfur-bound organometallic mercury as the majority component with around 20% of a minor inorganic component. The best fit, shown in Fig. 3.1, used β–HgS (metacinnabar) as the minor component, the kinetically preferred but thermodynamically less-stable of the mercuric sulfide dimorphs, which exhibits a zincblende structure[23] with four sulfurs bound to the metal. Other reasonable but poorer fits were found with other four-coordinate Hg–S species; we used the Hg L_{III} EXAFS to distinguish β–HgS from these possibilities, as we discuss below Since spectra are sensitive to local environment, specific molecular identities are not available from HERFD or conventional XAS.[24] For example, analogous methyl and ethyl mercury compounds have similar spectra (not illustrated) due to similarity in immediate coordination of mercury, such that our measurements cannot distinguish between different sulfur-bound organometallic mercury compounds. The predominant form of mercury in the cerebellum of Cat 717 is therefore identified as sulfur-bound organometallic mercury, with a minor phase that strongly resembles β–HgS.

Since selenium is important in mercury toxicology,[25–30] we also examined the Se K-edge HERFD,[21] (Fig. 3.2) and found no detectible involvement of mercury-selenium interactions in the brain tissue. However, even with the excellent resolution of HERFD, it is possible that a small fraction of an Hg–Se species may be present and remain undetected by our analyses, especially if this was a small fraction of the total Se present. Moreover, the linear combination method[22] is necessarily limited to the library of spectra for standard compounds that

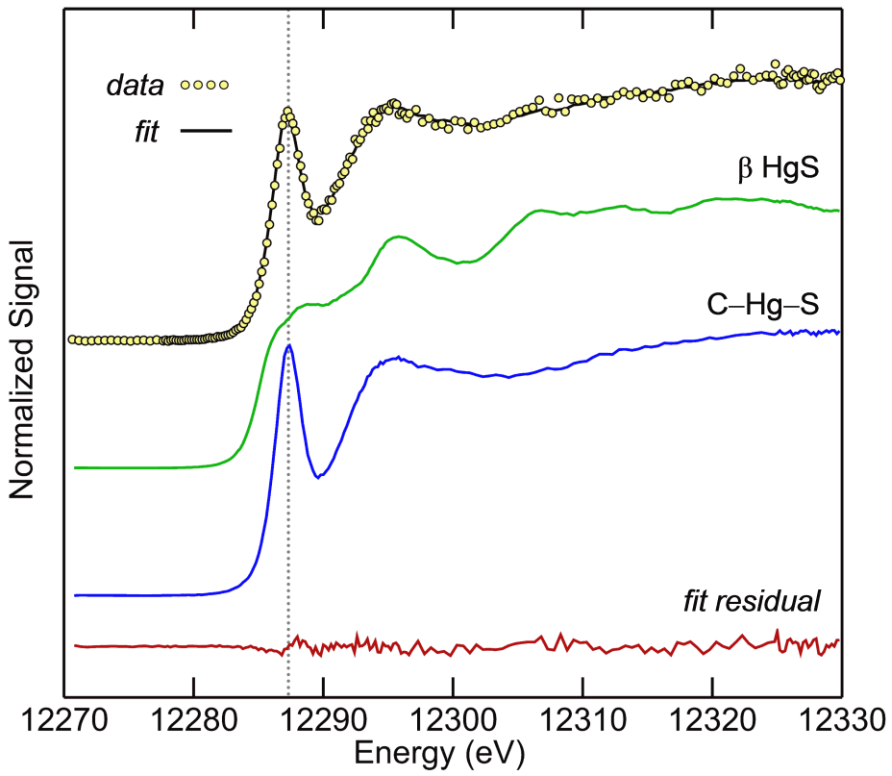

Figure 3.1: High energy resolution fluorescence detected Hg L_{III} Lα1 X-ray absorption near-edge spectra (HERFD-XAS). The HERFD-XAS spectrum of Cat 717 cerebellum (yellow circles) is compared with those of sulfur-bound organometallic mercury (C–Hg–S, modelled as methylmercury-L-cysteine), and β–HgS. The best fit (solid black line) was obtained with 78±4% C–Hg–S and 22±4% β–HgS; errors are three times the estimated standard deviation (99% confidence limits) from the diagonal of the variance-covariance matrix. The fit residual is calculated as the difference between the measured spectrum and best fit (solid red line). The vertical broken line is included to guide the eye.

Table 3.1: Top 10 best binary linear combination fits.

f_1	component 2 identity	f_2	$F^2 \times 10^6$	*fit-index*
0.775	β-HgS	0.225	1.5105	0.22
0.809	$[Hg(SR)_4]^{2-}$	0.191	1.8842	0.59
0.848	$[Hg(SPh)_4]^{2-}$	0.152	1.9211	0.63
0.824	*nano*-HgSe	0.176	1.9316	0.64
0.847	$[Hg(SR)_3]^-$	0.153	1.9579	0.66
0.833	$[Hg(SePh)_3]^-$	0.167	1.9790	0.68
0.658	CH_3Hg–Se(L–Cys)	0.342	2.1631	0.87
0.899	$[HgCl_4]^{2-}$	0.101	2.2316	0.94
0.903	$(CH_3)_2Hg$	0.097	2.2737	0.98
0.893	Hg(0)	0.107	2.4263	1.13

Binary linear combination fits of the Hg L_{III} HERFD-XAS spectrum of Cat 717 cerebellum were carried out using the EXAFSPAK program MATCHIT using a library of 21 different Hg L_{III} HERFD-XAS spectra. In all of the best 10 binary combinations (listed in the table, in order of decreasing goodness of fit) the first (majority) component was found to match C–Hg–S modeled as methylmercury L-cysteineate [CH_3Hg–S(L–Cys)], corresponding to fraction f_1 in the fits, with the remainder fraction (f_2) corresponding to the minor component identified in the table. Since HERFD-XAS cannot distinguish between different 2-coordinate organometallic thiolate-bound mercury species, we use methylmercury L-cysteineate as a generic surrogate for this type of compound. The function F^2 (often called χ^2, called F^2 here to distinguish it from the EXAFS χ) is defined by $F^2 = \sum(\mu - \mu_{calc})^2/(n-2)$ where μ and μ_{calc} are the experimental and computed signal, respectively, and the sum is over n data points included in the fit. The *fit-index* is given by $(F^2 - F_{min}^2) \times 10^6$, where F_{min}^2 is F^2 computed between Fourier filtered (free of high-frequency noise) data and raw data. The fit-index effectively and approximately lacks contributions from high-frequency noise, with a fit-index value of zero representing a best possible fit, and higher values representing poorer fits.

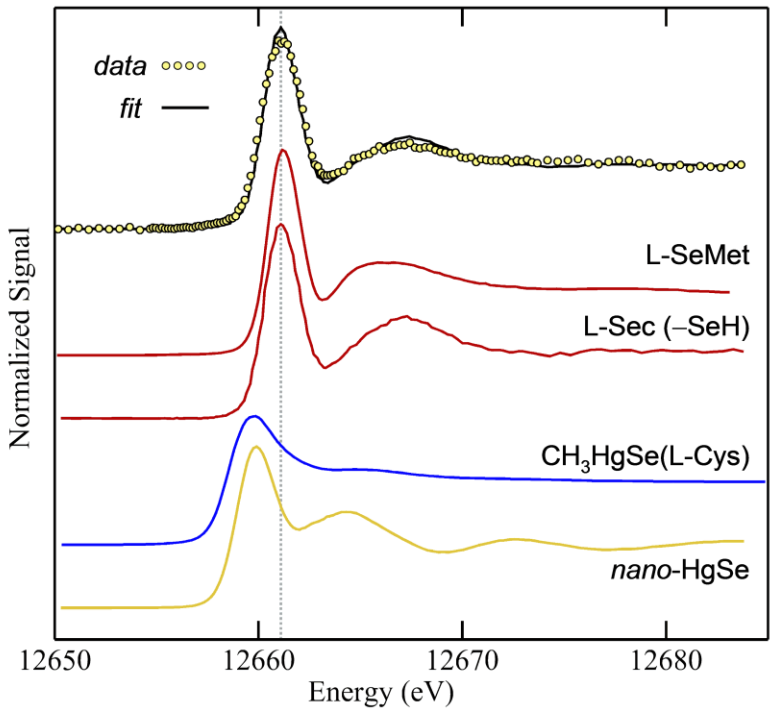

Figure 3.2: Se Kα1 HERFD-XAS of Cat 717, compared with spectra of selected standard compounds. L-selenomethionine (aqueous, pH 7.4), L-selenocysteine (aqueous, pH 4.0), methylmercury L-selenocysteinate (solid), and nanoparticulate–HgSe (colloidal) demonstrated. The fit shows no contributions from the two mercury-containing species. The vertical broken line is included to guide the eye.

are available. It is thus also possible that an Hg–Se species is present having a spectrum that is not represented in our library of standards. The Hg L_{III} and Se K HERFD spectra of a range of different standards, including some additional Hg–Se species are shown in supplementary material (Fig. S3.3).

We used Hg L_{III} and Se K HERFD absorption edge-jumps to estimate the effective concentration to be 70.9 μM Hg and 5.6 μM Se (wet weight), or some 13-fold excess of mercury. Previous conventional analysis of Cat 717 cerebellum[6] showed selenium below detection limits and total mercury dry weight of 62.5 $\mu g.g^{-1}$, which is commensurate with our value. Previous analyses also determined fractions of methylmercury and inorganic mercury to be 30% and 70%, respectively;[6] the analytical method for methylmercury, however, would be misleading if mercury was in a different organometallic form because the methods used in the previous analyses are based on chemical derivatization in combination with some measure of molecular mobility.

The Hg L_{III} extended X-ray absorption fine structure (EXAFS) spectra and corresponding Fourier transforms of Cat 717 cerebellum (Fig. 3.3) enable us to determine radial structural metrics of the mercury environments (Table 3.2). Curve-fitting analysis indicates 2.11 Å Hg–C and 2.37 Å Hg–S contacts, characteristic of the two-coordinate organometallic mercury observed as the dominant species in the HERFD. Consistent with a minor component of β–HgS or tetrathiolate Hg(II) species,[31,32] the EXAFS also shows a 2.55 Å Hg–S interaction characteristic of a four-coordinate site. The diagnostic weaker long-range Hg···Hg and Hg···S interactions[31] clearly distinguish the minor component as β–HgS. Constraining first-shell coordination numbers to the species fractions obtained from fitting the Hg L_{III} HERFD spectra gave the excellent fit shown in Fig. 3.3 with details given in Table 3.2. The substantial amplitude of the outer-shell β–HgS Hg···S_2 and Hg···Hg_2 EXAFS is large compared with the first shell Hg–S_2 which is due to the presence of 12 such interactions. The amplitudes of these interactions are actually less than crystalline β–HgS, and commensurate with amorphous β–HgS (not illustrated). The EXAFS is therefore quantitatively in agreement with the HERFD result that mercury in the cerebellum of Cat 717 is present as 78% sulfur-bound organometallic mercury, with 22% inorganic mercury as β–HgS.

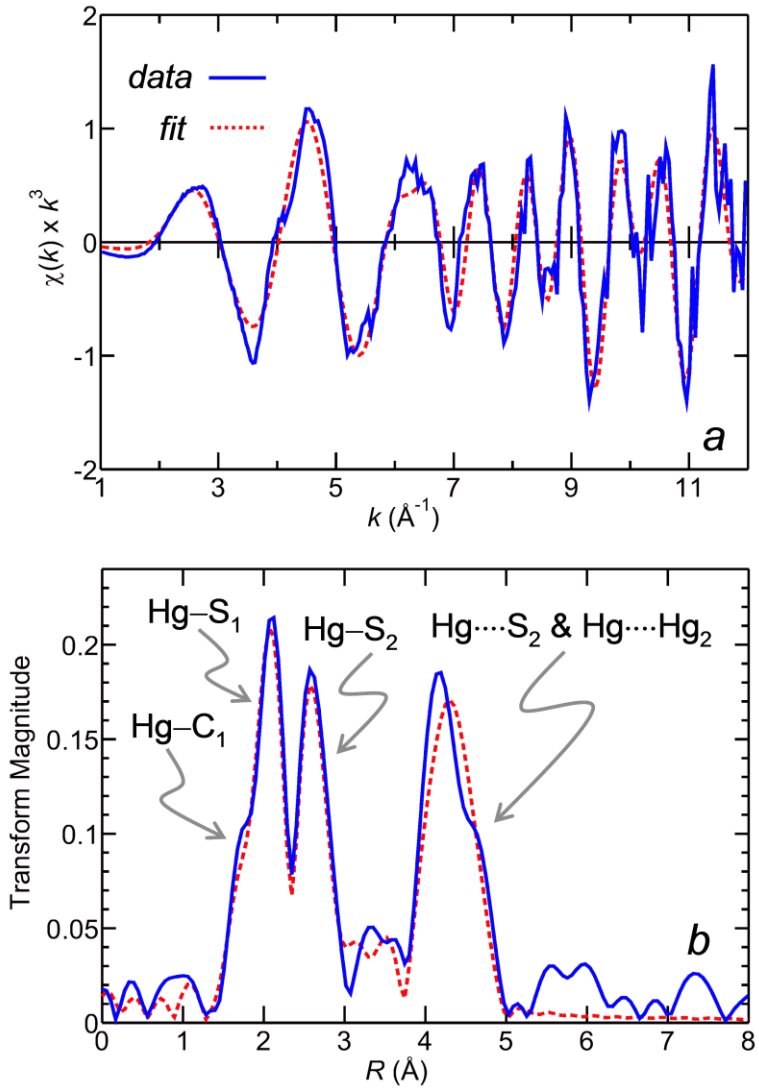

Figure 3.3: Extended X-ray absorption fine structure (EXAFS) spectra of Cat 717 cerebellum. (*a*) Hg L_{III}-edge EXAFS for Cat 717 cerebellum (solid blue line) is overlaid with the best fit (red dashed line); structural parameters are given in Table 3.2. (*b*) EXAFS Fourier transforms are phase-corrected for Hg–S backscattering, with specific backscattering interactions indicated. Hg–C_1 and Hg–S_1 are attributed to sulfur-bound organometallic mercury (species 1), and Hg–S_2, Hg⋯S_2 and Hg⋯Hg_2 to β–HgS (species 2).

Table 3.2: Hg L_{III} EXAFS curve-fitting results.

Interaction	*fraction*	*N*	*R* (Å)	σ^2 (Å^2)	ΔE_0 (eV)
Hg–C_1	0.78	1	2.111(5)	0.0027(3)	–15.6
Hg–S_1		1	2.371(3)	0.0026(3)	
Hg–S_2	0.22	4	2.546(3)	0.0023(3)	
Hg⋯Hg_2		4.2(1)	4.127(4)	0.0040(5)	
Hg⋯S_2		4.2(1)	4.841(8)	0.0050(6)	

Structural parameters for the best fit of the EXAFS spectrum of Cat 717 cerebellum, as shown in Fig. 3.3. Interactions Hg–C_1 and Hg–S_1 are attributed to organometallic mercury (species 1), and Hg–S_2, Hg⋯S_2 and Hg⋯Hg_2 to β–HgS (species 2). Values are given for the effective coordination numbers *N*, inter-atomic distances *R*, and the mean square deviation in *R*, σ^2, an index of thermal and static disorder. The threshold energy shift ΔE_0, taken from fits to standard compounds of known structure, was fixed at the same value for all interactions included in the analysis. Values in parentheses are the estimated standard deviations in the last digits obtained from the diagonal of the variance-covariance matrix (precisions). Coordination numbers in the fit for first-shell interactions were fixed according to the known value for the phase multiplied by the fraction determined from the HERFD-XAS analysis. For the outer shell interactions (beyond 4 Å) both *N* and σ^2 were allowed to vary and are not thought to be structurally representative. This is appropriate for disordered non-crystalline amorphous systems, such as mercury chalcogenides[25] including amorphous β–HgS, because the material will contain both disordered and ordered components, with the latter dominating the EXAFS. The interatomic distances (*R*) are, however, sensitive indicators of the nature of the material concerned.

3.5.2 Effluent released from industrial factory plausibly contained organometallic mercury

Because Cat 717 was given the acetaldehyde plant waste directly, our results provide experimental evidence related to the composition of the waste.[33] Since there are no chemically plausible pathways to convert inorganic to organometallic mercury in mammalian tissues, the presence of predominantly organometallic mercury in the brain of Cat 717 clearly shows that the primary mercury species in the plant waste was organometallic, and not inorganic as suggested in some early reports.[35,36] In agreement with this, the pathology exhibited by Cat 717[6] was that expected for organomercury poisoning, with severe tremor, moderate ataxia and severe paralysis but not inorganic mercury poisoning for which gastrointestinal signs including vomiting of mucoid material and bloody diarrhea would be evident.[37] The lack of any signs of inorganic mercury intoxication would argue that there were no large quantities of inorganic mercury in the plant waste, although smaller amounts of inorganic mercury were probably present.

3.5.3 α-mercuri-acetaldehyde a probable by-product of chemical plant processes

We have used computational chemistry to consider the chemical plant processes and expected side-products. The Chisso plant employed mercury catalysts to manufacture acetaldehyde through hydration of acetylene[3,38,39] using a catalytic method known as alkyne oxymercuration.[40] This factory, and others in Japan, had been using these methods since the early 1930's. However, no human poisonings were recognized in Minamata before 1953. Prior to that recognition in August 1952, the Chisso plant had modified their procedures, altering a catalyst regeneration process (see supplementary text).[3]

Fig. 3.4 summarizes the major chemical reactions, together with some reaction energies from our DFT calculations. Acetylene is bound to Hg^{2+} by a η^2 bond to both carbon atoms to form compound **1**, in which the carbon atoms are activated for attack by water to form **2** an α-mercuri-vinyl alcohol. Under acidic conditions protonolysis of the Hg–C bond regenerates inorganic catalyst forming vinyl alcohol, which undergoes acid-catalyzed 1,3-hydrogen migration keto-enol tautomerization to form the desired product acetaldehyde. However, **2** also undergoes similar keto-enol tautomerization to form the α-mercuri-acetaldehyde **3**, a stable compound of known structure.[41] Although **3** can also undergo protonolysis to form acetaldehyde, it is less susceptible to this reaction than **2**. Therefore, an energetically-favoured by-product of the Chisso plant, expected under low-acid conditions, is **3**, an α-mercuri-acetaldehyde which is distinct from methylmercury. It has been suggested that **3** oxidizes to α-mercuri-acetic acid species **4**, which

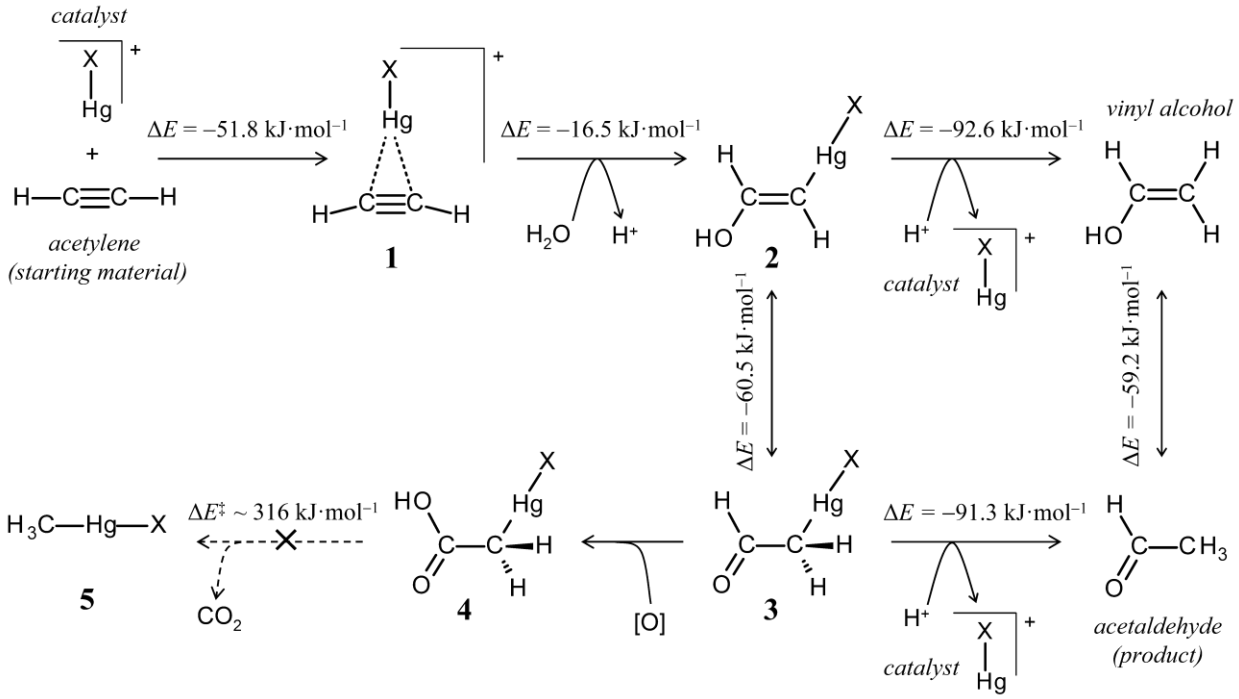

Figure 3.4: Chemistry of the Chisso chemical plant and potential side-products. DFT computed energy changes (ΔE in $kJ \cdot mol^{-1}$) are shown adjacent to each of the central reactions. The suggested loss of CO_2 from **4** to form methylmercury **5** is chemically very unlikely due to the very high activation energy $\Delta E^{\ddagger}$ of 316 $kJ \cdot mol^{-1}$. X represents a general substituent of mercury, like chloride, which was used for computations. The oxidation **3** to **4** might occur in the environment, after waste emission had occurred.

might spontaneously lose CO_2 to form methylmercury species **5**.[42] While the former is plausible, our calculations suggest that decarboxylation is improbable due to a substantial activation barrier of 316 kJ·mol^{-1}. In agreement with this, α-mercuri-acetic acids are known from the literature[43] to exhibit a stable C–C bond under oxidizing and acidic conditions, and upon heating,[44] and only insignificant methylmercury yields have been reported.[45] Taken together, the evidence is strong that the compound entering the waters of Minamata bay, that gave rise to the tragedy of Minamata disease, was species **3** or possibly **4**.

In living brain tissue organic mercury species are known to convert to inorganic forms over time, being transformed to highly insoluble HgSe.[27] However, since Cat 717 lived only a short time after initiation of dosing, these protective processes had no time to occur *in vivo*, likely accounting for the notable absence of HgSe. The brain tissues of Cat 717 were preserved by immersion in 10% formalin,[6] which is a standard method for fixing biological tissues.[46] Exposure to such formaldehyde-based fixatives will cross-link proteins, and alter the distributions of soluble ions such as Cl^- and K^+.[47] Insofar as our elements of interest are concerned, exposure of the brain tissue to formaldehyde preservative over decades would be expected to change its forms of selenium, but not of Hg. Selenocysteine residues (either selenolate R–Se$^-$ or selenol R–SeH) would react to form selanylmethanol derivatives, or cyclizing with the selenocysteine amino group to form 1,3-selenazolidine species. However, Hg–Se bonds would be expected to be stable, and in particular HgSe should be stable indefinitely. Thus the absence of HgSe or other compounds with Hg–Se bonds may be significant in relation to recent suggestions of inhibition of selenoenzymes as a contributor to mercury's toxicity.[48]

Plausibly, the presence of β-HgS in the cerebellum of Cat 717 may result from degradation of the original organometallic compounds during storage. The mechanism of conversion of organometallic to β-HgS might resemble that previously discussed by others for both β-HgS and HgSe.[49,50] Here organomercuri-cysteinate complexes would disproportionate to form *bis*-L-alanylsulfide and a *bis*-organomercuri-sulfide,[50] which would in turn eliminate HgS forming the di-organomercury compound which are known spontaneously react with H_2O in aqueous media to break one of the two Hg–C bonds. A schematic of this mechanism is shown in supplementary material Fig. S3.4. Conversely, our finding of a majority organometallic mercury species is unlikely to be an artifact of storage because there is no chemically plausible method of organometallic mercury derivatives forming.

We have shown through newly developed X-ray spectroscopic techniques that Cat 717 was exposed to primarily organometallic mercury compounds, and hence we can conclude that these were the dominant mercury species in the acetaldehyde plant waste. This is in agreement with the signs exhibited by the cat and with subsequent pathology investigations.[6] Our analysis of the chemistry indicates that the plant effluent probably contained an α-mercuri-acetaldehyde species (**3** or **4** in Fig. 3.4) and that that was the species that contaminated Minamata Bay and subsequently gave rise to the tragedy of Minamata disease. Because it seems that the mercury contamination introduced into Minamata Bay was already in the form of an organometallic compound, we believe this evidence indicates that natural biomethylative processes within Minamata Bay initially played no major role in the tragedy.

We further suggest that exposure to methylmercury compounds were not specifically involved in the Minamata tragedy. While α-mercuri-acetaldehyde and α-mercuri-acetic acid compounds have been chemically known for four decades and have been characterized as stable high-melting point solids,[41-44] their toxicologies are as yet unexplored. Although it seems probable from the historical cat experiments[6] that these may be similar to other organometallic compounds of mercury that have been investigated,[51] more work is required to explore the molecular toxicology of these species. Other uncertainties include how these compounds would behave in a marine environment such as Minamata Bay, and whether they would accumulate through the trophic levels, as has been observed for methylmercury compounds. In our rethinking of the cause of the Minamata tragedy, we conclude that there are multiple ramifications of a different organometallic mercury being responsible and that our views of this classic example of human toxicology should be evaluated.

3.6 Acknowledgements

We thank Professors Eric Block (University at Albany, State University of New York) and Dale Ward (University of Saskatchewan) for helpful comments on the manuscript. We also thank Professor Kaori Tanaka and Dominic George (University of Saskatchewan) for additional help. We acknowledge grant support from the Natural Sciences and Engineering Research Council of Canada (NSERC; IJP, PHK and GNG), the Canada Foundation for Innovation (CFI), John Evans Leader's Fund award (IJP) and Canada Research Chairs (IJP and GNG). SN acknowledges a Dr. Rui Feng Scholarship; AKJ and SN were Fellows and NVD an Associate in the Canadian Institutes of Health Research-Training grant in Health Research Using Synchrotron Techniques (THRUST). Use of the Stanford Synchrotron Radiation Lightsource, SLAC National Accelerator Laboratory, is supported by the U.S. Department of Energy, Office of Science, Office of Basic Energy Sciences under Contract No. DE-AC02-76SF00515. The SSRL Structural Molecular Biology Program is supported by the DOE Office of Biological and Environmental Research, and by the National Institutes of Health, National Institute of General Medical Sciences (including P41GM103393). The contents of this publication are solely the responsibility of the authors and do not necessarily represent the official views of NIGMS or NIH.

3.7 Supplementary Text

3.7.1 Historical perspective on Chisso acetaldehyde process

Acetaldehyde (ethanal), an important industrial chemical,[52] is produced on a large scale at many locations world-wide. Current production relies on oxidation of ethylene (ethene) using a copper/palladium homogeneous catalyst.[52] However, before mid-1960 acetaldehyde was manufactured by alkyne oxymercuration,[40] using an inorganic mercury catalyst to hydrate acetylene derived from calcium carbide. Othmer et al.[38] described the two main industrial processes for production of acetaldehyde used in 1956. The newer Chisso method, used at the Minamata plant from 1932 onward, differed from the older German method in using a lower reaction temperature, and in employing the heat generated by the hydration reaction to assist with distillation.[38] Both methods used a mercury catalyst, with manganese or iron compounds regenerating catalytically competent Hg(II) after reduction to Hg(0) due to side reactions.[38,52] From 1932 until 1952, aside from loss of production due to World War II bombing of the plant 1945-1946, the Minamata plant used MnO_2 in catalyst regeneration.[53] In 1952 this was changed to nitric acid and $Fe_2(SO_4)_3$,[53] which may be linked to the onset of large numbers of cases of Minamata disease. $Fe_2(SO_4)_3$ also was replaced by pyrite cinders, typically containing 80-90% Fe_2O_3 plus a range of other oxides, which may have led to process upsets necessitating discharge of mother liquor.[53] In 1955, the plant began adding seawater to the industrial water used for process hydration, resulting in high chloride concentrations in the reaction vessel. The drain of the rectifying column was observed to accumulate mercury compounds,[53] which were reported to be methylmercury compounds[53] although how this was determined is unclear. The first case of Minamata disease occurred in a child in 1953. Cats began showing signs of "dancing disease or epilepsy" and dying in 1954. Minamata disease was officially recognized in 1956 when four children were hospitalized with an unknown neurological disease.[53] The waste to which Cat 717 was exposed was collected in November 1960. When Chisso's acetaldehyde production stopped in 1966 the rate of occurrence of new cases of Minamata disease dropped quickly.[53]

3.8 Supplementary Figures

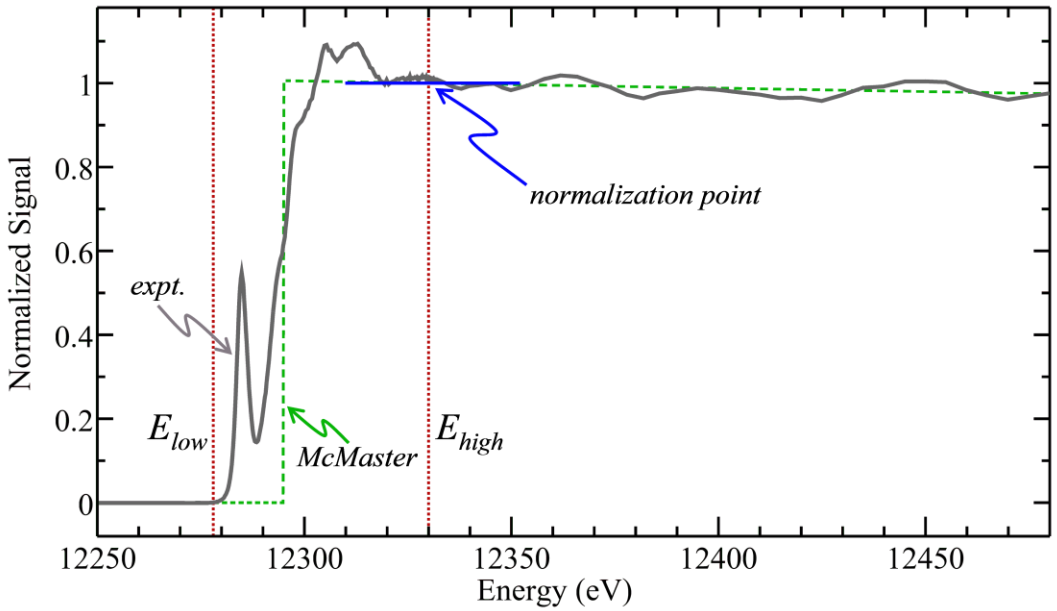

Figure S3.1: HERFD normalization to the absorption edge, illustrated using the Hg-L_{III} HERFD data for solid $HgSO_4$ (gray line). The raw signal intensity is scaled to the McMaster cross-section (shown with the green broken line)[17] excluding the most structured region between E_{low} and E_{high} (denoted by the red vertical broken lines). The normalization value is shown by the blue line.

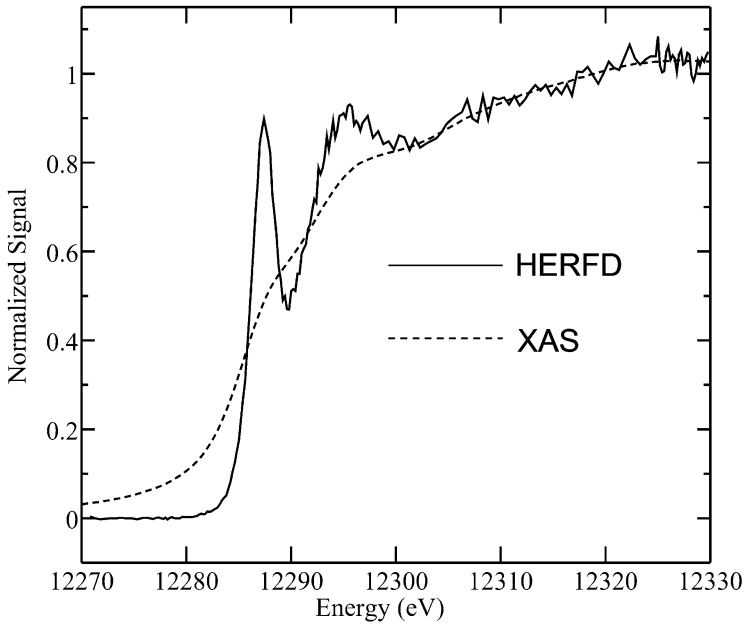

Figure S3.2: Comparison of Hg L_{III} HERFD-XAS and standard Hg L_{III} XAS of Cat 717 cerebellum showing the dramatically improved spectroscopic resolution obtained with HERFD-XAS.

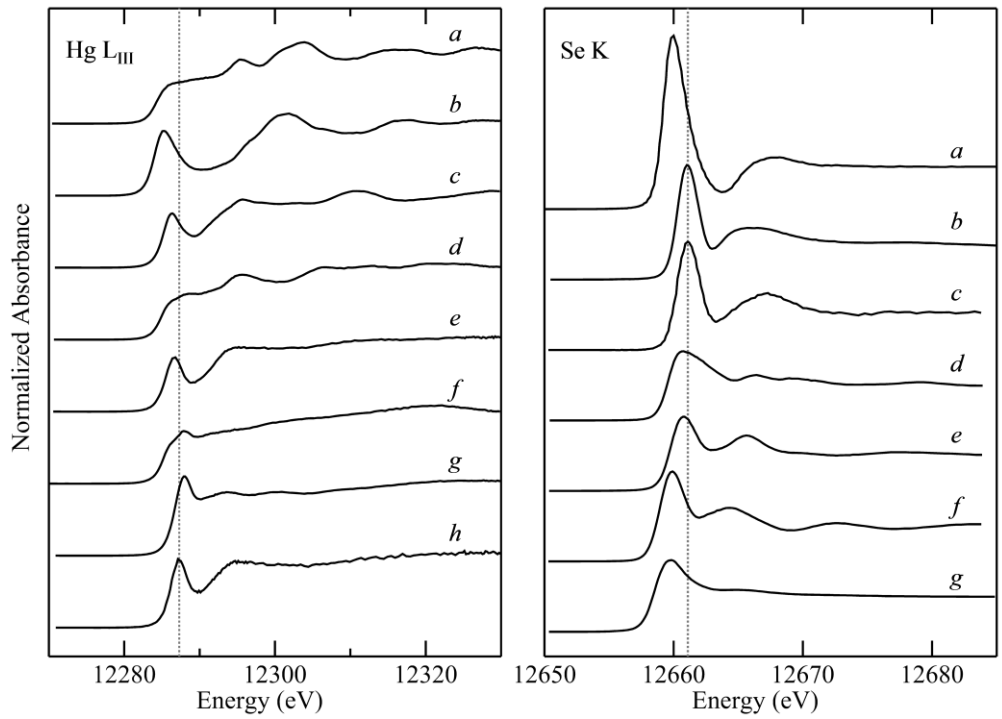

Figure S3.3: Hg L_{III}-edge and Se K-edge HERFD spectra of selected standards. The Hg L_{III}-edge spectra are those of *a* elemental mercury, *b* mercuric oxide, *c* α-mercuric sulfide, *d* β-mercuric sulfide, *e* $Hg(SR)_2$ [*bis*(L-cysteinato)-mercury(II)], *f* $[Hg(SR)_4]^{2-}$ [*tetrakis* (dimercaptopropanesulfonic acid)-mercury(II)],[54] *g* dimethylmercury, and *h* methylmercury-L-cysteinate. Spectrum *a* was collected using finely dispersed elemental mercury, spectra *b*–*d* were collected using finely divided solids diluted with boron nitride, and all others collected using dilute aqueous solution, apart from *g* which was in isopropanol solution. The Se K-edge spectra are those of *a* α-selenium, *b* L-selenomethionine, *c* L-selenocysteine, *d* $Hg(SePh)_2$ [*bis*(selenophenolato)mercury(II)], *e* $[Hg(SePh)_3]^-$ [tetrabutylammonium *tris*(selenophenolato)mercury(II)], *f* colloidal HgSe, *g* methylmercury-L-selenocysteinate. Spectra *a* and *f* were collected using finely dispersed compound in aqueous media, *b* and *c* using aqueous solutions, and *d*, *e* and *g* using finely ground solids diluted in boron nitride. The vertical broken lines are included to guide the eye.

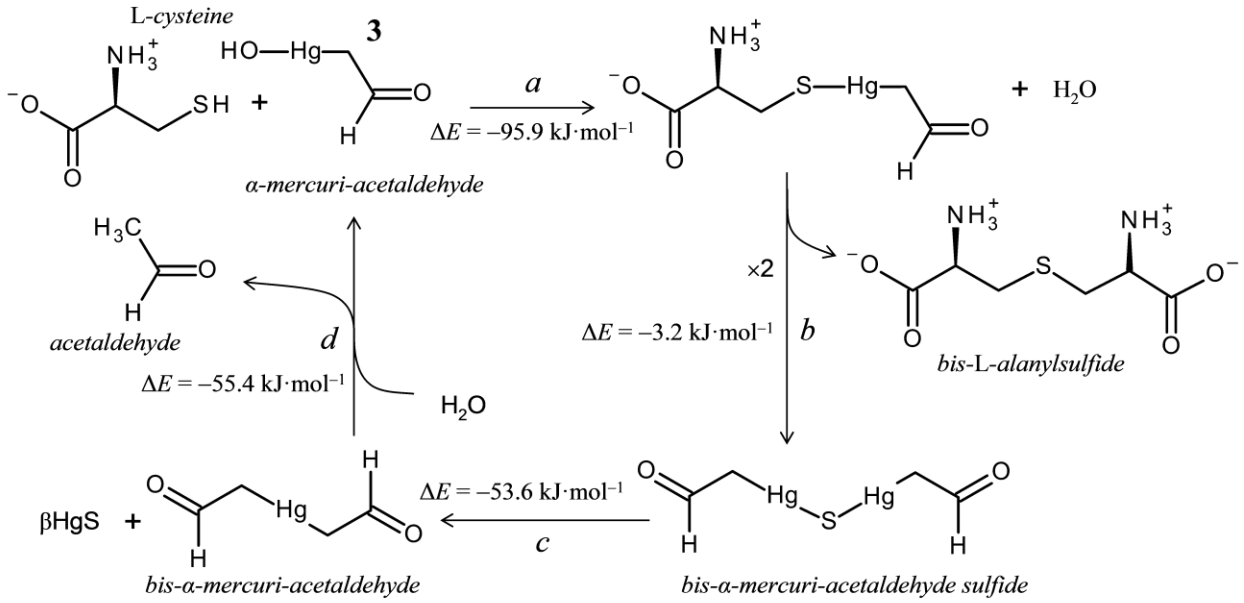

Figure S3.4: A possible mechanism of formation of β-HgS. The reactions are essentially those proposed by Asaduzzaman and Schreckenbach,[50] which were based on earlier work by Kahn and Wang on selenoaminoacids,[49] except that we have used α-mercuri acetaldehyde in place of methylmercury. Similar results can be anticipated for other organometallic compounds of mercury. Reaction energies were estimated as described for Figure 4. Reaction *a* follows the well-known affinity for thiols, and is expected to proceed rapidly, with the cysteine being part of a biomolecule and not necessarily the free amino acid. We include it here for the sake of forming a closed cycle. Reaction *b* is predicted to be only mildly thermodynamically favorable, and requires two α-mercuri acetaldehyde cysteine entities to be sufficiently close to react. This is consistent with β-HgS being only a minor component. The thermodynamics for reaction *c* was estimated by computing the enthalpy of formation of gas-phase HgS plus the previously reported sublimation enthalpy for HgS.[55] Reaction *d* follows the established chemistry of dialkylmercury species which are known to spontaneously undergo protonolysis in aqueous solution, in this case yielding acetaldehyde.

3.9 References

(1) Kurland, L. T., Faro, S. N., Siedler, H. Minamata disease. The outbreak of a neurologic disorder in Minamata, Japan, and its relationship to the ingestion of seafood contaminated by mercuric compounds. *World Neurol*. **1960**, *1*, 370–395.

(2) Takeuchi, T., Morikawa, N., Matsumoto, H., Shiraishi, Y. A pathological study of Minamata disease in Japan. *Acta Neuropath*. **1962**, *2*, 40–57.

(3) Eto, K., Marumoto, M., Takeya, M. The pathology of methylmercury poisoning (Minamata disease). *Neuropathology* **2010**, *30*, 471–479.

(4) Hunter, F., Russell, D.S. Focal cerebral and cerebellar atrophy in a human subject due to organic mercury compounds. *J. Neurol. Neurosurg. Psychiat*. **1954**, *17*, 235–241.

(5) K. Eto, K., Yasutake, A., Kuwana, T., Korogi, Y., Akima, M., Shimozeki, T., Tokunaga, H., Kaneko, Y. Methylmercury poisoning in common marmosets – A study of selective vulnerability within the cerebral cortex. *Toxicol. Pathol*. **2001**, *29*, 565–573.

(6) Eto, K., Yasutake, A., Nakano, A., Akagi, H., Tokunaga, H., Kojima, T. Reappraisal of the historic 1959 cat experiment in Minamata by the Chisso factory. *Tohoku J. Exp. Med*. **2001**, *194*, 197–203.

(7) Klaassen, C.D. Toxic Responses of the Ocular and Visual System. In *Casarett & Doull's Toxicology: The Basic Science of Poisons*; Fox, D.A., Boyes, W.K., Eds.; McGraw-Hill: New York, 2013, Ed. 8.

(8) Hoffmeyer, R., Singh, S. P., Doonan, C. J., Ross, A. R. S., Hughes, R. J., Pickering, I. J., George, G. N. Molecular mimicry in mercury toxicology. *Chem. Res. Toxicol*. **2006**, *19*, 753–759.

(9) Carty, A. J., Malone, S. F., Taylor, N. J., Canty, A. J. Synthesis, spectroscopic, and X-ray structural characterization of methylmercury-D,L-selenocysteinate monohydrate, a key model for the methylmercury(II)-selenoprotein interaction. *J. Inorg. Biochem*. **1983**, *18*, 291–300.

(10) Pickering, I. J., George, G. N., van Fleet-Stalder, V., Chasteen, T. G., Prince, R. C. X-ray absorption spectroscopy of selenium-containing amino acids. *J. Biol. Inorg. Chem*. **1999**, *4*, 791–794.

(11) Cramer, S. P., Tench, O., Yocum, M., George, G. N. A 13-element Ge detector for fluorescence EXAFS. *Nucl. Instr. Meth. A*. **1988**, *266*, 586–591.

(12) George, M. J. XAS-Collect: A computer program for X-ray absorption spectroscopic data acquisition. *J. Synchrotron Radiat*. **2000**, *7*, 283–286.

(13) Sokaras, D., Weng, T.-C., Nordlund, D., Alonso-Mori, R., Velikov, P., Wenger, D., Garachtchenko, A., George, M. J., Borzenets, V., Johnson, B., Rabedeau, T., Bergmann, U.

A seven-crystal Johann-type hard X-ray spectrometer at the Stanford Synchrotron Radiation Lightsource. *Rev. Sci. Instrum*. **2013**, *84*, 053102/1–8.

(14) George, G. N., Garrett, R. M., Prince, R. C., Rajagopalan, K. V. The molybdenum site of sulfite oxidase: A comparison of wild-type and the cysteine 207 to serine mutant using X-ray absorption spectroscopy. *J. Am. Chem. Soc*. **1996**, *118*, 8588–8592.

(15) Rehr, J. J., Mustre de Leon, J., Zabinsky, S. I., Albers, R. C. Theoretical X-ray absorption fine structure standards. *J. Am. Chem. Soc*. **1991**, *113*, 5135–5140.

(16) Mustre de Leon, J., Rehr, J. J., Zabinsky, S. I., Albers, R. C. Ab initio curved-wave X-ray-absorption fine structure. *Phys. Rev. B* **1991**, *44*, 4146–4156.

(17) McMaster, W.H., Del Grande, N.K., Mallett, J.H., Hubbell, J.H. Compilation of X-ray cross sections. Lawrence Livermore National Laboratory Report UCRL-50174, Sec II, Rev.1 1969.

(18) Delley, B. An all-electron numerical method for solving the local density functional for polyatomic molecules. *J. Chem. Phys*. **1990**, *92*, 508–517.

(19) Delley, B. From molecules to solids with the DMol3 approach. *J. Chem. Phys*. **2000**, *113*, 7756–7764.

(20) Peverati, R., Truhlar, D. G. M11-L: A local density functional that provides improved accuracy for electronic structure calculations in chemistry and physics. *J. Phys. Chem. Lett*. **2012**, *3*, 117–124.

(21) Nehzati, S., Dolgova, N.V., Sokaras, D., Kroll, T., Cotelesage, J.J.H., Pickering, I.J., George, G.N. A photochemically-generated selenyl free radical observed by high-energy resolution fluorescence detected X-ray absorption spectroscopy. *Inorg. Chem*. **2018**, *57*, 10867–10872.

(22) Pickering, I.J., Prince, R.C., Divers, T.C., George, G.N. Sulfur K-edge X-ray absorption spectroscopy for determining the chemical speciation of sulfur in biological systems. *FEBS Lett*. **1998**, *441*, 11–14.

(23) Lehmann, W. Röntgenographische Untersuchungen an Natürlichem und Synthetischem Metacinnabarit (HgS). *Z. Krystallog*. **1924**, *60*, 379–413.

(24) Dolgova, N.V., Nehzati, S., Choudhury, S., Regnier, N., Crawford, A.M., Ponomarenko, O., George, G.N., Pickering, I.J. X-ray spectroscopy and imaging of selenium in living systems. *Biochim. Biophys. Acta*. **2018**, *1862*, 2383–2392.

(25) Gailer, J., George, G.N., Pickering, I.J., Madden, S., Prince, R.C., Yu, E.Y., Denton, M.B., Younis, H.S., Aposhian, H.V. The structural basis of the antagonism between inorganic mercury and selenium in mammals. *Chem. Res. Toxicol*. **2000**, *13*, 1135–1142.

(26) Gailer, J. Arsenic–selenium and mercury–selenium bonds in biology. *Coord. Chem. Rev*. **2007**, *251*, 234–254.

(27) Korbas, M., O'Donoghue, J.L., Watson, G.E., Pickering, I.J., Singh, S.P., Myers, G.J., Clarkson, T.W., George, G.N. The chemical nature of mercury in human brain following poisoning or environmental exposure. *ACS Chem. Neurosci*. **2010**, *1*, 810–818.

(28) MacDonald, T.C., Korbas, M., James, A.K., Sylvain, N.J., Hackett, M.J., Nehzati, S., Krone, P.H., George, G.N., Pickering, I.J. Interaction of mercury and selenium in the larval stage zebrafish vertebrate model. *Metallomics* **2015**, *7*, 1247–1255.

(29) Bjørklund, G., Aaseth, J., Ajsuvakova, O.P., Nikonorov, A.A., Skalny, A.V., Skalnay, M.G., Tinkov, A.A. Molecular interaction between mercury and selenium in neurotoxicity. *Coord. Chem. Rev*. **2017**, *332*, 30–37.

(30) Dolgova, N.V., Nehzati, S., MacDonald, T.C., Summers, K.L., Crawford, A.M., Krone, P.H., George, G.N., Pickering, I.J. Disruption of selenium transport and function is a major contributor to mercury toxicity in zebrafish larvae. *Metallomics* **2019**, *11*, 621-631.

(31) Buckley H. E., Vernon, W. S. The crystal structures of the sulfides of mercury. *Mineral. Mag. J. M. Soc*., **1925**, *20*, 382–392.

(32) Govindaswamy, N., Moy, J., Millar, M., Koch, S. A. A distorted mercury $[Hg(SR)_4]^{2-}$ complex with alkanethiolate ligands: The fictile coordination sphere of monomeric $[Hg(SR)_x]$ complexes. *Inorg. Chem*. **1992**, *31*, 5343–5344.

(33) Normal levels of mercury in the brain tissues of cats fed a high-mercury predatory fish (tuna) are expected to be below 3 μM.

(34) Boyer, C.I., Jr., Andrews, E.J., deLahunta, A., Bache, C.A., Gutenmann, W.H., Lisk, D.J. Accumulation of mercury and selenium in kittens fed commercial cat food. *Cornell Vet*. **1978**, *68*, 365–374.

(35) Kurzel, R.B., Cetrulo, C.L. The effect of environmental pollutants on human reproduction, including birth defects. *Environ. Sci. Technol*. **1981**, *15*, 626-640.

(36) Kondo, K. Congenital Minamata disease: Warnings from Japan's experience. *J Child Neurol*. **2000**, *15*, 458-464.

(37) Von Burg, R. Toxicology update: Inorganic mercury. *J. Appl. Toxicol*. **1995**;*15*, 483–493.

(38) Othmer, D.F., Kon, K., Igarashi, T. Acetaldehyde by the Chisso process. *Ind. Eng. Chem*. **1956**, *48*, 1258–1262.

(39) The plant also supported a much smaller activity to manufacture vinyl chloride, also using mercury catalysts, which is not considered here.

(40) Larock, R.C. Solvomercuration/Demercuration Reactions in Organic Synthesis; Springer: Berlin, 2013

(41) Halfpenny, J., Small, R.W.H. Structure of (chloromercurio)acetaldehyde. *Acta Cryst. B* **1979**, *35*, 1239–1241.

(42) Takeuchi, T., Eto, K., Nakayama, H., Sumiyoshi, A. The pathology of Minamata disease: A tragic story of water pollution; Kyushu University Press Inc., 1999

(43) Grdenić, D., Korpar-Čolig, B., Matković-Čalogović, D., Sikirica, M., Popović, Z. Monomercurated acetic acid. The crystal structure of NO_3HgCH_2COOH. *J. Organomet. Chem*. **1991**, *411*, 19–23.

(44) Grdenić, D., Korpar-Čolig, B., Sikirica, M. Mercuretin as the condensation polymer of tris(acetoxymercuri)acetic acid. The crystal structure of $(ClHg)_3CCOOH \cdot DMSO$. *J. Organomet. Chem*. **1984**, *276*, 1–8.

(45) Kitamura, S., Sebe, E., Hayakawa, K., Sumino, K. Side reactions accompanying catalytic hydration of acetylene. IV. Miscellaneous reactions yielding alkyl mercury compounds. *Nippon Yakurigaku Zasshi*, **1968**, *64*, 531–543.

(46) Fox, C.H., Johnson, F.B., Whiting, J., Roller, P.P. Formaldehyde fixation. *J. Histochem. Cytochem*. **1985**, *33*, 845–853.

(47) Hackett, M.J., McQuillan, J.A., El-Assaad, F., Aitken, J.B., Levina, A., Cohen, D.D., Siegele, R., Carter, E.A., Grau, G.E., Hunt, N.H., Lay, P.A. Chemical alterations to murine brain tissue induced by formalin fixation: implications for biospectroscopic imaging and mapping studies of disease pathogenesis. *Analyst*. **2011**, *136*, 2941-2952.

(48) Ralston, N.V.C., Blackwell III, J.L., Raymond, L.J. Importance of molar ratios in selenium-dependent protection against methylmercury toxicity. *Biol. Trace Elem. Res*. **2007**, *119*, 255–268.

(49) Kahn, M.A.K., Wang, F. Chemical demethylation of methylmercury by selenoamino acids. *Chem. Res. Toxicol*. **2010**, *23*, 1202–1206.

(50) Asaduzzaman, A.M., Schreckenbach, G. Degradation mechanism of methyl mercury selenoamino acid complexes: A computational study. *Inorg. Chem*. **2011**, *50*, 2366–2372.

(51) Clarkson, T.W., Magos, L. The toxicology of mercury and its chemical compounds. *Crit. Rev. Toxicol*. **2006**, *36*, 609–662.

3.10 Additional References

(52) Eckert, M., Fleischmann, G., Jira, R., Bolt, H. M., Golka, K. Acetaldehyde. In: *Ullmann's Encyclopedia of Industrial Chemistry*, Wiley-VCH, 2007.

(53) Yokoyama, H. Mercury Pollution in Minamata. In: *Springer Briefs in Environmental Science*, Springer, 2018.

(54) George, G.N., Prince, R.C., Gailer, J., Buttigieg, G.A., Denton, M.B., Harris, H.H., Pickering, I.J. Mercury binding to the chelation therapy agents DMSA and DMPS, and the rational design of custom chelators for mercury. *Chem. Res. Toxicol*. **2004**, *17*, 999–1006.

(55) von Szentpály, L. Atom-based thermochemistry: Predictions of the sublimation enthalpies of group 12 chalcogenides and the formation enthalpies of their polonides. *J. Phys. Chem. A* **2008**, *112*, 12695–12701.

CHAPTER 4: MOLECULAR FATE OF MERCURY IN HUMAN BRAIN FOLLOWING ACUTE AND CHRONIC EXPOSURE

4.1 Preface

Chapter 4 is a continuation of the research on mercury and selenium species in brain tissue samples. Here, an opportunity arose to examine human brain tissue from various exposure scenarios which have been classified herein as either acute exposure with short term survival, acute exposure with long-term survival, or chronic exposure based off of a lifetime of consuming fish and seafood which can contain high levels of organometallic mercury. As with the feline brain tissue from the previous chapter, the human brain tissue samples examined here are extremely rare and important, and the opportunity to examine them was an invaluable opportunity. Given that both inorganic and organic mercury remained in the tissue of Cat 717, similar results were expected from these tissue samples, although perhaps with more inorganic mercury species as the brain of some of the following individuals had longer periods of time for defensive, demethylation mechanisms to take place. As well, questions were raised in Chapter 3 regarding potential changes in chemical form due to preservation method. Access to human brain tissue samples which were both frozen and fixed allowed for the opportunity to explore this further.

HERFD-XAS was used to investigate human brain tissue samples for mercury and selenium species in individuals who had experienced differing exposure conditions to organometallic mercury species. The results of this work showed, for the first time, that the chemical species of mercury is different when an individual is chronically exposed compared to acutely exposed. Mercury species in chronically exposed individuals remained organometallic in nature, while acutely exposed individuals had mercury primarily in inorganic forms, with small contributions from organometallic mercury compounds.

This chapter is currently being prepared for submission to *Environmental Science and Technology.*

James, A.K., Dolgova, N.V., Nehzati, S., Korbas, M., Cotelesage, J.J.H., Sokaras, D., Kroll, T., O'Donoghue, J.L., Watson, G.E., Myers, G.J., Pickering, I.J., George, G.N. Molecular fate of mercury in human brain following acute and chronic exposure.

A.K. James analyzed HERFD-XAS data and assisted in drafting the manuscript.

N.V. Dolgova collected and analyzed HERFD-XAS data and assisted in drafting the manuscript.

S. Nehzati collected HERFD-XAS data and edited the manuscript.

M. Korbas collected the X-ray fluorescence image.

J.J.H. Cotelesage assisted with HERFD-XAS data collection.

D. Sokaras and T. Kroll configured the HERFD-XAS beamline for the experiment.

J.L. O'Donoghue, G. Watson, and G.J. Myers provided the tissue samples and provided scientific input to the manuscript.

I.J. Pickering and G.N. George provided valuable scientific input, most especially with the chemistry aspects, and guidance, and provided funding for the research. G.N. George assisted in fitting the HERFD-XAS data. I.J. Pickering and G.N. George assisted in drafting the manuscript.

4.2 Abstract

Exposures of human populations to organometallic mercury compounds have been known to occur both historically and in present day. While acute toxicities have often been subject to great scientific and public interest, it is likely that the most common exposure of humans to organomercury occurs through chronic, low-level exposures. Numerous large-scale studies have focussed on the risks of chronic mercury exposure with conflicting results. Here, we examined human brain tissue samples from both acute and chronic organometallic mercury exposures using the advanced technologies of synchrotron high-energy resolution fluorescence detection X-ray absorption spectroscopy (HERFD-XAS). Unexpectedly, mercury speciation in brain tissue was revealed to have remained organic in nature in chronic exposures compared to acute exposures which contained inorganic mercury compounds with small contributions from organometallic mercury. Demethylation processes in brain tissue are discussed and considerations are made regarding stability of mercury and selenium ligands in cryopreserved and formalin-fixed tissues.

4.3 Introduction

Mercury is widely considered to be a deadly poison, with some amongst its compounds being more toxic than those of any other non-radioactive heavy element. Despite this toxicity, there is widespread and increasing environmental and human mercury exposure, with anthropogenic mercury pollution giving rise to 2-3 fold increased ocean surface levels,[1] and consequent estimated recent increases in human consumption of ~38%.[2] Mercury is listed by the World Health Organization amongst its top ten chemical health concerns,[3] and more than 100 nations have signed the *Minamata Convention* which is aimed at reducing anthropogenic mercury emissions.[4]

The toxic properties of inorganic and organometallic forms of mercury are remarkably different [5–7] with the detailed toxicology of each depending upon the exact chemical speciation.[8] The dreadful consequences of poisoning with organometallic mercury compounds are demonstrated explicitly by large-scale catastrophic acute poisonings that have occurred in Japan and in Iraq.[9] These tragic incidents revealed a debilitating neurotoxicity, which was particularly pronounced in fetuses and young children.[5,9–12] Organometallic mercury forms can typically cross both the blood brain barrier and the placenta. While adults may be severely impacted by exposure, their effects on the developing fetus can be devastating, resulting in microcephaly, cerebral palsy, seizures, mental retardation, blindness, paralysis and other very severe consequences.[5,6,9,10] The extreme toxicity of organometallic mercury to vertebrate fetuses was unknown until the Minamata mass-poisoning, where many severely handicapped children were born to relatively healthy mothers.[12] The numerous additional consequences of mercury poisoning include central nervous system defects, arrhythmias and cardiomyopathies, and kidney damage.[5,6,9,10] Mercury can also act as either an immunostimulant or an immunosuppressant, depending on the nature of the exposure, leading to a number of pathologic consequences.[5,6,9,10] One of the most perplexing phenomena in the toxicology of methylmercury species is that there can be significant latency between administration and onset of toxic symptoms,[13] which in humans can be as long as 150 days.[14] The causes of this latency remain as a major unanswered question in this field, and while a number of possible mechanisms have been suggested,[13] with recent work additionally suggesting a possible role for thyroid metabolism,[15] at present the reasons for the latency remain unclear.

While acute mercury exposures are of substantial concern when they do occur, most human exposure would be better described as chronic low-level exposure. Sources of chronic human exposure include dental amalgams, as well as food consumption of marine fish and other seafood, which naturally contains varying levels of methylmercury.[16,17] Current limits for human consumption of fish-borne mercury have been set in large part by referencing studies of human populations with high dietary mercury from seafood consumption. Three such studies are noteworthy, one based in the Faeroe Islands of the North Atlantic,[18] a second in the Seychelles Islands of the Indian Ocean[19,20] and the third in New Zealand.[7] Pilot whale consumption is the primary mercury source in the Faeroes study; traditional food includes both whale meat and rendered blubber, with the blubber containing high levels of polychlorinated biphenyls and dioxins,[21] plus other potentially toxic metals such as Cd.[22] In the New Zealand study the source was mostly shark skeletal muscle (prepared as "fish and chips"), [7] while in the Seychelles the source was marine fish with mercury levels similar to those consumed in North America and Europe. In all the studies, a cohort of pregnant women was evaluated for prenatal Hg exposure, with their children's development examined at varying ages for neuro-developmental deficits. The studies reach different conclusions regarding the hazards of Hg exposure from seafood consumption. The Faeroes study reported statistically significant adverse effects and has been the basis for US fish consumption advisories, whereas the New Zealand study was inconclusive, and the Seychelles study showed no substantial adverse effects.

It is increasingly realized that the pathophysiology of mercury toxicity and the biochemistry of selenium are inextricably linked.[15,17,23–28] Ralston and co-workers have put forward what has been called the selenium depletion hypothesis to explain mercury's toxic effects,[29] suggesting that inhibition of essential selenoenzymes is a primary mechanism of methylmercury's toxicity, and such inhibition has been shown to occur, at least *in vitro*.[30] Ralston et al. have boldly stated that consuming high-mercury fish is not only safe but beneficial, providing that the selenium content exceeds the mercury content.[31] However, some caution may be justified because the relationship between mercury and selenium is far from simple, and selenium can present either an antagonistic relationship, negating mercury toxicity,[15,23] or a synergistic relationship in which mercury's toxic effects are magnified in the presence of selenium,[15] with the effect changing depending upon chemical form and upon the order in which mercury and selenium are given.[15]

In previous work we have used conventional X-ray absorption spectroscopy (XAS) to examine brain tissue from individuals having different types of exposure, including tissues from chronic low-level and acute methylmercury exposure (poisoning).[24] Recently, high energy resolution X-ray fluorescence detection XAS (HERFD-XAS) has been exploited at both the Se K-edge[32,33] and the Hg L_{III} edge.[27,30,33] Here we use Hg Lα1 and Se Kα1 HERFD-XAS to probe mercury and selenium speciation in human brain tissue samples. We compare the results for individuals exposed to mercury through a lifetime of fish consumption, with the results for individuals exposed through poisoning with organometallic mercury compounds. Our results give insights into the molecular fates of mercury under conditions of chronic and acute exposure, and have relevance to guidelines on the human consumption of marine fish.

4.4 Materials and Methods

4.4.1 Sample preparation

Chemicals and reagents were purchased from Sigma-Aldrich (Oakville, Ontario, Canada) and were of the highest quality available. Solutions of standard compounds were prepared as previously described.[32–35] Tissue samples were loaded into 2 mm thick poly-acetal cuvettes closed with a metal-free polyimide "Kapton" adhesive tape window, and then frozen by immersion into a partly-frozen isopentane slurry with a temperature of approximately 120 K. The samples were transported and stored at liquid nitrogen temperatures, or in a –80°C freezer, until data acquisition. Solid standards were prepared as finely ground powders, which were mixed with boron nitride diluent so that they contained <1 wt.% mercury or selenium, and were packed into 1 mm thick aluminum plates which were sealed on either side with polyimide adhesive tape.

4.4.2 X-ray spectroscopy (XAS)

X-ray spectroscopy experiments were carried out at Stanford Synchrotron Radiation Lightsource (SSRL) with the SPEAR3 storage ring containing 500 mA at 3.0 GeV. Standard X-ray absorption spectroscopy (XAS) measurements used beamline 7-3 while high energy resolution fluorescence detected (HERFD) XAS experiments used beamline 6-2. On both beamlines in-hutch photon shutters were employed to prevent exposure of the sample to the X-ray beam when data were not being actively recorded. Samples were maintained at a temperature of 10 K using a helium flow cryostat (Oxford instruments, Abingdon, UK) and were mounted at an angle of 45° to the incident X-ray beam. The incident beam energies were calibrated with reference to the lowest-energy inflection of Hg-Sn amalgam foil for the Hg L_{III} edge, or a grey

hexagonal selenium foil for the Se K-edge, values for which were assumed to be 12284.0 eV and 12658.0 eV, respectively.

On 7-3 a Si(220) double crystal monochromator was used for the incident beam, with harmonic rejection accomplished by detuning the monochromator to 60% of peak intensity. Incident and transmitted X-rays were monitored using nitrogen-filled gas ionization chambers, while X-ray absorption was measured as the Hg Lα12 or Se Kα12 fluorescence excitation spectrum using an array of 30 germanium detectors (Canberra Ltd. Meriden, Connecticut, USA).[36] In order to maintain detector count-rates in the pseudo-linear regime, Ga_2O_3 and elemental arsenic X-ray filters were employed for Hg L_{III} and Se K-edge XAS respectively, to preferentially absorb scattered radiation, together with silver Soller slits (EXAFS Co., Pioche, Nevada, USA) to reject filter fluorescence. Data were collected using the XAS Collect data acquisition software.[37]

On 6-2 a Si(311) double crystal monochromator was used for the incident beam with harmonic rejection achieved through the cut-off energy (*ca*. 18 keV) of an upstream Rh-coated mirror. Incident and transmitted X-rays were monitored using gas ionization chambers filled with helium and nitrogen, respectively. High resolution X-ray fluorescence was measured by means of a 7-element array of spherically bent crystal analyzers, using Si(555) and Si(844) crystals[38] to select a very narrow energy band of the Hg Lα1 or Se Kα1 emission, respectively. The emission intensity was measured using a single-element silicon drift detector (Hitachi High-Technologies Science America Inc., Northridge, CA, USA). Aluminum filters upstream of the incident ion chamber were used to adjust the incident X-ray flux and to maintain the detector count-rates in the pseudo-linear regime for the most concentrated samples. Data were collected using the SPEC data acquisition software (Certified Scientific Software, Cambridge, Massachusetts, USA).

Data reduction and analysis were carried out as previously described[32,39] using the EXAFSPAK suite of computer programs.[40] Extended X-ray absorption fine structure (EXAFS) phase and amplitude functions were calculated using the program FEFF.[41,42] Data normalization was carried out using the EXAFSPAK program BACKSUB,[32] which employs tabulated X-ray cross sections.[43]

4.4.3 X-ray fluorescence imaging (XFI)

XFI experiments[44] were conducted on using the Advanced Photon Source Beamline 2-ID-D employing a Si(111) double crystal monochromator and using Fresnel zone plates (Xradia, Pleasanton, CA) to generate a micro-focused X-ray beam. An incident X-ray energy of 13450 eV

was used, which is below Br K-edge to avoid Br X-ray fluorescence from plastic components of the experimental setup. X-ray fluorescence was monitored using silicon-drift Vortex® detectors (Hitachi High-Technologies Science America Inc., Northridge, CA, USA). XFI data reduction and analysis followed established practices.[44]

4.4.4 Density functional theory (DFT) calculations

DFT geometry optimizations and energy calculations were carried out using DMol^3 and Biovia Materials Studio Version 2018 R1[45,46] using the meta-GGA approximation employing the M11-L functional both for the potential during the self-consistent field procedure, and for the energy.[47] DMol^3 double numerical basis sets included polarization functions for all atoms with all-electron relativistic core treatments.

4.4.5 Summary of tissue samples

Table 4.1 summarizes background information on the samples examined in the present study. Samples A–D originated from individuals who were lifetime residents of the Republic of Seychelles, where marine fish forms a large part of the normal diet. Samples A and B were from the same individual. None of these Seychellois suffered any known adverse effects attributable to the mercury in their diets. Samples E and F were from a 48 year old woman who died 10 months after accidental skin contact with an unknown volume of dimethylmercury in a research laboratory.[14,48]Sample G came from the daughter of a hog-farmer who as an 8-year old had eaten pork from an animal that had been given hog-feed that was contaminated with high levels of a methylmercury species.[49,50] She survived a further 21 years, but in a severely debilitated state, eventually succumbing to her poisoning.[51] Samples H and I originated from residents of Rochester, New York who had no known exposures to mercury.

4.5 Results and Discussion

4.5.1 HERFD-XAS nomenclature

The HERFD method depends upon measurement of the X-ray fluorescence with narrower energy resolution than the natural fluorescence linewidth, the lines of choice being the Se Kα1 and the Hg Lα1 for the Se K and Hg L_{III} edges, respectively. Here we use the nomenclature Se Kα1 and Hg Lα1 HERFD-XAS, rather than Se K-edge and Hg L_{III}-edge, because different fluorescence lines can in principle be used to record the HERFD-XAS for a given edge; for example, Swarbrick et al.[52] used the Pb Lβ5 line, rather than the Pb Lα1, to examine the Pb L_{III}

HERFD-XAS of lead species. Since the Hg Lα1 can only be used to record the Hg L_{III} HERFD-XAS, the nomenclature specifying the fluorescence line is more specific.

Sources of spectroscopic broadening in XAS experiments include the resolving power of the X-ray monochromator, but with conventional hard-X-ray XAS measurements the most substantial source of broadening typically arises from the short lifetime of the Se 1s or Hg $2p_{3/2}$ core-hole which is created by the primary X-ray photoexcitation. The energy resolution of HERFD-XAS is instead partly governed by the substantially longer lifetime of the hole created upon decay of an outer electron to fill the initial core hole, with concomitant emission of an X-ray fluorescent photon. HERFD-XAS probes the diagonal of what is known as the resonant inelastic X-ray scattering (RIXS) plane and shows dramatically improved energy resolution over conventional XAS. It has been called high-resolution XAS (HR-XAS), although strictly speaking this is inaccurate unless there are no off-diagonal RIXS contributions.[53] Fig. 4.1 shows an example of Hg Lα1 HERFD-XAS in comparison with conventional Hg L_{III}-edge XAS for a 1 mM frozen solution of dimethylmercury in propane-2-ol. The dramatic improvement in spectroscopic resolution beyond conventional XAS that is afforded by HERFD-XAS is immediately apparent. In particular, the lowest energy transition presents as a poorly resolved shoulder in the XAS but becomes a well-resolved prominent peak in the HERFD-XAS.

4.5.2 Sources of exposure

The data presented in the current study derive from samples representing three fundamentally different organometallic mercury exposure conditions. These are *chronic long-term low-level exposure*, *acute exposure with long-term survival* and *acute exposure with shorter-term survival*. The first category are Seychellois who were exposed to methylmercury, probably in the form of methylmercury-L-cysteinate,[16] from lifetime consumption of marine fish which form the primary dietary protein source for this population. While most marine fish typically contain substantial quantities of methylmercury bound to a thiolate donor,[16] recent reports show that blue marlin, a large predatory species, may contain predominantly inorganic mercury, in the form of mercuric selenide,[54] which is bio-unavailable because of its low solubility.

For the two acute exposures, we note that the organometallic mercury compounds to which the individuals were exposed differ, as does the time of survival following exposure. In the New Mexico poisoning of sample G, corresponding to *acute exposure with long-term survival*,

Table 4.1: Background information on brain tissue samples.

Sample	*Tissue*	*Gender*	*Age*	*Origin*	*Condition*	Hg [a]	Se [a]
A	Cerebellum [b]	M	67	Seychelles	frozen	0.80	5.0
B	Cerebellum [b]	M	67	Seychelles	formalin	0.51	1.8
C	Cerebellum [c]	M	67	Seychelles	frozen	0.42	5.7
D	Cerebellum [c]	M	67	Seychelles	formalin	0.23	2.9
E	Cerebellum [d]	F	48	Dartmouth	formalin	30.9	10.8–37.0
F	Cerebral Cortex [d]	F	48	Dartmouth	paraffin	59.0	9.5–44.0
G	Cerebral Cortex	F	29	New Mexico	paraffin	19.7	23.0–70.0
H	Cerebellum	F	57	Rochester	formalin	–	3.6
I	Cerebellum	F	57	Rochester	paraffin	–	6.0

a. Local levels of areas that were scanned spectroscopically, given in units of effective μM concentration, and estimated from the measured edge-jump.[33]

b. Samples were from the same individual.

c. Samples were from the same individual.

d. Samples were from the same individual.

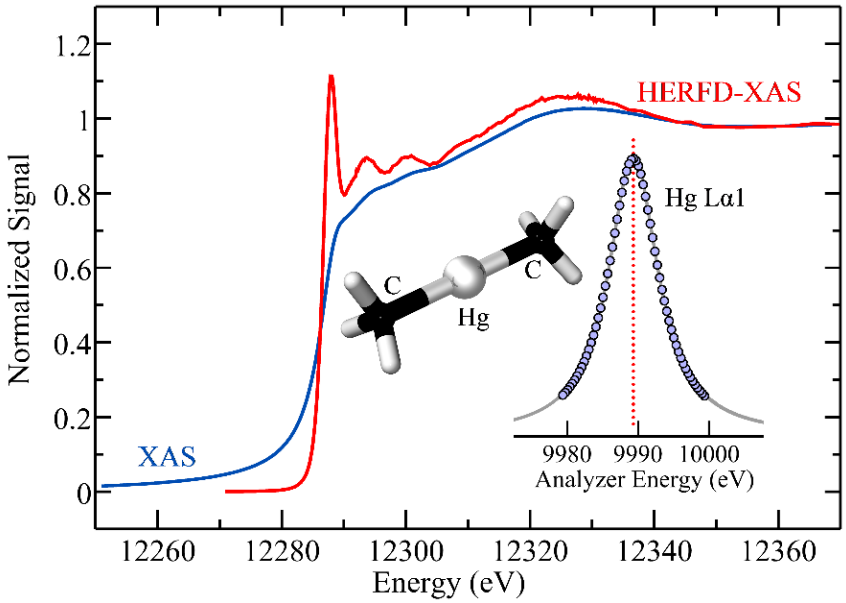

Figure 4.1: Hg Lα1 HERFD-XAS (red line) and Hg L_{III} XAS (blue line) of dimethylmercury. The insets show the structure of dimethylmercury (left) and Hg Lα1 emission (right) with the experimental spectrum (blue points) measured at the non-resonant excitation energy of 12 800 eV, together with a Lorentzian peak fit (gray line) showing the centroid energy selected for recording the HERFD-XAS.

methylmercury in the form of contaminated pig tissues were consumed. Unaware of the presence of deadly mercury compounds, a hog-farmer had fed his pigs grain dusted with the fungicide Panogen®, which is methylmercury cyanoguanidine (also known as methylmercury dicyanamide). One month later, one pig was slaughtered, presumably during the latency period where no toxic signs were in evidence, and was consumed by the farmer's family over a period of three months.[51] Various degrees of intoxication amongst family members became evident in the following month, approximately four months after the poisoned pork was first consumed.[51] Methylmercury cyanoguanidine has never been structurally characterized, but likely structures are those in which the $CH_3Hg–$ group is bound to one of the nitrogens of the guanidinium moiety, or to the nitrogen of the cyanide group. In either case the cyanoguanidine is expected to dissociate from the methylmercury *in vivo*, and to be rapidly replaced by a thiolate donor from abundant extracellular or intracellular thiols, most probably L-cysteine, to form compounds containing the $CH_3Hg–S$(L-Cys) linkage.

The Dartmouth poisoning (samples E and F), *acute exposure with shorter-term survival*, originated through skin absorption of an unknown volume of dimethylmercury in a research laboratory. A researcher was preparing a ^{199}Hg NMR standard, following approved safety guidelines, when she inadvertently spilled dimethylmercury upon the dorsum of her latex-gloved hand. While the popular scientific press has proliferated the notion that this spill comprised only a few drops,[55] the high mercury content of the tissues[14] would suggest a higher dose, perhaps more than 0.5 grams. Following exposure, unaware that she had assumed a lethal dose of mercury, the researcher went about her normal activities. After approximately 3 months, she began to experience weight loss, and at approximately 5 months developed rapidly worsening neurological symptoms. She received aggressive treatment with meso-dimercaptosuccininc acid, which acts to sequester Hg(II) as a monothiolate,[56] but died approximately 10 months after the initial exposure.[14] Dimethylmercury is a highly volatile compound, and is also a hydrophobic entity with an octanol-water partition coefficient K_{OW} of 200,[57] (compare K_{OW} for CH_3HgOH of 0.07[58]). Because of this, once internalized, it would be expected to cross cell membranes with ease and to partition into lipid-rich tissues. It is much more stable than other group 12 organometallics to water, but nonetheless will readily undergo protonolysis in aqueous media to form mono-methylmercury derivatives and methane.[59,60]

According to the elegant studies reported by Östlund,[61] mice injected with dimethylmercury labelled with ^{203}Hg rapidly exhaled 80-90% of the dose administered, and while no detectable dimethylmercury was found to be present after 16 hours, mono-methylmercury species were distributed in the tissues of the mice.[61] Östlund used autoradiography to investigate ^{203}Hg spatial distributions;[61] shortly after dimethylmercury injection the majority of the ^{203}Hg was present in fatty tissues, with very little in the central nervous systems or in the placenta of pregnant mice, until at four days after injection an increase in the central nervous system was observed.[61] Interestingly, at four days, the fetus of pregnant mice showed a marked uptake in the eye lens,[61] reminiscent of that observed for larval stage zebrafish.[8,62–64]

These results caused Östlund to conclude that "dimethyl mercury behaves as a chemically inert substance towards animal tissues" with toxic effects arising from degradation into other compounds.[61] This conclusion is chemically reasonable, as dimethylmercury itself is essentially coordinatively satisfied, and while it can form weak bonds with hard ligands,[65] it lacks the distinguishing affinity for chalcogenides that defines much of mercury chemistry. Overall, the evidence clearly indicates that protonolysis of one of the two C–Hg bonds of dimethylmercury had occurred in Östlund's mice mostly between 4 and 16 hours after injection. The same process seems probable to have occurred in the Dartmouth poisoning.

4.5.3 The molecular form of mercury in brain with different exposures

As we describe above, the two acute exposures were initially to quite different organometallic mercury compounds, and differences in localization might be expected in the hours following exposure, and (before dimethylmercury protonolysis). However, it seems likely that similar mono-methylmercury intoxication was ultimately responsible for the deaths in both acute cases. Fig. 4.2 compares the Hg Lα1 HERFD-XAS of samples A&B (combined), E, F and G. Sample AB represents chronic long-term exposure, E and F severe poisoning with survival of 10 months, and G severe poisoning with more protracted survival of 21 years. Linear-combination fitting of the A and B data shows that the mercury in the chronic exposure is present essentially exclusively in an organometallic form, with the CH_3Hg moiety coordinated to sulfur, most likely a cysteine thiolate as a CH_3Hg–S(L-Cys). An example of linear combination analyses is shown in Fig. 4.3. In contrast to A and B, samples E, F, and G show more complex mixtures of species (Table 4.2) including species of mercuric selenide and inorganic mercury bound to two

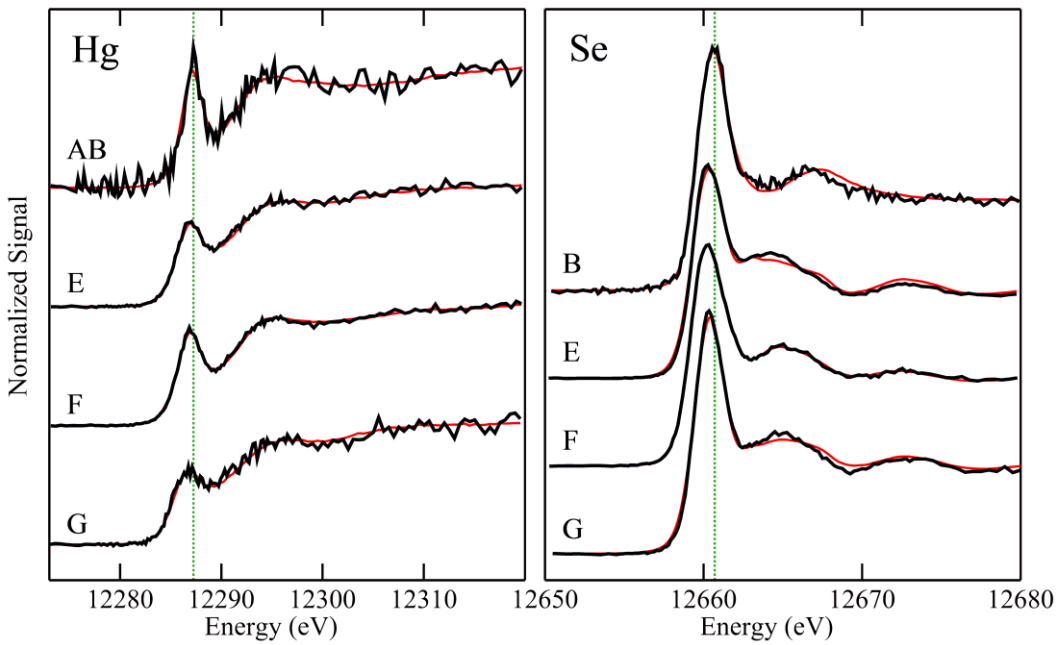

Figure 4.2: Hg Lα1 (left) and Se Kα1 (right) HERFD-XAS of brain tissue samples. Sample AB is the weighted average of the two data sets A and B. Sample details are given in Table 4.1. The black lines show experimental data, and the red lines show linear combination analyses according to the details given in Table 4.2. Green vertical broken lines are included to emphasize energy shifts in the spectra.

Table 4.2: Hg and Se linear combination speciation analysis.

	% mercury species		
Sample	HgSe	RS–Hg–SR	RS–Hg–CH_3
A+B	–	–	100 ± 1
E	45 ± 2 *nano*	29 ± 3	26 ± 2
F	18 ± 1 *solid*	49 ± 2	33 ± 2
G	61 ± 5 *nano*	34 ± 7	5 ± 4

	% selenium species				
Sample	HgSe	R–Se–R'	RS–Se–SR	R–Se–SR	oxidized Se
A	–	48 ± 3	34 ± 4	15 ± 8	3 ± 2
B	–	44 ± 1	25 ± 1	21 ± 3	10 ± 1
C	–	32 ± 2	24 ± 2	37 ± 4	7 ± 1
D	–	26 ± 2	7 ± 2	58 ± 3	9 ± 1
E	57 ± 2 *solid*	17 ± 1	11 ± 1	9 ± 3	6 ± 1
F	59 ± 1 *nano*	20 ± 1	11 ± 1	7 ± 1	3 ± 1
G	49 ± 2 *solid*	26 ± 1	21 ± 1	–	4 ± 1
H	–	67 ± 3	16 ± 2	–	17 ± 2
I	–	73 ± 4	6 ± 4	14 ± 8	7 ± 2

Percent contributions of each component in the fit, ± estimated standard deviations obtained from the diagonal of the variance-covariance matrix. For HgSe, both crystalline (*solid*) and nano-particulate (*nano*) forms were separately tested in fits of each sample, with the form giving the best fit presented in the table, as indicated adjacent to the value. Additional standard spectra used were as follows: RS–Hg–SR, mercury(II)-*bis*-L-cysteinate; RS–Hg–CH_3, methylmercury-L-cysteinate; R–Se–R', L-selenomethionine; RS–Se–SR, selenium-*bis*-S-glutathione; R–Se–SR, selenocysteine-cysteine selanylsulfide; oxidized Se, $[(CH_3)Se]^+$ as a generic oxidized selenium form, with floating energy shift in refinement.

sulfurs. The appearance of these species is addressed below. Dimethylmercury shows a highly distinctive spectrum (Fig. 4.1) and, as expected, both samples E and F gave zero fractions of this species when it was included in linear combination fits (not illustrated).

4.5.4 Mercuric selenide species

For samples E, F, and G (acute exposures), both the Hg Lα1 and Se Kα1 HERFD-XAS of the tissues examined clearly showed the presence of different amounts of mercuric selenide, HgSe, which has distinctive Hg Lα1 and Se Kα1 HERFD-XAS (Fig. 4.2, Fig. 4.3, Table 4.2). We have previously reported conventional XAS spectra for both crystalline and nano-particulate mercuric selenide (*nano*-HgSe), the latter exhibiting XAS spectra that are distinct from those of crystalline HgSe.[23,24] Manceau and co-workers[27] have also recently reported the Hg Lα1 HERFD-XAS of *nano*-HgSe, which is in reasonable agreement with our data. Fig. 4.4 compares the Se Kα1 and Hg Lα1 HERFD-XAS spectra of *nano*-HgSe with the conventional XAS spectra of the same samples. As expected, the HERFD-XAS spectra can be seen to be a better-resolved version of the conventional XAS, with distinctly similar spectra for crystalline and nano-particulate HgSe, but differing in the amplitudes of the post-edge structure, which is more pronounced for the crystalline material.

HgSe occurs mineralogically as Tiemannite, which has the zincblende structure; the wurtzite structure may plausibly occur in small particles,[66] although this has never been experimentally observed.[67] Both structures show four-coordinate Hg and four-coordinate Se, and are expected to be difficult to distinguish by EXAFS.[23] Naturally occurring tiemannite frequently occurs in combination with sulfur, as HgS_xSe_{1-x}, with nearly the entire range of x from β-HgS (x=1) to HgSe (x=0) having been observed.[68] Crystalline HgSe deposits have previously been identified in whale liver,[69] and we have previously identified mixed chalcogenide HgS_xSe_{1-x} nano-deposits in larval stage zebrafish treated with mercury compounds.[15,25] Our standard solution preparations of *nano*-HgSe stabilized with external glutathione linkages comprise black solutions, [23] and are approximately 100 atoms in each of Hg and Se, with a diameter of about 20 Å,[23] similar to the preparations of others.[67]

Fig. 4.5 shows high-resolution XFI data on an 8 μm thick section of cerebellum corresponding to sample G. The molecular layer, predominantly consisting of dendrites and axons derived from cells in other layers, is to the top right of the section, visible as the region that

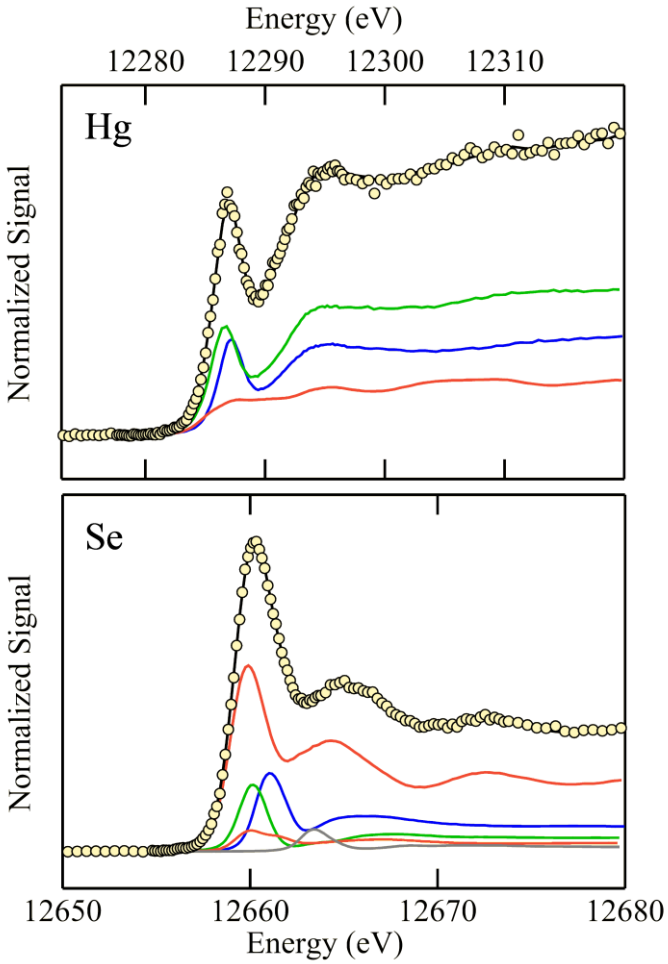

Figure 4.3: Example linear combination analyses for brain tissue sample F (Table 4.1), showing Hg Lα1 (top) and Se Kα1 (bottom) HERFD-XAS. Points indicate experimental measurements and the black lines the best fits. The colored lines beneath indicate the spectra of individual components, scaled according to their contributions. In both Hg and Se plots the red lines indicate HgSe. In the Hg plot the green and blue lines indicate mercury(II)-*bis*-thiolate and methylmercury-thiolate, respectively (Table 4.2). In the Se plot the green, blue, orange and gray indicate selenium-*bis*-S-glutathione, L-selenomethionine, selenocysteine-cysteine selanylsulfide, and oxidized Se, respectively (Table 4.2).

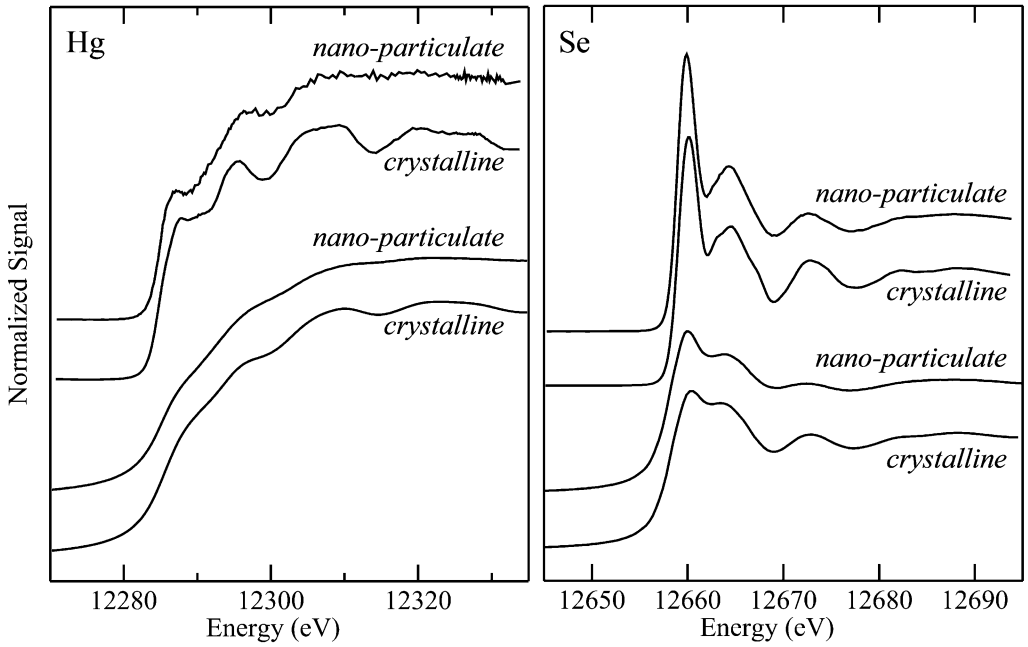

Figure 4.4: Comparison of HERFD-XAS and conventional XAS of nano-particulate and crystalline HgSe. The top pairs of spectra are the HERFD-XAS, and the bottom pairs of spectra the conventional XAS.

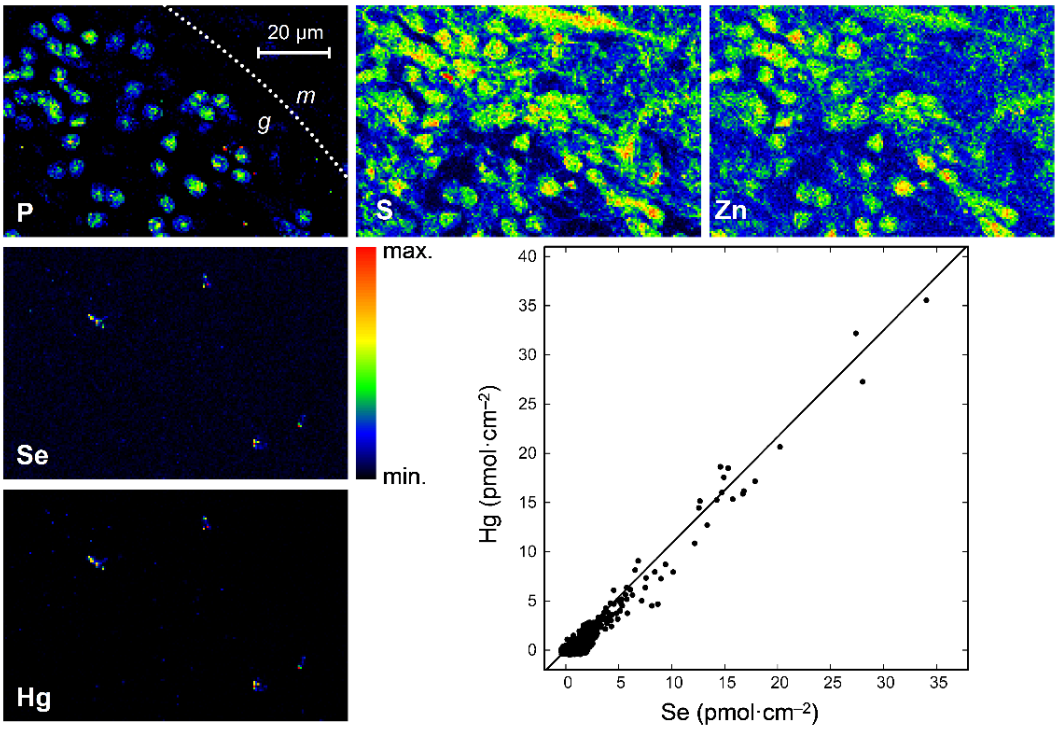

Figure 4.5: X-ray fluorescence imaging of an 8 µm thick section of cerebellar brain tissue corresponding to sample G. Maps of selected elements are shown, with maximum areal densities for P, S, Zn, Se and Hg of 42, 35, 13, 35 and 35 pmol·cm^{-2}, respectively. The minima in all the maps correspond to zero areal densities. The inset shows a correlation plot between the Hg and Se content of the image, with the best fit line shown (slope = 1.08).

is essentially devoid of nuclei. The granular layer, containing the granule cells is to the bottom right, with the cell nuclei clearly visible via their high phosphorus content. No Purkinje cells are obviously present in this section. The correlation plot (Fig. 4.5, inset) clearly shows a nearly 1:1 molar correspondence between concentrations of mercury and selenium, indicating the presence of HgSe in the sample. The spatial resolution of the experiment was 500 nm, and the observation of isolated hot-spots of Hg and Se that are approximately one pixel across suggest that clusters are smaller than this dimension. While Fig. 4.5 shows clearly discernable cell nuclei, the types of cells involved in the HgSe cannot be determined. For example, astrocytes are likely to phagocytose HgSe particles, which would then accumulate in lysosomes within these cells. It therefore seems likely that the highest levels of Fig. 4.5 may represent accumulations of several discrete HgSe particles, rather than large single isolated particles. Fig. 4.5 has discernable pixels containing both Hg and Se with areal densities[44] of 2 to 5 pmol·cm^{-2} in both Hg and Se, and if these are due to a single HgSe particle then this would correspond to a nano-particle comprised of approximately 3,000 to 7,000 atoms of both Hg and Se, which would be 60 to 80 Å in diameter.

Our previous conventional XAS EXAFS analysis,[24] also gives clues as to the size of the clusters in brain tissues. The major structural differences between the core of an HgSe nano-particle compared with crystalline material, are expected to be related to disorder in both short and long-range interatomic distances. For smaller particles, disorder is predicted to be greater and the amplitudes of long-range EXAFS contributions would be damped due to the presence of substantial static Debye-Waller factors. Thus, both crystalline and nano-particulate HgSe show intense first-shell EXAFS from four Hg–Se bonds at 2.61 Å, with outer shell features giving rise to peaks in the Fourier transform at ~4.3 Å.[24] The amplitudes in EXAFS of brain tissue samples previously studied[24] are more pronounced than for the ~$Hg_{100}Se_{100}$ *nano*-HgSe previously investigated,[23] and much less intense than those observed with crystalline HgSe. Thus, the likely size of the HgSe clusters in the brain tissue is between 80 and 20 Å. In agreement with this, we find that in some cases the *nano*-HgSe standard fits the data better, whereas in other crystalline HgSe shows better fits (Table 4.2).

4.5.5 Inorganic mercury bound to two thiolate donors

The second major component revealed by linear combination analysis of the samples derived from acute exposures is Hg(II) bound to two thiolate donors (e.g. $Hg(Cys)_2$) (Table 4.2). This was also detected using conventional XAS,[24] and indeed, it almost appears that it may be a

signature of catastrophic intoxication. We have previously shown that methylmercury compounds can coordinate the selenolate of the selenoenzyme thioredoxin reductase,[70] but thioredoxin itself has previously been suggested as a toxicological target of both inorganic and organometallic forms of mercury.[71–73] Both thioredoxin 1 and its mitochondrial counterpart thioredoxin 2 are abundant in human brain, with their active sites both containing a CXXC motif at their active sites (CPYC and CGPC in thioredoxin 1 and 2, respectively). Vertebrate tissues also contain a number of other proteins that are important in redox homeostasis that share similar CXXC active sites, such as the glutaredoxins.[74] Such active sites configurations can readily accommodate inorganic mercury as a linear digonal *bis*-thiolate complex, and it seems plausible that the $Hg(SR)_2$ present in the brain tissue samples from acute exposures might be derived from inhibited thioredoxin and other proteins with the CXXC motif *in vivo*.

4.5.6 Organometallic mercury bound to chalcogenide donors

Of the two acute cases, linear combination analysis (Table 4.2) indicated that both samples from the *acute exposure with shorter-term survival* case (E and F) contained thiolate-bound methylmercury, but at slightly different levels, 26 and 33% for cerebellum and cerebral cortex, respectively. In contrast, the sample from the *acute exposure with long-term survival* case (sample G) showed only relatively small amounts of this species, and we conclude that the sample has no detectible thiolate-bound methylmercury.

We also examined the possibility of other mercury chemical species, in particular methylmercury L-selenocysteinate,[70] which when incorporated into the linear combination fitting schemes did show subtly improved fits in some cases. As we have previously noted,[33] the Hg Lα1 HERFD-XAS spectra of methylmercury L-selenocysteinate and methylmercury L-cysteinate are very similar, but the features of the Hg Lα1 HERFD-XAS for the selenium congener are shifted slightly to lower energy.[70] Such coordination might originate through inhibition of essential selenoenzymes, and we have recently shown that methylmercury inhibits the essential selenoenzyme thioredoxin reductase through covalent binding of the selenolate of the active site selenocyteine residue.[70] Significantly, no improvements in the fitting of the chronic exposure samples were obtained when methylmercury L-selenocysteinate was incorporated in the linear combination analysis, and the improvements in fits for acute exposure samples the tended to be marginal (not illustrated), with the selenium congener replacing the methylmercury L-cysteinate. However, little correspondence was observed between fits of the Hg Lα1 and Se Kα1 HERFD-

XAS, and we conclude that the presence methylmercury L-selenocysteinate cannot be demonstrated with confidence.

4.5.7 Molecular form of selenium in brain tissues

The Se Kα1 HERFD-XAS show distinctive spectra for the low-level exposure, compared with the samples from the acute exposures. In all cases the acute exposures showed significant HgSe, as described above, whereas this was not found to be component of the chronic exposures. No other species of selenium bound to mercury could be identified with confidence in any of the samples, and the presence of HgSe may be another human indicator of catastrophic poisoning. The remainder of the selenium was modelled as a range of organic selenium species which may represent essential selenium not bound to mercury, such as in selenoenzymes. However, as we note below, such organic selenium is expected to be more strongly affected by the preservation method.

The final linear combination analyses for all samples for both Hg Lα1 and Se Kα1 HERFD-XAS are shown in Fig. 4.2 and summarized in Table 4.2. We have noted that the presence of Hg(II) bound to two thiolate donors may be a signal of poisoning. The second major form that was detected is HgSe, but this can only be benign because of its very low solubility (solubility product ~10^{-59}).[75] Any mercury present as HgSe will therefore be rendered bio-unavailable and effectively excluded from any involvement in biological processes. The third mercury form, methylmercury bound to one thiolate donor, was present in the *shorter-term survival* poisoning case, and less-pronounced in the *long-term survival* case.

4.5.8 In-vivo origins of mercuric selenide

As noted above, the relationship between selenium and mercury is complex. The toxicological antagonism between selenium and inorganic mercury in vertebrates is well-established at doses corresponding to acute exposures.[15,23] With inorganic mercury, nano-particulate HgS_xSe_{1-x} forms with endogenous selenium,[25] and mercury's toxic effects are dramatically reduced when selenium is pre-administered (as L-selenomethionine), with formation of nano-particulate HgSe, but not if the order is reversed and mercury is given before selenium.[15] With methylmercury, administration of selenium (as L-selenomethionine) magnifies the methylmercury toxicity, irrespective of the order, via an unknown mechanism.[15] Both inorganic mercury and methylmercury inhibit selenium transport, possibly by binding to the selenoprotein P transporter; selenium is depleted from tissues and levels are not restored by subsequent L-

selenomethionine treatments,[15] and thyroid metabolism, which depends upon selenoenzymes, is severely disrupted by both mercury forms.[15]

The studies of Dolgova et al.,[15] are insightful but spanned only a few days. It is clear that while conversion of methylmercury to inorganic forms occurs in the vertebrate brain, this process is relatively slow,[76] and the mechanisms by which it occurs are unclear. It has long been known that methylmercury complexes of selenium can spontaneously decompose to form HgSe. Thus, in our hands, solutions of methylmercury L-selenocysteinate,[77] are stable at high pH but near to neutral pH rapidly precipitate HgSe, as identified by powder X-ray diffraction.[24] Even the crystalline solid of methylmercury L-selenocysteinate slowly decomposes to form HgSe on storage at room temperature. The mechanism of this reaction is thought to involve two methylmercury L-selenocysteinate molecules combining to form *bis*-methylmercuric selenide $(CH_3Hg)_2Se$,[78] and *bis*-L-alanylselenide.[79] $(CH_3Hg)_2Se$ will spontaneously eliminate HgSe forming dimethylmercury,[78] and as we have discussed above, dimethylmercury will undergo spontaneous protonolysis to form methane and mono-methylmercury, which can then participate in further cycles of the reaction.[79]

A related mechanism can operate with methylmercury-L-selenocysteinate and methylmercury-L-cysteinate, which can form $(CH_3Hg)_2Se$ and *bis*-L-alanylsulfide.[79] For this mechanism to operate *in vivo*, two molecules of methylmercury L-(seleno)cysteinate would need to come into close enough proximity to react chemically. In our studies of thioredoxin reductase inhibited with methylmercury,[70] which contains methylmercury L-selenocysteineate at the active site, we have observed that the protein, unlike free methylmercury L-selenocysteineate, is stable in solution. This is probably because the protein prevents individual methylmercury L-selenocysteineate groups from coming into sufficiently close proximity to react. This bimolecular requirement may explain the slow observed rates of demethylation of methylmercury *in vivo*, if this mechanism does in fact occur to any appreciable extent.

Manceau and co-workers have suggested that methylmercury binding to multiple selenocysteine residues at the C-terminal end of selenoprotein P may cause the mercury to demethylate.[27] This is a chemically plausible suggestion, as we predict that multiple selenolate donors will increase the charge distribution across the Hg–C bond, effectively catalyzing protonolysis. The resulting inorganic complex could form a four-coordinate $[Hg(SeCys)_4]^{2-}$ core

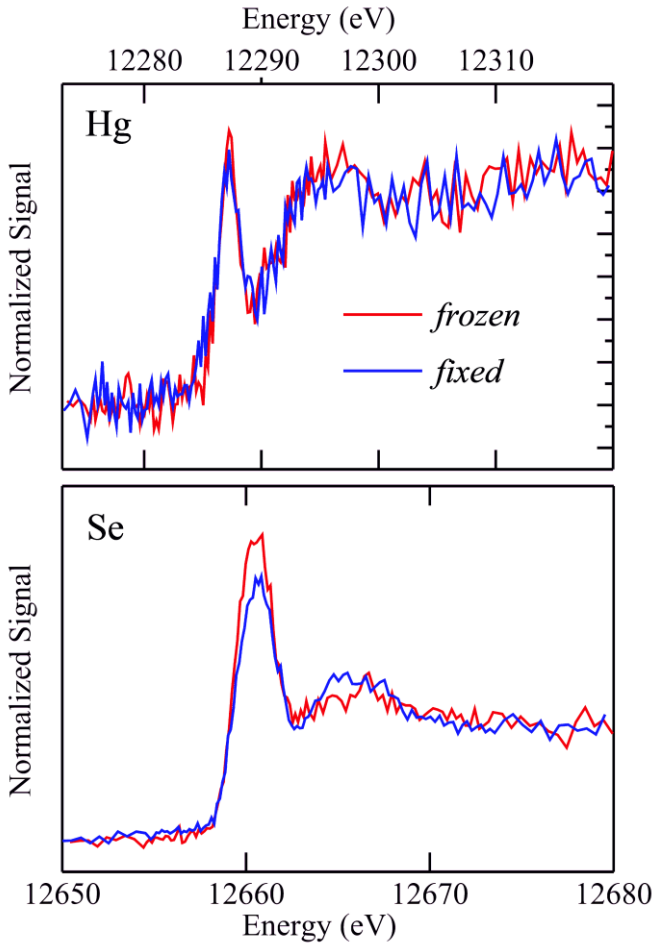

Figure 4.6: Comparison of Hg Lα1 (top; samples A and B) and Se Kα1 (bottom; samples C and D) HERFD-XAS for frozen (red) and fixed (blue) tissue.

within the protein, which might deplete essential selenium, and with time could form HgSe deposits.[27,28]

4.5.9 Comparison of speciation in fixed versus cryopreserved specimens

Our study depends upon the availability of human tissue samples, some of which are from irreproducible historical acute poisoning events and are only available as fixed samples. Our previous speciation studies[32] have been criticized as lacking relevance because of possible chemical changes caused by fixation, and in particular that the mercury content will be lost to the formalin fixative.[80] While this has already been extensively discussed,[32,81] here we compare frozen and formalin fixed tissues taken from the same individual, samples A and B. Fig. 4.6 compares Hg Lα1 and Se Kα1 HERFD-XAS of two pairs of cerebellum samples taken from two different individuals; one sample from each individual was fixed in formalin as per normal medical practice, while the other was frozen and stored at –80°C. Concentrations are low, particularly for mercury, but within the noise the observed spectra show no observable changes for mercury. The selenium Se Kα1 HERFD-XAS, however, shows distinctive differences between fixed and frozen samples. This finding is in agreement with our earlier discussions.[32]

Commercial formalin fixative solutions consist of aqueous formaldehyde (HCHO) with some methanol (CH_3OH) which serves to inhibit formaldehyde polymerization that would otherwise precipitate as paraformaldehyde over time. Because of its low molecular weight and solubility in both lipid and aqueous phases, formaldehyde will diffuse rapidly throughout tissue samples, and will serve to fix the sample through cross-linking of proteins. Previous work has shown that fixation in formalin will dramatically alter the distributions of soluble tissue components such as Cl^- and K^+.[82] As we have previously discussed[32] compounds of mercury are likely to be chemically stable to exposure to formaldehyde. Similarly, selenium present as the insoluble and inert HgSe is unlikely to be affected in either localization or chemical form by exposure to formaldehyde. However, organo-selenium compounds such as selenocysteine are expected to react with formaldehyde to form selanylmethanol derivatives, which in turn may cyclize by reacting with amino groups.[32] Using the edge jump of the HERFD-XAS as an indicator of concentration we find similar mercury levels in the two samples, with the fixed tissue at 0.80 μM and the frozen slightly lower at 0.51 μM. The fact that the frozen sample showed lower concentrations than the fixed sample is probably due to the fact that different physical regions were necessarily studied. This result is consistent both with our earlier discussions,[32,33,82]

and with the findings of others indicating that mercury is not lost from tissues into formalin-based fixative solutions.[83]

The work presented here shows that the molecular-level fates of methylmercury compounds differ remarkably between chronic low-level long-term exposure and acute poisoning. With acute exposure we find that the relationship with selenium appears to be very important, with formation of biologically inert nano-particulate HgSe deposits, and occurrence of Hg(II)-*bis*-thiolate complexes, which may be a marker for methylmercury poisoning. In contrast, the chemical form of mercury in chronic low-level methylmercury exposure, from marine fish consumption with no evident adverse effects, remains essentially unchanged from that observed for marine fish. The implications of this finding are that mechanistic studies involving acute exposures of animal models may have little or no relevance to the vast majority of human exposure to methylmercury, which is chronic low-level in nature, and derives from consumption of marine fish.

4.6 Acknowledgements

We acknowledge grant support from the Natural Sciences and Engineering Research Council of Canada (NSERC; IJP and GNG), the Canada Foundation for Innovation (CFI; IJP), John Evans Leader's Fund award (IJP) and Canada Research Chairs (IJP and GNG). SN acknowledges a Dr. Rui Feng Scholarship; AKJ and SN were Fellows and NVD an Associate in the Canadian Institutes of Health Research (CIHR)-Training grant in Health Research Using Synchrotron Techniques (THRUST). The Canadian Light Source, a national research facility of the University of Saskatchewan, is supported by the CFI, NSERC, the National Research Council (NRC), CIHR, the Government of Saskatchewan, and the University of Saskatchewan. Use of the Stanford Synchrotron Radiation Lightsource, SLAC National Accelerator Laboratory, is supported by the U.S. Department of Energy, Office of Science, Office of Basic Energy Sciences under Contract No. DE-AC02-76SF00515. The SSRL Structural Molecular Biology Program is supported by the DOE Office of Biological and Environmental Research, and by the National Institutes of Health, National Institute of General Medical Sciences (including P41GM103393). The contents of this publication are solely the responsibility of the authors and do not necessarily represent the official views of NIGMS or NIH. This research used resources of the Advanced Photon Source, an Office of Science User Facility operated for the U.S. Department of Energy (DOE) Office of Science by Argonne National Laboratory, and was supported by the U.S. DOE under Contract No. DE-AC02-06CH11357, and the Canadian Light Source (CLS) and its funding partners.

4.7 References

(1) Lamborg, C. H., Hammerschmidt, C. R., Bowman, K. L., Swarr, G. J., Munson, K. M., Ohnemus, D. C., Lam, P. J., Heimbürger, L.-E., Rijkenberg, M. J. A., Saito, M. A. A global ocean inventory of anthropogenic mercury based on water column measurements. *Nature* **2014**, *512*, 65–68.

(2) Lavoie, R. A., Bouffard, A., Maranger, R., Amyot, M. Mercury transport and human exposure from global marine fisheries. *Sci. Rep*. **2018**, *8*, 6705/1–9.

(3) WHO. Mercury and Health: Key Facts; https://www.who.int/en/news-room/fact-sheets/detail/mercury-and-health.

(4) UNEP. Minamata Convention on Mercury; United Nations Environment Programme: Geneve, Switzerland, 2013.

(5) Clarkson, T. W.; Magos, L.; Myers, G. J. The toxicology of mercury – current exposures and clinical manifestations. *N. Engl. J. Med.* **2003**, *349*, 1731–1737.

(6) Clarkson, T. W., Magos, L. The toxicology of mercury and its chemical compounds. *Crit. Rev. Toxicol.* **2006**, *36*, 609–662.

(7) Goyer, R. A., Aposhian, H. V., Arab, L., Bellinger, D. C., Burbacher, T. M. Toxicological effects of methylmercury. National Research Council, National Academy Press, Washington DC, 2000.

(8) Korbas, M., MacDonald, T. C., Pickering, I. J., George, G. N., Krone, P. H. Chemical form matters: differential accumulation of mercury following inorganic and organic mercury exposures in zebrafish larvae. *ACS Chem. Biol.* **2012**, *7*, 411–420.

(9) Clarkson, T. W. Human toxicology of mercury. *J. Tr. Elem. Exp. Med.* **1998**, *11*, 303–317.

(10) Clarkson, T. W. The three modern faces of mercury. *Env. Health Persp.* **2002**, *110*, 11–23.

(11) Tchounwou, P. B., Ayensu, W. K., Ninashvili, N., Sutton, D. Environmental exposure to mercury and its toxicopathologic implications for public health. *Env. Toxicol.* **2003**, *18*, 149–175.

(12) Harada, M. Minamata disease: methylmercury poisoning in Japan caused by environmental pollution. *Crit. Rev. Toxicol.* **1995**, *25*, 1–24.

(13) Weiss, B., Clarkson, T. W., Simon, W. Silent latency periods in methylmercury poisoning and in neurodegenerative disease. *Env. Health Persp*. **2002**, *110* (suppl. 5), 851–854.

(14) Nierenberg, D. W., Nordgren, R. E., Chang, M. B., Siegler, R. W., Blayney, M. B., Hochberg, F., Toribara, T. Y., Crenichiari, E., Clarkson, T. Delayed cerebellar disease and death after accidental exposure to dimethylmercury. *New England J. Med.* **1998**, *338*, 1672–1676.

(15) Dolgova, N.V., Nehzati, S., MacDonald, T.C., Summers, K.L., Crawford, A.M., Krone, P.H., George, G.N., Pickering, I.J. Disruption of selenium transport and function is a major contributor to mercury toxicity in zebrafish larvae. *Metallomics* **2019**, *11*, 621–631.

(16) Harris, H. H., Pickering, I. J., George, G. N. The chemical form of mercury in fish. *Science* **2003**, *381*, 1203.

(17) George, G. N., Singh, S. P., Prince, R. C., Pickering, I. J. The chemical forms of mercury and selenium in fish following digestion with simulated gastric fluid. *Chem. Res. Toxicol.* **2008**, *21*, 2106–2110.

(18) Choi A. L., Grandjean, P. Methylmercury exposure and health effects in humans. *Environ. Chem*. **2008**, *5*, 112–120.

(19) Myers, G. J., Thurston, S. W., Pearson, A. T., Davidson, P. W., Cox, C., Shamlaye, C. F., Cernichiari, E., Clarkson, T. W. Postnatal exposure to methyl mercury from fish consumption: A review and new data from the Seychelles child development study *NeuroToxicol*. **2009**, *30*, 338–349.

(20) van Wijngaarden, E., Thurston, S. W., Myers, G. J., Harrington, D., Cory-Slechta, D. A., Strain, J. J., Watson, G. E., Zareba, G., Love, T., Henderson, J., Shamlaye, C. F., Davidson, P. W. Methyl mercury exposure and neurodevelopmental outcomes in the Seychelles Child Development Study Main cohort at age 22 and 24 years. *Neurotoxicol. Teratol*. **2017**, *59*, 35–42.

(21) Needham, L. L., Grandjean, P., Heinzow, B., Jørgensen, P. J., Nielsen, F., Patterson, Jr. D. G., Sjdin, A., Turner, W. E., Weih, P. Partition of environmental chemicals between maternal and fetal blood and tissues. *Environ. Sci. Technol.* **2011**, *45*, 1121–1126.

(22) Andersen, A., Julshamn, K., Ringdal, O., Moerkoere, J. Trace elements intake in the Faroe Islands II. Intake of mercury and other elements by consumption of pilot whales (*Globicephalus meleanus*). *Sci. Tot. Environ.* **1987**, *65*, 63–68.

(23) Gailer, J., George, G. N., Pickering, I. J., Madden, S., Prince, R. C., Yu, E. Y., Denton, M. B., Younis H. S., Aposhian, H. V. Structural basis of the antagonism between inorganic mercury and selenium in mammals. *Chem. Res. Toxicol*. **2000**, *13*, 1135–1142.

(24) Korbas, M., O'Donoghue, J. L., Watson, G. E., Pickering, I. J., Singh, S. P., Myers, G. J., Clarkson, T. W.; George, G. N. The chemical nature of mercury in human brain following poisoning or environmental exposure. *ACS Chem. Neurosci*. **2010**, *1*, 810–818.

(25) MacDonald, T. C., Korbas, M., James, A. K., Sylvain, N. J., Hackett, M. J., Nehzati, S., Krone, P. H., George G. N., Pickering, I. J. Interaction of mercury and selenium in the larval stage zebrafish vertebrate model. *Metallomics* **2015**, *7*, 1247–1255.

(26) Spiller, H. A. Rethinking mercury: the role of selenium in the pathophysiology of mercury toxicity. *Clin. Toxicol.* **2018**, *56*, 313–326.

(27) Manceau, A., Bourdineaud, J.-P., Oliveira, R. B., Sarrazin, S. L. F., Krabbenhoft, D. P., Eagles-Smith, C. A., Ackerman, J. T., Stewart, A. R., Ward-Deitrich, C., del Castillo Busto, M. E., Goenaga-Infante, H., Wack, A., Retegan, M., Detlefs, B., Glatzel, P., Bustamante, P., Nagy, K. L., Poulin, B. A. Demethylation of methylmercury in bird, fish, and earthworm. *Environ. Sci. Technol*. **2021**, *55*, 1527–1534.

(28) Manceau, A., Gaillot, A.-C., Glatzel, P., Cherel, Y., Bustamante, P. In vivo formation of HgSe nanoparticles and Hg–tetraselenolate complex from methylmercury in seabirds–implications for the Hg–Se antagonism. *Environ. Sci. Technol*. **2021**, *55*, 1515–1526.

(29) Ralston, N. V. C., Raymond, L. J. Mercury's neurotoxicity is characterized by its disruption of selenium biochemistry. *Biochim. Biophys. Acta Gen. Subj*. **2018**, *1862*, 2405–2416.

(30) Pickering, I. J., Cheng, Q., Mendoza Rengifo, E., Dolgova, N. V., Kroll, T., Sokaras, D., George, G. N., Arnér, E. S. J. Direct observation of methylmercury and auranofin binding to selenocysteine in thioredoxin reductase. *Inorg. Chem*. **2020**, *59*, 2711–2718.

(31) Ralston, N. V. C., Ralston, C., Raymond, L. J. Selenium health benefit values: Updated criteria for mercury risk assessments. *Biol. Trace Elem. Res*. **2016**, *171*, 262–269.

(32) Nehzati, S., Dolgova, N. V., Sokaras, D., Kroll, T., Cotelesage, J. J. H., Pickering, I. J., George, G. N. A photochemically-generated selenyl free radical observed by high-energy resolution fluorescence detected X-ray absorption spectroscopy. *Inorg. Chem*. **2018**, *57*, 10867–10872.

(33) James, A. K., Nehzati, S., Dolgova, N. V., Sokaras, D., Kroll, T., Eto, K., O'Donoghue, J. L., Watson, G., Myers, G. J., Krone, P. H., Pickering, I. J., George, G. N. Rethinking the Minamata tragedy: What mercury species was really responsible? *Environ. Sci. Technol*. **2020**, *54*, 2726–2733.

(34) Hoffmeyer, R., Singh, S. P., Doonan, C. J., Ross, A. R. S., Hughes, R. J., Pickering, I. J., George, G. N. Molecular mimicry in mercury toxicology. *Chem. Res. Toxicol*. **2006**, *19*, 753–759.

(35) Pickering, I. J., George, G. N., van Fleet-Stalder, V., Chasteen, T. G., Prince, R. C. X-ray absorption spectroscopy of selenium-containing amino acids. *J. Biol. Inorg. Chem*. **1999**, *4*, 791–794.

(36) Cramer, S. P., Tench, O., Yocum, M., George, G. N. A 13-element Ge detector for fluorescence EXAFS. *Nucl. Instr. Meth. A*. **1988**, *266*, 586–591.

(37) George, M. J. XAS-Collect: A computer program for X-ray absorption spectroscopic data acquisition *J. Synchrotron Radiat*. **2000**, *7*, 283–286.

(38) Sokaras, D., Weng, T.-C., Nordlund, D., Alonso-Mori, R., Velikov, P., Wenger, D., Garachtchenko, A., George, M. J., Borzenets, V., Johnson, B., Rabedeau, T., Bergmann, U.

A seven-crystal Johann-type hard X-ray spectrometer at the Stanford Synchrotron Radiation Lightsource. *Rev. Sci. Instrum.* **2013**, *84*, 053102/1–8.

(39) George, G. N., Garrett, R. M., Prince, R. C., Rajagopalan, K. V. The molybdenum site of sulfite oxidase: A comparison of wild-type and the cysteine 207 to serine mutant using X-ray absorption spectroscopy. *J. Am. Chem. Soc*. **1996**, *118*, 8588–8592.

(40) George, G. N. https://www-ssrl.slac.stanford.edu/exafspak.html (2001).

(41) Rehr, J. J., Mustre de Leon, J., Zabinsky, S. I., Albers, R. C. Theoretical X-ray absorption fine structure standards. *J. Am. Chem. Soc.* **1991**, *113*, 5135–5140.

(42) Mustre de Leon, J., Rehr, J. J., Zabinsky, S. I., Albers, R. C. Ab initio curved-wave X-ray-absorption fine structure. *Phys. Rev. B* **1991**, *44*, 4146–4156.

(43) McMaster, W. H., Del Grande, N. K., Mallett, J. H., Hubbell, J. H. Compilation of X-Ray Cross Sections. Lawrence Livermore National Laboratory Report UCRL-50174, Sec II, Rev.1 **1969**.

(44) Pushie, M. J., Pickering, I. J., Korbas, M., Hackett, M. J., George, G. N. Elemental and chemically specific X-ray fluorescence imaging of biological systems. *Chem. Rev*. **2014**, *114*, 8499–8541.

(45) Delley, B. An all-electron numerical method for solving the local density functional for polyatomic molecules. *J. Chem. Phys*. **1990**, *92*, 508–517.

(46) Delley, B. From molecules to solids with the DMol^3 approach. *J. Chem. Phys*. **2000**, *113*, 7756–7764.

(47) Peverati, R., Truhlar, D. G. M11-L: A local density functional that provides improved accuracy for electronic structure calculations in chemistry and physics. *J. Phys. Chem. Lett*. **2012**, *3*, 117–124.

(48) Siegler, R. W., Nierenberg, D. W., Hickey W. F. Fatal poisoning from liquid dimethylmercury: a neuropathologic study. *Hum. Pathol.* **1999**, *30*, 720–723.

(49) Curley, A., Sedlak, V. A., Girling, E. F., Hawk, R. E., Barthel, W. F., Pierce, P. E., Likosky, W. H. Organic mercury identified as the cause of poisoning in humans and hogs. *Science* **1971**, *172*, 65–67.

(50) Piper, R. C., Miller, V. L., Dickinson, E. O. Toxicity and distribution of mercury in pigs with acute methylmercurialism. *Amer. J. Vet. Res*. **1971**, *32*, 263–273.

(51) Davis, L. E., Kornfeld, M., Mooney, H. S., Fiedler, K. J., Haaland, K. Y., Orrison, W. W., Cernichiari, E., Clarkson, T. W. Methylmercury poisoning: Long-term clinical, radiological, toxicological, and pathological studies of an affected family. *Ann. Neurol*. **1994**, *35*, 680–688.

(52) Swarbrick, J. C., Skyllberg, U., Karlsson, T., Glatzel, P. High energy resolution X-ray absorption spectroscopy of environmentally relevant lead(II) compounds. *Inorg. Chem.* **2009**, *48*, 10748–10756.

(53) Baker, M. L., Mara, M. W., Yan, J. L., Hodgson, K. O., Hedman, B., Solomon, E. I. K- and L-edge X-ray absorption spectroscopy (XAS) and resonant inelastic X-ray scattering (RIXS) determination of differential orbital covalency (DOC) of transition metal sites. *Coord. Chem. Rev*. **2017**, *345*, 182–208.

(54) Manceau, A., Azemard, S., Hédouin, L., Vassileva, E., Lecchini, D., Fauvelot, C., Swarzenski, P. W., Glatzel, P., Bustamante, P., Metian, M. *Environ. Sci. Technol. Lett*. **2021**, (*in the press*, doi: 10.1021/acs.estlett.1c00217)

(55) Cavanaugh, R. The dangers of dimethylmercury. *Chemistry World*, Feb. 19, 2019.

(56) George, G. N., Prince, R. C., Gailer, J. G., Buttigieg, G. A., Denton, M. B., Harris, H. H., Pickering, I. J. Mercury binding to the chelation therapy agents DMSA and DMPS and the rational design of custom chelators for mercury. *Chem. Res. Toxicol.* **2004**, *17*, 999–1006.

(57) Wasik, S.P. 1978. Partition of Organoelements in Octanol/Water/Air Systems. In Brinckman, F.E. and J.M. Bellama (eds.). Organometals and Organometalloids Occurrence and Fate in the Environment. ACS Symposium Series 82. American Chemical Society, Washington, DC.

(58) Major, M. A., Rosenblatt, D. H., Bostian, K.A. The octanol/water partition coefficient of methylmercuric chloride and methylmercuric hydroxide in pure water and salt solutions. *Environ. Tox. Chem*. **1991**, *10*, 5–8.

(59) Ni, B., Kramer, J. R., Bell, R. A., Werstiuk, N. H. Protonolysis of the Hg-C Bond of chloromethylmercury and dimethylmercury. A DFT band QTAIM study. *J. Phys. Chem. A.* **2006**, *110*, 9451–9458.

(60) Asaduzzaman, A.M., Schreckenbach, G. Degradation mechanism of methyl mercury selenoamino acid complexes: A computational study. *Inorg. Chem*. **2011**, *50*, 2366–2372.

(61) Östlund, K. Metabolism of methyl mercury and dimethyl mercury in mice. *Acta Pharmacol. Toxicol.* **1969**, *27* (suppl.), 1–132.

(62) Korbas, M., Blechinger, S., Krone, P. H., Pickering, I. J., George, G. N. Localizing organomercury uptake and accumulation in zebrafish larvae at the tissue and cellular level. *Proc. Natl. Acad. Sci. USA.* **2008**, *105*, 12108–12112.

(63) Korbas, M., Krone, P. H., Pickering, I. J., George, G. N. Dynamic accumulation and redistribution of methylmercury in the lens of developing zebrafish embryos and larvae. *J. Biol. Inorg. Chem*. **2010**, *15*, 1137–1145.

(64) Korbas, M., Lai, B., Vogt, S., Gleber, S.-C., Karunakaran, C., Pickering, I. J., Krone, P. H., George, G. N. Methylmercury targets photoreceptor outer segments. *ACS Chem. Biol*. **2013**, *8*, 2256–2263.

(65) Schumann, H., Freitag, S., Girgsdies, F., Hemling, H., Kociok-Köhn, G. Homoleptic organometallic compounds of zinc, cadmium, and mercury, Intramolecularly stabilized by amine ligands. *Eur. J. Inorg. Chem*. **1998**, 245–252.

(66) Torres, D. D., Banerjee, P., Pamidighantam, S., Jain, P. K. A non-natural wurtzite polymorph of HgSe: A potential 3D topological insulator. *Chem. Mater.* **2017**, *15*, 6356–6366.

(67) Kuno, M., Higginson, K. A., Qadri, S. B., Yousuf, M., Lee, S. H., Davis B. L., Mattoussi, H. Molecular clusters of binary and ternary mercury chalcogenides: colloidal synthesis, characterization, and optical spectra. *J. Phys. Chem. B* **2003**, *107*, 5758–5767.

(68) Boctor, N. Z., Brady, J. B. Interdiffusion of sulfur and selenium in tiemannite. *Amer. Mineral*. **1980**, *65*, 797–799.

(69) Martoja, R., Berry, J. P. Identification of Tiemannite as a probable product of demethylation of mercury by selenium in cetaceans. A complement to the scheme of the biological cycle of mercury. *Vie Milieu* **1980**, *30*, 7–10.

(70) Pickering, I. J., Cheng, Q., Mendoza Rengifo, E., Dolgova, N. V., Kroll, T., Sokaras, D., George, G. N., Arnér, E. S. J. Direct observation of methylmercury and auranofin binding to selenocysteine in thioredoxin reductase. *Inorg. Chem.* **2020**, *59*, 2711–2718.

(71) Carvalho, C. M. L., Chew, E.-H., Hasemy, S. I., Lu, J., Holmgren, A. Inhibition of the human thioredoxin system. A molecular mechanism of mercury toxicity. *J. Biol. Chem.* **2006**, *283*, 11913–11923.

(72) Branco, V., Carvalho, C. The thioredoxin system as a target for mercury compounds. *Biochim. Biophys. Acta* **2019**, *1863*, 129225/1–9.

(73) Manceau, A., Nagy, K. L., Glatzel, P., Bourdineaud, J.-P. Acute toxicity of divalent mercury to bacteria explained by the formation of dicysteinate and tetracysteinate complexes bound to proteins in *Escherichia coli* and *Bacillus subtilis*. *Environ. Sci. Technol.* **2021**, *55*, 3612−3623.

(74) Foloppe, N., Nilsson, L. The glutaredoxin –C–P–Y–C motif: Influence of peripheral residues. *Structure* **2004**, *12*, 289–300.

(75) Clever, H. L., Johnson, S. A., Derrick, M. E. The solubility of mercury and some sparingly soluble mercury salts in water and aqueous electrolyte solutions. *J. Phys. Chem. Ref. Data* **1985**, *14*, 631–680.

(76) Lind, B., Friberg, L., Nylander, M. Preliminary studies on methylmercury biotransformation and clearance in the brain of primates: II. Demethylation of mercury in brain. *J. Trace Elem. Exp. Med.* **1988**, *1*, 49–56.

(77) Carty, A. J., Malone, S. F., Taylor, N. J., Canty, A. J. Synthesis, spectroscopic, and X-say structural characterization of methylmercury-D,L-selenocysteinate monohydrate, a key model for the methylmercury(II)-selenoprotein interaction. *J. Inorg. Biochem*. **1983**, *18*, 291–300.

(78) Kahn, M. A. K., Wang, F. Chemical demethylation of methylmercury by selenoamino acids. *Chem. Res. Toxicol*. **2010**, *23*, 1202–1206.

(79) Asaduzzaman, A. M., Schreckenbach, G. Degradation mechanism of methyl mercury selenoamino acid complexes: A computational study. *Inorg. Chem*. **2011**, *50*, 2366–2372.

(80) Balogh, S. J., Tsz-Ki Tsui, M. T.-K. Comments on 'Rethinking the Minamata tragedy: What mercury species was really responsible?' *Environ. Sci. Technol*. **2020**, *54*, 8482–8483.

(81) James, A. K., Nehzati, S., Dolgova, N. V., Sokaras, D., Kroll, T., O'Donoghue, J. L., Watson, G., Myers, G. J., Krone, P. H., Pickering, I. J., George, G. N. Reply to comments on 'Rethinking the Minamata tragedy: What mercury species was really responsible?' *Environ. Sci. Technol.* **2020**, *54*, 8484–8485.

(82) Hackett, M. J., McQuillan, J. A., El-Assaad, F., Aitken, J. B., Levina, A., Cohen, D. D., Siegele, R., Carter, E. A., Grau, G. E., Hunt, N. H., Lay, P. A. Chemical alterations to murine brain tissue induced by formalin fixation: implications for biospectroscopic imaging and mapping studies of disease pathogenesis. *Analyst* **2011**, *136*, 2941-2952.

(83) Mottet, K., Friberg, L. O., Vahter, M., Body, R.., Lind, B., Shen, D., Burbacher, T. Effects of perfusion, fixation, and freezing on the concentration and chemical form of mercury in the brain of rats exposed to methylmercury. *J. Trace Elem. Exp. Med*. **1993**, *6*, 23–30.

CHAPTER 5: PRESERVATION METHOD INFLUENCES ON MEASURED ELEMENTAL LOCALIZATIONS AND CONCENTRATIONS IN LARVAL ZEBRAFISH

5.1 Preface

The method of preservation of the historical samples in Chapter 3 raised the question of how preservation method might affect the speciation of mercury and endogenous elements. In Chapter 4, these differences were explored using brain tissue samples from a single individual which had been either cryopreserved or undergone fixation in formalin. Here, the vertebrate model organism, zebrafish (*Danio rerio*) was utilized to compare fish which had been experimentally exposed to mercury and subsequently cryopreserved or fixed using the JB-4 methacrylate embedding technique, a highly utilized preservation method in histology. Direct comparisons were made using X-ray fluorescence imaging (XFI) maps of similar sections of larval zebrafish which had been prepared using differing preservation techniques. The results of this work demonstrated that the previously mentioned preservation techniques have little effect on the accumulation or distribution of mercury in larval zebrafish. However, changes in both were noted in endogenous elements investigated.

This chapter is currently being prepared for submission to *Journal of Analytical Atomic Spectrometry*.

James, A.K., Dolgova, N.V., Summers, K.L., Krone, P.H., George, G.N., Pickering, I.J. Preservation method influences on measured elemental localizations and concentrations in larval zebrafish.

A.K. James conducted experimental and laboratory work, collected and analyzed XFI data and drafted the manuscript.

N.V. Dolgova assisted in editing the manuscript.

K.L. Summers assisted with XFI data collection.

I.J. Pickering, G.N. George and P.H. Krone contributed scientific input and guidance and provided funding for the research as well as commented on and edited the manuscript.

5.2 Abstract

Preservation of experimental samples is a common practice in many fields where immunostaining or histological analyses are important. Largely studied have been the effects of the commonly used formalin-fixation technique, including on the distribution and levels of endogenous elements. These effects have been contrasted with another commonly used method of preservation, cryopreservation. The JB-4 methacrylate preservation protocol, a well-described preservation technique has been studied very little in comparison, and no studies exist which qualitatively and quantitatively compare methacrylate fixation to cryopreservation in relation to elemental distributions and concentrations both of endogenous elements and of mercury, post-exposure. Here, zebrafish (*Danio rerio*) were exposed to organometallic mercury and subsequently preserved using either methacrylate fixation or cryopreservation techniques. X-ray fluorescence imaging (XFI) was utilized to both visualize potential changes in elemental distributions as well as to quantitatively compare concentrations in different tissues between methods. Mercury was not seen to be significantly affected by preservation method; however endogenous elements were affected to varying degrees, dependent on the tissues measured.

5.3 Introduction

Twenty-eight of the one hundred and eighteen known chemical elements are recognized to play essential roles in living organisms; many of the heavier elements, such as transition metal ions, are vital for many of the most important chemistry that drives life.[1] A large number of other elements can be toxic to life, and the mechanisms by which both functional and toxic elements exert their effects[2–13] are of considerable interest. Living organisms possess inherent structure, with length scales ranging from nanometers and below, to millimeters and above, and the spatial distribution of chemical elements is essential information for understanding their function. X-ray fluorescence imaging (XFI)[14] is an increasingly used method for the study of elemental localization on a range of length scales from subcellular to whole (small) organisms. Quantitation of elemental concentrations and correlation of these levels between the various elements can be achieved on a pixel by pixel basis. Moreover, the elemental distribution between and within structures such as organs, tissues and subcellular compartments can be identified and visualized, especially if the XFI is correlated with conventional histological images or other probes such as Fourier transform infrared imaging. However, the preservation and preparation methods used for tissue samples to be investigated by XFI should ideally reflect the elemental distribution in the living organism and may necessitate different preparation approaches for different analyses.

Since the pathlength of XFI in soft biological tissues is a few millimeters at most for heavier elements, and considerably less for lighter elements, preparation of sections is required for almost all tissue examination. In addition, since access to synchrotron facilities, essential for conducting XFI analysis of trace elements in biological tissues, is often distant from home laboratories and sporadic in nature, preservation of tissues is necessary. In some cases, in particular autopsy samples which may have been preserved for other reasons, there may be little control over the preservation methods. However, in the case of laboratory experiments in which tissues are intended for XFI analysis, there may be choice over the preservation method utilized. The ideal method will provide excellent preservation of the physical structures while maintaining the elemental distribution of the endogenous and exogenous elements. Previous work has investigated the effect of preservation method on the distribution of endogenous elements including mammalian brain tissue[15,16] and in adherent mammalian cells.[17] Studies have highlighted the challenges with fixation of mobile elements such as chloride and potassium, and have shown that cryopreservation more faithfully preserves the majority of biological elements.[15]

Zebrafish have been demonstrated as a versatile model for investigating vertebrate development; our group has developed XFI of zebrafish to investigate the effects of toxic elements, especially different forms of mercury and its relationships with other elements.[3–19] Here we present a study of larval stage zebrafish exposed to methylmercury L-cysteinate (MeHg-L-Cys) and quantitatively compare elemental distributions from XFI images using standard microscopy methods for sectioning with those obtained using frozen samples and a cryomicrotome. The present study focuses on mercury, as a widespread toxic element, as well as endogenous biological elements, and highlights distributions and concentrations within different tissue types. The advantages and limitations of the different preservation methods are discussed.

5.4 Materials and Methods

5.4.1 Zebrafish

Zebrafish were raised and maintained in the Lab Animals Services Unit (LASU) at the University of Saskatchewan. All experiments conducted using zebrafish were approved by the University of Saskatchewan Ethics Board. Wildtype zebrafish of the Tübingen strain were utilized for this work. Zebrafish larvae collected post-mate were rinsed in system water for debris removal and were subsequently distributed into Petri dishes containing embryo media. Petri dishes contained no more than 50 embryos per dish with embryo media solution changed daily along with removal of debris including hatched chorions and dead embryos removed daily up to the point of hatching, 3 days post-fertilization (dpf). Growing larvae as well as larvae utilized for experimental treatment groups were maintained in an incubator which was kept at 28°C. Upon initiation of experiment zebrafish larvae numbers were reduced to 20 larvae per Petri dish with a minimum of 5 Petri dishes per treatment group. Stock solutions of MeHg-L-Cys were made using a 1 M aqueous solution of methylmercury hydroxide (Strem Chemicals Inc. Newburyport, MA), L-cysteine (Millipore Sigma, Oakville, ON) and deionized water (Millipore) as previously described.[3,4]

Experiments began at 3 dpf when all larvae are completely hatched from their chorions. Treatment groups included an experimental group (0.2 µM MeHg-L-Cys) and a control group (embryo media alone). Experimental solutions were changed every 24 hours with deaths and deformities noted at the same time point. Exposure continued to 5 dpf upon which any remaining living larvae were euthanized with 0.2% Tricaine.

5.4.2 Preservation techniques

Here, two individual preservation methods were utilized. The first was a cryopreservation technique whereby whole euthanized larvae were embedded and properly oriented in a cryomold filled with OCT media. This mold was subsequently immersed into isopentane cooled using liquid nitrogen which is ideal for rapid freezing, prevention of ice crystal formation and well preserved tissues.[20,21] Zebrafish larvae were then sectioned to 10 µm using a SBE Scientific HM550 cryostat microtome (Markham, ON, Canada) with sections intended for X-ray fluorescence imaging (XFI) being mounted on Thermanox plastic coverslips and adjacent sections intended for histology and optical microscopy were mounted onto Fisherbrand Superfrost Plus microscope slides.

The second preservation method utilized was methacrylate embedding. Briefly, euthanized larvae were immersed in 4% paraformaldehyde in 30 mM PBS for two hours followed by graded ethanol dehydration completed in 5-minute washes (0, 25, 50, 75, 100% ethanol) using ethanol and 30 mM PBS with 0.1% Tween 20 (PBST). Larvae were stored overnight at 4°C or in this state until needed. This was followed by a graded ethanol rehydration (0, 25, 50, 75, 100% PBST) the reverse of the previous step in 5-minute washes back to 100% PBST. Larvae were then carefully and quickly oriented into small molds which were filled with heated 1% agarose gel. Upon hardening of the gel, blocks were carefully cut out around the larvae and dehydrated in 100% ethanol while gently rotating at 4°C for a 5-8 hour time period. Blocks were subsequently immersed in infiltration solution A from the JB-4 methacrylate kit (Polysciences, Warrington, PA, USA) and left gently rotating overnight at 4°C. Solution A was changed the following day and gently rotated again at 4°C for another 5-6 hours. Here the infiltrated blocks were carefully oriented into embedding molds which were subsequently filled with JB-4 Solution B and fresh infiltration solution and then having aluminum mounting chucks placed on top. These blocks were left to polymerize overnight at 4°C with the molds being placed on ice and wrapped in plastic. Once hardened, a microtome and glass knives were utilized to section blocks containing zebrafish larvae at 10 µm. Again, sections intended for XFI were mounted onto Thermanox plastic coverslips with adjacent sections mounted on Fisherbrand Superfrost Plus microscope slides for histology and optical microscopy.

5.4.3 X-ray fluorescence imaging (XFI)

All X-ray fluorescence images were collected at the 7 GeV Advanced Photon Source (APS, Argonne, IL) operating in top-up mode with a ring current of 102 mA. Images were recorded on undulator beamline 20-ID-B employing a Si(111) double crystal monochromator and using Rh-coated Kirkpatrick Baez (KB) mirrors to provide a focussed microbeam. The incoming X-ray beam was set to an energy of 13 450 eV to maximize trace element collection while including mercury L_{III} fluorescence and eliminating bromine K-edge fluorescence. Samples were mounted at a 45° angle to the incoming X-ray beam, with the beam located at a 90° angle to the 4-element silicon drift Vortex® detector (Hitachi High-Technologies Science America Inc., Northridge, CA, USA) which was retrofitted with a collimator. Samples which were mounted on 6.3 μm polypropylene film were "raster scanned" with a pixel size of 5 μm × 5 μm and a dwell time of 600 ms/pixel.

5.4.4 Statistical analysis

GraphPad Prism (Version 8.4.3) was utilized for detecting significant differences in quantitation of elements. Differences were detected in multiple target organs, as well as for whole sections using two-sample, unpaired *t*-tests. We note that XFI maps for methylmercury L-cysteine cryopreserved head and trunk sections had an n=4, while methacrylate preserved treatment groups had an n=3 for head sections and an n=2 for trunk sections. We additionally note that the use of statistical tests based on normal distributions is standard practice in XFI analyses; however, the correct probability distribution function for XFI data is clearly not a normal distribution as values can never be negative. Hence, a log-normal or gamma distribution function will be more appropriate. Nonetheless, we have employed these standard tools here. A detailed discussion of the correct statistical treatment of XFI is outside the scope of the present work.

5.5 Results and Discussion

5.5.1 Optical images

A comparison hematoxylin and eosin stained histological images of both head and trunk sections of zebrafish larvae which have been either cryopreserved (Fig. 5.1A, C) or methacrylate embedded (Fig. 5.1B, D) can be seen in Fig. 5.1. Sections 5.1B and 5.1D also highlight relevant anatomical features present in these respective sections including the brain (br), retinal pigmented epithelium (rpe), optic nerve (on) and eye lens (el) in the head section (Fig. 5.1B), and the liver

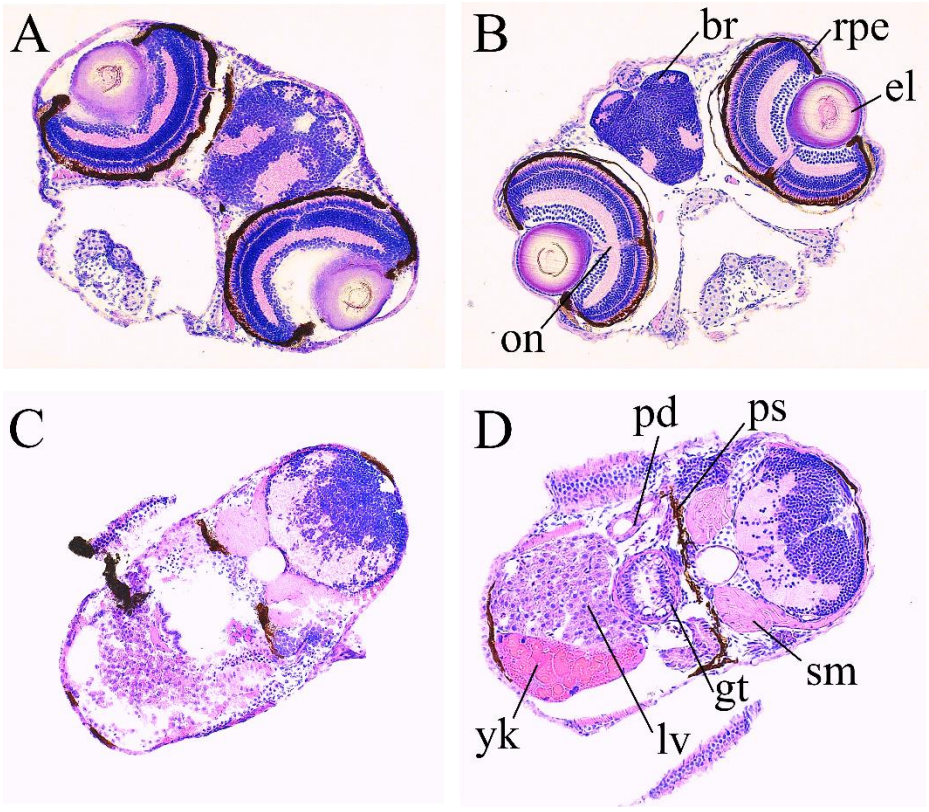

Figure 5.1: Optical images of larval zebrafish aged 5 dpf 10 µm head and liver sections preserved using either a cryopreservation technique (A,C) or a methacrylate embedding technique (B,D). A representative image of a head and liver section (B,D) denotes various important anatomical features including the lens (el), brain (br), optical nerve (on), retinal pigmented epithelium (rpe) and liver (lv), yolk sac (yk), gut tube (gt), pronephric duct (pd), somatic muscle (sm) and pigment spot (ps) in representative sections.

(lv), the gut tube (gt), yolk sac (yk), the pronephric duct (pd), somatic muscle (sm) and pigment spots (ps) in the trunk section (Fig. 5.1D).

It is apparent from Fig. 5.1 that anatomical structures are much better preserved in the embedded (Fig. 5.1B, D) compared with the cryopreserved sections (Fig. 5.1A, C). For the sections prepared by cryopreservation, minor tearing was present around the lens of the eye in Fig. 5.1A as well as tearing in the trunk section near the gut tube in Fig. 5.1C. Considering all of the sections, cryopreserved tissue was generally more susceptible to tears when compared with methacrylate preservation. A subtle "smearing effect" was also noted in the trunk section (Fig. 5.1C), with the lower half of the section appearing to be slightly asymmetrical. This was another consequence of cryopreservation which occurred relatively frequently. In contrast, the methacrylate embedding technique resulted in sections which consistently had remarkably intact anatomy (Fig. 5.1B, D). Here, single layers of cells were very easy to visualize. However, also noticeable in the methacrylate embedded sections (in optical images, not illustrated) is a series of parallel diagonal lines crossing the image and obscuring some of the anatomy. This was a pitfall specific to the embedding technique and is assumed to be due to slight imperfections in the glass knives. This effect was not seen in cryopreserved tissue.

5.5.2 Effect on distributions of individual elements

Before considering the specific effects, or otherwise, of the preparation techniques, we briefly consider other sources of variation. When considering quantitation of whole sections irrespective of preservation, differences in the longitudinal depth within the larva of the section collected can change the volume of relevant organs present within the section, which may slightly influence the values collected by quantitating XFI images. As an example, a head section taken at a slightly shallower depth in the head of the larval zebrafish will contain less of the eye lens and substantially more brain tissue than a section taken tens of microns deeper. Small differences in volume of organs present due to biological variability between larvae are possible, though expected to be small. Homogeneity of elements, or lack of it, across specific tissues or organs would also add complexity to the quantitation. Interestingly, research using autopsy materials has shown that essential elements are nearly homogenous in liver and kidney tissue with a slight increase being noted between different areas of the brain for copper, iron and calcium, among others.[22] Toxic metals were seen to be more variable in kidneys and brain tissue.[22] In addition, any variability in the thickness of individual sections would give rise to an additional systematic

error; here we expect those small differences to be negligible due to the consistency in sectioning. It is important to achieve consistency when sectioning which is easier accomplished cutting tissues which have been embedded in methacrylate compared to those which have been cryopreserved. For an excellent review on microtomy using frozen and fixed sections, refer to Spencer et al.[21]

5.5.3 Mercury

Fig. 2 highlights mercury fluorescence in zebrafish larvae of the same age (5 dpf) and having received the same exposure to 0.2 µM MeHg-L-Cys. Those in Fig. 5.2A and C were cryopreserved while those in Fig. 5.2B and D were methacrylate embedded. Fig. 5.3 shows the XFI distributions of endogenous elements in the same head sections as in Fig. 5.2A and B, with quantitative analysis of elements shown in Fig. 5.4. Fig. 5.5 displays the additional elements for the trunk sections, with the corresponding results of quantitative analysis in Fig.5.6. The colour bars in all XFI images represent the gradient of elemental concentrations present within the section, with black indicating a very low to almost negligible concentration moving through the colour spectrum to red which represents the highest concentration of that specific element (here, mercury) in that section. The methacrylate images (Fig. 5.2B, D) are scaled to the highest concentration of mercury present in the cryopreserved images (Fig. 5.2A, C) to visually highlight similarities or differences in average mercury concentrations present. The distribution of mercury clearly remains the same in both head and trunk sections irrespective of preservation method. Target organs for MeHg-L-Cys include the lens of the eye and the brain, as well as the liver and kidneys, as has been observed previously.[3,4,6-8,18,19] Quantitative analysis of zebrafish sections as seen in Fig. 5.4 indicates no significant differences between cryopreserved and methacrylate embedded sections in head sections in the levels of mercury determined in the brain, lenses and total-head sections; the cryopreserved showed slightly higher average concentrations in the brain as well as the whole image although these differences were not significant. The mercury concentration averaged slightly higher in the lenses of the methacrylate images, but also not significantly so (Fig 5.4). Fig. 5.6 demonstrates a trend of slightly higher mercury concentrations in cryopreserved sections, specifically in the liver, the kidneys as well as the trunk sections in their entirety, which encompass all tissues present. No significant differences existed for mercury in trunk sections (Fig 5.6).

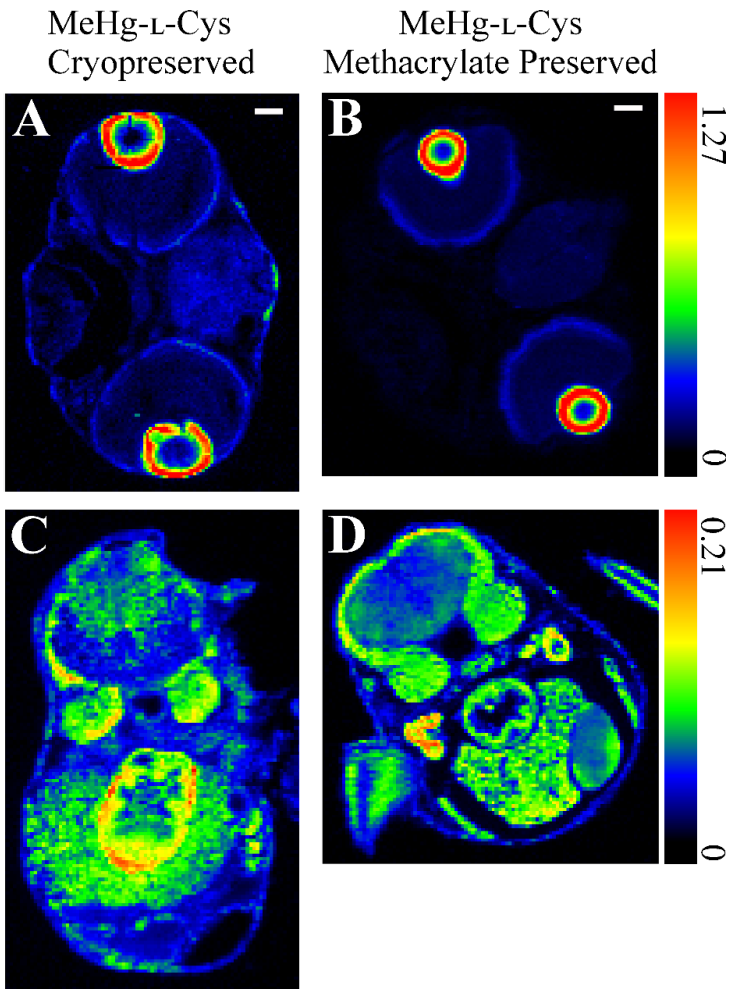

Figure 5.2: Mercury X-ray fluorescence imaging of zebrafish larvae aged 5 dpf after exposure to 0.2 µM MeHg-L-Cys for 48 hours. Upon euthanization larvae were preserved using a methacrylate embedding technique (2B, D) or a cryopreservation method using OCT media (2A, C) and sectioned into 10 µm head and trunk sections. Both methacrylate preserved images are scaled to the highest concentration present in cryopreserved images. Colour bar indicates highest concentration of mercury present in units of areal density (µg/cm^2). Scale bar denotes 50 µm.

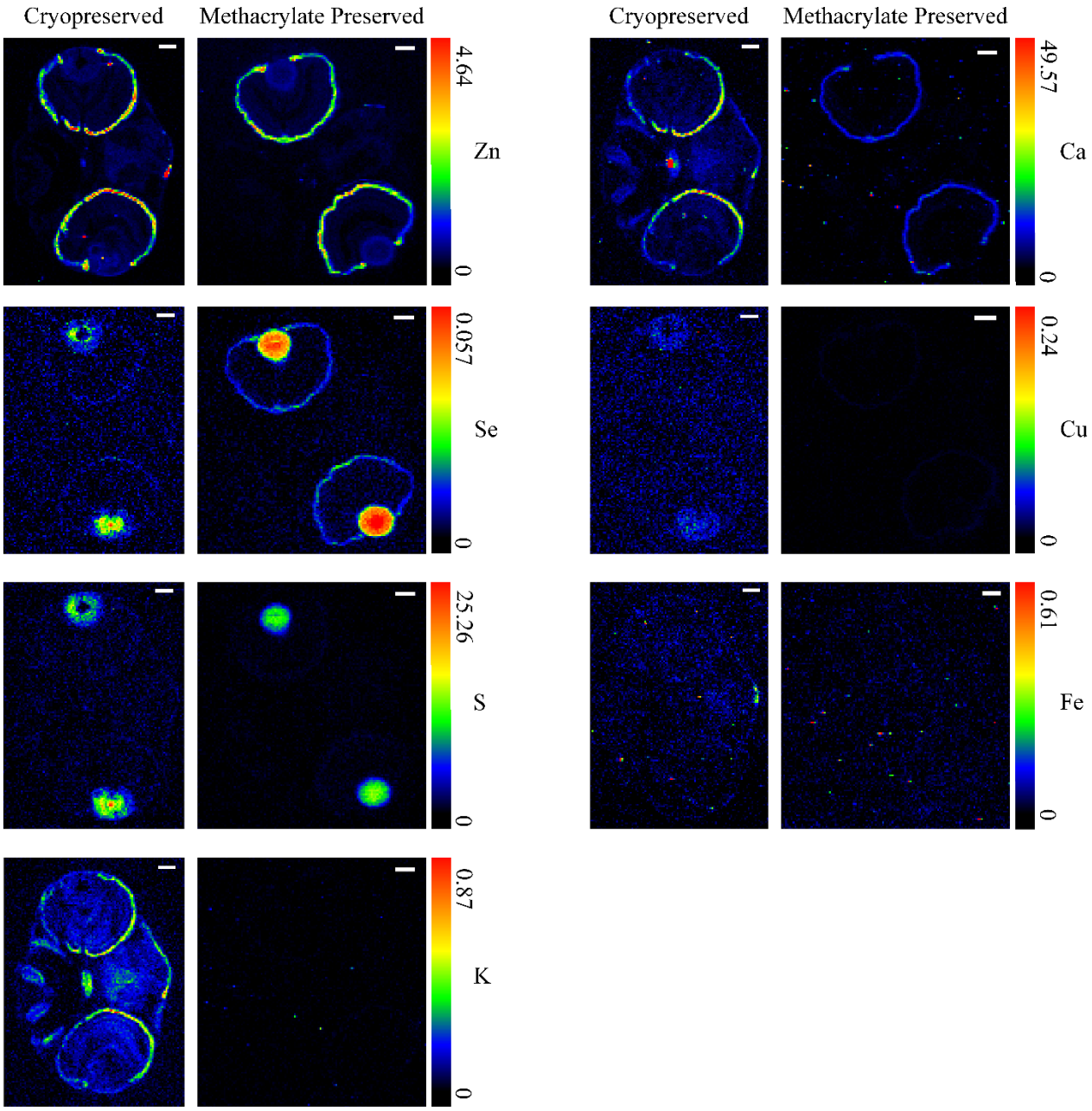

Figure 5.3: X-ray fluorescence images of head sections of 5 dpf larval zebrafish exposed to 0.2 µM MeHg-L-Cys and subsequently preserved in methacrylate (right columns) or cryopreserved in OCT media (left columns). Concentrations and distributions of various elements (µg/cm^2) including zinc, calcium, selenium, copper, sulfur, iron and potassium are compared for the two preservation methods. Images are scaled to the concentration present in the cryopreserved image to emphasize similarities or differences in concentration when present. Colour bar indicates maximum concentration of each element present. Scale bar is 50 µm.

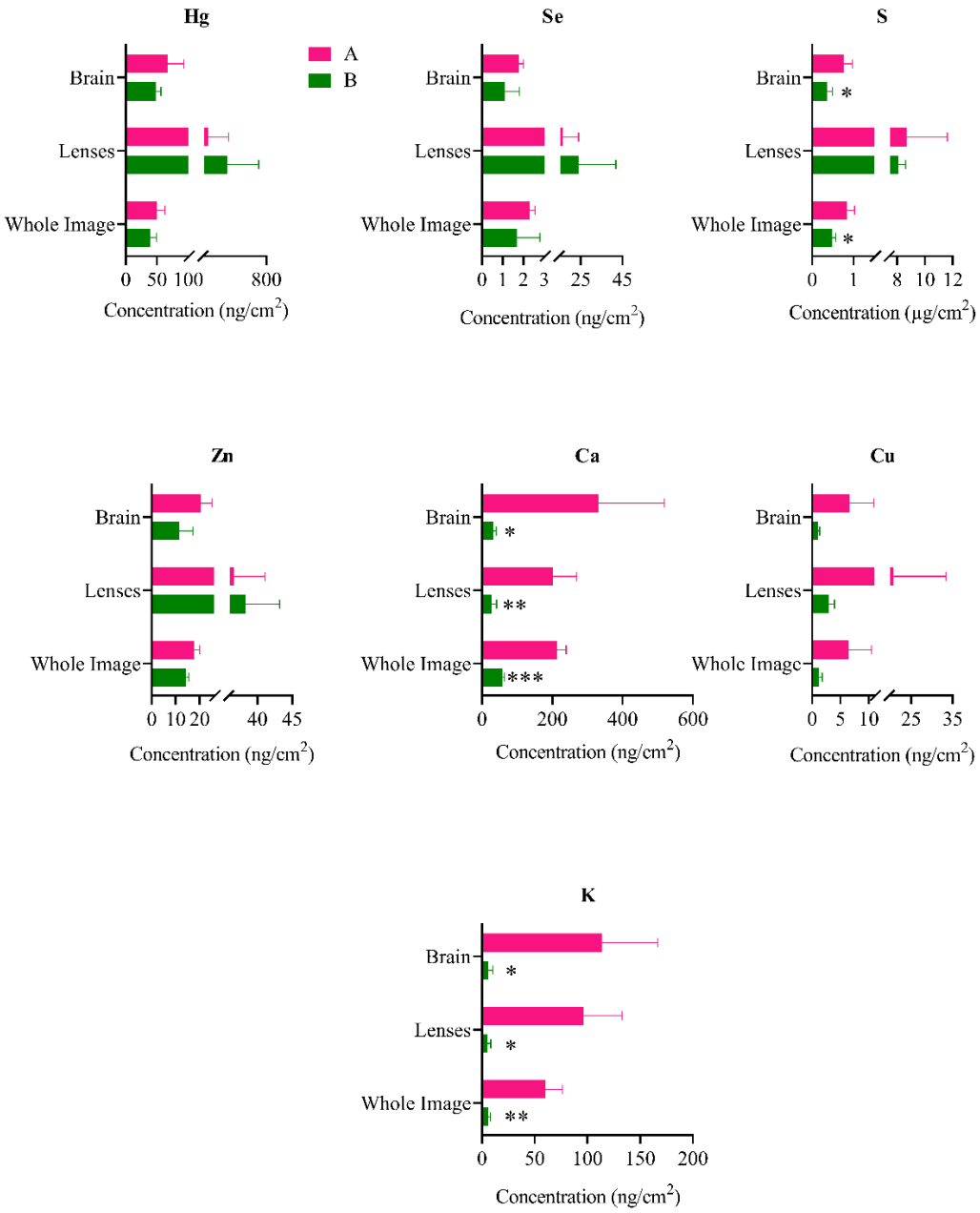

Figure 5.4: Quantitative analysis of head sections of larval zebrafish X-ray fluorescence images. All mercury, selenium, sulfur, zinc, calcium, copper and potassium were averaged together in the image in its entirety as well as in target organs including the lenses and the brain. Treatment groups included MeHg-L-Cys, cryopreserved (pink bars) and MeHg-L-Cys, methacrylate preserved (green bars), respectively. Significant differences in the concentration of each element present (µg/cm^2 or ng/cm^2) between preservation methods are indicated as (*$p \leq 0.05$, **$p \leq 0.001$, ***$p < 0.001$) as determined by two sample unpaired t-test. Error bars indicate ± SD.

5.5.4 Zinc

In the head section, zinc was seen to have very similar localization patterns in both methods, being most concentrated in the retinal pigmented epithelium as well as in pigment spots, when present (Fig. 5.3). No significant differences were found in any part of the head sections analyzed (Fig. 5.4), although whole head section comparisons were found to be approaching significance (p=0.057). The highest average concentration of zinc (approximately 40 ng/cm^2) was found in the lenses of the eyes of the methacrylate embedded larvae, a concentration slightly higher than its cryopreserved counterpart. In contrast, the brain and the whole head section concentrations averaged slightly higher in the cryopreserved larvae.

In the trunk section, zinc was seen in both preservation methods to accumulate highly in the dorsal, midline and ventral pigment spots in XFI trunk sections of zebrafish larvae (Fig. 5.5), which visually appeared similar in the two methods. Zinc fluorescence in the remainder of the tissues was noticeably fainter in the methacrylate image when placed on the same scale as the cryopreserved image. However, there was not a significant difference between methods for whole trunk sections (Fig. 5.6), which is consistent with the measurement being dominated by the strong accumulation of zinc in the pigment spots in both measurements. Zinc accumulation in the livers of the cryopreserved larvae was significantly greater than methacrylate sections (**$p \leq$ 0.001) but not for kidney sections. Cryopreserved kidneys had the highest zinc concentrations out of all measurements taken at approximately 36 ng/cm^2.

5.5.5 Selenium

Selenium distribution did not vary between methods in head sections, with accumulation occurring highly in the lenses of the eyes as well as in the retinal pigmented epithelium (Fig. 5.3). As with zinc, the methacrylate preserved sections had slightly higher selenium concentrations in the lenses, although the selenium in the brain and in the whole section was higher for cryopreserved (Fig. 5.4). No differences in head sections were found to be statistically significant.

In the trunk sections, selenium fluorescence was noticeably fainter in methacrylate sections when displayed on the same scale as cryopreserved (Fig. 5.5). Distribution of selenium in the cryopreserved XFI image appears to be diffuse throughout the trunk section, with notable accumulation in the pigment spots located along the midline of the section as well as dorsally and ventrally. Accumulated selenium in pigment spots was visible using both methods.

Quantitatively, selenium concentrations were significantly higher in cryopreserved sections in the whole sections when compared to methacrylate embedded sections (Fig. 5.6). Selenium concentrations in the liver and the kidneys were increased in cryopreserved compared to methacrylate preserved, and while not statistically significant the differences approached significance (p=0.064 and p=0.056, respectively). In both methods, average concentrations of selenium in liver, kidneys as well as whole sections were very similar, approximately 2 ng/cm^2 in cryopreserved and 1 ng/cm^2 for methacrylate preserved, indicating that most of the selenium present in the section is found in these two organs.

5.5.6 Sulfur

When examining the sulfur XFI images of the head sections the distribution pattern appears similar (Fig. 5.3), with sulfur accumulating in high concentrations in the lenses of the eyes in both methods. The quantity of sulfur visually appears to be nearly equal in these two XFI images, but quantitative analysis (Fig. 5.4) showed that sulfur concentrations were significantly higher in the brain ($*p \leq 0.05$) as well as the whole section ($*p \leq 0.05$) when cryopreservation was utilized rather than methacrylate embedding. The quantity of sulfur present in the lenses was not significantly different between methods.

In the trunk sections, while the overall distributions of sulfur look similar, the greater concentrations of sulfur in the cryopreserved image is apparent based on the colour scale (Fig. 5.5). Indeed, sulfur quantification (Fig. 5.6) revealed a significant difference in sulfur concentrations in the whole trunk sections between methods ($*p \leq 0.05$). Accumulation appears ubiquitous throughout both, with obvious accumulations occurring in the liver, kidneys, somatic muscle as well as the gut tube. An interesting pattern of accumulation is seen in the brain, with what appears to be a higher concentration of sulfur in the exterior brain tissue with sulfur present at a lower concentration in the interior brain tissue. Sulfur concentrations in liver and kidneys were higher in cryopreserved trunk tissues compared to methacrylate embedded, but not significantly so.

5.5.7 Potassium

Of all the elements studied, potassium provides the most striking case of differences between preservation methods in the head section, with the dramatic loss of potassium in the methacrylate XFI image compared to its cryopreserved counterpart (Fig. 5.3). Potassium is found in significantly higher concentrations in the cryopreserved sections in the brain ($*p \leq 0.05$), the

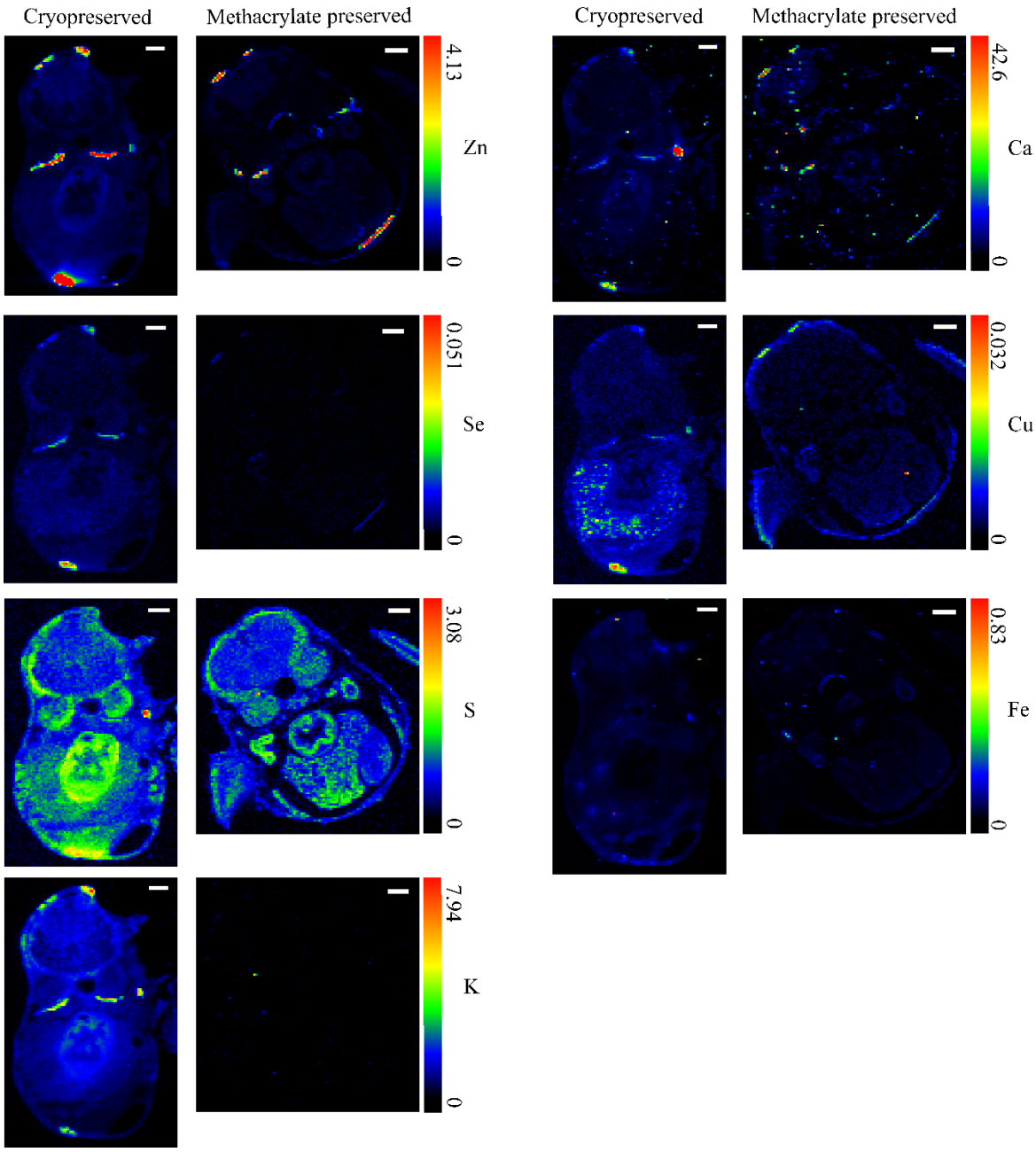

Figure 5.5: X-ray fluorescence images of trunk sections of 5 dpf larval zebrafish exposed to 0.2 µM MeHg-L-Cys and subsequently preserved in methacrylate (right columns) or cryopreserved in OCT media (left columns). Concentrations and distributions of various elements (µg/cm^2) including zinc, calcium, selenium, copper, sulfur, iron and potassium are compared between the two preservation methods. Images are scaled to the concentration present in the cryopreserved image to emphasize similarities or differences in concentration when present. Colour bar indicates maximum concentration of each element present. Scale bar is 50 µm.

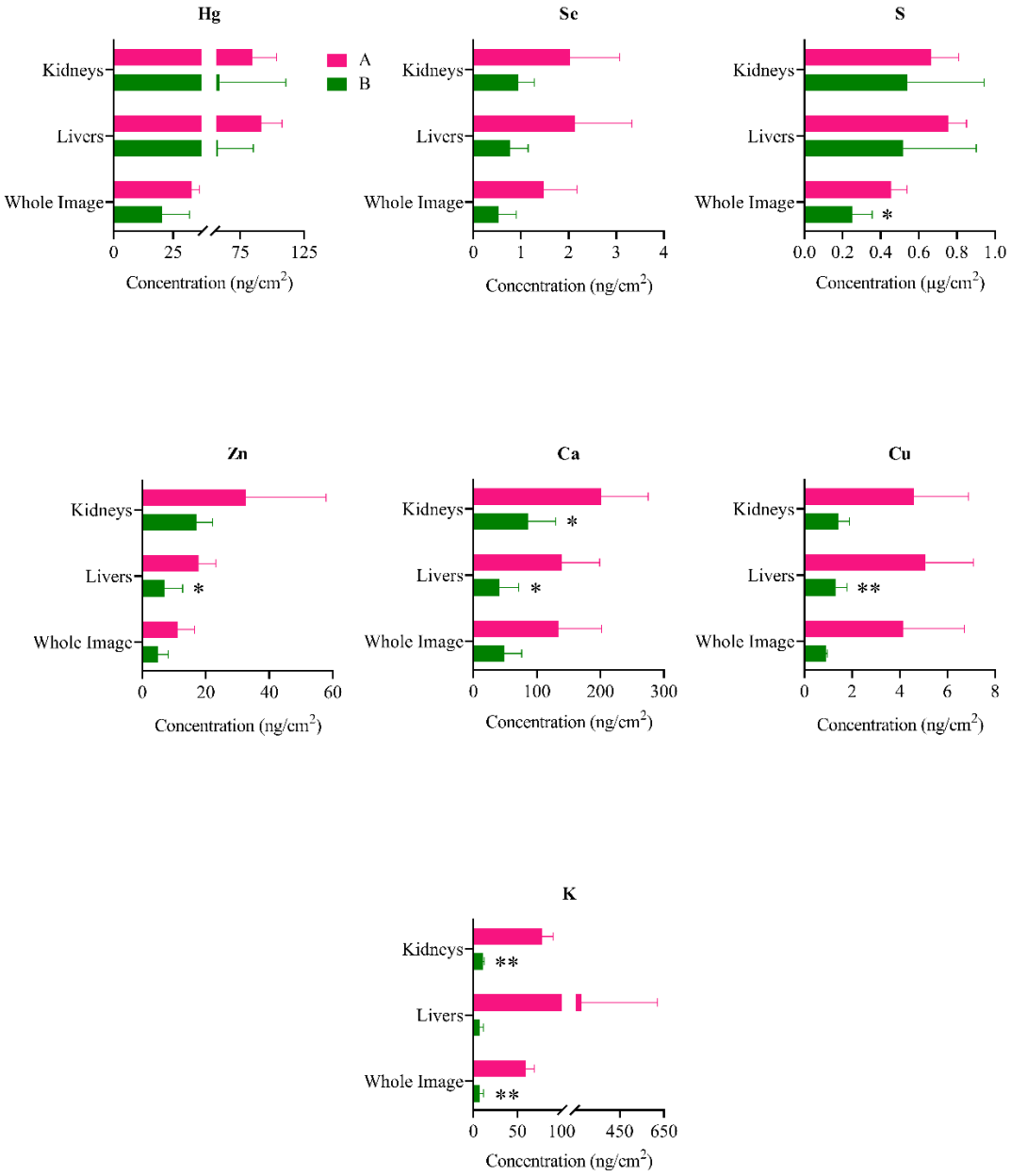

Figure 5.6: Quantitative analysis of trunk sections of larval zebrafish X-ray fluorescence images. Mercury, selenium, sulfur, zinc, calcium, copper and potassium were all quantified in the image in its entirety as well as in target organs including the liver and the kidneys. Treatment groups included MeHg-L-Cys, cryopreserved (pink bars) and MeHg-L-Cys, methacrylate preserved (green bars), respectively. Significant differences in the concentration of each element present (µg/cm^2 or ng/cm^2) between preservation methods are indicated as (*$p \leq 0.05$, **$p \leq 0.001$, ***$p < 0.001$) as determined by two sample unpaired t-test. Error bars indicate ± SD.

lenses (*$p \leq 0.05$) and in the whole head section (**$p \leq 0.001$) compared to the methacrylate preserved zebrafish larvae (Fig. 5.4). The highest concentration of potassium was found in the brain at approximately 125 ng/cm^2.

In the trunk sections, accumulations of potassium in methacrylate embedded sections appeared non-existent compared to cryopreserved when placed on the same scale (Fig. 5.5), as was seen in the head sections. Potassium in the cryopreserved XFI image was present throughout the entire section, with hotspots of potassium apparent in dorsal, midline and ventral pigment spots. Concentrations of potassium were significantly greater than those found in methacrylate sections (Fig. 5.6) for both the whole image (**$p \leq 0.001$) as well as the kidneys (**$p \leq 0.001$). Liver concentrations were not found to be significantly different, although concentrations found in cryopreserved were greater than in methacrylate embedded. Lack of significance is presumed to be due to the high variability found in these sections.

5.5.8 Calcium

Calcium was also strongly affected by preservation method. In the cryopreserved head section (Fig. 5.3) calcium is visible distributed across the image in its entirety, with an apparent "hotspot" in what might be the trabecular bar, cartilage of the chondrocranium. A high concentration of calcium is also found in the retinal pigmented epithelium which is visible in both methods. In the methacrylate section, calcium is no longer apparent in the brain or in any other part of the image besides the retinal pigmented epithelium. The speckling present on the image is presumed to be debris. Fig. 5.4 shows that although visually dimmed in the XFI image by the high concentrations found in discrete locations within the head section, the brain contains substantial calcium, averaging approximately 330 ng/cm^2 in the cryopreserved section. Here we see significant differences between the two methods (*$p \leq 0.05$), with the methacrylate section averaging less than 40 ng/cm^2. Increasingly significant differences were also seen between cryopreserved and methacrylate sections in the lenses (**$p \leq 0.001$) as well as in the head section in its entirety (***$p < 0.001$).

In the trunk sections, calcium distributions appeared similar between methods, however the cryopreserved XFI image had more intense fluorescence than the methacrylate embedded (Fig. 5.5). Calcium was prominently accumulated within the dorsal, midline and ventral pigment spots in both methods. As with the methacrylate head section XFI image, the methacrylate preserved trunk section XFI image appeared to be speckled with debris. Quantified calcium

concentrations were significantly greater in the kidneys as well as the livers of cryopreserved compared to methacrylate (*$p \leq 0.05$). No significant difference was found between whole trunk section concentrations, although the concentrations found in cryopreserved were greater (Fig. 5.6). Calcium in the pigment spots visually appeared stronger in the methacrylate section compared with the cryopreserved, whereas in the zinc they appeared comparable. Pigment spots could not be quantified reliably due to their shape and variable appearance in the images. The whole section concentration measurements of calcium may be dominated by isolated strong spots, such as is seen in the cryopreserved calcium map.

5.5.9 Copper

Copper distribution in the methacrylate head section is barely visible when put on the same scale as the cryopreserved section (Fig. 5.3). As well, the distribution pattern has changed, with much of the copper in the cryopreserved section localized to the lens compared to existing primarily within the retinal pigmented epithelium in the methacrylate preserved section. A two sample, unpaired *t*-test showed a significant difference in the copper present in the retinal pigmented epithelium between preservation methods (**$p \leq 0.001$, data not shown), demonstrating that the distribution change is real and not simply dimmed due to higher concentrations of copper seen elsewhere in the image. For both cryopreserved and methacrylate embedded head sections, the copper distribution was not uniform throughout the section but highest in the lenses and then nearly equal in the brain and whole quantified section (Fig. 5.4). The lenses of the eyes of the cryopreserved zebrafish larvae contained the highest copper concentration, approximately 25 ng/cm^2 compared to all other target organs which averaged around 4-8 ng/cm^2. Fig. 5.4 shows that copper concentrations were higher in cryopreserved sections in all areas of the section measured, but with no significant differences found between the two methods. However, significance was approached in whole head sections (p=0.076), lenses (p=0.062) and brain (p=0.076).

Distribution of copper in the cryopreserved trunk section was clearly highest in the liver while still present in lower concentrations throughout other parts of the anatomy present in the trunk section (Fig. 5.5) and overall was higher in concentration than seen for copper in the head section. The corresponding methacrylate XFI image had lower fluorescence throughout without any obvious target organs except perhaps being slightly higher in the liver as well. Quantitatively (Fig. 5.6), copper concentrations were significantly higher in the livers of the cryopreserved

sections (***$p < 0.001$), while approaching significance in the kidneys (p=0.056) and the whole section (p=0.064). Copper concentrations were nearly uniform in trunk sections with liver, kidneys and the entire quantified section all averaging similar concentrations within preservation method, indicating that most of the copper present in those sections resides in those two organs.

5.5.10 Iron

Iron distributions were more visible in the cryopreserved head section compared to the methacrylate sections (Fig. 5.3). Iron appears to be present diffusely throughout the anatomy of the section with a slight accumulation within the dorsal pigment spot present in the cryopreserved. Head sections of both preservation methods exhibit have numerous spots of debris obscures features in the rest of the section. Since these debris spots are not directly correlated with anatomy, the quantitative analyses of organs and whole sections was highly variable and is not included in Fig. 5.4.

In the trunk sections, iron localizations appeared similar in the XFI images of both preservation methods (Fig. 5.5). The low intensity of the fluorescence indicates lower iron concentrations which are diffuse throughout, with no intense accumulations in any specific area of the section. Similar to the head sections, debris spots complicated quantification, which was not further pursued for this element.

5.5.11 Comparison and implications

Fig. 5.7 summarizes the comparison in quantitation between fixed and frozen treatments for all the tissues examined. Each element is displayed in a different colour, with quantitation of brain, lens, liver, kidneys, head section and trunk section shown as the six points. The diagonal gray solid line indicates equivalency between the two methods of measurements. Points which lie below this line show lower values in the methacrylate sections compared with the frozen sections. Successive broken diagonal lines indicate where the methacrylate values constitute 50%, 10% and 1% of frozen values.

Fig. 5.7 clearly demonstrates the differential impact of methacrylate preservation on some of the elements. Mercury is least impacted, with essentially all points lying on the line of equivalency within the error bars. Sulfur, selenium and zinc follow with lower impact; some points show equivalent levels in the two methods, but others lie closer to the 50% line. Calcium and copper are severely impacted, falling between 50% and 10% of the cryosection values.

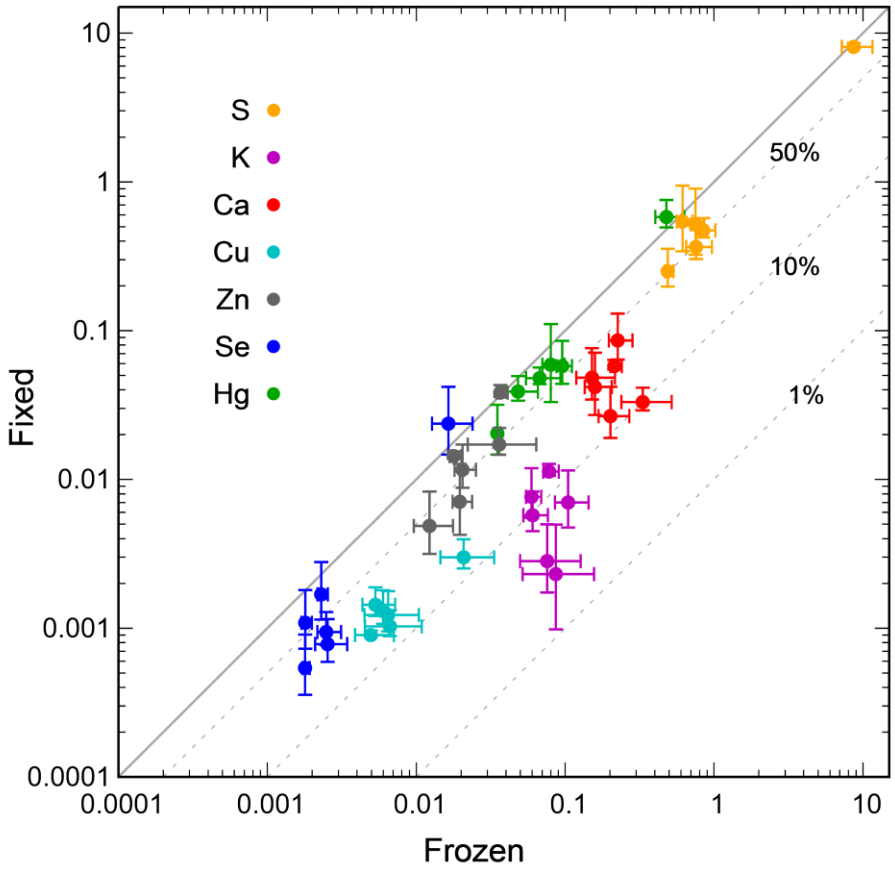

Figure 5.7: Summative plot of quantitative analysis of zebrafish larval sections. Values from the quantitative analyses of Fig.5. 4 and Fig. 5.6 are plotted with values from methacrylate embedded sections on the ordinate and those from the cryopreservation on the abscissa. Both axes show areal concentrations in units of µg/cm^2 on a log scale. For each element, which is coded by colour, the six points correspond to mean areal concentrations in eye lens, brain, liver, kidneys, and whole head and trunk sections. The use of error bars as a visual guide of uncertainty is important, but because the ± one standard deviation (σ) crosses zero these cannot be used in our log-log plot. Both gamma and log-normal distributions are asymmetric close to zero and to reflect this we have used asymmetric error bars of – σ/2 to + σ, which is a reasonable approximation for a gamma probability distribution function. The solid diagonal line corresponds to equivalent values for both preservation methods. Dashed diagonal lines indicate when the fixed values are 50, 10 and 1% of the frozen values.

Finally, potassium shows the most dramatic differences in the methacrylate preservation, essentially between 10% and 1% of the levels in the cryosections.

Methacrylate embedding is an involved technique which requires many steps, each of which may cause leaching or changes in distribution of mobile elements within tissue. To date, information on the effects of methacrylate embedding on elemental quantities or distributions is extremely limited, while literature on effects of formalin-fixation is vast. The first step of methacrylate embedding, however, is immersion in 4% paraformaldehyde for a minimum of two hours. Paraformaldehyde, $HO(–CH_2O–)_nCH_2OH$, is an oligomeric (n~8) or polymeric (n>100) form of formaldehyde that will spontaneously and reversibly form from hydrated formaldehyde (methanediol, $H_2C(OH)_2$) with elimination of water. Paraformaldehyde solutions fix protein containing tissues through the equilibrium formation of methanediol in solution, which will cross link proteins by reacting with nitrogen groups (e.g. those of lysine, arginine and histidine residues) irreversibly forming methylene linkages between them ($=N–CH_2–N=$).[23] Identical chemistry is responsible for formaldehyde fixation, and very similar cross-linking reactions occur with glutaraldehyde fixation. Thus, similar chemical and physical processes are responsible for the initial steps of both methacrylate embedding and formalin fixation and some cautious parallels may be in order.

We were especially interested in the potential effects on mercury, as research focussing on mercury has previously utilized the methacrylate embedding technique due to it being an established technique in histology with impeccable preservation of anatomy.[24] Here we observed that the differences in mercury concentration compared between cryopreserved and methacrylate embedded head sections (Fig. 5.2A, B) and their respective trunk sections (Fig. 5.2C, D) are very small and non-significant ($p > 0.05$). In addition, the distribution patterns for mercury are essentially invariant, being found in high concentrations in the lens of the eye and the brain as well as in the liver, kidneys, somatic muscle and gut tube in the trunk sections. We attributed the fact that mercury is unaffected by this embedding technique compared to cryopreservation that the mercury is relatively immobile once absorbed into all the tissues considered. Indeed, this has been seen in other research. Early work by Bush et al.[22] noted no detectable changes in various elements including mercury in brain, kidneys, liver, heart, bone, and muscle tissue from autopsy studies where half of the tissue was fresh and analyzed immediately and the other half of the tissue being preserved in formalin and then analyzed at both six and twelve months later. More

recently, Gellein et al.[25] reported that leaching of mercury, silver, nickel and lead from human brain tissue samples preserved in formalin into the formalin in which they were preserved was minimal when compared the concentrations of these very same elements in fresh, unused formalin solutions. Other research[26] has examined the concentration of mercury within rat brain tissue between three treatment groups that had been exposed to mercury and then either frozen directly after being sacrificed, perfused with saline and then frozen, or perfused with saline and then fixed. The treatment group that was frozen directly after sacrifice was determined to have a significantly higher amount of total mercury than the other two groups ($p < 0.05$). They attributed this higher concentration of mercury with the mercury present in the trapped blood due to lack of perfusion and to the fact that rats have a higher accumulation of organic mercury in the blood than other species.

XFI images of both head and trunk sections with corresponding quantifications highlighted some interesting differences in elemental localizations and quantities between preservation methods. Whether significantly different or not, elemental quantities of mercury, selenium, sulfur, zinc, calcium, copper and potassium were lower in almost every part of methacrylate embedded trunk tissue compared to that of the cryopreserved. As the cryopreservation technique utilized here is considered to be excellent in maintenance of biological elemental profiles, these values are assumed as near as possible to what was present at the time of euthanization. Some of these results contrast with what is has been seen in the literature regarding differences between cryopreservation and formalin fixation which is an increase using the latter method in copper, zinc, calcium or aluminum among others resulting from presumed metal contamination from the formalin fixation process.[15,22,27–29] Other, more recent work observing possible leaching effects of numerous trace and toxic elements in formalin-fixed and frozen dolphin tissue noted increased concentrations of copper and zinc in frozen compared with formalin-fixed tissues.[30] Head sections herein demonstrated slight increases in mercury, selenium and zinc in the lenses of the eyes of the methacrylate embedded sections (Fig. 5.4); while contamination may be responsible for the increase in zinc, it seems unlikely to be the case for mercury or selenium. A different suggestion for the variation in mercury, selenium and zinc is that the lenses show substantially higher concentrations of these elements than other tissues, and also present a much smaller volume than other tissues surveyed; the tearing which is apparent in the cryopreserved sections (Fig. 5.1) may contribute to the

quantitation being slightly low in these small, high concentration areas. Alternatively, these increases might be attributable to redistribution due to the embedding process, in which elements mobilized from other tissues have an affinity for this tissue, but if so the effect is minor.

Excellent work has been done using PIXE and FTIR to compare formalin-fixed murine brain tissue to fresh cryofixed which saw increases in calcium, iron, copper and zinc in formalin-fixed tissues.[15] Metal contamination was attributed to the fixative process. These authors also reported OCT media containing copper concentrations comparable to those found in standard phosphate-buffered formalin solution but noted OCT media will not penetrate the brain tissue due to its hydrophilic nature, and therefore not result in contamination. As well, Pushie et al.[14] noted that methacrylate embedding materials contain elements of low atomic number which would not affect an experiment done in the energy range that these experiments were completed in. Copper was not seen to be increased in the brain tissue of any sections measured, or indeed in any other anatomy measured herein.

Leaching of soluble ions of potassium, chloride and sodium after formalin fixation has been reported many times in the literature, and, as discussed above, similar effects are expected in the initial stage of the methacrylate embedding. The substantial concentrations of potassium present in XFI cryopreserved sections was in stark contrast to the complete lack of potassium in the methacrylate XFI sections, like that seen in formalin-fixation. This effect is clearly seen in potassium maps in Fig. 5.3 and Fig. 5.5. Sulfur was also seen to be significantly lower in brain tissue, as previously observed for formalin-fixation of murine brain[15] which is consistent with its presence in leachable forms such as in glutathione. However, the observation that there was no significant change in sulfur levels in the eye lens in consistent with sulfur being present in unleachable species. Calcium in bone and associated tissues, as well as calcium existing as Ca^{2+} ions which are important in a great number of biological processes are, like K^{+}, expected to wash out easily. This is substantiated by the visual distributions in the sections, in which small, high concentration areas are observed in the methacrylate embedded sections whereas the broad, low-level distribution of calcium seen in the cryopreserved sections is greatly reduced. The natural heterogeneity of calcium's distribution contributes to the larger error bars in this case.

No element measured herein demonstrated a complete lack of change in either elemental quantification or distribution between preservation methods, significant or otherwise. There is a large amount of literature regarding alteration of elements due to formalin fixation of tissues

compared to frozen tissue, but a lack of information regarding comparisons of frozen tissue to tissue which has been embedded in methacrylate or other resin-type materials, and none specific to zebrafish. Acrylic resins are ideal for XFI studies of elemental analyses due not only to the impeccable conservation of anatomical features for histological analyses but also due to their rapid polymerization, colourless block formation, ease of sectioning thin sections (≤ 10 μm), stability in an electron beam[31] and apparent lack of metal contamination compared to formalin-fixed tissue. Thus, if the intent is to measure quantification and distribution in mercury alone, along with histology, the methacrylate embedding method appears to be more appropriate. However, if the purpose of the research is to estimate elemental quantities other than mercury, potential for leaching of selenium, sulfur, zinc, calcium, copper and potassium, which may also be specific to tissue sub-type, must be considered. Cryopreservation is highly regarded for its maintenance of biological elemental profiles and lack of extraneous elemental contamination which is the most ideal for studies which involve research on dynamics or quantification of specific elements *in situ*. However, the authors acknowledge that fresh frozen tissue is not always available, especially for autopsy samples, and that formalin-fixed and other resin-embedded tissues are essential for storage of samples over long periods of time.

When planning an experiment, emphasis needs to be placed on what the specific needs from the preservation technique are in order to determine which method will assist in achieving research goals. This work demonstrated that when analyzing mercury fluorescence and performing subsequent quantifications, methacrylate embedded sections work as well as cryopreserved; however, as samples are typically analyzed within months of experiment completion, and histological information is not necessarily pertinent to the experimental goals, the excellent anatomical preservation provided by methacrylate embedded sections could be sacrificed in favour of achieving the most accurate possible elemental compositions and distributions which is a hallmark of cryopreservation. As ever, forward thinking and good decision-making in experimental design is an integral part of the scientific process.

5.6 Acknowledgements

We acknowledge support from the Natural Sciences and Engineering Research Council of Canada (NSERC; GNG and IJP) and the Canada Foundation for Innovation (CFI; IJP). AKJ and KLS were Fellows, and NVD was an Associate in the Canadian Institutes of Health Research – Training Grant in Health Research Using Synchrotron Techniques (IJP). GNG and IJP are Canada Research Chairs. This research used resources of the Advanced Photon Source, an Office of Science User Facility operated for the U.S. Department of Energy (DOE) Office of Science by Argonne National Laboratory and was supported by the U.S. DOE under Contract No. DE-AC02-06CH11357, and the Canadian Light Source and its funding partners.

5.7 References

(1) Chellan, P., Sadler, P.J. The elements of life and medicines. *Phil. Trans. R. Soc. A.* **2015**, *373*, article number 20140182.

(2) George, G.N., Pickering, I.J., Doonan, C.J., Korbas, M., Singh, S.P., Hoffmeyer, R. Inorganic molecular toxicology and chelation therapy of heavy metals and metalloids. *Adv. Mol. Toxicol.* **2008**, *2*, 125-155.

(3) Korbas, M., Blechinger, S., Krone, P.H., Pickering, I.J., George, G.N. Localizing organomercury uptake and accumulation in zebrafish larvae at the tissue and cellular level. *Proc. Natl. Acad. Sci. USA.* **2008**, *105*, 12108–12112.

(4) Korbas, M., Krone, P. H., Pickering, I. J., George, G. N. Dynamic accumulation and redistribution of methylmercury in the lens of developing zebrafish embryos and larvae. *J. Biol. Inorg. Chem.* **2010**, *15*, 1137-1145.

(5) Korbas, M., O'Donoghue, J. L., Watson, G. E., Pickering, I. J., Singh, S. P., Myers, G. J. Clarkson, T. W., George, G. N. The chemical nature of mercury in human brain following poisoning or environmental exposure. *ACS Chem. Neurosci*. **2010**, *1*, 810-818.

(6) Korbas, M., MacDonald, T. C., Pickering, I. J., George, G. N., Krone, P. H. Chemical form matters: differential accumulation of mercury following inorganic and organic mercury exposures in zebra fish larvae. *ACS Chem. Biol.* **2012**, *7*, 411–420.

(7) Korbas, M., Lai, B., Vogt, S., Gleber, S.-C., Karunakaran, C., Pickering, I. J., Krone, P. H., George, G. N. Methylmercury targets photoreceptor outer segments. *ACS Chem. Biol.* **2013**, *8*, 2256-2263.

(8) MacDonald, T. C., Korbas, M., James, A. K., Sylvain, N. J., Hackett, M. J., Nehzati, S., Krone, P. H., George G. N., Pickering, I. J. Interaction of mercury and selenium in the larval stage zebrafish vertebrate model. *Metallomics* **2015**, *7*, 1247–1255.

(9) Dolgova, N. V., Hackett, M. J., MacDonald, T. C., Nehzati, S., James, A. K., Krone, P. H., George, G. N., Pickering, I. J. Distribution of selenium in zebrafish larvae after exposure to organic and inorganic selenium forms. *Metallomics* **2016**, *8*, 305–312.

(10) Dolgova, N. V., Nehzati, S., Choudhury, S., MacDonald, T. C., Regnier, N. R., Crawford, A. M., Ponomarenko, O., George, G. N., Pickering, I. J. X-ray spectroscopy and imaging of selenium in living systems. *Biochim. Biophys. Acta – General Subjects* **2018**, *1862*, 2383-2392.

(11) Dolgova, N. V., Nehzati, S., Macdonald, T. C., Summers, K. L., Crawford, A. M., Krone, P. H., George, G. N., Pickering, I. J. Disruption of selenium transport and function is a major contributor to mercury toxicity in zebrafish larvae. *Metallomics* **2019**, *11*, 621–631.

(12) Pickering, I. J., Cheng, Q., Mendoza Rengifo, E., Dolgova, N. V., Kroll, T., Sokaras, D., George, G. N., Arnér, E. S. J. Direct observation of methylmercury and auranofin binding to selenocysteine in thioredoxin reductase. *Inorg. Chem.* **2020**, *59*, 2711–2718.

(13) James, A. K., Nehzati, S., Dolgova, N. V., Sokaras, D., Kroll, T., Eto, K., O'Donoghue, J. L., Watson, G., Myers, G. J.; Krone, P. H., Pickering, I. J., George, G. N. Rethinking the Minamata tragedy: What mercury species was really responsible? *Environ. Sci. Technol.* **2020**, *54*, 2726–2733.

(14) Pushie, M. J., Pickering, I. J., Korbas, M., Hackett, M. J., George, G. N. Elemental and chemically specific X-ray fluorescence imaging of biological systems. *Chemical Reviews* **2014**, *114*, 8499-8541.

(15) Hackett, M.J., McQuillan, J.A., El-Assaad, F., Aitken, J.B., Levina, A., Cohen, D.D., Siegele, R., Carter, E.A., Grau, G.E., Hunt, N.H., Lay, P.A. Chemical alterations to murine brain tissue induced by formalin fixation: implications for biospectroscopic imaging and mapping studies of disease pathogenesis. *Analyst* **2011**, *136*, 2941-2952.

(16) Pushie, M. J., Hollings, A., Reinhardt, J., Webb, S. M., Lam, V., Takechi, R., Mamo, J. C., Paterson, P. G., Kelly, M. E., George, G. N., Pickering, I. J., Hackett, M. J. Sample preparation with sucrose cryoprotection dramatically alters Zn distribution in the rodent hippocampus, as revealed by elemental mapping. *J. Anal. At. Spectrom.* **2020**, *35*, 2498-2508.

(17) Jin, Q., Paunesku, T., Lai, B., Gleber, S.-C., Chen, S.I., Finney, L., Vine, D., Vogt, S., Woloschak, G., Jacobsen, C. Preserving elemental content in adherent mammalian cells for analysis by synchrotron-based X-ray fluorescence microscopy. *J. Microsc.* **2018**, *265*, 81-93.

(18) MacDonald, T.C., Nehzati, S., Sylvain, N.J., James, A.K., Korbas, M., Caine, S., Pickering, I.J., George, G.N., Krone, P.H. Phenylthiourea alters toxicity of mercury compounds in zebrafish larvae. *J. Inorg. Biochem.* **2015**, *151*, 10-17.

(19) MacDonald, T.C., Sylvain, N.J., James, A.K., Pickering, I.J., Krone, P.H., George, G.N. Effects of inorganic mercury on the olfactory pits of zebrafish larvae. *Metallomics* **2016**, *8*, 514-517.

(20) Shiurba, R. Freeze-substitution: Origins and applications. In *International Review of Cytology;* Jeon, K.W., Ed.; Academic Press: San Diego, 2001, Vol. 206.

(21) Spencer, L.T. Microtomy for paraffin and frozen sections. In *Bancroft's Theory and Practice of Histological Techniques;* Suvarna, S.K., Layton, C., Bancroft, J.D., Eds.; Elsevier Limited, 2019, Ed. 8.

(22) Bush, V.J., Moyer, T.P., Batt, K.P., Parisi, J.E. Essential and toxic element concentrations in fresh and formalin-fixed human autopsy tissues. *Clin. Chem.* **1995**, *41*, 284-294.

(23) Kallen, R.G., Jencks, W.P. Equilibria for the reaction of amines with formaldehyde and protons in aqueous solution. *J. Biol. Chem.* **1966**, *241*, 5864-5878.

(24) Sullivan-Brown, J., Bisher, M.E., Burdine, R.D. Embedding, serial sectioning and staining of zebrafish embryos using JB-4 resin. *Nat. Protoc.* **2011**, *6*, 46-55.

(25) Gellein, K., Flaten, T.P., Erikson, K.M., Aschner, M., Syversen, T. Leaching of trace elements from biological tissue by formalin fixation. *Biol. Trace Elem. Res.* **2008**, *121*, 221-225

(26) Mottet, K., Friberg, L., Vahter, M., Body, R., Lind, B., Shen, D., Burbacher, T. Effects of perfusion, fixation, and freezing on the concentration and chemical form of mercury in the brain of rats exposed to methylmercury. *J. Trace. Elem. Exp. Med.* **1993**, *6*, 23-30.

(27) Bonta, M., Török, S., Hegedus, B., Döme, B., Limbeck, A. A comparison of sample preparation strategies for biological tissues and subsequent trace element analysis using LA-ICP-MS. *Anal. Bioanal. Chem.* **2017**, *409*, 1805-1814.

(28) Schrag, M., Dickson, A., Jiffry, A., Kirsch, D., Vinters, H.V., Kirsch, W. The effect of formalin fixation on the levels of brain transition metals in archived samples. *Biometals* **2010**, *23*, 1123-1127.

(29) Chwiej, C., Szczerbowska-Boruchowska, M., Lankosz, M., Wojcik, S., Falkenberg, G., Stegowski, Z., Setkowicz, Z. Preparation of tissue samples for X-ray fluorescence microscopy. *Spectrochim. Acta B* **2005**, *60*, 1531-1537.

(30) McCormack, M.A., Jackson, B.P., Dutton, J. Effects of formalin fixation on trace element concentrations in bottlenose dolphin (*Tursiops truncates*) tissues. *Environ. Toxicol. Chem.* **2020**, *39*, 1149-1164.

(31) Stirling, J.W., Woods, A.E. Resin (plastic) embedding for microscopy and tissue analysis. In *Bancroft's Theory and Practice of Histological Techniques;* Suvarna, S.K., Layton, C., Bancroft, J.D., Eds.; Elsevier Limited, 2019, Ed. 8.

CHAPTER 6: EXPLORING THE ROLE OF L-SYSTEM TRANSPORTERS (LAT) IN THE UPTAKE OF ORGANOMETALLIC MERCURY IN LARVAL ZEBRAFISH

6.1 Preface

The research in Chapters 3 and 4 focussed on speciation of mercury and selenium in a variety of brain tissue samples. Not considered in the aforementioned chapters was how organometallic species of mercury cross the highly regulated blood-brain barrier to exert their toxicity. The research herein Chapter 6 stemmed from discussions regarding the currently accepted mechanisms of transportation of methylmercury within the human body, and how those concepts might be explored using the same zebrafish model organism which was utilized in Chapters 5 and 7.

Here, larval stage zebrafish were exposed to methylmercury- L-cysteine alone or in combination with a variety of compounds which ultimately inhibited transportation into target organs and resulted in increased survival. As well, comparisons were made between D- and L-enantiomers of methylmercury, with results indicating that transporters of methylmercury may not be entirely stereoselective.

This chapter is currently being prepared for submission to *Metallomics*.

James, A.K., Dolgova, N.V., MacDonald, T.C., Summers, K.L., Nehzati, S., Korbas, M., Krone, P.H., George, G.N., Pickering, I.J. Exploring the role of L-system transporters (LAT) in the uptake of organic mercury in larval zebrafish.

A.K. James conducted experimental work, collected and analyzed XFI data and drafted the manuscript.

N.V. Dolgova assisted in editing the manuscript.

K.L. Summers assisted with XFI data collection.

S. Nehzati assisted with zebrafish exposures.

M. Korbas performed initial experimental work which provided direction to the project.

I.J. Pickering, G.N. George and P.H. Krone contributed scientific input and guidance and provided funding for the research as well as commented on and edited the manuscript. G.N. George conducted computational calculations.

6.2 Abstract

Transportation of methylmercury compounds has long been attributed to L-system transport, specifically via LAT1 and LAT2. This has been studied *in vivo* and *in vitro* using various substrates and inhibitors of LAT. Here, the effects of disturbing LAT transport on organ specific accumulations of mercury were investigated using X-ray fluorescence imaging (XFI). Zebrafish (*Danio rerio*), a well-described vertebrate model organism, were exposed to methylmercury-L-cysteine alone or in conjunction with various LAT blockers, or to methylmercury-D-cysteine, to determine whether survival and mercury accumulations in target organs would be affected. A drastic increase in survival in larvae exposed to methylmercury-L-cysteine co-exposed with various LAT blockers was observed when compared to treatment groups exposed to methylmercury-L-cysteine alone. Additionally, significant differences were noted in mercury concentrations in known target organs including the eye lens and brain when treatment groups were compared. Exposure to methylmercury-D-cysteine led to slightly lower mercury in brain and greatly increased survival compared with methylmercury-L-cysteine exposure; a concomitant decrease in selenium and increase in sulfur was also observed. Overall, the study highlights the important role of LAT transporters in methylmercury uptake *in vivo*.

6.3 Introduction

Organometallic compounds of mercury are known to be potent neurotoxins with the ability to cross the blood-brain barrier (BBB).[1,2] Of these, methylmercury compounds are the most extensively studied, primarily due to their presence in fish and seafood products and consequent potential health risks to humans.[3–6] The transport and distribution of organometallic mercury compounds was at one time thought to be due to their lipid solubility or via simple diffusion and partitioning. It has since been hypothesized that active transport may be more important due to coordination with biological thiolates giving products that are substrates for endogenous amino acid transporters.[7,8] The term *molecular mimicry* has been used to describe this notion, and it has been explicitly suggested that methylmercury-L-cysteine (MeHg-L-Cys) is a molecular mimic of L-methionine, and that this is responsible for its transport. More recent work has quantitatively examined the molecular similarities between MeHg-L-Cys and L-methionine and concluded that these are too dissimilar to provide a *bona-fide* example of molecular mimicry,[9] and instead concluded the uptake is more likely due to the very broad substrate specificity of the transporters.[10]

System L transporters, specifically LAT1 and LAT2 have been postulated to be responsible for the rapid uptake and distribution of methylmercury in target locations within the human body such as the brain, placenta and liver cells.[11–14] Human amino acid transporters can be categorized into transport families called solute carrier (SLC) families which are either sodium dependent (SLC1, SLC6, SLC38) or sodium independent (SLC7 and SLC16) and have differing substrate selectivities.[15] System L ("leucine-preferring") transport falls under the SLC7 family and is comprised of bidirectional heterodimeric transporters. The human System L transporter LAT1 (L-type amino acid transporter 1), also referred to as SLC7A5 is a light protein monomer comprised of 12 transmembrane segments linked to the 4F2 cell surface antigen heavy chain (4F2hc, also known as CD98hc or SLC3A2) through a disulfide bridge.[16,17] LAT2 is referred to as SLC7A8, being of a similar structure to LAT1. LAT1 mRNA is expressed in multiple tissues including the placenta, the brain, the spleen, testis and colon,[18] while LAT2 shows highest expression in the kidneys but is also strongly expressed in placenta, brain, liver, spleen, skeletal muscle, small intestines and lungs.[19] Both LAT1 and LAT2 transport large neutral amino acids, while LAT2 additionally transports some smaller amino acids including alanine and glutamine.[19] LAT1 is responsible for the transport of many large neutral amino acids across plasma

membranes including phenylalanine, methionine, leucine, isoleucine, tryptophan, valine, tyrosine and histidine with high affinity, as well as glutamine and asparagine with a somewhat lower affinity.[18,20] System L transporters are localized both at the luminal (blood-facing) and abluminal (brain-facing) sides of the BBB.[11] The affinity of System L for amino acids in peripheral tissues in rats has been shown to be substantially lower than at the BBB.[21,22] System A is a sodium-dependent transport system for neutral amino acids such as alanine and proline[15] and is also located at the BBB although exclusively at the abluminal side.[23] It has been shown that co-treatment of MeHg-L-Cys or substrate L-leucine with α-methylaminoisobutyric acid (MeAIB), a System A analog has no negative effect on the uptake of MeHg-L-Cys or L-leucine, demonstrating that their uptake is specific to System L.[11]

As LAT1 and LAT2 (hereafter referred to as LAT) are postulated to at least in part be responsible for *in vivo* methylmercury uptake and distribution, it follows that substrates or inhibitors of these transporters would result in a reduction in the uptake of methylmercury compounds as well as in reduced overall toxicity. This has been studied *in vivo* in earlier work employing co-administration of organometallic mercury compounds with various thiol compounds to rats, leading to the conclusion that organometallic mercury transport involved neutral amino acid transporters.[24–26] More recently, *in vitro* studies have shown MeHg-L-Cys uptake to be inhibited when various cell types were exposed in combination with LAT specific inhibitor 2-aminobicyclo-(2,2,1)-heptane-2-carboxylic acid (BCH) and/or various LAT substrates such as L-phenylalanine, L-methionine, L-leucine, L-histidine and L-valine.7,[13,27]

While the effect of substrates and inhibitors on uptake and toxicity has been demonstrated, the effect on organ- and tissue-specific distributions of mercury has not previously been determined. We therefore turned to zebrafish (*Danio rerio*) which are a versatile model organism for the developing foetus and also an established target for organometallic mercury toxicity. Zebrafish demonstrate high fecundity with larvae that develop rapidly and have well established laboratory breeding and maintenance protocols. Zebrafish larvae have been extensively used to study the uptake and accumulation of mercury compounds using X-ray fluorescence imaging (XFI).[28–34]

Here we report a comparison of the toxicity of MeHg-L-Cys to larval zebrafish in the presence and absence of the LAT inhibitor BCH or the LAT substrates L-phenylalanine and L-methionine, which are expected to act as competitive inhibitors of MeHg-L-Cys transport. We

used XFI to quantify mercury and endogenous elemental concentrations in target organs including the lens of the eye, brain, liver and kidney of larval zebrafish following exposure to all treatment groups. Additionally, differences in survival as well as target organ accumulations of mercury were compared between MeHg-L-Cys and MeHg-D-Cys treatment groups.

6.4 Materials and Methods

6.4.1 Chemicals

Methylmercury hydroxide (1 M aqueous solution) was purchased from Strem Chemicals Inc. (Newburyport, MA, USA) and used to make stock solutions of methylmercury L-cysteine as previously described.[30,32] L-cysteine, D-cysteine, L-phenylalanine L-methionine and 2-amino-2-norbornanecarboxylic acid (BCH) were purchased from Sigma-Aldrich (St. Louis, MO, USA).

6.4.2 Zebrafish husbandry and breeding

Adult zebrafish (*Danio rerio*) were raised and maintained in a dedicated aquatic facility kept at 22°C and run on a 14 : 10 h light : dark cycle with system water kept at 27.5°C. Fish were fed a mixed diet of Tetramin fish flakes and previously frozen shrimp and blood worms. Zebrafish used for experimental work were of the Tübingen wildtype variety. All live animal work was conducted in accordance with the Guidelines of the Canadian Council of Animal Care (CCAC) and approved by the University of Saskatchewan's Ethics Board.

Adult zebrafish mates were conducted in breeding tanks which were separate from rearing tanks. A 2:1 female-to-male ratio was used for maximal breeding success, with dividers separating genders throughout the night until the beginning of the light cycle when dividers were removed. Resulting embryos were collected the later the same day and raised to 3 days post-fertilization (dpf) in Petri dishes containing embryo media[34] which was changed daily and with daily removal of debris including empty chorions and dead embryos.

6.4.3 Experimental set-up

Experimental groups included a system water control, three individual LAT inhibiting groups (100 µM BCH, 100 µM L-phenylalanine, 100 µM L-methionine), two methylmercury exposure groups (0.2 µM methylmercury L-cysteine and 0.2 µM methylmercury-D-cysteine) and three experimental groups consisting of each LAT blocker in combination with methylmercury L-cysteine using the concentrations listed above. All stock solutions were prepared in deionized water (Millipore).

Larval zebrafish exposures began at 3 dpf, the time-point at which most larvae are hatched from their protective chorion. Each treatment group consisted of a minimum of 100 zebrafish larvae divided between five 10 cm Petri dishes (20 larvae/dish) with 25 mL of chemical solutions changed daily. Deformities and lethalities were recorded daily with all dead embryos and other debris removed daily. All exposures lasted 48 hours to 5 dpf upon which embryos were euthanized using 0.2% Tricaine.

All treatments began on 3 dpf and extended to 5 dpf. Treatment solutions were changed daily. 3 dpf is the point at which larval zebrafish hatch from their protective chorion; any larvae remaining within the chorion on day three were manually extracted. Range-finding studies were conducted at concentrations of 0 (control), 0.2, 1, 2, 10 and 25 µM MeHg-L-Cys. Larval zebrafish exposed to a concentration of 1 µM and above did not survive longer than 24 hours. Given the results of MeHg-L-Cys treatments, larval zebrafish were also exposed in a similar fashion to MeHg-D-Cys at concentrations of 0 (control), 0.2, and 2 µM, with survival reduced to zero by 72 hours into 2 µM MeHg-D-Cys treatment. 0.2 µM was the concentration chosen for both MeHg-L-Cys and MeHg-D-Cys experimental treatments. Mortality data was combined from exposures of 360 zebrafish in MeHg-L-Cys treatment groups and 160 zebrafish in MeHg-D-Cys treatment groups.

After euthanization 5 dpf larval zebrafish were rinsed three times in triple distilled water for removal of excess externally adherent mercury. They were then embedded in optimal cutting temperature (OCT) media (Tissue-Tek) and flash frozen in a partly frozen slurry of cold isopentane, chilled with liquid nitrogen. All frozen larvae were stored at -80 °C until sectioning. Relevant anatomy including both the zebrafish head (containing both the fore-brain and eye lens) and trunk (containing the liver, yolk sac and pronephros) regions were collected as 10 µm thick sections using an ESBE Scientific HM550 cryostat microtome (Markham, ON, Canada). Sections intended for synchrotron X-ray fluorescence imaging were collected on Thermanox plastic coverslips while adjacent sections collected for histological analysis were mounted on Fisherbrand Superfrost Plus microscope slides and stained using hematoxylin & eosin.

6.4.4 X-ray fluorescence imaging (XFI)

All X-ray fluorescence images were collected at the 7 GeV Advanced Photon Source (APS) at the US Department of Energy's Argonne National Laboratory on beamline 20-ID-B. Ring current was operating at 102 mA in top-up mode. A focussed microbeam with minimal

scatter was achieved using Rh-coated Kirkpatrick-Baez (KB) mirrors and Si(111) double crystal monochromator. The 4-element silicon-drift Vortex® detector (Hitachi High-Technologies Science America Inc., Northridge, CA, USA) with an optimally placed collimator responsible for monitoring the X-ray fluorescence was located at a 90° angle to the incident beam while the sample was mounted onto 6.3 µm polypropylene film and is located at an angle of 45° to the incident X-ray beam.[28] The sample was continuously raster scanned at an energy set to 13 450 eV so as to be just below the bromine K-edge, since bromine is present at trace levels in many plastics, while also allowing for monitoring of Hg $L\alpha_{1,2}$ and other elements of interest. Images were collected with a beam size of 5 µm × 5 µm and dwell time of 600 milliseconds per pixel. X-ray fluorescence imaging data was analyzed using the program SMAK software using established procedures.[28] All statistical analyses on X-ray fluorescence images and mortality data were carried out using GraphPad version 8.4.3. Between three and seven head section X-ray fluorescence maps were collected per treatment group. Trunk sections can be seen in Figure C.6.1 (Appendix C) as constraints on allotted beamtime necessarily allowed for a maximum of one replicate for each LAT treatment group.

6.4.5 Computational chemistry

Density function theory (DFT) calculations employed DMol^3 and visualized with Biovia Materials Studio Version 2018 R2, and Biovia Discovery Studio 2016.[35,36] Calculations employed the meta-GGA approximation, with the hybrid M11-L functional[37] for the self-consistent field procedure and for the energies. Double numerical basis sets were used, including polarization functions for all atoms, with all electron core treatments for all atoms. The M11-L functional is specifically designed to accurately model weak intermolecular interactions, and hence is useful for proteins and other biological molecules.

6.5 Results and Discussion

6.5.1 Survival studies of MeHg-ʟ-Cys and MeHg-ᴅ-Cys

Initial toxicity tests, including monitoring of mortality and deformities, of each compound used were conducted prior to survival studies. Signs or deformities commonly observed prior to mortality included lethargic or moribund behavior, edema, and spinal disturbances including lordosis (pronounced downward curvature) and kyphosis (pronounced upward curvature of the spine). LAT substrates L-phenylalanine and L-methionine and LAT inhibitor BCH were not

predicted to be toxic to larval zebrafish and indeed, no mortality, deformities or adverse signs were observed with these compounds at 0 (control), 25, 50, 100 and 200 µM.

Fig. 6.1 highlights the survival of larval zebrafish at 24 and 48 hours of exposure. Clearly seen is the reduced survival of zebrafish in the MeHg-L-Cys treatment group at 48 hours in comparison to all treatment groups which included both MeHg-L-Cys and either a LAT substrate or inhibitor. At the 48 hour time point, larvae in all LAT substrate treatment groups were visibly healthier than in treatment groups with MeHg-L-Cys alone, although some larvae did exhibit one or more of the adverse signs listed above. Statistically significant differences were determined using one-way ANOVA followed by Tukey's multiple comparisons test. Significant differences in survival were noted between MeHg-L-Cys treatment group and control group as well as between MeHg-L-Cys and each of the LAT treatment groups (***$p > 0.001$). Other work has noted similar results, with a co-exposure of MeHg-L-Cys and L-methionine resulting in increased rates of eclosion (an indicator of development into adulthood) in the Drosophila model organism when compared to treatment groups of MeHg-L-Cys alone.[38]

Significant differences in survival were also seen between two different forms of organometallic mercury, MeHg-L-Cys and MeHg-D-Cys (***$p > 0.001$) as noted in Fig. 6.2. Strikingly similar to what is seen in Fig. 6.1, where survival of zebrafish remains high in treatment groups of MeHg-L-Cys in combination with various LAT inhibitors at the 48-hour exposure time point compared to MeHg-L-Cys alone, the treatment group of MeHg-D-Cys alone also resulted in increased survival compared to its enantiomer, MeHg-L-Cys. Indeed, survival in MeHg-D-Cys treatment group continued until euthanization at 7 dpf, while MeHg-L-Cys zebrafish did not survive past 5 dpf.

6.5.2 Co-exposure of MeHg-L-Cys with LAT blockers decreases mercury accumulation

XFI experiments showing the accumulation and distributions of mercury, zinc, selenium and sulfur in head sections of all treatment groups including control (A), 0.2 µM MeHg-L-Cys (B), 0.2 µM MeHg-D-Cys (C), 0.2 µM MeHg-L-Cys + 100 µM BCH (D), 0.2 µM MeHg-L-Cys + 100 µM L-phenylalanine (E) and 0.2 µM MeHg-L-Cys + 100 µM L-methionine (F) are seen in Fig. 6.3. This figure highlights one individual replicate from each group. Head section XFI mercury images in Fig. 6.3 are all scaled to MeHg-L-Cys treatment (B) for visual comparison of differences in uptake of mercury as a result of various treatment groups (C-F). The colour bar in

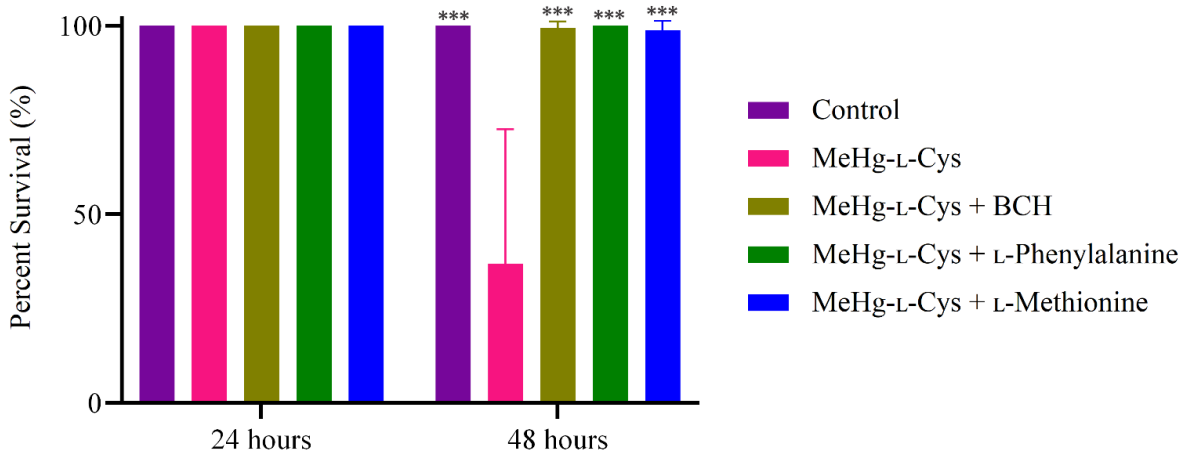

Figure 6.1: Percent survival of larval zebrafish in multiple treatment groups including 0.2 µM MeHg-L-Cys alone and in combination with 100 µM of LAT inhibitor BCH or LAT substrates L-phenylalanine and L-methionine in comparison with no-treatment control. Exposure to various chemical treatments occurred for a total of 48 hours with chemical solutions changed every 24 hours. Survival is denoted as a percentage with errors bars representing standard deviation. Note the reduced survival in MeHg-L-Cys at 48 hours compared to treatment groups at the same time point which also contained a LAT transport inhibitor or substrate. Significant differences in survival were noted between the MeHg-L-Cys treatment group and other treatment groups (*$0.01 \geq p \leq 0.05$, **$p \leq 0.001$, ***$p > 0.001$) using one-way ANOVA followed by Tukey's multiple comparisons test.

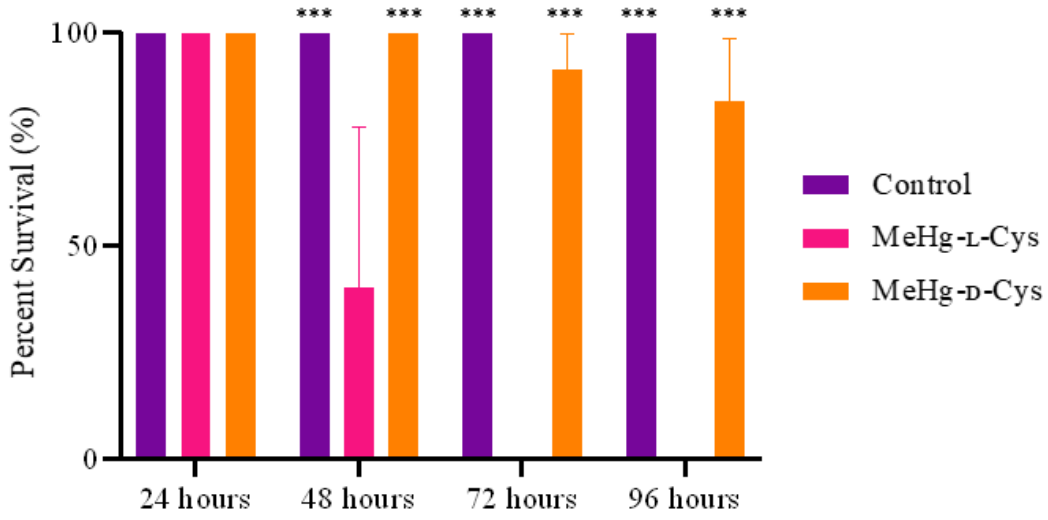

Figure 6.2: Comparison of effects of MeHg-L-Cys and MeHg-D-Cys exposure on survival of larval zebrafish. Zebrafish were exposed to treatments of 0.2 µM MeHg-L-Cys or 0.2 µM MeHg-D-Cys from 3 to 7 dpf. Note that survival in MeHg-L-Cys falls to zero after 48 hours while survival in MeHg-D-Cys remains high. Significant differences in survival are seen between MeHg-L-Cys and both control and MeHg-D-Cys groups at 48 hours and beyond (***$p > 0.001$) determined using one-way ANOVA followed by Tukey's multiple comparisons test.

each row indicates the maximum elemental concentrations for mercury, selenium, sulfur and zinc found in the zebrafish larvae in the MeHg-L-Cys treatment group (B) in units of areal density ($\mu g/cm^2$). Here it is easy to visualize the classical uptake pattern of organometallic mercury into the outer layer of the eye lens, which has been seen in previous work on zebrafish larvae.[29,30] It can also be seen that treatment groups containing a competing LAT substrate have a smaller accumulation of mercury in the eye lens, seen in the figure as a cooler colour vs. a warm, red-toned colour (Fig. 6.3C-F vs. Fig. 6.3B). The same effect is also observed in the brain, although the differences in concentration in the brain in Fig. 6.3 are not as visually dramatic due to the contrast with much greater accumulations in the eye lens.

To quantify the comparison between treatments, the levels of mercury in the whole image and specific areas of the eye lens and brain were determined; data presented in Fig. 6.4 (Hg panel). Fig. 6.4 shows average concentrations of mercury in the sections of a minimum of three different zebrafish larvae. Exposure to MeHg-L-Cys resulted in the highest level of mercury accumulation among all examined conditions (Fig. 6.4, Hg panel). Mercury levels in the whole head section and specifically in eye lens and the brain, are significantly decreased in the case of co-exposure of zebrafish to MeHg-L-Cys and BCH and L-phenylalanine as opposed to exposure to MeHg-L-Cys alone, with the difference being statistically significant (Fig. 6.4, Hg panel). Interestingly, co-exposure of zebrafish to MeHg-L-Cys and L-methionine lead only to a slight and statistically insignificant decrease in mercury level in the head section of zebrafish (Fig. 6.3, Fig. 6.4 Hg panel), even though presence of L-methionine provided the same protection against MeHg-L-Cys toxicity as L-phenylalanine and BCH, at least within the time frame of our experiment.

Consistent with the lower observed toxicity of MeHg-D-Cys compared to MeHg-L-Cys discussed above (Fig. 6.2), exposure to MeHg-D-Cys resulted in a lower mercury burden in the whole head section compared to MeHg-L-Cys exposure, although the decrease was not statistically significant (Fig. 6.4, Hg panel). Interestingly, the largest difference was observed in the brain, potentially indicating that the presence of D-cysteine decreases the ability of mercury to cross the blood-brain barrier.

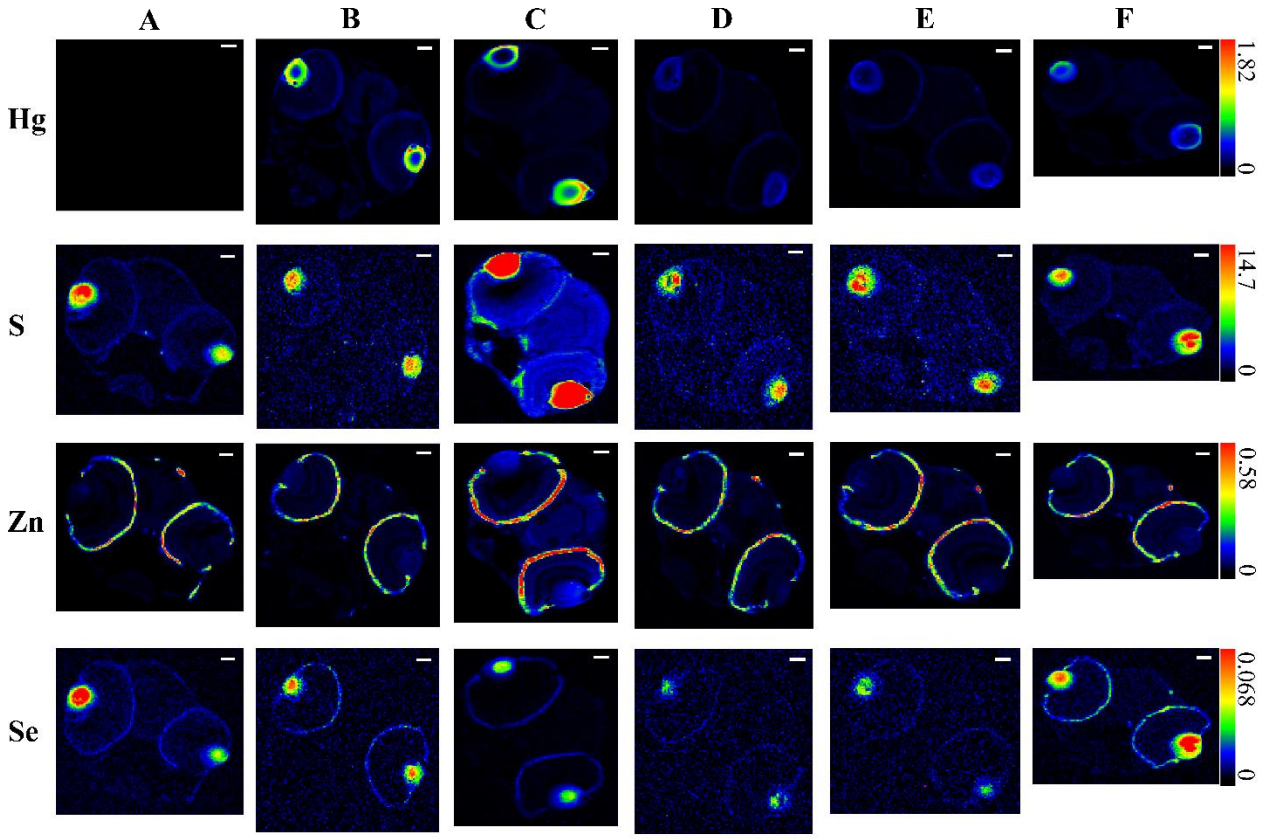

Figure 6.3: X-ray fluorescence images of elemental distributions of mercury, sulfur, selenium and zinc in head sections of 5 dpf larval zebrafish which have been cryopreserved and sectioned at 10 µm. Treatment groups are as follows: (A) control, (B) MeHg-L-Cys, (C) MeHg-D-Cys, (D) MeHg-L-Cys + BCH, (E) MeHg-L-Cys + L-phenylalanine, (F) MeHg-L-Cys + L-methionine. Color bar represents the areal density scale and indicates the maximum value (µg/cm^2) common to all the images in each row, corresponding to each element. The MeHg-L-Cys (B) treatment was chosen for the common intensity scales in order to compare differences in Hg and the effect on other elements as a function of the different treatments (A, C-F). Scale bar of 50 µm is denoted for reference.

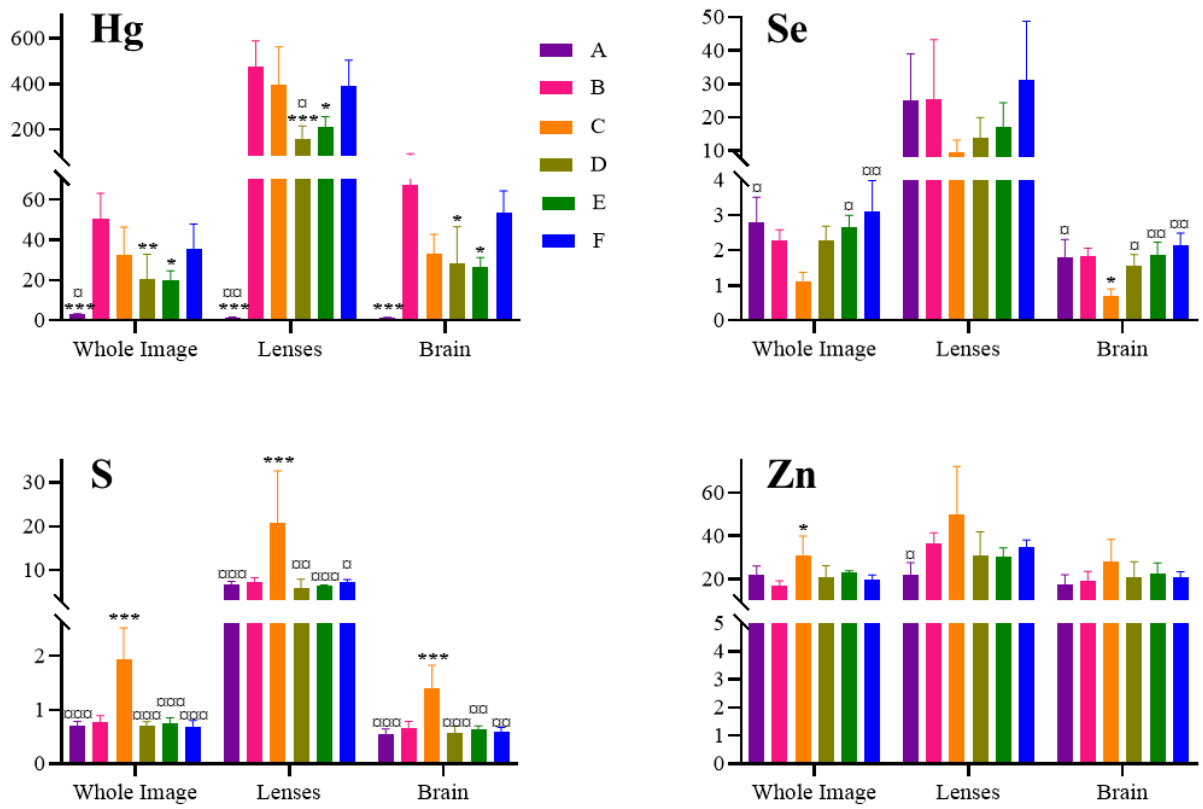

Figure 6.4: Quantification of mercury, selenium, sulfur and zinc in head sections of larval zebrafish derived from XFI images. Treatment groups A-F are the same as indicated in Fig. 6.3: (A) control, (B) MeHg-L-Cys, (C) MeHg-D-Cys, (D) MeHg-L-Cys + BCH, (E) MeHg-L-Cys + L-phenylalanine, (F) MeHg-L-Cys + L-methionine. Values given in units of µg/cm^2 represent the average concentrations of mercury, selenium, sulfur and zinc present in each tissue type after exposure to various treatments or control. Significant differences in mercury concentrations were determined between MeHg-L-Cys (*$p \leq 0.05$, **$p \leq 0.001$, ***$p > 0.001$) and all other treatment groups as well as between MeHg-D-Cys (¤$p \leq 0.05$, ¤¤$p \leq 0.001$, ¤¤¤$p > 0.001$) and all other treatment groups using one-way ANOVA followed by Tukey's multiple comparison post-hoc test.

6.5.3 MeHg-L-Cys exposure protects zebrafish from selenium depletion

Selenium is a known regulator of mercury toxicity.[39–42] Mercury compounds are known to have very high affinity to selenols and selenides, which leads to formation of biologically inactive mercury-selenium complexes and decreases mercury toxicity. Thiols and sulfides also have high affinities for mercury, although lower than corresponding selenium compounds. Because of the known interactions between mercury, selenium and sulfur, we quantified levels of selenium and sulfur in addition to mercury levels in zebrafish (Fig. 6.4, Se and S panels). Zinc concentrations were also quantified (Fig. 6.4, Zn panel), as zinc fluorescence occurs diffusely throughout zebrafish head sections and more strongly in specific structures, allowing for ease of visualization of whole sections. Concentrations of zinc were observed to be significantly higher in MeHg-D-Cys exposures when compared to MeHg-L-Cys exposures in whole head sections and compared to control groups in eye lenses (Fig. 6.4, Zn panel).

Previously we reported that exposure to mercuric chloride and methylmercury chloride leads to selenium depletion, specifically in the brain of zebrafish larvae.[43] In this study methylmercury exposure was performed with MeHg-L-Cys instead of methylmercury chloride; strikingly, MeHg-L-Cys exposure does not result in significant depletion of selenium in zebrafish larvae head sections nor does it alter the level of selenium in the brain (Fig. 6.4, Se panel). This finding suggests that the presence of an extra source of sulfur (L-cysteine) may protect the organism from selenium depletion, which is underscored by the increase in selenium levels after co-exposure to MeHg-L-Cys and L-methionine (Fig. 6.4, Se panel). Interestingly, only L-forms of sulfur containing amino acids appear to grant protection against selenium depletion; exposure to MeHg-D-Cys leads to depletion of selenium comparable to that observed after $HgCl_2$ exposure.[43]

6.5.4 Fit within the LAT active site of MeHg-L-Cys and other LAT substrates

LAT substrates and analogs have been shown to be effective in reducing uptake of endogenous substances such as L-leucine but also in reducing uptake of MeHg-L-Cys, which is currently assumed to utilize System L transport to wreak toxic havoc on various target organs such as the brain and liver within the human body. Recent cryogenic electron microscopy (cryo-EM) work has given insights into the molecular structure of LAT1/CD98hc.[16] This work gives first clues as to the structure of LAT1, but has limited resolution. Fig. 6.5 shows one of the raw cryo-EM maps of Yan et al.,[16] which serves to illustrate some of the resolution limitations, but

nevertheless, clearly shows LAT1 as a bundle of alpha-helices (bottom of figure) in complex with the 4F2hc (SLC3A2) cell-surface antigen heavy chain (top of figure).

Yan et al.[16] have successfully resolved the overall polypeptide fold, and have approximately located the inhibitor BCH within the active site. The structure, shown in Fig. 6.6 is comprised of a bundle of alpha-helical regions with a large central channel, which are thought to penetrate the cell membrane. The interior of the channel comprised of the alpha-helical bundle contains a large number of amino acid residues which are conserved between different species. BCH was observed to be located within the alpha-helical tract, which is thought to serve to transport the amino acid substrates across the cell membrane. We have used computational chemistry to examine the structure of the BCH binding site and whether various substrates including: MeHg-L-Cys, MeHg-D-Cys, L-methionine, L-leucine, and L-phenylalanine fit into this part of the active site channel. In order to conform to the experimental structure of Yan and coworkers,[16] the polypeptide backbone was restricted to coordinate locations that were deposited in the protein data bank. Appropriate protons were added and density functional theory geometry optimizations were used to examine the fit of different substrates at the BCH binding location, with the locations of the amino acid side chains and substrate being subject to no constraints or restraints.

Refinement of the BCH-bound structure suggested a small translation from the experimentally obtained position, which given the limitations of the experimental data (Fig. 6.5) is not surprising (not illustrated), and we conclude that our computational results are consistent with the structure of Yan et al.[16] All of the amino acid substrates that were tested fit well into the BCH binding site, which includes the alternative organometallic mercury compound α-mercuri-acetaldehyde (Chapter 3, not illustrated). We note that comparing the relative binding energies for different substrates is not simple. Density functional theory computes total energies – which correspond to the energetic difference between the energy of geometry-optimized structure and the energy in which all nuclei and electrons are removed to infinity. However, comparison of energies for different enantiomers is a simple matter, and because of the possibility of transport of the D-enantiomers, we compared the relative energies of L- and D- substrates. This is shown in Table 6.1. Perhaps surprisingly, in the case of each compound, the geometry-optimized D-enantiomer was energetically preferable to the L-enantiomer (Table 6.1).

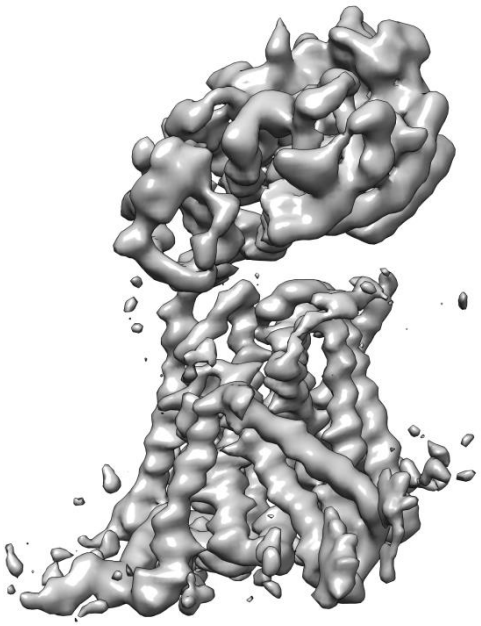

Figure 6.5: Raw cryo-EM map of human LAT1 (SLC7A5) amino acid transporter.[16] The raw map illustrates the limited resolution of some cryo-EM structures. (Source: https://www.ebi.ac.uk/pdbe/entry/emdb/EMD-0678, visualized with UCSF Chimera v1.14).

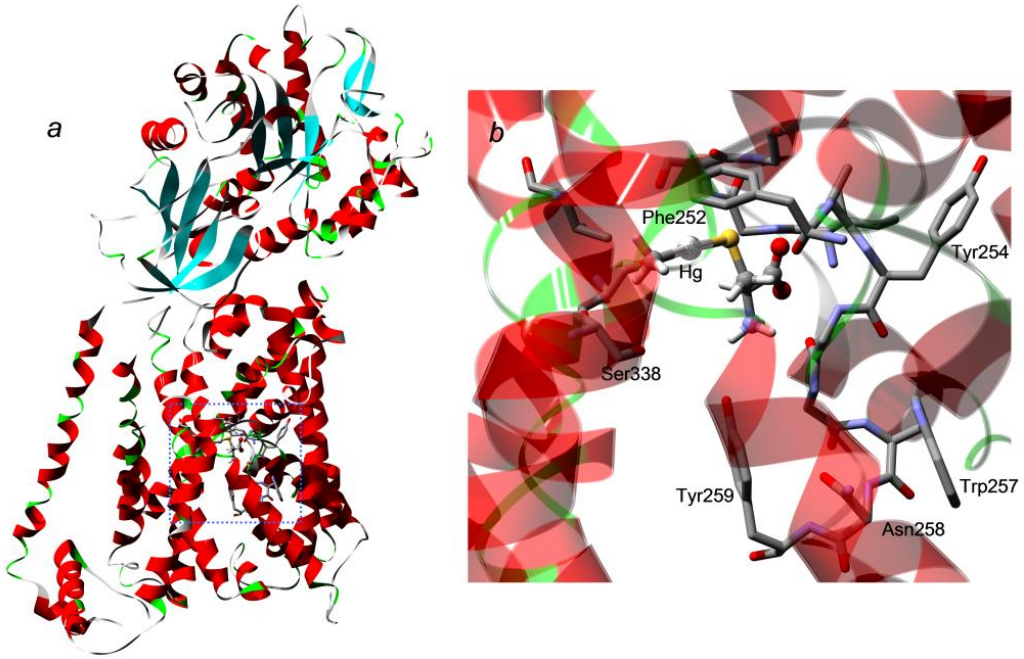

Figure 6.6: Visualization of the LAT1 complex and binding sites. *a*) Overall structure of the LAT1 complex, incorporating the geometry optimized BCH binding sites of the active site channel (see Section 6.4.5). *b*) Detail of the region indicated by the broken line rectangle in *a*, with MeHg-L-Cys in the BCH binding site with the polypeptide chain being rendered transparent to reveal the active site binding. Selected amino acid residues are labelled. All protein protons have been hidden to simplify the structure.

Table 6.1: Energy difference between L- and D-enantiomers of methylmercury-L-cysteine and LAT substrates bound to BCH active site.

Substrate	*Energy change* (L-D) ($kJ \cdot mol^{-1}$)
MeHg-Cys	36.8
Methionine	68.9
Phenylalanine	26.4
Leucine	35.8

The table shows the energetic differences between geometry optimized energy-minimized structures with the L- and D- enantiomeric substrates bound in the site observed for BCH binding. Coordinates of the polypeptide backbone were constrained to the locations reported from the cryo-EM structure.

For example, the binding of MeHg-D-Cys was energetically preferable by approximately 36 kJ mol^{-1} and calculations suggested a somewhat different orientation for the two enantiomers within the BCH-binding pocket. LAT preferentially transports L-enantiomers, but its selectivity is not complete, and we conclude that whatever parts of the overall active site confer enantiomeric selectivity, it is not the region in which BCH was observed to be bound. Other work has shown that inhibitory effects on LAT uptake of the substrate L-leucine can be seen in the presence of D-methionine, D-phenylalanine and D-leucine *in vitro*[44,45] which not only indicates the potential for the binding of D-enantiomers, but also that it occurs in a location which is effective in halting or reducing transport. Other research using microinjection of various methylmercury compounds into LAT1-4F2hc and LAT2-4F2hc expressing *Xenopus laevis* oocytes showed that while the uptake was greatest for MeHg-L-Cys, MeHg-D-Cys was also taken up, albeit at a level that was somewhat less than 25% of MeHg-L-Cys within the same time frame.[8]

The LAT/4F2hc heterodimer has been a subject of study for some time in part due to its implication in various human cancers as well as its upregulation in various cancerous cell lines.[20,46,47] Its increased expression under these circumstances is thought to be related to increased cell proliferation, as neutral amino acid transport via LAT/4F2hc is involved in the mTOR pathway in several cell lines.[46] Indeed, an increased presence of LAT1 transporters has been linked with certain types of cancer which can be correlated with a negative prognosis.[46] Some research has focussed on inhibition of LAT transport as a therapeutic strategy for certain cancers.[46,47]

Here we used zebrafish larvae, a commonly used vertebrate model for the developing foetus to study competitive inhibition of two forms of organometallic mercury in the presence of various LAT substrates and an inhibitor to investigate whether a modulation of uptake of either form of organometallic mercury would occur and whether the result would be a corresponding modulation in toxicity. Although uptake of MeHg-L-Cys and MeHg-D-Cys via LAT transporters has been studied quite extensively in *in vitro* models, the involvement of these transporters in methylmercury transport *in vivo* has been studied less, and not in zebrafish, to our knowledge. Besides competitive inhibition by other amino acids, transport of MeHg-L-Cys can also be modulated by changes in LAT1 and LAT2 expression. For example, LAT1 expression is reduced as a result of high blood glucose in patients with diabetes,[48] which can potentially result in reduced MeHg-L-Cys uptake by the brain.

The importance of understanding interactions between LAT transporters and methylmercury *in vivo* can be highlighted by the possibilities of significant modulation of mercury uptake by specific physiological conditions, for example, the presence of higher concentration of amino acids in the blood. The results herein demonstrate that co-exposure of MeHg-L-Cys and each individual LAT competitor resulted in increased survival of zebrafish larvae when compared with MeHg-L-Cys alone, suggesting that toxic effects of methylmercury exposure can possibly be modulated by the presence of nutrients such as amino acids in the blood stream or other tissues. Amino acids are commonly found in protein-rich foods. Given the heightened survival and the reduced concentrations of mercury in target organs in larvae treated with excesses of amino acids, it is possible that the presence of these amino acids affords some protection against this organometallic compound. One might further speculate that the uptake rates of MeHg-L-Cys through the intestinal tract might be decreased if organometallic mercury was a constituent of a protein-rich meal, similar to the protection afforded by the selenium content of fish when consumed at the same time as organometallic mercury.

While all examined LAT substrates and inhibitor were successful in decreasing mercury toxicity, not all of them influenced mercury accumulation in zebrafish tissues in the same way. L-phenylalanine and BCH co-exposure with MeHg-L-Cys resulted in a statistically significant decreases in mercury accumulation in whole sections, including the brain. Co-exposure with L-methionine resulted in only slight attenuation in mercury accumulation, which might be partly explained by a lower affinity of LAT transporters to L-methionine compared to L-phenylalanine.[16,49] Higher levels of mercury in zebrafish co-exposed with L-methionine compared to fish co-treated with L-phenylalanine or BCH could also indicate that initial uptake is not the only determinant of mercury bioaccumulation. Methionine itself can bind mercury and other work has noted that excess cysteine can accelerate the uptake of methylmercury.[11,50] As well, methionine catabolism can result in the formation of sulfides[51] that are known to form stable and biologically inert HgS compounds,[52] which may also explain the decrease in toxicity and only slight change in mercury burden.

The mercury burden in the brain as a result of MeHg-D-Cys exposure was approximately two-fold lower than the mercury concentration resulting from MeHg-L-Cys (Fig. 6.4, Hg panel), which at least in part can be explained by the lower affinity of LAT transporters towards MeHg-D-Cys compared to the L-enantiomer. As well, the relatively long exposure time used in this study

might have allowed for significant catabolic changes of D-cysteine. There are few known pathways for D-cysteine metabolism in vertebrates. One pathway includes production of hydrogen sulfide;[53] here, increased availability of D-cysteine may lead to elevated production of hydrogen sulfide and sulfane sulfur in tissues, resulting in enhanced protection of neurons and kidneys.[54] As previously mentioned, hydrogen sulfide and many sulfane species efficiently protect tissues and organs against mercury toxicity by forming biologically inactive mercury sulfide complexes such as mercuric sulfide. Moreover, hydrogen sulfide plays an important role in demethylation of organometallic mercury.[55] It is possible that the presence of high levels of sulfides as a result of MeHg-D-Cys catabolism resulted in some level of demethylation of organometallic mercury; this may explain the reduced transport of MeHg-D-Cys into the brain (Fig. 6.4, Hg panel) and subsequent increased survival (Fig. 6.2).

Our earlier work has shown that exposure of zebrafish larvae to mercuric chloride leads to depletion of selenium from melanophores that normally contain high levels of selenium, as well as redistribution of this element into the kidneys as a complex with mercury, presumably as part of the process of mercury excretion from the body.[43] We also observed that both mercuric chloride and methylmercury chloride exposure leads to statistically significant selenium depletion from the brain of zebrafish larvae.[43] It was therefore somewhat surprising to discover that in this work, exposure of zebrafish larvae to MeHg-L-Cys did not result in selenium depletion, further highlighting the importance of chemical form in toxicity.[29] This finding suggests that consuming fish which contain mercury in the form of MeHg-L-Cys[56] may not lead to selenium depletion, but may instead result in selenium enrichment with additional physiological and cognitive benefits due to the high selenium content in most fish species.[57] Interestingly, co-exposure to L-methionine together with MeHg-L-Cys slightly increased the level of selenium above the level of that observed in control fish, although this increase was not statistically significant.

Significant depletion of selenium was observed in all tissues in zebrafish exposed to MeHg-D-Cys, and especially in the brain. This depletion is consistent with what is observed in zebrafish after exposure to methylmercury chloride or mercuric chloride[43] and highlights the importance of the involvement of the metabolically active L-cysteine form vs. the D-cysteine form that is very limited in the possible catabolism pathways discussed above. The combined observations of decreased toxicity of MeHg-D-Cys compared to MeHg-L-Cys, without a significant decrease in mercury burden in tissues, along with significant differences in their

effects on selenium and sulfur abundance in zebrafish suggest that the toxicity of mercury and its effects on selenium and sulfur metabolism are determined not only by the level of mercury in the tissues and its chemical form, but also by the presence of other nutrients and physiologically active compounds that can significantly modulate the outcome of exposure.

In conclusion, the current work highlights an important role of LAT transporters in methylmercury uptake *in vivo*. We also show that mercury toxicity and accumulation is influenced by other nutrients, with an especially important role of sulfur-containing amino acids like L-methionine. Moreover, exposure to methylmercury complexed with D-cysteine leads to significant selenium deficiency in zebrafish larvae tissues, consistent with the results of exposure to methylmercury chloride and mercuric chloride, while L-cysteine complexed with methylmercury does not result in selenium depletion.

6.6 Acknowledgements

This work was supported by the Natural Sciences and Engineering Research Council of Canada (NSERC; GNG and IJP), the Canada Foundation for Innovation (CFI; IJP) and by Canadian Institutes of Health Research – Training Grant in Health Research Using Synchrotron Techniques (CIHR-THRUST; IJP). AKJ, TCM, SN and KLS were CIHR-THRUST Fellows, and NVD was a CIHR-THRUST Associate. GNG and IJP are Canada Research Chairs. This research used resources of the Advanced Photon Source, an Office of Science User Facility operated for the U.S. Department of Energy (DOE) Office of Science by Argonne National Laboratory, and was supported by the U.S. DOE under Contract No. DE-AC02-06CH11357, and the Canadian Light Source and its funding partners.

6.7 References

(1) Sanfeliu, C., Sebastià, J., Christòfol, R., Rodriguez-Farré, E. Neurotoxicity of organomercurial compounds. *Neurotox. Res*. **2003**, *5*, 283-306.

(2) Clarkson, T.W. The toxicology of mercury and its chemical compounds. *Crit. Rev. Toxicol*. **2006**, *36*, 609-662.

(3) Harada, M. Minamata Disease: Methylmercury poisoning in Japan caused by environmental pollution. *Crit. Rev. Toxicol*. **1995**, *25*, 1-24.

(4) Davidson, P.W., Strain, J.J., Myers, G.J., Thurston, S.W., Bonham, M.P., Shamlaye, C.F., Stokes-Riner, A., Wallace, J.M.W., Robson, P.J., Duffy, E.M., Georger, L.A., Sloane-Reeves, J., Cernichiari, E., Canfield, R.L., Cox, C., Huang, L.S., Janciuras, J., Clarkson, T.W. Neurodevelopmental effects of maternal nutritional status and exposure to methylmercury from eating fish during pregnancy. *Neurotoxicology* **2008**, *29*, 767-775.

(5) Grandjean, P., Weihe, P., White, R.F., Debes, F., Araki, S., Yokoyama, K., Murata, K., Sorensen, N., Dahl, R., Jorgensen, P.J. Cognitive deficit in 7-year old children with prenatal exposure to methylmercury. *Neurotoxicol. Teratol*. **1997**, *19*, 417-428.

(6) Tchounwou, P.B., Ayensu, W.K., Ninashvili, N., Sutton, D. Environmental exposure to mercury and its toxicopathologic implications for public health. *Environ. Toxicol*. **2003**, *18*, 149-175.

(7) Mokrzan, E.M., Kerper, L.E., Ballatori, N., Clarkson, T.W. Methylmercury-thiol uptake into cultured brain capillary endothelial cells on amino acid system L. *J. Pharmacol. Exp. Ther*. **1995**, *272*, 1277-1284.

(8) Simmons-Willis, T.A., Koh, A.S., Clarkson, T.W., Ballatori. N. Transport of a neurotoxicant by molecular mimicry: the methylmercury-L-cysteine complex is a substrate for the human L-type large neutral amino acid transporter (LAT) 1 and LAT2. *Biochem. J*. **2002**, *367*, 239-246.

(9) Hoffmeyer R., Singh, S.P., Doonan, C.J., Ross, A.R.S., Hughes, R.J., Pickering, I.J., George, G.N. Molecular mimicry in mercury toxicology. *Chem. Res. Toxicol*. **2006**, *19*, 753-759.

(10) George. G.N., Pickering, I.J., Doonan, C.J., Korbas, M., Singh, S.P., Hoffmeyer, R. Inorganic molecular toxicology and chelation therapy of heavy metals and metalloids. In: Advances in Molecular Toxicology; Fishbein, J.C., Ed.; Elsevier Science: Amsterdam, 2008, Vol. 2

(11) Kerper, L.E., Ballatori, N., Clarkson, T.W. Methylmercury transport across the blood-brain barrier by an amino acid carrier. *Am. J. Physiol-Reg*. **1992**, *262*, 761-765

(12) Kajiwara Y., Yasutake, A., Hirayama, K. Methylmercury transport across the placenta via neutral amino acid carrier. *Arch. Toxicol*. **1996**, *70*, 310-314.

(13) Wang, W., Clarkson, T.W., Ballatori, N. γ-glutamyl transpeptidase and L-cysteine regulate methylmercury uptake by HepG2 cells, a human hepatoma cell line. *Toxicol. Appl. Pharm.* **2000**, *168*, 72-78.

(14) Balthasar, C., Stangl, H., Widhalm, R., Granitzer, S., Hengstschläger, M., Gundacker, C. Methylmercury uptake into BeWo cells depends on LAT2-4F2hc, a system L amino acid transporter. *Int. J. Mol. Sci*. **2017**, *18*, 1730.

(15) Kanai, Y., Endou, H. Heterodimeric amino acid transporters: Molecular biology and pathological and pharmacological relevance. *Curr. Drug Metab*. **2001**, *2*, 339-354.

(16) Yan, R., Zhao, X., Lei, J., Zhou, Q. Structure of the human LAT1-4F2hc heteromeric amino acid transporter complex. *Nature* **2019**, *568*, 127-+.

(17) Lee, Y.,Wiriyasermkul, P., Jin, C., Quan, L., Ohgaki, R., Okuda, S., Kusakizako, T., Nishizawa, T., Oda, K., Ishitani, R., Yokoyama, T., Nakane, T., Shirouzu, M., Endou. H., Nagamori, S., Kanai, Y., Nureki, O. Cryo-EM structure of the human L-type amino acid transporter 1 in complex with glycoprotein CD98hc. *Nat. Struct. Mol. Biol*. **2019**, *26*, 510-+.

(18) Kanai, Y., Segawa, H., Miyamoto, K., Uchino, H., Takeda, E., Endou, H. Expression cloning and characterization of a transporter for large neutral amino acids activated by the heavy chain of 4F2 antigen (CD98). *J. Biol. Chem*. **1998**, *273*, 23629-23632.

(19) Pineda, M., Fernández, E., Torrents, D., Estévez, R., López, C., Camps, M., Lloberas, J., Zorzano, A., Palacín, M. Identification of a membrane protein, LAT-2, that co-expresses with 4F2 heavy chain, an L-type amino acid transport activity with broad specificity for small and large zwitterionic amino acids. *J. Biol. Chem*. **1999**, *274*, 19738-19744.

(20) Fuchs, B.C., Bode, B.P. Amino acid transporters ASCT2 and LAT1 in cancer: Partners in crime? *Semin. Cancer Biol*. **2005**, *15*, 254-266.

(21) Pardridge, W.M. Brain metabolism: A perspective from the blood-brain barrier. *Physiol. Rev*. **1983**, *63*, 1481-1535.

(22) Miller, L.P., Pardridge, W.M., Braun, L.D., Oldendorf, W.H. Kinetic constants for blood-brain barrier amino acid transport in conscious rats. *J. Neurochem*. **1985**, *45*, 1427-1432.

(23) Betz, A.L., Goldstein, G.W. Polarity of the blood-brain barrier: Neutral amino acid transport into isolated brain capillaries. *Science* **1978**, *202*, 225-227.

(24) Hirayama, K. Effect of amino acids on brain uptake of methyl mercury. *Toxicol. Appl. Pharmacol*. **1980**, *55*, 318-323.

(25) Hirayama, K. Effects of combined administration of thiol compounds and methylmercury chloride on mercury distribution in rats. *Biochem. Pharmacol*. **1985**, *34*, 2030-2032.

(26) Kerper, L.E., Ballatori, N., Clarkson, T.W. Methylmercury transport across the blood-brain barrier by an amino acid carrier. *Am. J. Physiol*. **1992**, *262*, R761-R765.

(27) Heggland, I., Kaur, P., Syversen, T. Uptake and efflux of methylmercury in vitro: Comparison of transport mechanisms in C6, B35 and RBE4 cells. *Toxicol. In Vitro* **2009**, *23*, 1020-1027.

(28) Pushie, M.J., Pickering, I.J., Korbas, M., Hackett, M.J., George, G.N. Elemental and chemically specific X-ray fluorescence imaging of biological systems. *Chem. Rev*. **2014**, *114*, 8499-8541.

(29) Korbas, M., MacDonald, T.C., Pickering, I.J., George, G.N., Krone, P.H. Chemical form matters: Differential accumulation of mercury following inorganic and organic mercury exposures in zebrafish larvae. *ACS Chem. Biol*. **2012**, *7*, 411-420.

(30) Korbas, M., Krone, P.H., Pickering, I.J., George, G.N. Dynamic accumulation and redistribution of methylmercury in the lens of developing zebrafish embryos and larvae. *J. Biol. Inorg. Chem*. **2010**, *15*, 1137-1145.

(31) MacDonald, T.C., Korbas, M., James, A.K., Sylvain, N.J., Hackett, M.J., Nehzati, S., Krone, P.H., George, G.N., Pickering, I.J. Interaction of mercury and selenium in the larval stage zebrafish vertebrate model. *Metallomics* **2015**, *7*, 1199-1292.

(32) Korbas, M., Blechinger, S.R., Krone, P.H., Pickering, I.J., George, G.N. Localizing organomercury uptake and accumulation in zebrafish larvae at the tissue and cellular level. *PNAS* **2008**, *105*, 12108-12112.

(33) Korbas, M., Lai, B., Vogt, S., Gleber, S.-C., Karunakaran, C., Pickering, I. J., Krone, P. H., George, G. N. Methylmercury targets photoreceptor outer segments. *ACS Chem. Biol*. **2013**, *8*, 2256-2263.

(34) Dolgova, N.V., Hackett, M.J., MacDonald, T.C., Nehzati, S., James, A.K., Krone, P.H., George, G.N., Pickering, I.J. Distribution of selenium in zebrafish larvae after exposure to organic and inorganic selenium forms. *Metallomics* **2016**, *8*, 305-312.

(35) Delley, B. An all-electron numerical method for solving the local density functional for polyatomic molecules. *J. Chem. Phys*. **1990**, *92*, 508-517.

(36) Delley, B. From molecules to solids with the DMol3 approach. *J. Chem. Phys*. **2000**, *113*, 7756-7764.

(37) Peverati, R., Truhlar, D.G. M11-L: A local density functional that provides improved accuracy for electronic structure calculations in chemistry and physics. *J. Phys. Chem. Lett*. **2012**, *3*, 117-124.

(38) Rand, M.D., Vorojeikina, D., Peppriell, A., Gunderson, J., Prince, L.M. Drosophotoxicology: Elucidating kinetic and dynamic pathways of methylmercury toxicity in a Drosophila model. *Front. Genet*. **2019**, *10*, article number 666.

(39) Gailer, J. Arsenic-selenium and mercury-selenium bonds in biology. *Coord. Chem. Rev*. **2007**, *251*, 234-254.

(40) Hatfield, D.L., Tsuji, P.A., Carlson, B.A., Gladyshev, V.N. Selenium and selenocysteine: roles in cancer, health, and development. *Trends Biochem. Sci*. **2014**, *39*, 112-120.

(41) Berry, M.J., Ralston, N.V.C. Mercury toxicity and the mitigating role of selenium. *EcoHealth* **2008**, *5*, 456-459.

(42) Gerson, J.R., Walters, D.M., Eagles-Smith, C.A., Bernhardt, E.S., Brandt, J.E. (2020) Do two wrongs make a right? Persistent uncertainties regarding environmental selenium−mercury interactions. *Environ. Sci. Technol*. **2020**, *54*, 9228-9234.

(43) Dolgova, N.V., Nehzati, S., MacDonald, T.C., Summers, K.L., Crawford, A.M., Krone, P.H., George, G.N., Pickering, I.J. Disruption of selenium transport and function is a major contributor to mercury toxicity in zebrafish larvae. *Metallomics* **2019**, *11*, 621-631.

(44) Morimoto, E., Kanai, Y., Kim, D.K., Chairoungdua, A., Choi, H.W., Wempe, M.F., Anzai, N., Endou, H. Establishment and characterization of mammalian cell lines stably expressing human L-type amino acid transporters. *J. Pharmacol. Sci*. **2008**, *108*, 505-516.

(45) Yanagida, O., Kanai, Y., Chairoungdua, A., Kim, D.K., Segawa, H., Nii, T., Ho Cha, S., Matsuo, H., Fukushima, J., Fukasawa, Y., Tani, Y., Taketani, Y., Uchino, H., Kim, J.Y., Inatomi, J., Okayasu, I., Miyamoto, K., Takeda, E., Goya, T., Endou, H. Human L-type amino acid transporter 1 (LAT1): characterization of function and expression in tumor cell lines. *Biochim. Biophys. Acta* **2001**, *1514*, 291-302.

(46) Fotiadis, D., Kanai Y., Palacin, M. The SLC3 and SLC7 families of amino acid transporters. *Mol. Aspects. Med*. **2013**, *34*, 139-158.

(47) Satou, M., Wang, J., Nakano-Tateno, T., Teramachi, M., Suzuki, T., Hayashi, K., Lamothe, S., Hao, Y., Kurata, H., Sugimoto, H., Chik, C., Tateno, T. L-type amino acid transporter 1, LAT1, in growth hormone-producing pituitary tumor cells. *Mol. Cell. Endocrinol*. **2020**, *515*, 110868-

(48) Yamamoto, Y., Sawa, R.,Wake, I., Morimoto, A., Okimura, Y. Glucose-mediated inactivation of AMP-activated protein kinase reduces the levels of L-type amino acid transporter 1 mRNA in C2C12 cells. *Nutr. Res*. **2017**, *47*, 13–20.

(49) Segawa, H., Fukasawa, Y., Miyamoto, K., Takeda, E., Endou, H., Kanai, Y. Identification and functional characterization of Na+-independent neutral amino acid transporter with broad substrate selectivity. *J. Biol. Chem*.**1999**, *274*, 19745-19751.

(50) Hirayama, K. Effects of combined administration of thiol compounds and methylmercury chloride on mercury distribution in rats. *Biochem. Pharmacol*. **1985**, *36*, 1919-1924.

(51) Stipanuk, M.H. Metabolism of sulfur-containing amino acids: How the body copes with excess methionine, cysteine, and sulfide. *J. Nutr*. **2020**, *150*, 2494-2505.

(52) Korbas, M., O'Donoghue, J. L., Watson, G. E., Pickering, I. J., Singh, S. P., Myers, G. J., Clarkson, T. W., George, G. N. The chemical nature of mercury in human brain following poisoning or environmental exposure. *ACS Chem. Neurosci*. **2010**, *1*, 810–818.

(53) Olson, K.R., Straub, K.D. The role of hydrogen sulfide in evolution and the evolution of hydrogen sulfide in metabolism and signaling. *Physiology* **2016**, *31*, 60-72.

(54) Shibuya, N., Koike, S., Tanaka, M., Ishigami-Yuasa, M., Kimura, Y., Ogasawara, Y., Fukui, K., Nagahara, N., Kimura, H. A novel pathway for the production of hydrogen sulfide from D-cysteine. *Nat. Commun*. **2013**, *4*, article number 1366.

(55) West, J., Graham, A.M., Liem-Nguyen, V., Jonsson, S. Dimethylmercury degradation by dissolved sulfide and mackinawite. *Environ. Sci. Technol*. **2020**, *54*, 13731-13738.

(56) Harris, H.H., Pickering, I.J., George, G.N. The chemical form of mercury in fish. *Science* **2003**, *301*, 1203.

(57) Berr, C., Akbaraly, T., Arnaud, J., Hininger, I., Roussel, A.-M., Gateau, P.B. Increased selenium intake in elderly high fish consumers may account for health benefits previously ascribed to omega-3 fatty acids. *J. Nutr*. **2009**, *13*, 14-18.

CHAPTER 7: CAN SKIN-ASSOCIATED MUCOUS CHEMICALLY PROTECT AGAINST LOW-LEVEL MERCURY IN TELEOST FISH?

7.1 Preface

The final experimental chapter of this thesis is focussed on potential defensive mechanisms against mercury toxicity. Inspiration for this work came at least partly from the research in Chapter 4 which dealt with potential mechanisms for demethylation of organometallic mercury compounds in human brain tissue. Mercury is also thought to become demethylated within the intestinal tract of humans, prior to excretion.

Prior work conducted within this research group noted an unusual phenomenon of accumulation of mercury in what appeared to be the exterior, mucosal-producing epithelial layer of larval zebrafish after exposure to an inorganic mercury compound. Previous work had presumed this to be mercury bound through non-physiological adsorption from the treatment solution and sought to dampen undesirable mercury fluorescence in (presumed) non-target locations in XFI images by rinsing euthanized zebrafish prior to preservation. This work considered the possibility that accumulation in this location was, instead, a target for mercury accumulation, and even toxicity. This was further explored by treating larval zebrafish, the model organism of choice in this thesis, to various other organic and inorganic mercury species. The potential for demethylation to occur here was realized and investigated by titrating a range of concentrations using both an organometallic and inorganic mercury species. Demethylation was seen to occur in the lowest methylmercury concentration used.

This chapter will be submitted for publication following the completion of additional work.

James, A.K., MacDonald, T.C., Dolgova, N.V., Summers, K.L., Krone, P.H., Pickering, I.J., George, G.N. Can skin-associated mucous chemically protect against low-level mercury in teleost fish?

A.K. James collected trout mucosa from Wild West Steelhead, conducted experimental and laboratory work, collected and analyzed XFI data, analyzed XAS data and drafted the manuscript.

T.C. MacDonald conducted initial studies with inorganic mercury and noted accumulations in the epithelial layer of larval zebrafish.

N.V. Dolgova assisted with the Ellman's assay and collected sulfur XAS.

K.L. Summers assisted with mercury XFI data collection.

G.N. George, I.J. Pickering and P.H. Krone contributed scientific input and guidance and provided funding for the research as well as commented on and edited the manuscript.

7.2 Abstract

Demethylation of organometallic mercury compounds is known to occur within the brain and the intestinal tract of humans as a mechanism of protection against toxicity, although this process is not yet fully understood. Similar protective mechanisms against organometallic mercury are known to occur in many animal species. Here the potential for demethylation in a previously un-studied target location, the mucosa of a teleost fish was examined. X-ray absorption spectroscopy (XAS) was used to determine mercury speciation after titration of various concentrations of an organometallic and inorganic mercury compound with mucosa harvested from steelhead trout (*Oncorhynchus mykiss*) from a local aquaculture facility. Demethylation of organometallic mercury was seen at the lowest concentration used. As well, the accumulation of mercury in a previously unseen location, the exterior epithelial layer, was investigated using X-ray fluorescence imaging (XFI) and larval zebrafish, a well-established model organism in vertebrate development which had been exposed to either organometallic or inorganic mercury compounds. Accumulation of mercury in this exterior target location was seen after exposure to all mercury compounds used and was additionally seen to increase over time after exposure to inorganic mercury.

7.3 Introduction

Mucosal-associated tissues occur in all vertebrates,[1] with fish and amphibians being distinct from mammals, reptiles and birds in having a mucosal-covered epidermis. This mucosal exterior has functions that include sensory perception (e.g. in fish nasal mucosa), assisting locomotion by providing lubrication, helping with both thermal and ionic regulation and in providing a protective barrier against the environment (e.g. water) in which it is in constant contact.[2,3] Günther et al.[4] has called the epithelial layer the first line of defense for an organism which is in intimate contact with its environment. This protective function can be argued to be especially important for an aquatic organism as it is the barrier between the organism itself and its environment. As such, skin-related diseases are more commonly found in aquatic organisms when compared with terrestrial organisms, hence the large body of literature on aquaculture and related topics.[5–8]

The epidermal layer of a teleost fish contains cellular components which are thought to be ubiquitous amongst teleost fish species, including goblet cells, club cells, Merkel cells, sacciform cells and undifferentiated cells, amongst others, although their quantity and distribution may vary between species.[3] Secretions from goblet mucous cells, club cells and sacciform cells are thought to be the primary components of fish epidermal mucous. Goblet cells produce mucins which are the primary component of mucous and are composed of high molecular weight sulfated or neutral glycoproteins and which are responsible for the gel-like texture of the secreted mucous.[9] Other components of mucous include additional proteins such as lysozymes and lectins, and a variety of immune related components which have been previously summarized.[10]

Some research has shown that the number of mucous cells present within the skin epithelia may be altered in response to environmental stressors.[9] It is known that in adverse conditions such as changes in salinity, light, pH, or presence of heavy metals, fish epithelial cells will secrete an over-abundance of mucous as a protective mechanism. Shephard et al.[2] noted that excess secretions of mucous on the surface of epithelial cells may provide ideal conditions for binding of mucosa to toxicants such as heavy metals which could then be shed to prevent ingestion or uptake. However, they also noted that this was pure theory and that it has not been otherwise proven.

Zebrafish (*Danio rerio*) have been used extensively as a model in toxicology[11] for studying heavy metals, including mercury.[12–14] Our laboratory has developed and demonstrated

the use of X-ray fluorescence imaging of zebrafish larval sections with the purpose of investigating target organs and tissues for toxic effects of mercury and other biologically relevant elements, as well as extensive research using X-ray absorption spectroscopy techniques as a tool for probing the molecular structure of heavy metals in biological tissues. In this work, we used EXAFS to investigate the chemical modifications of mercury compounds on mucosal secretions of mature *Oncorhynchus mykiss* collected from a local aquaculture facility. Further to this, we utilized XFI to demonstrate the uptake of various organic and inorganic mercury species into the epithelial layer of the model organism, *Danio rerio*.

7.4 Materials and Methods

7.4.1 Husbandry and experimental

Zebrafish were raised and maintained in a dedicated aquatic facility, the Lab Animals Service Unit (LASU) at the University of Saskatchewan using a 14:10 h light : dark cycle and with water temperatures constant at 27.5 °C. Mates were conducted by placing Tübingen wildtype zebrafish in separate tanks with females and males kept separate through use of a divider until the start of the light cycle in the morning. Dividers were then removed, and embryo collection occurred several hours later.

Viable embryos were rinsed with system water and carefully transferred to Petri dishes of no more than 50 embryos/dish. Petri dishes were filled with embryo media, which has been previously described[15] and placed into an incubator maintaining a constant temperature of 28°C. Embryo media were changed daily up to 3 days post-fertilization (dpf) with dishes being cleaned of dead embryos and debris concurrently.

Methylmercury hydroxide (1 M) aqueous solution was purchased from Strem Chemicals Inc. (Newburyport, MA, USA) and was diluted with triple-distilled water to make a stock solution of 4 mM. All other chemicals were purchased from Sigma-Aldrich (St. Louis, MO, USA) except when otherwise stated, and were of the highest quality available. L-cysteine stock solutions were made in 30 mM phosphate-buffered saline (PBS). Appropriate aliquots of stock solutions were mixed to produce a 1 mM solution with a 20% excess of L-cysteine for methylmercury-L-cysteine (MeHg-L-Cys).[16,17] Final exposure solutions of 0.2 µM MeHg-L-Cys were made up using 1 mM stocks and embryo media. A stock solution of 1 mM mercuric chloride ($HgCl_2$) was produced by mixing mercuric chloride crystals into triple-distilled water. A 1 mM stock solution of mercuric bis-L-cysteine [$Hg(Cys)_2$] was made by slowly mixing the stock

solution of $HgCl_2$ into a 2.5 mM solution of L-cysteine made up in 100 mM HEPES solution.[18] A final exposure concentration of 100 µM $Hg(Cys)_2$ was made from the stock solution and embryo media. A 4 mM aqueous stock solution of methylmercury chloride (MeHgCl) was purchased from Alfa Aesar and diluted to 100 µM using triple-distilled water. Mercuric chloride crystals were used to produce a 1 mM stock solution in triple-distilled water. Both stock solutions were used to create final exposure concentrations of 0.2 µM MeHgCl and 4 µM $HgCl_2$ which were made up in embryo media.

University of Saskatchewan Ethics Board approved all animal work which was conducted following the Guidelines of the Canadian Council of Animal Care (CCAC). Exposures to all mercury solutions began at 3 dpf and ended at between 4 and 7 dpf. Exposure concentrations for each mercury chemical form were based on previous work and we intended to ensure survival of the larvae while still exhibiting significant accumulation of mercury within tissues. Previous (unpublished) lethality work has shown that zebrafish larvae can survive a concentration of 0.2 µM MeHg-L-Cys for up to 48 hours. A similar concentration of 0.2 µM MeHgCl was chosen with reference to MeHg-L-Cys lethality work as well as lethality work involving an additional 100 zebrafish larvae. The exposure concentration of 4 µM $HgCl_2$ and duration of 48 hours was based on previous work.[19] $Hg(Cys)_2$ has been shown to be less toxic to zebrafish larvae[18] surviving at 100 µM for up to 96 hours based off previous work (unpublished) as well as additional lethality studies involving 100 zebrafish larvae. Larvae from 0.2 µM MeHg-L-Cys, 0.2 µM MeHgCl and 4 µM $HgCl_2$ exposures were all collected for preservation at 48 hours, while those from 100 µM $Hg(Cys)_2$ were collected at 24h, 48h, 72h, and 96h time points. All stock solutions were kept cold at 4°C with exposure solutions made fresh and changed in exposure Petri dishes every 24 hours. Petri dishes with zebrafish larvae were kept in an incubator for the duration of the experiment. Upon experimental completion, all larvae were euthanized using 0.2% Tricaine and either rinsed multiple times using triple-distilled water (as specified by previous work[16-21] specifically for eliminating mercury which may have accumulated on the exterior of the zebrafish epidermis) or directly moved, unrinsed, towards preservation.

7.4.2 JB-4 methacrylate preservation

Zebrafish larvae were preserved using the commercial JB-4 Plus embedding kit (Polysciences, Warrington, PA, USA), the general protocol of which has been described elsewhere.[16–18] Following preservation, zebrafish larvae were sectioned to 10 µm using a

microtome equipped with glass knives. Sections intended for X-ray fluorescence imaging (XFI) were mounted on Thermanox plastic coverslips while adjacent sections were collected onto Fisherbrand Superfrost Plus microscope slides for histological staining.

7.4.3 X-ray fluorescence imaging (XFI)

X-ray fluorescence imaging data were collected at the Advanced Photon Source (APS) which is a U.S. Department of Energy facility. The APS is a 7 GeV synchrotron containing 60 operational beamlines running at a ring current of 102 mA and in top-up mode. Beamline 20-ID-B is an undulator beamline employing a Si(111) double-crystal monochromator with Kirkpatrick-Baez (KB) mirrors and a Rh-coated mirrors for production of a focussed microbeam with a resolution of approximately 5 µm. A silicon drift Vortex® detector (Hitachi High-Technologies Science America Inc., Northridge, CA, USA), fitted with a collimator was used to record X-ray fluorescence. The plastic coverslip on which the samples are located was mounted onto 6.3 µm polypropylene film and situated at an angle of 45° from the incoming X-ray beam and at a 90° angle to the detector. Incident X-ray energy was set to 13 450 eV for capturing of mercury and other trace element fluorescence without exciting bromine fluorescence. Each sample was scanned from the bottom-left corner fluidly to the top-right corner in 5 µm × 5 µm step sizes with a dwell time of 600 milliseconds per step.

X-ray fluorescence imaging data was also collected on beamline 2-ID-D which has significantly greater resolution than 20-ID-B at approximately 200 µm. This resolution is achieved using Fresnel zone plates (X-radia, Pleasanton, CA) rather than the KB mirrors utilized at 20-ID-B. All other set-up parameters were the same excepting the step size which was 400 nm × 400 nm and the dwell time which was 400 milliseconds. X-ray fluorescence imaging analysis was carried out as previously described.[16–21]

7.4.4 Ellman's assay and mercury-mucosa experimental

Oncorhynchus mykiss mucosa samples were collected at a local aquaculture facility (Wild West Steelhead, Lucky Lake, SK, CA). Mucosa was collected as composite samples from approximately 10 trout which had been euthanized moments before using electrocution (standard operating procedure at the facility). Approximately 90 mL of mucosa was collected which was noted to be very viscous at the time of collection. Samples were stored on ice for transport and frozen at -20°C upon arrival at the laboratory.

Ellman's assay was utilized for estimation of thiol content of the trout mucosa collected which utilizes the Ellman's reagent, 5,5'-dithiobis (2-nitrobenzoic acid), also called DTNB for reaction with thiols in peptides or proteins. A calibration curve using glutathione was created for quantitation and absorbance off the plate was read at 412 nm. Average thiol content was determined to be 2.5 mM after trout mucosa was mixed with the reagent DTNB and read using a plate-reader.

Mucosa samples for X-ray absorption spectroscopy (XAS) were titrated with varying concentrations of organic and inorganic mercury to probe any changes in the mercury molecular environment in presence of the mucosa. Forms of mercury included one organic (MeHgCl) and one inorganic form ($HgCl_2$) with concentrations of 100, 400 and 700 µM chosen for both organic and inorganic mercury. Mucosa-only control samples were also made. All XAS samples contained 25% glycerol for protection against ice artifacts, although samples were monitored carefully as some work has shown that the addition of cryoprotectants may lead to photoreduction,[22,23] even in the case of mercury,[24] which can alter spectra and influence interpretation of results. All samples intended for mercury XAS were loaded into metal-free plastic cuvettes with mylar tape for windows flash frozen in liquid nitrogen cooled isopentane. Samples intended for sulfur XAS were treated slightly differently due to the low penetration of X-rays at the sulfur edge, with mucosa being coated as thin films on Thermanox plastic coverslips which were dried in a desiccator and then transported attached to microscope slides.

7.4.5 X-ray absorption spectroscopy (XAS)

All XAS experiments were run at the 3 GeV Stanford Synchrotron Radiation Lightsource (SSRL, Menlo Park, CA) which maintains a ring current of ~500 mA through top-up operational mode. Mercury L_{III}-edge XAS was collected using beamline 7-3 and sulfur K-edge XAS was collected on beamline 4-3. Both beamlines are powered by essentially identical flat-top field profile 20-pole 2T permanent magnet wigglers. Beamline 7-3 is equipped with a Si(220) double-crystal monochromator responsible for X-ray energy selection with a single upstream Rh-coated mirror for focussing the X-ray beam. End station set-up at 7-3 includes a liquid-helium cooled cryostat which maintains the sample at a temperature of 10K as well as two nitrogen-filled ion chambers which measure both the incident and the transmitted X-rays. Mercury fluorescence is collected by a Canberra solid-state 30-element germanium detector equipped with gallium filters and Soller slits for exclusion of unwanted confounding fluorescence. To calibrate the incident X-

ray beam energy, transmittance of X-rays through a Hg-Sn amalgam standard metal foil located downstream of the ion chambers is analyzed simultaneously to mercury fluorescence emitted from the sample, using a third nitrogen-filled ion chamber. The lowest energy inflection of the Hg-Sn amalgam is assumed to be 12 284 eV.

Beamline 4-3 is optimized for lower X-ray energies than 7-3 and employs a Si(111) double-crystal monochromator with an upstream vertically collimating bare silicon mirror which was set at an appropriate angle to achieve harmonic rejection. Samples were maintained at room temperature in a helium flight path and total X-ray fluorescence was monitored using a large-area PIN diode (Canberra Industries, Meriden, CT, USA). Visible light was excluded by employing an aluminized mylar window on the face of the detector, and by darkening the experimental hutch. The incident X-ray energy was calibrated with reference to the spectrum of solid sodium thiosulfate measured immediately prior to the sample spectrum. The first intense peak of sodium thiosulfate was assumed to be 2469.2 eV.[25]

Near-edge analysis of sulfur K-edge spectra was carried out using the program DATFIT included in the EXAFSPAK suite of programs.[26] EXAFSPAK was also utilized for data reduction and analysis of both mercury L_{III}-edge and sulfur K-edge EXAFS data, as previously described.[27,28]

7.5 Results and Discussion

7.5.1 XFI demonstrates surface mercury accumulation irrespective of rinsing

Fig. 7.1 shows an example of X-ray fluorescence imaging (XFI) of zebrafish larval sections. XFI is an element-specific technique which allows the visualization of distributions of elements.[29] The sections in Fig. 7.1 depict the trunk, where mercury associated with the outer layer of the zebrafish larvae appears as a low intensity “halo”. The highest intensities of mercury in the trunk section are seen in the liver, kidneys and yolk sac. Fig. 7.1 shows the effect of rinsing on the fluorescence maps. Well-established protocols for embedding using the JB-4 methacrylate kit were followed here,[30] as had been used extensively in previous mercury research.[19-21] The first step in the protocol (developed in-lab) was to rinse euthanized larvae with deionized water three times, to remove mercury which may have accumulated on the exterior of the larvae which if picked up using XFI would potentially confound accumulations present in other parts of the anatomy.

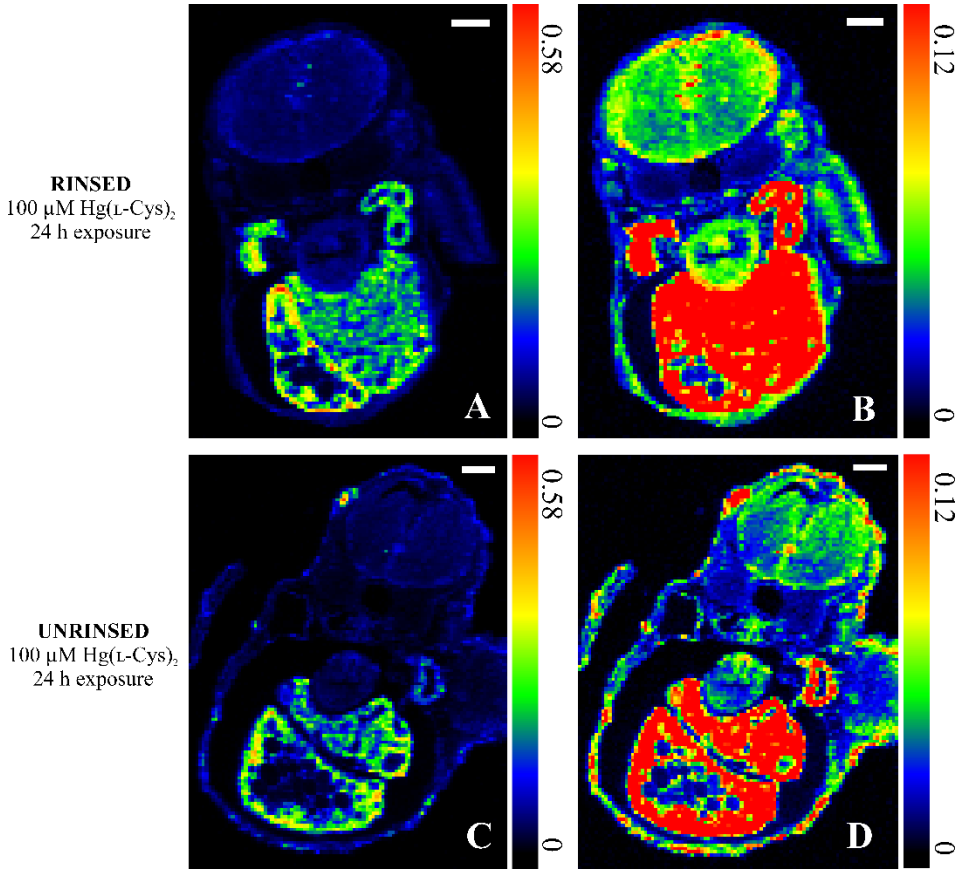

Figure 7.1: Comparison of mercury distributions in rinsed and unrinsed zebrafish larval sections. Zebrafish larvae were exposed to 100 µM $Hg(L\text{-}Cys)_2$ at 3 dpf for 24 hours. (A), (B): rinsed three times, (C), (D): unrinsed. In both cases larvae were embedded prior to sectioning and then were imaged using XFI. Maximum for colour bar: 0.58 µg/cm^2 for (A) and (C) while (B) and (D) were set to a maximum concentration of 0.12 µg/cm^2, for direct comparison and in order to highlight accumulation of mercury in the outermost regions, specifically in the epidermal layer. Scale bar shows 50 µm.

In Fig. 7.1, zebrafish larvae were either rinsed and not rinsed following the same exposure scenarios of 100 µm Hg(L-Cys)$_2$ over a period of 24 hours starting at 3 dpf to examine whether rinsing significantly decreased what mercury existed on the exterior of the larvae. Fig. 7.1A and C show two representative larvae, rinsed and unrinsed scaled to the same maximum concentration of 0.58 µg/cm^2 for ease of comparison. Here, mercury is not apparent in the surrounding epidermal layer of the larvae due to the high concentration of mercury present within the liver tissues. Fig. 7.1B and D demonstrate the same sections, with the mercury concentration scaled down to 0.12 µg/cm^2 where the mercury present in the epidermis becomes clear. Qualitatively, mercury shows slightly higher levels in the epidermis of the unrinsed section, while still being present in the rinsed section; due to the narrowness of this layer compared to the pixel size, this difference could not be quantified with any certainty.

7.5.2 Mercury accumulation in epidermis increases with time

Multiple exposures were conducted with exposure time periods ranging from 24 to 96 hours in order to examine how the phenomenon of mercury in the epidermis might evolve with larval zebrafish age. Fig. 7.2 highlights this work, demonstrating both lens and trunk sections from zebrafish larvae which were all exposed to 100 µm Hg(L-Cys)$_2$. Fig. 7.2A and B head sections and Fig. 7.2B and D trunk sections are scaled to the same maximum concentration of 0.18 and 0.27 µg/cm^2, respectively, for comparison. Clearly seen again is the typical accumulation locations after an inorganic mercury exposure, with mercury accumulating within the liver, yolk sac, and the single visible pronephric duct in Fig. 7.2C. Mercury accumulation is also seen in the epidermal layer in all Fig 7.2 images. Both Fig. 7.2A compared with 7.2B and Fig. 7.2 C compared to 7.2D show a convincing (but unquantified) increase in mercury accumulation in the epidermal layer occurring over time.

Mercury is very clearly accumulating at the exterior/epidermal layer in zebrafish larvae, however, even at the excellent resolution of 5 µm utilized in Figs. 7.1 and 7.2 it becomes difficult to pinpoint the exact location of this accumulation. In Fig. 7.3 and Fig. 7.4, XFI imaging with a resolution of 400 nm was utilized to determine more precisely where mercury was accumulating in an embedded larval zebrafish exposed to 100 µm Hg(L-Cys)$_2$ for 48 hours. The location which was chosen for XFI imaging is denoted on the H&E stained image. This spot was chosen to include both brain matter as well as epidermal tissue. Maps of sulfur and phosphorus accumulations were included to highlight the cellular level resolution made possible at such a

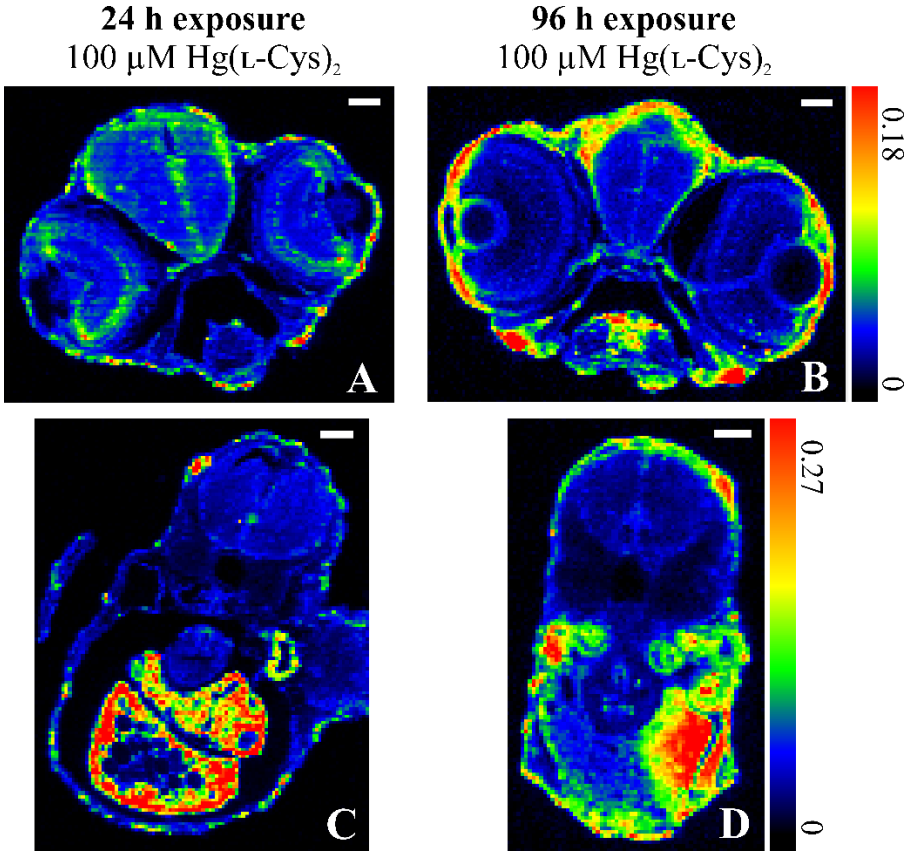

Figure 7.2: XFI images demonstrating increases in mercury accumulation in the outer epithelial layer over time. Images (A) and (C) represent the lens and trunk sections of unrinsed embedded larval zebrafish following a 24-hour exposure to 100 µM $Hg(L\text{-}Cys)_2$ between 3 and 4 dpf, while images (B) and (D) demonstrate the same treatment over an exposure period of 96 hours, lasting from 3 to 7 dpf. Maximum for colour bar: (A) and (B) set to 0.18 µg/cm^2; (C) and (D) set to 0.27 µg/cm^2 to highlight increases in mercury accumulations at epidermal layer. Scale bar shows 50 µm.

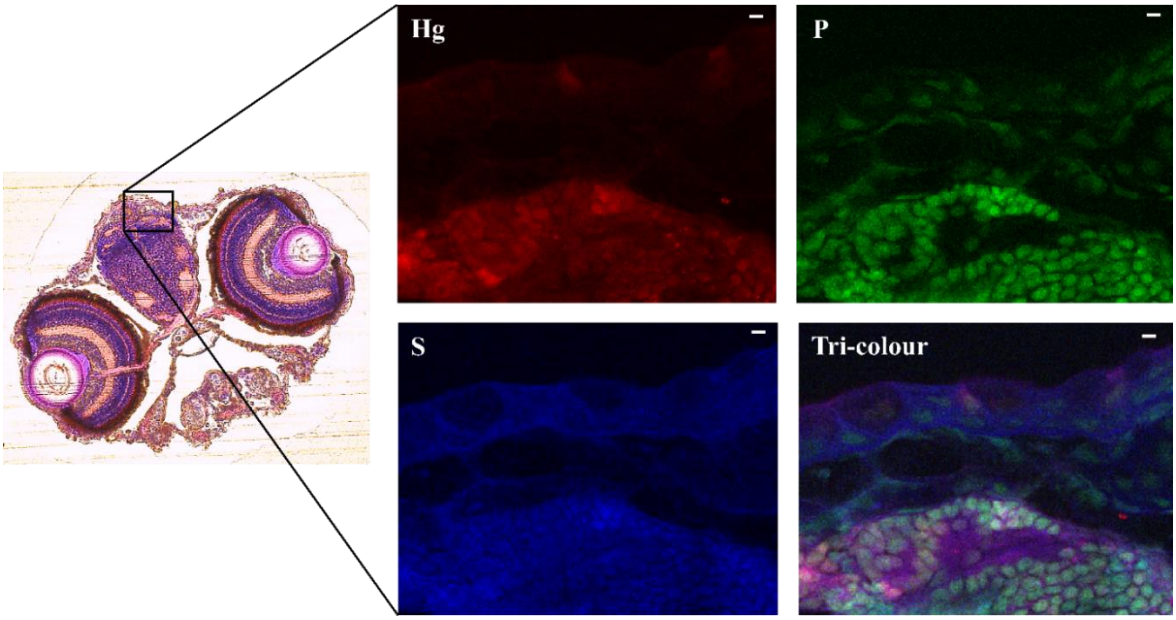

Figure 7.3: High-resolution XFI image containing both epithelial layer and brain tissue of embedded 3 dpf larval zebrafish exposed to 100 µM $Hg(L\text{-}Cys)_2$ over 48 hours. H&E stained image specifies the area selected for the XFI image from the embedded and sectioned zebrafish. Elemental maps demonstrate mercury, sulfur and phosphorus accumulations in the selected area. Included is a tri-colour plot which consists of overlaid XFI maps of mercury, sulfur and phosphorus accumulations. Scale bar shows 4 µm.

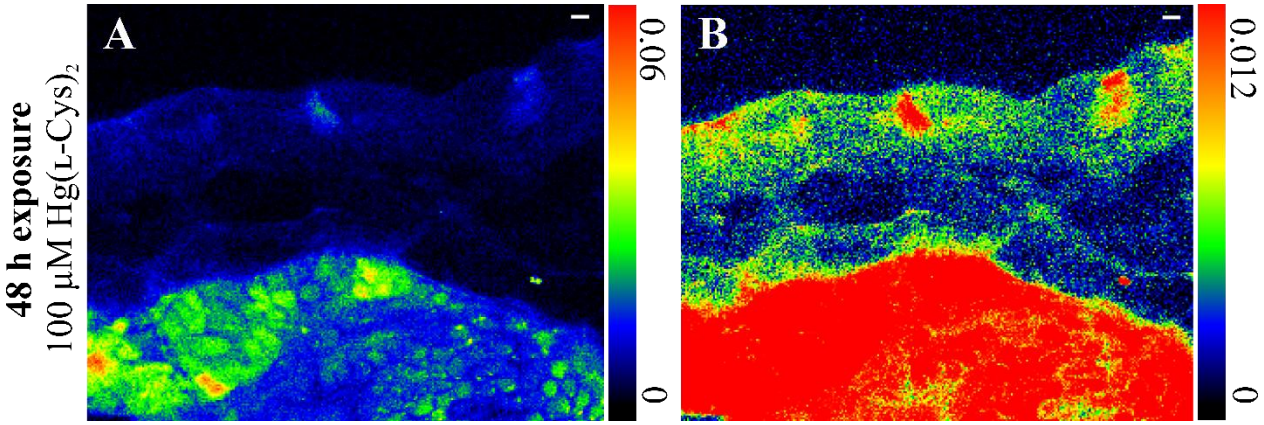

Figure 7.4: High-resolution mercury XFI of embedded zebrafish larvae exposed to 100 µM Hg(L-Cys)$_2$ over 48 hours. Image is the same as that seen in Fig. 7.3 with a different filter applied for easier visualization of mercury accumulation in brain and epidermal tissues. Image (A) is the XFI image at full intensity with a maximum mercury concentration of 0.06 µg/cm^2 and (B) is the same image scaled to a threshold of 0.012 µg/cm^2 to visualize mercury distributions in epidermal layer. Scale bar denotes a distance of 4 µm.

small resolution. Mercury map shows accumulation occurring diffusely throughout the image, with higher accumulation present in the brain tissue compared to the epidermal layer. However, the accumulation of mercury in the outermost epidermal layer is visible in this map. Included is a tri-colour map with all three elements overlaid each other, creating an XFI image rich in cellular and elemental accumulation detail.

7.5.3 Mercury accumulation observed with range of different mercury species

Together, these results show that, following $Hg(L\text{-}Cys)_2$ exposure, mercury accumulates in the outermost epidermal layer, and that the concentration apparently increases with duration of exposure. Moreover, the phenomenon of accumulation may extend to other chemical forms of mercury. Fig. 7.5 shows XFI distributions of mercury in zebrafish larvae following treatment with different mercury forms including an additional inorganic mercury species ($HgCl_2$) and two methylmercury species (MeHgCl, MeHg-L-Cys). While unquantified, in each case these images qualitatively suggest that mercury is accumulating in the epidermal layers following exposure to a range of different mercury chemical forms.

7.5.4 XAS of chemical interactions of mucosa with mercury species

Informed by the observation of mercury associating with the epidermal/mucosal layer, we addressed the question of whether the mucosa itself could interact chemically with mercury species. We therefore used X-ray absorption spectroscopy to investigate the chemical forms of sulfur in the mucosa and the nature of any chemical association between organic and inorganic mercury and mucosa harvested from trout.

X-ray absorption spectroscopy relies upon the photoelectric effect whereby an incoming X-ray beam excites strongly-bound core-level electrons to outer shell levels or, with sufficiently high energy, expels them to the continuum. The energy at which these electrons are excited is elementally specific and is called the electron-binding energy, which for the Hg L_{III}-edge is around 12 284 eV and for S K-edge is around 2469 eV. Information can be extracted from the energy range close to the absorption edge, which probes the bound-state transitions. These spectra are referred to as near-edge spectra (sometimes called XANES) and contain unique features specific to the element coordination, oxidation state and geometry of the ligands.[31] The near-edge spectrum of a specific chemical species of an element can thus be thought of as a distinctive “signature” or “fingerprint” of that species.[31] These spectra are commonly analyzed

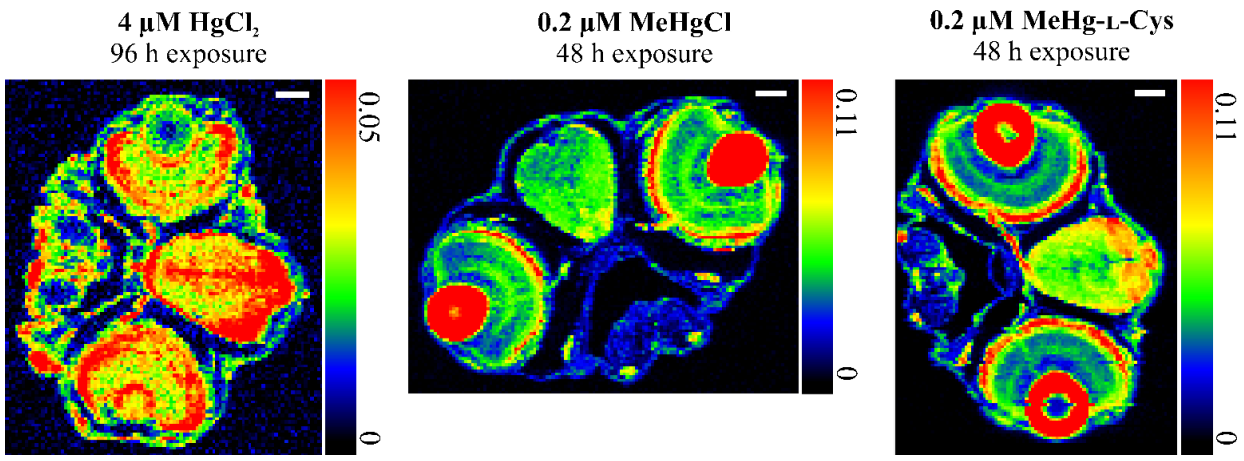

Figure 7.5: Blocked XFI images showing Hg in epidermal layer following exposure to different mercury species. Inorganic mercury shown on left-hand side (4 µM $HgCl_2$, exposure occurring between 3 and 7 dpf) and methylmercury species shown in middle (MeHgCl) and on right-hand side (MeHg-L-Cys; both 0.2 µM exposures occurring between 3 and 5 dpf). Mercury accumulation in the outermost layers are observed in all three treatments. Colour scale shows areal density in µg/cm^2 with scales adjusted to highlight increases in mercury accumulations in the epidermal layers. Scale bars show 50 µm.

against an existing library of standard compounds using linear combination fitting, which can provide information on the type of chemical species present in a complex sample, such as a biological tissue.[31] However, it is important to note that the information extracted from the near-edge is limited to the library of compounds available to the researcher, and informs on the local environment of the atom, rather than identifying molecules explicitly.

Accompanying the excitation and ejection from core-levels is the concomitant decay of a higher level electron to the vacant hole, resulting in the release of a fluorescent photon. This fluorescence is also specific to element and may be analyzed as characteristic X-ray emission energies. Mercury $L\alpha_{1,2}$ and sulfur $K\alpha_{1,2}$ fluorescence emission lines were monitored here as a sensitive probe of XAS from these dilute samples. Extending the range of the incident X-ray energy up to 700 eV beyond the absorption edge enabled the collection of extended X-ray absorption fine structure (EXAFS), which results from constructive and destructive interference between the outgoing ejected photoelectron and backscattering from neighbouring atoms. EXAFS allows for the accurate determination of bond lengths between the absorbing atom (here, mercury or sulfur) and backscattering atoms, the number of backscattering atoms as well as the elements to which the element of interest is bound to in dilute samples which have undergone little to no pre-treatment. Mercury EXAFS data were collected to a *k*-range of 12 $Å^{-1}$, while sulfur spectra were collected in the near-edge energy range.

7.5.5 Sulfur content of trout mucosa

Sulfur K-edge XAS is well-established as a probe of the distribution of sulfur chemical forms in complex biological systems, providing a sensitive probe of sulfur functional groups.[28,32–34] We used sulfur K-edge XAS to survey the sulfur types present in the trout mucosa. The sulfur K-edge is shown in Fig. 7.6 upper panel, with the second derivative spectrum in the lower panel. The second derivative spectrum was fit to a linear combination of spectra of biologically relevant standards. Fig. 7.6 lower panel shows the second derivative spectra, overlaid by the best fit, with the individual components shown below. The numerical results of the fit are shown in Table 7.1. Six major types of sulfur species are identified by the fit. The lowest energy peak in the absorbance spectrum at around 2470-2472 eV encompasses three species: disulfides, thiols and sulfides, which are partially separated in the second derivative spectrum. The peak at around 2474 eV corresponds to the sulfinates, while the prominent double peak at around 2477-2481 eV is attributable to sulfonates and O-linked sulfate esters.

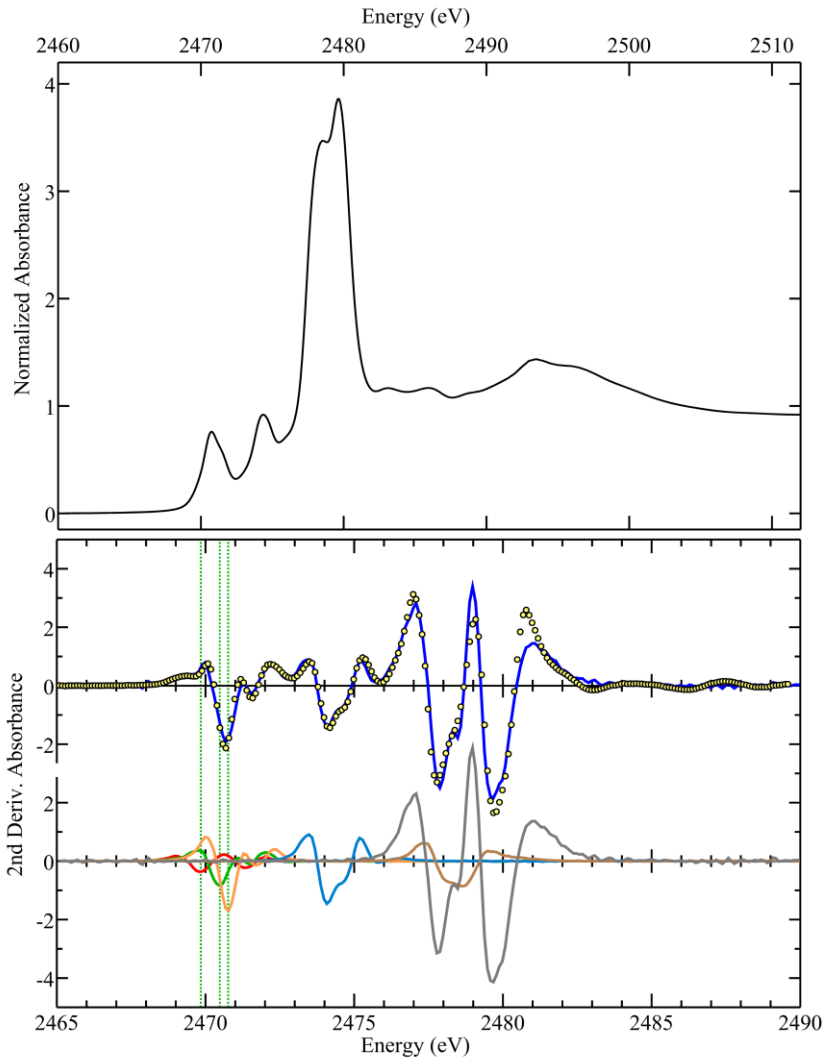

Figure 7.6: Sulfur K near-edge X-ray absorption spectrum of trout mucosa. The normalized absorption spectrum (upper panel) is dominated by transitions between 2477 and 2481 eV due to oxidized species. The corresponding second derivative (lower panel) is shown on an expanded energy scale. Experimental data points are shown as yellow dots overlaying the blue line corresponding to the best fit (top). Sulfur components which comprised the best fit of the data (bottom) are shown as red (disulfides), green (thiols), yellow (sulfides), light blue (sulfinate) and brown (sulfonate) and grey (O-linked sulfate esters); components are scaled to their contributions in the fit. Vertical green dashed lines are meant to aid in visualizing the peaks of the reduced sulfur forms which are diminished in comparison to the oxidized forms. Linear combinations fitting parameters are found in Table 7.1.

Table 7.1: S K-edge best linear combination fit results from trout mucosa.

Standard	*Sulfur site*	*%*	*esd (%)*
disulfide	R–S–S–R	3.0	1.1
thiol	R–SH	9.0	1.6
sulfide	R–S–R	13.7	1.4
sulfinate	$R–SO_2^-$	8.6	0.7
sulfonate	$R–SO_3^-$	7.6	0.9
O-linked sulfate ester	$RO–SO_3^-$	58.2	1.4

Linear combination fits of S K-edge trout mucosa were performed using the program DATFIT in the EXAFSPAK suite of programs. Experimental data were fit using a library of spectra of sulfur standards. Best fit of experimental data includes sulfur components listed above recorded in percentages of the total fit with estimated standard deviations also given as percentages.

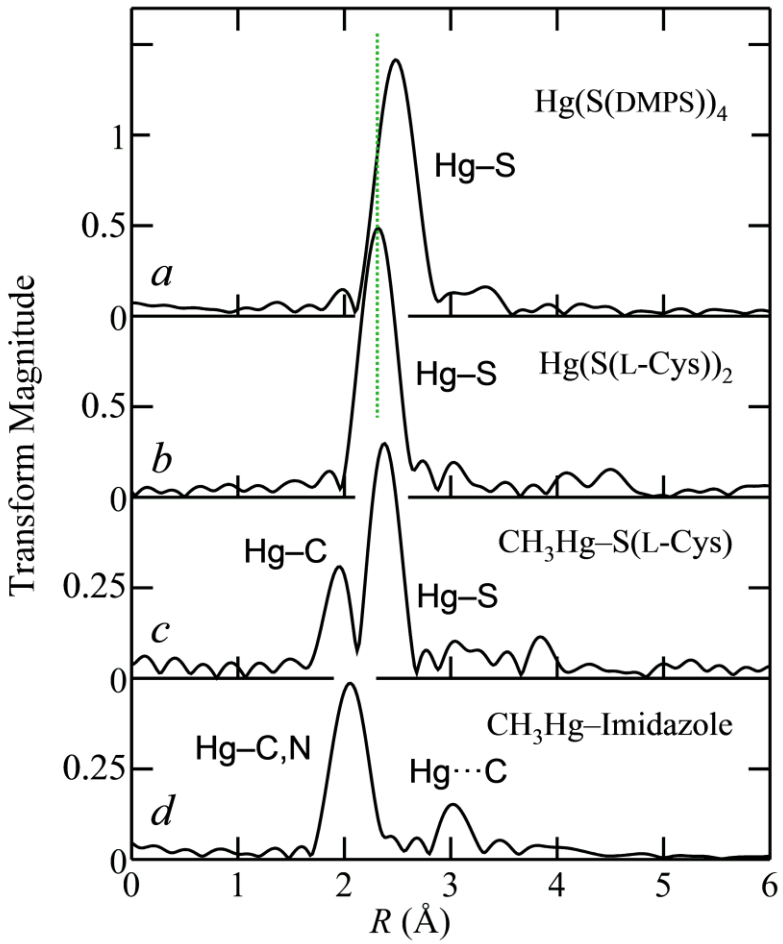

Figure 7.7: Fourier-transformed data of standards Hg L_{III}-edge EXAFS of mercury solution standards. *a*. Hg bound to 4 sulfurs, as modelled by Hg with an excess of DMPS. *b*. Hg bound to 2 sulfurs, as modelled by Hg(L-Cys)$_2$. *c*. Hg bound to a methyl carbon and a single sulfur, as modelled by CH_3Hg(L-Cys). *d*. Hg bound to a methyl carbon and a nitrogen from imidazole, as modelled by CH_3Hg-imidazole. Fourier transforms have been phase-corrected for first shell interactions (Hg–S) for *a*-*c* or (Hg–N) for *d*. *a* and *b* have a modified intensity scale compared with *c* and *d* due to the much larger transform magnitude for the multiple sulfur ligands.

7.5.6 Mercury EXAFS of standards

In order to survey the possible chemical interactions, we chose one inorganic form ($HgCl_2$) and one organic form (MeHgCl). In each case, three concentrations of mercury were chosen for titration with trout mucosa, representing a low, medium and high (100 µM, 400 µM, 700 µM) mercury dose. EXAFS Fourier transforms of standard mercury solutions are shown in Fig. 7.7. The phase-corrected Fourier transforms can be considered to be radial distribution functions, with peaks approximately corresponding to bonded or nearby atoms surrounding the central mercury. Four sulfurs coordinating to mercury gives rise to a prominent Hg–S peak at around 2.5 Å, whereas two sulfurs result in a substantially shorter Hg–S interatomic distance at about 2.3 Å (Fig. 7.7*a* and *b*). Binding to a methyl carbon and a single sulfur results in Hg-S also around 2.3 Å with a clearly resolved Hg–C at a shorter distance around 2.0 Å (Fig. 7.7*c* and *d*). In methylmercury-imidazole, in which mercury binds to a carbon and nitrogen, the EXAFS results in an unresolved first-shell peak at around 2 Å with an additional peak at approximately 3 Å attributable to more distant atoms in the 5-membered ring.

7.5.7 Interactions of inorganic mercury with trout mucosa

The EXAFS and corresponding Fourier transforms of inorganic mercury in the form of $HgCl_2$ titrated with trout mucosa at low, medium and high levels (100, 400 and 700 µM Hg) are shown in Fig. 7.8. Inorganic mercury at the lowest level (100 µM) to trout mucosa gave rise to large amplitude EXAFS with a corresponding strong single peak in the Fourier transform at around 2.3 Å. The medium and high inorganic mercury treatments show a substantial decrease both of the total EXAFS amplitude and of this 2.3 Å peak, with the appearance of a second, weaker peak at a shorter distance. EXAFS curve-fitting results (Table 7.2) show that the 100 µM sample EXAFS fits well to a single first shell interaction of 2 Hg–S bonds at 2.32 Å. This is consistent with the inorganic mercury being completely coordinated by thiols from the trout mucosa. To fit the 400 and 700 µM inorganic mercury samples, an additional peak modelled as Hg–O was included, refining to a value of 2.05-2.07 Å. In both cases, the total coordination number was held at 2, and then the proportion of Hg–S and Hg–O bonds varied. From resulting coordination numbers in Table 7.2, the proportion of Hg–S to total first shell bonds are 1, 0.8 and 0.2 for 100, 400 and 700 µM mercury as inorganic mercury, respectively. We interpret the Hg–O as residual hydrated mercury in the 400 and 700 µM mercury samples, in which there are insufficient thiols to fully coordinate the mercury.

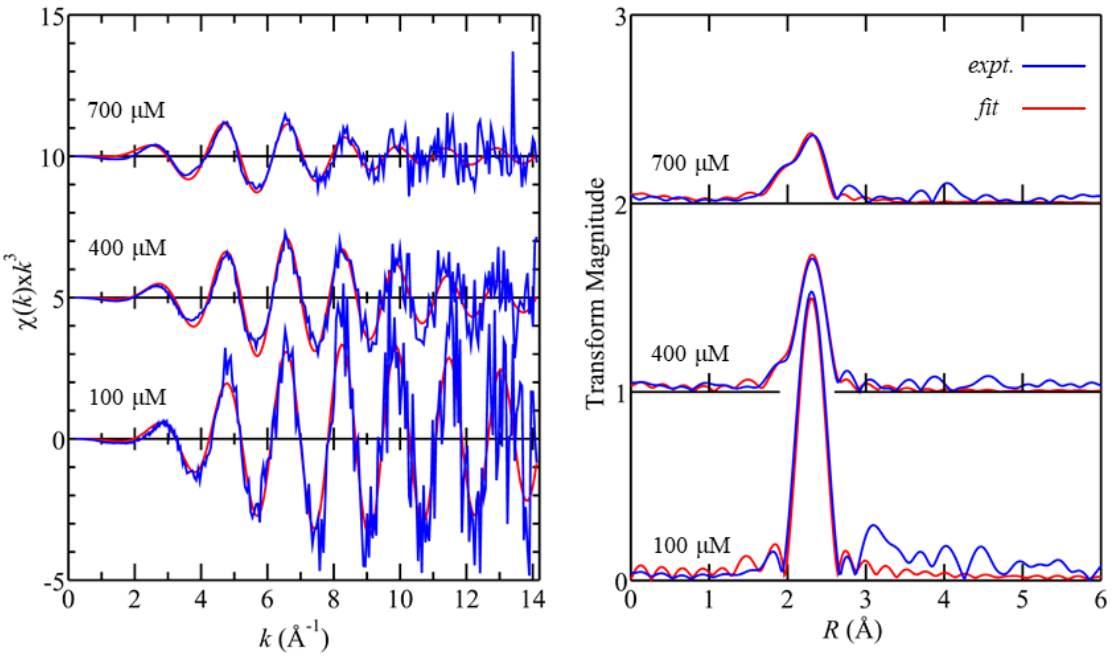

Figure 7.8: Mercury EXAFS of inorganic mercury-treated trout mucosa. Hg L_{III}-edge EXAFS and Fourier transforms of 100 µM $HgCl_2$ + trout mucosa (bottom), 400 µM $HgCl_2$+ trout mucosa (middle) and 700 µM $HgCl_2$+ trout mucosa (top). In all cases, blue line indicates experimental data with overlaid red line indicating best fit of data. Hg Fourier transforms are phase-corrected for Hg–S backscattering. Relevant curve-fitting parameters can be found in Table 7.2.

7.5.8 Interactions of methylmercury with trout mucosa

In contrast to the results for the inorganic mercury titration (Fig. 7.8), the EXAFS of the high and medium organic mercury concentrations titrated with the trout mucosa (Fig. 7.9) demonstrated bonds lengths which are well cited in the literature and are consistent with a linear, 2-coordinate organic mercury species resembling methylmercury-cysteinate.[27] The shorter Hg–C contact at 2.07 Å is characteristic of the bond in methylmercury while an Hg–S contact at 2.35 Å is attributable to binding to the thiols of the mucosa. Unexpectedly, when 100 µM MeHgCl was combined with trout mucosa the resulting EXAFS showed a substantially less intense Hg–C contact, which would indicate the diminished presence of an organic mercury species compared with what was seen in the 400 and 700 µM concentration groups. Similar to the 400 and 700 µM treatments, an Hg–S bond is present at 2.34 Å, although with an increased intensity. This substantial decrease in the intensity of the Hg–C contact indicates that demethylation of the methylmercury has occurred in the presence of the trout mucosa, suggesting a hitherto unidentified protective property of the mucosa.

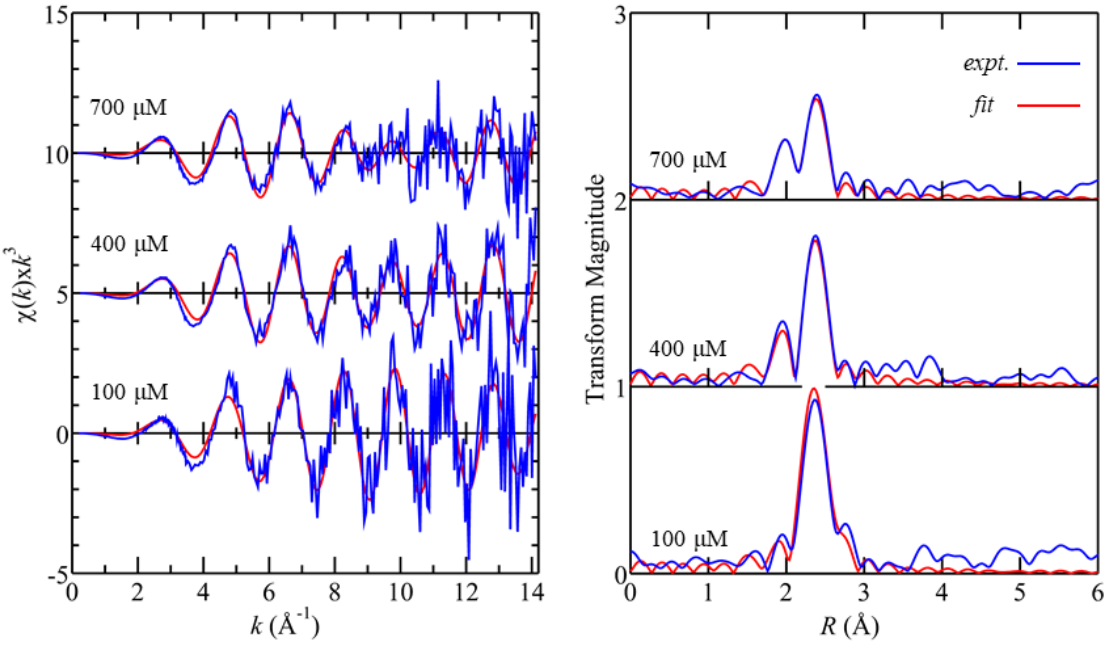

Figure 7.9: Mercury EXAFS of methylmercury-treated trout mucosa. Hg L_{III}-edge EXAFS and Fourier transforms of 100 µM MeHgCl + trout mucosa (bottom), 400 µM MeHgCl + trout mucosa (middle) and 700 µM MeHgCl + trout mucosa (top). In al cases, blue line indicates experimental data with overlaid red line indicating best fit of data. Hg Fourier transforms are phase-corrected for Hg–S backscattering. Relevant curve-fitting parameters can be found in Table 7.2.

Table 7.2: Hg L_{III}-edge EXAFS curve-fitting results from samples combining trout mucosa with increasing concentrations of MeHgCl or $HgCl_2$.[a]

Addition	*Concentration*	*Interaction*	*N*	*R* (Å)	σ^2 (Å^2)
Hg^{2+}	100 μM	Hg–S	2	2.323(2)	0.0023(2)
	400 μM	Hg–S	1.62(6)[b]	2.327(2)	0.0056(2)
		Hg–O	0.38(6)[b]	2.049(9)	0.0028(10)
	700 μM	Hg–S	0.41(9)[b]	2.339(6)	0.0037(13)
		Hg–O	1.59(9)[b]	2.068(6)	0.010(1)
CH_3Hg^+	100 μM	Hg–S	1.60[c]	2.339(7)	0.0035(5)
		Hg–C	0.40[c]	2.068(6)	0.0016[d]
		Hg–S	0.40[e]	2.624(7)	0.0026(6)
	400 μM	Hg–S	1	2.346(3)	0.0019(2)
		Hg–C	1	2.073(6)	0.0016[d]
	700 μM	Hg–S	0.82(4)[b]	2.346(3)	0.0026(6)
		Hg–O	0.18(4)[b]	2.06(2)	0.0026(6)
		Hg–C	1	2.068(5)	0.0016[d]

a. Coordination number *N*, interatomic distance *R* (Å), and Debye-Waller factor σ^2 (Å^2). All fits used a fixed ΔE_0 value of –17.43 eV determined from curve fitting of standard compounds

b. Hg–S and Hg–O coordination numbers were constrained in refinements so that the fraction of each summed to a total coordination number of 2.0

c. Hg–S and Hg–C coordination numbers were allowed to vary in increments of 0.1 and constrained to a total coordination number of 2.0. The noise level of the data did not support free-floating of the coordination number and σ^2, because of high mutual correlation coefficients in the refinement

d. The value for σ^2 was fixed at the value determined for methylmercury-L-cysteine

e. An additional long-range interaction was needed for an adequate fit, approximated as a long Hg–S, *e.g.* a bond to an organic sulfide such as methionine sulfur.

The mucosa-producing epidermal layer of teleost fish is inherently important in innate immunity. This layer contains goblet cells which are partly responsible for the production of mucous, which contains glycosylated glycoproteins as well as many immune-related components such as proteases, immunoglobins, lysozymes, complement, among others.[35] A known response of teleost fish to adverse conditions such as the presence of heavy metals is the over-production of mucous[36,37] which, among others, may serve the purpose of binding to pathogens followed by sloughing off for protection of susceptible anatomy. Interest in mucosal immunity has increased recently with many studies investigating the impacts of adverse conditions to integral components of fish mucous and their relationship to various aspects of immunity. It has been noted that such changes can impact overall fish health and even cause genetic changes which may have population level effects.[2] To our knowledge, very little work has focussed on the effect of heavy metals on fish skin mucous, and further to that, only relatively few studies were found which specifically studied the effects caused by mercury which is a persistent global contaminant. The current work explores the accumulation of mercury in the epidermal/mucosal exterior layer of zebrafish larvae as well as the possibility of mercury binding to elemental components of *Oncorhynchus mykiss* mucous.

Increased mucosal production has been seen in numerous fish species as a reaction to the presence of heavy metals.[2,36,38] Furthermore, research has shown that upregulation of mucosal-producing goblet cells may occur under circumstances of environmental stress.[2] However, the issue of whether said mucosa has the capability of binding to these heavy metals as a form of protection against toxicity or otherwise has remained a point of contention.[2] Here we used X-ray fluorescence imaging to demonstrate the accumulation of mercury in the epidermal layer of larvae zebrafish after exposure to inorganic mercuric *bis*-cysteinate (Fig. 7.2, 7.3, 7.4) as well as an apparent increasing accumulation of mercury over an extended time period given the same exposure conditions (Fig. 7.2). Exposure to other species of mercury, both organic and inorganic, also give rise to this accumulation (Fig. 7.5) and the accumulation was present whether sections were rinsed or unrinsed (Fig. 7.1).

The epidermal layer of teleost fish contains goblet cells which are responsible for the production and secretion of mucous which is known to be composed largely of glycoproteins. Guardiola et al.[39] noted that fish mucous typically has an overall negative charge and that it is likely polyanionic which would be useful in binding to heavy metals, although others have

suggested that fish mucous is neutral, bordering on acidic if it contains elevated levels of components such as carboxylated or sulphated monosaccharides.[2] It is very likely that this differs somewhat between fish species and is also related to the stress levels of the animal which are known to trigger changes in epidermal composition.[2,40] The trout mucosa used in this work measured at a pH of 8.

An Ellman's assay was performed on trout mucosa. This assay was utilized for quantifying free sulfhydryl groups; it determined a relatively high concentration of approximately 2.5 mM of sulfur compounds when estimated against a glutathione calibration curve. Mercury is known to have a very high affinity to sulfur compounds. Varying species of mercury can bind to albumin in blood plasma[41,42] and be transported ubiquitously throughout the body after exposure, leading to accumulations and toxicities in many target organs. Mercury has been shown to disrupt normal metabolic activity through binding to cysteine resides in many biologically important enzymes.[43] Some examples include glutathione peroxidase which functions as an antioxidant and whose disruption may result in oxidative stress particularly in the cardiovascular system[44] as well as sulfur transferases which are involved in cysteine metabolism and have been seen to be disrupted in adult *Xenopus laevis* after exposure to $HgCl_2$ resulting in reduced levels of sulfane sulfur various tissues,[45] to name a few. Methylmercury may also bind to cysteine residues in tubulin which is thought to lead to depolymerisation of tubulin and ultimately halts production of microtubulins which are essential components of the cellular cytoskeleton.[21,46,47]

Analysis of trout mucus for sulfur compounds using EXAFSPAK program DATFIT identified the presence of several types of sulfur species in the trout mucosa (Fig. 7.6). This method of analysis does not identify individual molecules, but rather chemical types. Thus, the proportion of thiols, in which the sulfur is bound to one organic carbon and a proton (R-SH), might represent the amino acid cysteine, unbound or in a peptide chain or protein, or possibly in the endogenous thiol glutathione. Disulfide might arise from a similar environment in which two RS-H environments are oxidized to form a RS-SR moiety. Similarly, sulfide (R-S-R) represents methionine or a similar environment where the sulfur is bound to two aliphatic carbons. Sulfonates may include the molecule taurine, which is widely distributed in cells of animals including fish. Sulfinates may represent oxidized thiols, such as cysteine sulfinic acid which is an intermediate in the conversion of cysteine to taurine. The O-linked sulfate esters represent sulfated polysaccharide components of the mucosa as previously observed[2], and account for some

58% of the total sulfur. Some 9% of the total sulfur was observed to be present as thiols, which are predicted to coordinate to the mercury when exposed.

Addition of 100 µM mercuric chloride to trout mucosa (Fig. 7.8) shows a prominent peak in the EXAFS Fourier transform attributable to two Hg–S bonds. Addition of the higher concentrations of 400 and 700 µM show a sequentially decreased intensity for the Hg–S contact, with the bonds replaced by oxygen from the solvent. We attribute this to having sufficient thiols available for the 100 µM $HgCl_2$ sample, whereas for the higher concentrations there are insufficient thiols available. Interestingly, this suggests that there may be a lower concentration of accessible and reactive thiols available than were estimated by the Ellman's reagent. It is possible that while Ellman's reagent estimates all accessible thiols, only certain pairs of thiols, those that can form a near linear S–Hg–S, will react with the inorganic mercury.

Additions of 400 and 700 µM methylmercury chloride to trout mucosa (Fig. 7.9) resulted Hg L_{III} EXAFS which fit to one carbon and one sulfur donor at bond lengths of 2.073(6) and 2.346(3) Å, respectively, resembling a linear 2-coordinate mercury-L-cysteine species (Table 7.2). Magnitude of Fourier transforms of methylmercury chloride additions at 700 µM appear diminished in comparison to additions of 400 µM which is likely due to the lack of available sulfur donors in an overwhelming mercury presence. This might also be the reason for the additional Hg-O contact seen at 2.06(2) Å suggested in the best experimental fit (Table 7.2). The striking observation in Fig. 7.9 is with the lowest concentration of 100 µM, in which the near-lack of the shorter 2 Å peak corresponding to the methyl carbon, which is so prominent in the higher concentrations, indicates that demethylation of the methylmercury has occurred in the presence of the trout mucosa.

Methylation and demethylation of mercury occurs naturally in the environment, with biomethylation of inorganic mercury by sulfate-reducing bacteria,[48] iron-reducing bacteria[49] and methanogens[50] considered to be appreciable sources of increased methylmercury in aquatic environments.[51] Past work has shown that some of these bacteria, including sulfate-reducing and methanogens also have the ability to demethylate organic mercury.[52] Demethylation of organic mercury is known to take place in abiotic and biotic environments and has been seen to occur through both oxidative and reductive pathways. Figueiredo et al.[53] found microorganisms present in both aerobic and anaerobic environments to play a key role in demethylation of methylmercury in both anoxic and oxygenated estuarine sediments.

Given the high thiol content of the slime determined using Ellman's assay, and mercury's known affinity for thiols, exploratory work investigating what mixtures of the two would produce was undertaken. In the past, the question had been raised concerning whether the removal of heavy metal ions via mucous was truly an adapted mechanism of surface layer protection or whether it was simply a natural result of the adverse conditions an animal finds itself in.[2] Here we see for the first time, the implication that trout skin mucosa might be utilized as a direct defense against heavy metal ions, specifically methylmercury, through the action of demethylation at low-level concentrations.

A highly diminished Hg–C contact was seen when a concentration of 100 µM MeHgCl was combined with trout mucosa in Hg L_{III} EXAFS analysis (Fig. 7.9). While an organic portion remains, it is apparent that the majority of the methyl contacts in the sample have been cleaved resulting in a predominantly inorganic mercury species. Past research has demonstrated that *in vivo* demethylation is possible, particularly in areas which are likely to contain mucosal surfaces. Ludwicki et al.[54] demonstrated increasing demethylation of methylmercury chloride as well as phenylmercuric acetate to Hg^0 incubated over a time period of 24 - 72 hours with the intestinal contents of rats, although they also noted that this process was likely to be slower than the absorption of methylmercury in the gastrointestinal tract. Interestingly, the yield of elemental mercury produced by the degradation of phenylmercury acetate was noted to be higher than that produced by methylmercury chloride in the same time frame, which may speak to the vulnerability of different mercury-carbon bonds to protonolysis. Indeed, varying strains of intestinal microbia including *E. coli*, *Bacteroides* and *Bifidobacteria* from humans and *E. coli* from rats incubated with methylmercury resulted in its volatilization, and although the authors could not specify the end product they suggested it to be a volatile sulfur derivative of methylmercury.[55] Microbial action has been seen to play a part in intestinal demethylation of mercury in fish and mammals. In turn, it is a possibility that the demethylation of low-level concentrations of methylmercury chloride occurring in trout skin mucous is due to similar microbial activity. A review of intestinal demethylation of methylmercury species in mammals and fish demonstrated that reductive demethylation rather than oxidative occurs predominantly.[56] An overlap exists in phyla of bacteria that have been found in human gut microbiota[57] as well as in the mucous found on the skin of farmed Atlantic salmon (*Salmo salar*).[58] Data from both studies pointed to the phyla Proteobacteria as being the most abundant, followed by Firmicutes

and Acidobacteria in salmon and Firmicutes, Actinobacteria and Bacteroidetes being equally abundant in the human microbiome. No data could be found on the specific microbial communities in trout mucosa, however it is likely that some redundant bacterial species exist between most fish species.

In this work, we demonstrated that the complex mucosal layer of the teleost fish, *Oncorhynchus mykiss* has the capability of binding to the toxic heavy metal, mercury. Further to that, we highlighted the novel possibility of demethylation of low-levels of organic mercury occurring in this mucosa. As well, we showed that over a short time period, mercury will accumulate in the epidermal layer of zebrafish larvae exposed to the same concentration of inorganic mercury, in addition to other well-known target organs, and that these accumulations appear to increase over time given constant exposure to inorganic mercuric *bis*-cysteine. Ongoing work may include improving resolution and certainty of mercury compounds in the mucosa of *Oncorhynchus mykiss* mucosa using high energy resolution fluorescence detected X-ray absorption spectroscopy (HERFD-XAS).

7.6 Acknowledgements

This work was supported by the Natural Sciences and Engineering Research Council of Canada (NSERC; GNG and IJP), the Canada Foundation for Innovation (CFI; IJP) and by Canadian Institutes of Health Research – Training Grant in Health Research Using Synchrotron Techniques (CIHR-THRUST; IJP). AKJ, TCM, SN and KLS were CIHR-THRUST Fellows, and NVD was a CIHR-THRUST Associate. GNG and IJP are Canada Research Chairs. The Canadian Light Source (CLS), a national research facility of the University of Saskatchewan, is supported by the CFI, NSERC, the National Research Council (NRC), CIHR, the Government of Saskatchewan, and the University of Saskatchewan. Use of the Stanford Synchrotron Radiation Lightsource, SLAC National Accelerator Laboratory, is supported by the U.S. Department of Energy, Office of Science, Office of Basic Energy Sciences under Contract No. DE-AC02-76SF00515. The SSRL Structural Molecular Biology Program is supported by the DOE Office of Biological and Environmental Research, and by the National Institutes of Health, National Institute of General Medical Sciences (including P41GM103393). The contents of this publication are solely the responsibility of the authors and do not necessarily represent the official views of NIGMS or NIH. This research used resources of the Advanced Photon Source, an Office of Science User Facility operated for the U.S. Department of Energy (DOE) Office of Science by Argonne National Laboratory, and was supported by the U.S. DOE under Contract No. DE-AC02-06CH11357, and the Canadian Light Source and its funding partners.

7.7 References

(1) Randall, T.D., Mebius, R.E. The development and function of mucosal lymphoid tissues: a balancing act with micro-organisms. *Mucosal Immunol.* **2014**, *7*, 456-466.

(2) Shephard, K.L. Functions for fish mucus. *Rev. Fish Biol. Fish*. **1994**, *4*, 401-429.

(3) Zaccone, G., Kapoor, B.G., Fasulo, S., Ainis, L. Structural, histochemical and functional aspects of the epidermis of fishes. In *Advances in Marine Biology*; Southward, A., Ed.; Academic Press: London, 2001, Vol. 40.

(4) Günther, J., Seyfert, H-M. The first line of defence: insights into mechanisms and relevance of phagocytosis in epithelial cells. *Semin. Immunopathol.* **2018**, *40*, 555-565.

(5) Noga, E.J. Skin ulcers in fish: *Pfiesteria* and other etiologies. *Toxicol. Pathol.* **2000**, *28*, 807-823.

(6) de Bruijn, I., Liu, Y., Wiegertjes, G.F., Raaijmakers, J.M. Exploring fish microbial communities to mitigate emerging diseases in aquaculture. *FEMS Microbiol. Ecol.* **2018**, *94*, 1-12.

(7) Lieke, T., Meinelt, T., Hoseinifar, S.H., Pan, B., Straus, D.L., Steinberg, C.E.W. Sustainable aquaculture requires environmental-friendly treatment strategies for fish diseases. *Rev. Aquac.* **2020**, *12*, 943-965.

(8) Erkinharju, T., Dalmo, R.A., Hansen, M., Seternes, T. Cleaner fish in aquaculture: review on diseases and vaccination. *Rev. Aquac.* **2021**, *13*, 189-237.

(9) Esteban, M.A. An overview of the immunological defenses in fish skin. *ISRN Immunol.* **2012**, *2012*, Article ID 853470.

(10) Brinchmann, M.F. Immune relevant molecules identified in the skin mucus of fish using –omics technologies. *Mol. BioSyst.* **2016**, *12*, 2056-2063.

(11) Garcia, G.R., Noyes, P.D., Tanguay, R.L. Advancements in zebrafish applications for 21st century toxicology. *Pharmacol. Ther.* **2016**, *161*, 11-21.

(12) Hill, A.J., Teraoka, H., Heideman, W., Peterson, R.E. Zebrafish as a model vertebrate for investigating chemical toxicity. *Toxicol. Sci.* **2005**, *86*, 6-19.

(13) Dai, Y.J., Jia, Y.F., Chen, N., Bian, W.P., Li, Q.K., Ma, Y.B., Chen, Y.L., Pei, D.S. Zebrafish as a model system to study toxicology. *Environ. Toxicol. Chem.* **2014**, *33*, 11-17.

(14) Green, A.J., Planchart, A. The neurological toxicity of heavy metals: A fish perspective. *Comp. Biochem. Physiol. C. Toxicol.* **2018**, *208*, 12-19.

(15) Dolgova, N.V., Hackett, M.J., MacDonald, T.C., Nehzati, S., James, A.K., Krone, P.H., George, G.N., Pickering, I.J. Distribution of selenium in zebrafish larvae after exposure to organic and inorganic selenium forms. *Metallomics* **2016**, *8*, 305-312.

(16) Korbas, M., Blechinger, S.R., Krone, P.H., Pickering, I.J., George, G.N. Localizing organomercury uptake and accumulation in zebrafish larvae at the tissue and cellular level. *Proc. Natl. Acad. Sci.* **2008**, *105*, 12108-12112.

(17) Korbas, M., Krone, P.H., Pickering, I.J., George, G.N. Dynamic accumulation and redistribution of methylmercury in the lens of developing zebrafish embryos and larvae. *J. Biol. Inorg. Chem.* **2010**, *15*, 1137-1145.

(18) Korbas, M., MacDonald, T.C., Pickering, I.J., George, G.N., Krone, P.H. Chemical form matters: Differential accumulation of mercury following inorganic and organic mercury exposures in zebrafish larvae. *ACS Chem. Biol*. **2012**, *7*, 411-420.

(19) MacDonald, T.C., Nehzati, S., Sylvain, N.J., James, A.K., Korbas, M., Caine, S., Pickering, I.J., George, G.N., Krone, P.H. Phenylthiourea alters toxicity of mercury compounds in zebrafish larvae. *J. Inorg. Biochem.* **2015**, *151*, 10-17.

(20) MacDonald, T.C., Korbas, M., James, A.K., Sylvain, N.J., Hackett, M.J., Nehzati, S., Krone, P.H., George, G.N., Pickering, I.J. Interaction of mercury and selenium in the larval stage zebrafish vertebrate model. *Metallomics* **2015**, *7*, 1199-1292.

(21) MacDonald, T.C., Sylvain, N.J., James, A.K., Pickering, I.J., Krone, P.H., George, G.N. Effects of inorganic mercury on the olfactory pits of zebrafish larvae. *Metallomics* **2016**, *8*, 514-517.

(22) Nienaber, K.H., Pushie, M.J., Cotelesage, J.J.H., Pickering, I.J. George, G.N. Cryoprotectants severely exacerbate X-ray induced photoreduction. *J. Phys. Chem. Lett.* **2018**, *9*, 540-544.

(23) Summers, K.L., Schilling, K.M., Roseman, G., Markham, K.A., Dolgova, N.V., Kroll, T., Sokaras, D., Millhauser, G.L., Pickering, I.J., George, G.N. X-ray absorption spectroscopy investigations of copper(II) coordination in the human amyloid β peptide. *Inorg. Chem.* **2019**, *58*, 6294-6311.

(24) Nienaber, K.H., Nehzati, S., Cotelesage, J.J.H., Pickering, I.J., George, G.N. X-ray induced photoreduction of Hg(II) in aqueous frozen solution yields nearly monatomic Hg(0). *Inorg. Chem.* **2018**, *57*, 8205-8210.

(25) Sekiyama, H., Kosugi, N., Kuroda, H., Ohta, T. Sulfur K-edge absorption spectra of Na_2SO_4, Na_2SO_3, $Na_2S_2O_3$, and $Na_2S_2O_x$ (x=5-8). *Bull. Chem. Soc. Jpn.* **1986**, *59*, 575-579.

(26) George, G.N. https://www-ssrl.slac.stanford.edu/exafspak.html (2001).

(27) George, G.N., Singh, S.P., Prince, R.C., Pickering, I.J. Chemical forms of mercury and selenium in fish following digestion with stimulated gastric fluid. *Chem. Res. Toxicol.* **2008**, *21*, 2106-2110.

(28) Pickering, I.J., Prince, R.C., Divers, T., George, G.N. Sulfur K-edge X-ray absorption spectroscopy for determining the chemical speciation of sulfur in biological systems. *FEBS Lett.* **1998**, *441*, 11-14.

(29) Pushie, M. J., Pickering, I. J., Korbas, M., Hackett, M. J., George, G. N. Elemental and chemically specific X-ray fluorescence imaging of biological systems. *Chem. Rev.* **2014**, *114*, 8499-8541.

(30) Sullivan-Brown, J., Bisher, M.E., Burdine, R.D. Embedding, serial sectioning and staining of zebrafish embryos using JB-4 resin. *Nat. Protoc.* **2011**, *6*, 46-55.

(31) George, G.N., Pickering, I.J. X-ray Absorption Spectroscopy of Metals in Biology. In Encyclopedia of Biophysics; Roberts, G.C. Ed.; Springer: Berlin, Heidelberg, 2013.

(32) Hackett, M.J., Smith, S.E., Paterson, P.G., Nichol, H., Pickering, I.J., George, G.N. X-ray absorption spectroscopy at the sulfur K-edge: a new tool to investigate the biochemical mechanisms of neurodegeneration. *ACS Chem. Neurosci.* **2012**, *3*, 178-185.

(33) Hackett, M.J., Paterson, P.G., Pickering, I.J., George, G.N. Imaging taurine in the central nervous system using chemically specific X-ray fluorescence imaging at the sulfur K-edge. *Anal. Chem.* **2016**, *88*, 10916-10924.

(34) Hackett, M.J., George, G.N., Pickering, I.J., Eames, B.F. Chemical biology in the embryo: in situ imaging of sulfur biochemistry in normal and proteoglycan-deficient cartilage matrix. *Biochemistry*, **2016**, *55*, 2441-2451.

(35) Easy, R.H., Ross, N.W. Changes in Atlantic salmon (*Salmo salar*) epidermal mucus protein composition profiles following infections with sea lice (*Lepeophtheirus salmonis*). *Comp. Biochem. Phys D.* **2009**, *4*, 159-167.

(36) Eddy, F.B., Fraser, J.E. Sialic acid and mucus production in rainbow trout (*Salmo gairdneri Richardson*) in response to zinc and seawater. *Comp. Biochem. Physiol.* **1982**, *73C*, 357-359.

(37) Lock, R.A.C., van Overbeeke, A.P. Effects of mercuric chloride and methylmercuric chloride on mucus secretion in rainbow trout, *Salmo gairdneri Richardson*. *Comp. Biochem., Physiol. C.* **1981**, *69C*, 67-73.

(38) Westfall, B.A. Coagulation film anoxia in fishes. *Ecology* **1945**, *26*, 283-287.

(39) Guardiola, F.A., Dioguardi, M., Parisi, M.G., Tranpani, M.R., Meseguer, J., Cuesta, A., Cammarata, M., Esteban, M.A. Evaluation of waterborne exposure to heavy metals in innate immune defences present on skin mucus of gilthead seabream (*Sparus aurata*). *Fish Shellfish Immunol.* **2015**, *45*, 112-123.

(40) Rajan, M.T., Banerjee, T.K. Histopathological changes induced by acute toxicity of mercuric chloride on the epidermis of freshwater catfish – *Heteropneustes fossilis* (Bloch). *Ecotoxicol. Environ. Safety* **1991**, *22*, 139-152.

(41) Li, Y., Yan, X.P., Chen, C., Xia, Y.L., Jiang, Y. Human serum albumin – Mercurial species interactions. *J. Proteome Res.* **2007**, *6*, 2277-2286.

(42) Ajsuvakova, O.P., Tinkov, A.A., Aschner, M., Rocha, J.B.T., Michalke, B., Skalnaya, M.G., Skalny, A.V., Butnariu, M., Dadar, M., Sarac, I., Aaseth, J., Bjørklund, G. Sulfhydryl groups as targets of mercury toxicity. *Coord. Chem. Rev.* **2020**, *417*, Article Number 213343

(43) Ynalvez, R., Gutierrez, J., Gonzalez-Cantu, H. Mini-review: toxicity of mercury as a consequence of enzyme alteration. *Biometals* **2016**, *29*, 781-788.

(44) Azevedo, B.F., Furieri, L.B., Peçanha, F.M., Wiggers, G.A., Vassallo, P.F., Simões, M.R., Florim J., Rossi de Batista, P., Fioresi, M., Rossoni, L., Stefanon, I., Alonso, M.J., Salaices, M., Vassallo, D.V. Toxic effects of mercury on the cardiovascular and central nervous systems. *J Biomed. Biotechnol.* **2012**, *2012*, 1-11.

(45) Sura, P., Bronowicka-Adamska, P., Furtak, E., Wróbel, M. Effect of mercury ions on cysteine metabolism in *Xenopus laevis* tissues. *Comp. Biochem. Phys C.* **2011**, *154*, 180-186.

(46) Vogel, D.G., Margolis, R.L., Mottet, N.K. The effects of methyl mercury binding to microtubules. *Toxicol. Appl. Pharmacol.* **1985**, *80*, 473-486.

(47) Philbert, M.A., Billingsley, M.L., Reuhl, K.R. Mechanisms of injury in the central nervous system. *Toxicol. Pathol.* **2000**, *28*, 43-53.

(48) King, J.K., Harmon, S.M., Fu, T.T., Gladden, J.B. Mercury removal, methylmercury formation, and sulfate-reducing bacteria profiles in wetland mesocosms. *Chemosphere* **2002**, *46*, 859-870.

(49) Kerin, E.J., Gilmour, C.C., Roden, E., Suzuki, M.T., Coates, J.D., Mason, R.P. Mercury methylation by dissimilatory iron-reducing bacteria. *Appl. Environ. Microbiol.* **2006**, *72*, 7919-7921.

(50) Hamelin, S., Amyot, M., Barkay, T., Wang, Y., Planas, D. Methanogens: Principal methylators of mercury in lake periphyton. *Environ. Sci. Technol.* **2011**, *45*, 7693-7700.

(51) Celo, V., Lean, D.R.S., Scott, S.L. Abiotic methylation of mercury in the aquatic environment. *Sci. Total Environ.* **2006**, *368*, 126-137.

(52) Oremland, R.S., Culbertson, C.W., Winfrey, M.R. Methylmercury decomposition in sediments and bacterial cultures: Involvement of methanogens and sulfate reducers in oxidative demethylation. *Appl. Environ. Microbiol.* **1991**, *57*, 130-137.

(53) Figueiredo, N., Serralheiro, M.L., Canario, J., Duarte, A., Hintelmann, H., Carvalho, C. Evidence of mercury methylation and demethylation by the estuarine microbial communities

obtained in stable Hg isotope studies. *Int. J. Environ. Res. Public Health*. **2018**, *15*, Article Number 2141

(54) Ludwicki, J.K. *In vitro* methylation and demethylation of mercury compounds by the intestinal contents. *Bull. Environ. Contam. Toxicol.* **1991**, *44*, 357-362.

(55) Rowland, I.R., Davies, M.J., Grasso, P. Metabolism of methylmercuric chloride by the gastro-intestinal flora of the rat. *Xenobiotica* **1978**, *1*, 37-43.

(56) Li, H., Lin, X., Zhao, J., Cui, L., Wang, L., Li, B., Chen, C., Li, Y-F. Intestinal methylation and demethylation of mercury. *Bull. Environ. Contam. Toxicol.* **2019**, *102*, 597-604.

(57) Thursby, E., Juge, N. Introduction to the human gut microbiota. *Biochem. J.* **2017**, *474*, 1823-1836.

(58) Minniti, G., Hagen, L.H., Porcellato, D., Jørgensen, S.M., Pope, P.B., Vaaje-Kolstad, G. The skin-mucus microbial community of farmed Atlantic salmon (*Salmo salar*). *Front. Microbiol.* **2017**, *8* Article Number 2043.

CHAPTER 8: GENERAL DISCUSSION

Methylmercury is widely recognized as a highly neurotoxic molecular compound with the ability to cause multi-organ system effects, including devastating toxicity if exposure occurs *in utero*. Exposure of human populations to this toxicant occurs primarily through consumption of contaminated fish or seafood. One should not abstain from consumption however, as there are many proven health benefits of consuming fish and seafood. Many countries, including Canada have advisories to recommend acceptable quantities of consumption for different fish species. These advisories are based off risk of the likelihood of increased (or decreased) contamination with mercury. To safely consume fish and seafood, one must simply be aware of the varying risks of mercury contamination. For example, Health Canada currently recommends eating no more than 150 g (a single serving, or an amount nearly equivalent to the amount of fish present in a can of tuna) a week (combined) of the following: shark, fresh/frozen tuna, swordfish, orange roughy, escolar or marlin.[1] Further to that, women pregnant, breastfeeding, or intending to become pregnant should consume no more than this same amount per month.[1] Many of these fish species are considered to be top predator fish, tend to be quite large when caught, and have been seen to contain high levels of mercury. Children 5-11 years of age should consume no more than 125 g per month of the above specified species, and younger children aged 1-4 should consume no more than 75 g. Canned tuna (excepting albacore canned tuna) are under no restrictive guidelines. This is because any canned tuna categorized as “light” comes from smaller, younger fish species including yellowfin, tongol or skipjack tuna which are unlikely to contain high levels of mercury. Recommendations for canned albacore only exist for women who are or may become pregnant or are breastfeeding. Here, consumption is suggested to be limited quantities of no more than 300 g (approximately 2 cans) per week, with slightly more restrictive recommendations for younger children.

It has been estimated that over a billion people globally depend on fish and seafood as their primary protein source.[2] While it might be said that Canadians generally eat less fish or seafood than these populations, there are certain populations within Canada having potentially increased risk for methylmercury consumption due to dietary habits. These may include: populations where fish is intertwined as a part of a traditional lifestyle with traditional practices which may include a reliance on fish or whale caught as part of the diet, immigrant populations coming from countries where consumption rates are generally higher, or populations residing in

coastal areas compared to interior areas (e.g. the Prairies) of the country. For example, trends of seasonally increased scalp hair mercury concentrations have been seen in pregnant Inuit women consuming beluga whale, a traditional dietary source.[3] Here, scalp hair mercury concentrations were seen to increase during summer months and decrease during the winter months when other dietary sources, including lake trout became dominant.[3]

It has been noted that indigenous cultures may be more at risk for methylmercury exposure (among other pollutants) due to the close proximity of traditional hunting and fishing grounds to local industries such as pulp and paper mills, hydroelectric, or mining activities.[4] This has come to be socially referred to as "environmental racism." Cree Nation populations in the James Bay area of northern Quebec, Canada have been seen to have increased blood mercury concentrations in areas where traditional fishing grounds overlapped with varying industries, especially hydroelectric and pulp and paper.[4] Methylmercury concentrations of fish including pike, trout and walleye in these regions were commonly elevated.[4] First Nations communities located in Grassy Narrows, Ontario were also severely impacted when inorganic mercury-contaminated waste from a chlor-alkali facility was released into the English-Wabigoon river system over a period of 8 years, from 1962-1970.[5] Inorganic mercury was methylated by sulfate-reducing bacteria within the river system to the highly toxic form of methylmercury, which was consumed by local human populations fishing and hunting in the river system areas. Recent research has shown that mercury contamination of the varying lakes in the English-Wabigoon river system has decreased since the 1970s. However, total mercury concentrations in fish tissue are, at the low concentration end, averaging around or slightly higher than the Health Canada tolerable daily intake value of 0.2 mg/kg body weight per day[6], and at the high concentration end, up to 12 times higher than the tolerable daily intake value.[5] Controversy surrounding the issue of remediation and compensation in the Grassy Narrows area is ongoing.

Rarely in history has there been such a devastating example of methylmercury intoxication via consumption of contaminated fish and seafood as what occurred in Minamata, Japan in the 1950s-1960s. The opportunity to investigate such rare and valuable specimens as those which were obtained for the work in Chapter 3 truly became the cornerstone for this entire body of research. Chapter 3 saw the examination of feline brain tissue from the famous Cat 717 experiments of the late 1950s, which had a hand in elucidating the source of the disease which was spreading rampantly throughout Minamata City, Japan, at that time, and later through

Niigata, Japan. Mercury high energy resolution fluorescence detected X-ray absorption spectroscopy (HERFD-XAS) analysis of this brain tissue revealed the majority of mercury remaining to be in an organic form, resembling methylmercury-L-cysteine (MeHg-L-Cys), with a smaller inorganic portion in the form of inorganic mercuric sulfide.[7] This not only demonstrated that the effluent being released from the factory contained organic mercury (originally assumed to be inorganic mercury which became methylated within Minamata Bay), but also demonstrates the impressive stability of mercury ligands in biological tissue. The sample obtained was quite old and had been preserved in formalin for approximately 40 years, however, the organic and inorganic ligands of mercury in the feline brain tissue remained.

Density functional theory was utilized to re-create the chemical processes occurring in the chemical factory which lead to the presumed production of methylmercury. However, the calculations indicated methylmercury to be an unlikely by-product. This work determined that an alternative mercury species, α-mercuri-acetaldehyde, was the most likely by-product of the chemical process, and then further to that, was the compound likely being released into Minamata Bay during the years the process was used.[7] While this work appeared to be found quite interesting by the general community,[8–11] this particular observation was received as very controversial in the scientific community, with a plethora of articles and discussion surrounding it.[12–17] A theory on the discussion surrounding this publication is that a great deal of what is known regarding methylmercury toxicokinetics and toxicodynamics was acquired from the Minamata tragedy. In turn, if the chemical compound suggested to be the root of the toxicity was not in fact, methylmercury, then perhaps what is "known" about methylmercury toxicity can be questioned. Regardless of the reason for the somewhat heated discussion, it raises an interesting question about the toxicities of alternative organic mercury species. A search of the Cambridge Crystal Structure Database indicates that 1604 organometallic mercury compounds have been structurally characterized. Even while recognizing that not every one of these 1604 species is biologically or environmentally relevant, research on organic species is primarily focussed on one single species, methylmercury. Methylmercury is by and far the most commonly studied organic mercury species, likely due to its known prevalence in the environment, particularly in aquatic settings. A logical question seems to be: what other species might be biologically or environmentally relevant that have not been researched? Under what circumstances are they likely to become problematic in an environmental or biological setting? Might it be reasonable to

suggest that organic species beyond methylmercury (or dimethylmercury) exist in the environment? And if so, how might their properties differ from methylmercury? For example, if α-mercuri-acetaldehyde was the dominant contaminant of the effluent waste in the in the Minamata tragedy, future research should focus on its toxicity and on understanding what transformations might have occurred within the environment as well as within aquatic organisms. In this case, the clinical symptoms exhibited by Cat 717 appeared to be reflective of methylmercury intoxication.[18] It is likely that this compound is metabolized into a species resembling methylmercury. Further work is necessary to characterize this organic mercury compound.

The work completed in Chapter 3 and Chapter 4 demonstrated the strength of X-ray absorption near-edge analysis, EXAFS and HERFD techniques in analyzing historical biological tissue for *in situ* metals having dilute concentrations. With these techniques, samples require little to no pre-treatment, and any phase (gas, liquid, solid) can be examined. Examination of a variety of historical samples has been seen in other fields using XAS techniques (including X-ray fluorescence imaging). A handful of recent publications on such samples has ranged from XFI and XAS analysis of ancient weapons from early Medieval times to investigate metal processing techniques,[19] XAS analysis of elemental composition on thin layers of paint from famous Leonardo da Vinci paintings, including the Mona Lisa, to further understand his meticulous painting techniques of flesh tones,[20] and XFI to investigate copper, zinc and lead in toenails of a seaman who was part of the Franklin Expedition of 1845 to 1848 to the result of determining that perhaps the leading cause of death was not excessive lead exposure but rather due to zinc deficiency related to diet.[21] Future work related to Chapter 3 includes the analysis of mercury species in hair samples and umbilical cord samples from victims of Minamata disease in Niigata, Japan, which occurred shortly after that in Minamata, Japan and under similar circumstances. Additional work completed (not shown here, and unpublished) includes mercury and selenium HERFD-XAS on a range of fish species including swordfish, whale, and tuna which are known to bioaccumulate toxic concentrations of mercury.

Chapter 4 saw the examination of a variety of rare and unique human brain tissue samples collected from individuals who had experienced either an acute exposure or were classified as having a chronic exposure to mercury given a lifetime of consuming marine fish and seafood which may contain elevated mercury concentrations. This chapter revealed that, at least in the

brain tissue samples examined, the chemical species of mercury were different when comparing an acute and chronic exposure. Specifically, inorganic mercury species dominated historical cases of acute exposures to organometallic mercury while the mercury present in individuals considered to have chronic, low-level exposures remained entirely organic in nature. The implications of this will likely be controversial. Nevertheless, this result indicates that acute exposures to mercury may not be a reliable reference for chronic mercury exposure, which occurs globally and arguably, far more frequently in human populations.

A direct comparison of brain tissue preserved in formalin and that which had been cryopreserved, being taken from the same individual, revealed no differences in mercury speciation in Chapter 4. The question of the effects of differing preservation methods on mercury, specifically regarding accumulation and distribution were further examined in Chapter 5. Conclusions were that methacrylate embedding had no major impact on either accumulation or distribution of mercury in the vertebrate model organism (*Danio rerio*) in the larval stage after exposure to MeHg-L-Cys and when compared with similarly aged and treated larval zebrafish which had been cryopreserved. However, the same conclusion could not be made for many of the other endogenous elements investigated, including potassium, calcium, copper, sulfur and zinc. This might prove a cautionary tale to researchers interested in chemical form in biological tissue. Further work could include performing chemically specific imaging on comparable sections of larval zebrafish which had undergone differing preservation methods to determine whether differences also existed in the chemical form of elements present, as that was not investigated in this work. Briefly, chemically-specific imaging allows for the creation of XFI maps of different chemical forms of an element, and can be taken further by pin-pointing elemental "hotspots" using the image created and determining their specific chemical form using X-ray absorption near-edge spectra (at beamlines which have this capability). These two techniques were first demonstrated together by investigating the qualitative and quantitative distributions of different forms of selenium in the selenium-accumulating plant *Astragalus bisulcatus*.[22]

Chapter 6 also utilized larval zebrafish as a vertebrate model, but here to investigate the effect of compounds which were assumed to competitively inhibit the toxicologically insidious compound MeHg-L-Cys for L-type neutral amino acid transporters (LAT1 and LAT2). These transporters are currently assumed to aid in the transportation of organometallic mercury in the human body, specifically at the blood-brain and blood-placental barrier. Here we had

hypothesized that competitive inhibition from a variety of LAT substrates (L-phenylalanine, L-methionine) and a LAT analog (BCH) would result in reduced mortality in zebrafish which were co-exposed with one of the above concurrently with MeHg-L-Cys, which was seen. A significant reduction in mercury concentration in a variety of target organs was also seen using XFI. However successful the mortality assays were, the results of XFI indicated that even while mercury concentrations were significantly reduced in target organs, the LAT "blockers" utilized were only moderately preventative in terms of accumulation, as mercury was still present in all target organs. This could indicate that the competitive inhibition of these particular blockers is not entirely efficient, or that transportation of organomercury is still occurring via other transporters or mechanisms (passive diffusion), or that both of these are occurring. Further work might include extending the experimental timeline to observe how much longer zebrafish which had been co-exposed to methylmercury and LAT blockers survived compared to the methylmercury treated group alone. Perhaps they would expire shortly after the timeline utilized in this experiment, which would then indicate that inhibiting LAT is relatively ineffective for reducing longer term exposure to methylmercury, at least when using mortality as an endpoint. Or perhaps the protectiveness of the blood-brain barrier would increase, as the blood-brain barrier of larval zebrafish has been estimated to become mature between 3-10 dpf,[23] with the mRNA encoding LAT1 been seen to be expressed at 18 hours post-fertilization.[24]

Future research investigating LAT transport of methylmercury using zebrafish might include a focus on increasingly frontal transverse head sections which include less eye lens and more brain matter. It could be interesting to attempt to visualize changes in accumulations or distributions within the brain tissue in methylmercury-exposed larval zebrafish in small increments of time, such as 4, 8, 12, 24, 36, 48 hours post-exposure. If visualization proved possible, it might be helpful to utilize a beamline such as BioXAS (Canadian Light Source, Saskatoon, SK) which has the ability to alternate between micro- and nano-modes in fluorescence imaging. At such a beamline, one could collect a micro-scale fluorescence map, identify areas of interest, and collect fluorescence maps at a nano-scale during the same beamtime. As an example, recent research has shown the formation of mixed chalcogenide $HgS_xSe_{(1-x)}$ particles in various target tissues of larval zebrafish after exposure to inorganic mercury in the relatively short time frame of 24-36 hours of exposure beginning at 3 dpf.[25] Here, mercury sequestration was clearly very fast, but more might be learned if sections were collected in a series beginning at earlier

time points. Using this set-up, it should be possible to see how quickly mercury accumulates in different target tissues.

Future work might also explore the differing toxicities of MeHg-L-Cys compared to methylmercury-D-cysteine (MeHg-D-Cys). This compound was included in Chapter 6 to demonstrate the stereoselectivity of LAT transporters (L-system transporters) but with an unexpected result. Here we saw that MeHg-D-Cys was taken up in target organs in head sections in concentrations which were not significantly different from MeHg-L-Cys, and yet, survival of zebrafish in MeHg-D-Cys was markedly increased compared to MeHg-L-Cys. The reason for this was unclear. The stereoselectivity of LAT is well reported in the literature. However, less frequently, the opposite has also been demonstrated. Wang et al. exposed a human hepatoma cell line to various organomercury compounds including complexes of methylmercury with L- and D-cysteine and observed that while uptake was certainly less when in the complex with D-cysteine, it did occur to some extent.[26] Mokrzan et al. found the uptake of MeHg-D-Cys to be lower compared to MeHg-L-Cys when the same concentration of both was used to treat cultured brain capillary endothelial cells which are an *in vitro* model for the blood-brain barrier.[27] Yet other work is in agreement, demonstrating that MeHg-D-Cys is taken up in the brain of a rat model when injections occurred via the carotid, even while this uptake was reduced compared to MeHg-L-Cys.[28] Recent work has focussed on re-evaluating what is typically accepted about LAT stereoselectivity, suggesting that D- and L- enantiomers exhibit different binding behaviors[29] which may explain the differing affinities.

A final thought on work involving zebrafish pertains to the observed differing susceptibilities of various wildtype zebrafish strains to methylmercury toxicity. During the course of the described research, two well-established strains of adult wildtype zebrafish were available for mating; AB and Tübingen (TU) which were reared in the new LASU facility on campus. Prior to that, in research not included in this thesis but nevertheless assisted in and published,[25,30,31] a wildtype zebrafish strain purchased from a generic pet store was maintained in a fish facility located in Health Sciences. The biggest difference in sensitivity to methylmercury was seen between the pet store variety and both AB and TU strains, where the former could be exposed to concentrations ranging from 0.2-100 µM, surviving an exposure period of 24 hours at the highest concentration and 84 hours at the lowest concentration,[32] and concentrations of 1-2 µM methylmercury chloride and MeHg-L-Cys being commonly used for 36 hour exposures.[33,34]

In marked contrast, through range-finding assays it was determined that 0.2 μM was the highest concentration usable for a 48-hour exposure to MeHg-L-Cys using AB and TU strains. Differences between AB strains and TU strains were also noticed in regards to methylmercury sensitivity, with AB being more sensitive to methylmercury toxicity. This idea was not further explored in this theses, however, because of this difference the wildtype zebrafish used was exclusively TU. It is interesting to note that a work colleague observed a similar pattern of increased sensitivity of the AB strain to selenium exposures. A reason for this might simply be genetic background. Interestingly, this increased sensitivity did not appear to translate when $HgCl_2$ was utilized (see Chapter 7). The concentration of this compound was based off of earlier work which was done using the pet store wildtype zebrafish,[30] with no increased sensitivity noted in TU strains. A commonly utilized zebrafish information network (ZFIN)[35] lists 32 different wildtype strains, a list which may not be exhaustive. It could be interesting to examine differences in sensitivity more thoroughly. This has been explored using various behavioral endpoints,[36,37] but not with mercury toxicity.

Chapter 7 explored the accumulations and distributions of organic and inorganic mercury species in the mucosal-associated tissue of larval zebrafish as well as the interactions between organic and inorganic mercury and mucosa which had been collected from steelhead trout (*Oncorhynchus mykiss)* reared in a local aquaculture facility. This work demonstrated a target area of accumulation of both organic and inorganic mercury in larval zebrafish that, to our knowledge, has never been identified. The discovery of this was quite accidental, and became the beginning of this exploration of a possible mechanism of defense against mercury species in at least one teleost fish, steelhead trout. Mercury was seen to increase in this target area over time in larval zebrafish after exposure to one form of inorganic mercury. This accumulation was (statically) observed in more than one mercury species (inorganic and organometallic). The most surprising result came from the comparison between titrations of an organic and inorganic mercury species with the trout mucosa, which, at the lowest organometallic mercury concentration used, appeared to have become nearly demethylated.

One observation that came from this work was the elevated mercury concentrations present in the gut tube of organomercury-treated zebrafish. This can initially be difficult to visualize until one begins changing the intensity scale of the image, as was being done here to observe the mercury in the mucosal-associated epithelial layer. This is in contrast to what is seen

in zebrafish treated with inorganic mercury where changing the intensity scale does not reveal increased mercury concentrations in this location. Methylmercury is known to be highly absorbed (approximately 95%) in the gastrointestinal tract[38] while inorganic mercury absorption in this area is thought to be very low (7-15%).[39] The intestinal tract has also been shown to be a location where demethylation of organic mercury via the gut microbiome occurs.[38] This could be interesting to study in larval zebrafish, as accumulation is clearly occurring in the gut tube after organomercury exposure. Future work might include collecting fluorescence maps of exposed zebrafish throughout an extended time frame followed by collecting XAS spectra to see if mercury species are primarily organic nature at earlier time points followed by inorganic mercury at later time points where mercury had become demethylated.

Increased replication is needed for this data, especially in the lower concentration methylmercury titrations which produced such a unique result. If this result could be confirmed in trout mucosa it would certainly be of interest to observe whether demethylation occurs in the mucosa of other fish, including both freshwater and marine species. As well, this work would likely benefit from using the HERFD-XAS technique to increase confidence in the mercury species being identified. The same could be said for sulfur, as the sulfur species were rather difficult to identify. However, the resolution at the sulfur K-edge using the HERFD-XAS technique is currently limited by monochromator resolution. The technology and methodology behind the methods employing synchrotron radiation is continually improving. The newer, 4th generation synchrotron radiation sources give the opportunities for enhancements of many techniques, especially those that are brilliance limited, such as XFI and HERFD-XAS. The availability of smaller spot sizes should allow for improved spectrometer resolution, and the advantages of higher resolution monochromator designs might provide additional advantages. However, increased energy resolution can be hindered by the limitations on flux density. As well, one must be cautious of photo-damage effects that may be a result of the smaller spot size and resulting increased flux density in the HERFD-XAS technique. Mercury has been seen to be vulnerable to photoreduction effects. To circumvent this, a new area of the sample was interrogated for each sweep of the data (Chapters 3 and 4), with shutters being employed to prevent X-rays from interacting with the sample in any moment besides active data collection. With the new sources, combining HERFD-XAS and XFI is a possibility. Here, the ability to

rapidly scan a HERFD-XAS spectrum for each pixel of an XFI image could give vastly improved capabilities.

Human populations are exposed to various forms of organic and inorganic mercury through a wide variety of sources, both natural and anthropogenic. The leading source of anthropogenic emissions of mercury into the environment occurs through the generation of coal-fired power. An updated estimate places current atmospheric anthropogenic mercury contributions at 450% greater than what might be expected from natural sources.[40] This value includes what is referred to as "legacy emissions," defined as non-current emissions which continue to cycle throughout the environment in the present day. This same assessment on the current state of global mercury estimates East and Southeast Asia as the largest contributors to atmospheric mercury from anthropogenic sources, with large contributions coming from fuel combustion, various industrial sectors, product waste and artisanal and small-scale gold mining.[40] The only other areas of the world which surpassed these contributions in any of the listed sectors were South American and sub-Saharan African contributions from artisanal and small-scale gold mining.[40] Locally, Saskatchewan relies on the burning of coal for approximately 30% of provincial power which comes from three large coal-fired power plants including Boundary Dam (Estevan, SK), Shand Power Station (Estevan, SK) and Poplar River Power Station (Coronach, SK).[41] Provincial plans regarding coal-fired power currently include retiring facilities which are older than 50 years as well as retrofitting existing facilities to accommodate carbon capture and storage by the year 2030.[41] Current global initiatives regarding mercury include the Minamata Convention on Mercury, an international treaty introduced in 2013 dedicated to reducing global mercury pollution for protection of both human health and the environment.[42] Aims of this treaty broadly apply to supply and trade of mercury-containing products, emissions of mercury into environmental compartments from industrials processes, proper waste management and reduction or elimination of mercury mining or mining operations which cause the release of mercury, to name a few.[42] This treaty currently has 128 signatories and 130 ratifications; Canada signed in 2013.[42]

Despite the toxicity of mercury and the potential for acute and chronic exposure in human populations, the mechanisms of mercury's rapid transport throughout the human body, of its toxicity, and of the human body's defenses are still not fully characterized. Exposure of human populations to mercury is a worldwide health concern given rising industrial and mining

activities, increasing global temperatures resulting in melting of permafrost and polar ice which can contain high levels of mercury, and the large human populations which regularly consume fish and seafood which have increased risk for mercury contamination. The aim of this research was to increase knowledge on organometallic mercury toxicity and dynamics in human brain tissue as well as in the zebrafish vertebrate model. Here we were able to uncover complexities regarding the transportation of organic mercury in the human body, raise new questions about defensive mechanisms in teleost fish against organic and inorganic mercury, highlight the importance of careful selection of preservation method in the study of endogenous elements, dive deeper into the root cause of a most infamous, historic example of mass organic mercury poisoning, and perhaps most importantly, present an entirely new perspective on the differences between acute and chronic exposures of humans to organometallic mercury compounds.

8.1 References

(1) Health Canada. Mercury in fish: Question and Answers. Retrieved from: https://www.canada.ca/en/health-canada/services/food-nutrition/food-safety/chemical-contaminants/environmental-contaminants/mercury/mercury-fish-questions-answers.html

(2) World Health Organization. Global and regional food consumption patterns and trends. Retrieved from: https://www.who.int/dietphysicalactivity/publications/trs916/en/gsfao_global.pdf

(3) de Moraes Pontual, M., Ayotte, P., Little, M., Furgal, C., Boyd, A.D., Muckle, G., Avard, E., Ricard, S., Gauthier, M-J., Anassour-Laouan Sidi, E., Lemire, M. Seasonal variations in exposure to methylmercury and its dietary sources among pregnant Inuit women in Nunavik, Canada. *Sci. Tot. Environ.* **2021**, *755*, article number 143196.

(4) Moriarity, R.J., Liberda, E.N., Tsuji, L.J.S. Using a geographic information system to assess local scale methylmercury exposure from fish in nine communities of the Eeyou Istchee territory (James Bay, Quebec, Canada). *Environ. Res.* **2020**, 191, article number 110147.

(5) Kinghorn, A., Solomon, P., Chan, H.M. Temporal and spatial trends of mercury in fish collected in the English-Wabigoon river system in Ontario, Canada. *Sci. Total Environ*. **2007**, *372*, 615-623.

(6) Legrand, M., Feeley, M., Tikhonov, C., Schoen, D., Li-Muller, A. Methylmercury blood guidance values for Canada. *Can. J. Public Health* **2010**, *101*, 28-31.

(7) James, A.K., Nehzati, S., Dolgova, N.V., Sokaras, D., Kroll, T., Eto, K., O'Donoghue, J.L., Watson, G.E., Myers, G.J., Krone, P.H., Pickering, I.J., George, G.N. Rethinking the Minamata tragedy: What mercury species was really responsible? *Environ. Sci. Technol*. **2020**, *54*, 2726-2733.

(8) CBC Radio interview. February 27, 2020. https://www.cbc.ca/news/canada/saskatoon/mercury-poisoning-discovery-minamata-disease-saskatchewan-research-cat-brain-1.5476569

(9) University of Saskatchewan media release. February 13, 2020. https://news.usask.ca/media-release-pages/2020/usask-research-identifies-potential-cause-of-minamata-mercury-poisoning.php

(10) SLAC National Accelerator Laboratory media release. February 21, 2020. https://www6.slac.stanford.edu/news/2020-02-21-researchers-identify-new-culprit-minamata-mercury-poisoning-tragedy.aspx

(11) Science Daily news release. February 13, 2020. https://www.sciencedaily.com/releases/2020/02/200213135755.htm

(12) Science Magazine news article. March 24, 2020. https://www.sciencemag.org/news/2020/03/mysterious-chemical-found-dead-cats-brain-reopens-debate-over-mercury-poisoning

(13) Smithsonian magazine news article. March 26, 2020. https://www.smithsonianmag.com/smart-news/debate-over-mercury-poisoning-disaster-revived-dead-cats-brain-180974515/

(14) Tohyama, C. Comment on "Rethinking the Minamata tragedy: What mercury species was really responsible?" *Environ. Sci. Technol.* **2020**, *54*, 8486-8487.

(15) James, A.K., Nehzati, S., Dolgova, N.V., Sokaras, D., Kroll, T., O'Donoghue, J.L., Watson, G.E., Myers, G.J., Krone, P.H., Pickering, I.J., George, G.N. Reply to comments on "Rethinking the Minamata tragedy: What mercury species was really responsible?" *Environ. Sci. Technol*. **2020**, *54*, 8488-8490.

(16) Balogh, S.J., Tsui, M.T-K. Comment on "Rethinking the Minamata tragedy: What mercury species was really responsible?" *Environ. Sci. Technol.* **2020**, *54*, 8482-8483.

(17) James, A.K., Nehzati, S., Dolgova, N.V., Sokaras, D., Kroll, T., O'Donoghue, J.L., Watson, G.E., Myers, G.J., Krone, P.H., Pickering, I.J., George, G.N. Reply to comments on "Rethinking the Minamata tragedy: What mercury species was really responsible?" *Environ. Sci. Technol*. **2020**, *54*, 8484-8485.

(18) Eto, K., Yasutake, A., Nakano, A., Akagi, H., Tokunaga, H., Kojima, T. Reappraisal of the historic 1959 cat experiment in Minamata by the Chisso factory. *Tohoku J. Exp. Med*. **2001**, *194*, 197-203.

(19) Grolimund, D., Senn, M., Trottmann, M., Janousch, M., Bonhoure, I., Acheidegger, A.M., Marcus, M. Shedding new light on historical metal samples using micro-focused synchrotron X-ray fluorescence and spectroscopy. *Spectrochim. Acta B*. **2004**, *59*, 1627-1635.

(20) de Viguerie, L., Walter, P., Laval, E., Mottin, B., Solé, V.A. Revealing the sfumato technique of Leonardo da Vinci by X-ray fluorescence spectroscopy. *Angew. Chem. Int. Ed*. **2010**, *49*, 6125-6128.

(21) Christensen, J.R., McBeth, J.M., Sylvain, N.J., Spence, J., Chan, H.M. Hartnell's time machine: 170-year-old nails reveal severe zinc deficiency played a greater role than lead in the demise of the Franklin Expedition. *J. Archaeol. Sci. Rep*. **2017**, *16*, 430-440.

(22) Pickering, I.J., Prince, R.C., Salt, D.E., George, G.N. Quantitative, chemically specific imaging of selenium transformation in plants. *Proc. Natl. Acad. Sci. USA*. **2000**, *97*, 10717-10722.

(23) Fleming, A., Diekmann, H., Goldsmith, P. Functional characterisation of the maturation of the blood-brain barrier in larval zebrafish. *PLOS One* **2013**, *8*, article number e77548.

(24) Walter, K.M., Dach, K., Hayakawa, K., Giersiefer, S., Heuer, H., Lein, P.J., Fritsche, E. Ontogenic expression of thyroid hormone signaling genes: An in vitro and in vivo species comparison. *PLOS One* **2018**, *14*, article number e0221230.

(25) MacDonald, T.C., Korbas, M., James, A.K., Sylvain, N.S., Hackett, M.J., Nehzati, S., Krone, P.H., George, G.N., Pickering, I.J. Interaction of mercury and selenium in the larval stage zebrafish vertebrate model. *Metallomics* **2015**, *7*, 1247-1255.

(26) Wang, W., Clarkson, T.W., Ballatori, N. γ-glutamyl transpeptidase and L-cysteine regulate methylmercury uptake by HepG2 cells, a human hepatoma cell line. *Toxicol. Appl. Pharmacol*. **2000**, *168*, 72-78.

(27) Mokrzan, E.M., Kerper, L.E., Ballatori, N., Clarkson, T.W. Methylmercury-thiol uptake into cultured brain capillary endothelial cells on amino acid system L. *J. Pharmacol. Exp. Ther*. **1995**, *272*, 1277-1284.

(28) Kerper, L.E., Ballatori, N., Clarkson, T.W. Methylmercury transport across the blood-brain barrier by an amino acid carrier. *Am. J. Physiol*. **1992**, *262*, R761-R765.

(29) Chien, H.C., Colas, C., Finke, K., Springer, S., Stoner, L., Zur, A.A., Venteicher, B., Campbell, J., Hall, C., Flint, A., Augustyn, E., Hernandez, C., Heeren, N., Hansen, L., Anthony, A., Bauer, J., Fotiadis, D., Schlessinger, A., Giacomini, K.M., Thomas, A.A. Reevaluating the substrate specificity of the L-type amino acid transporter (LAT1). *J. Med. Chem*. **2018**, *61*, 7358-7373.

(30) MacDonald, T.C., Nehzati, S., Sylvain, N.J., James, A.K., Korbas, M., Caine, S., Pickering, I.J., George, G.N., Krone, P.H. Phenylthiourea alters toxicity of mercury compounds in zebrafish. *J. Inorg. Biochem*. **2015**, *151*, 10-17.

(31) MacDonald, T.C., Sylvain, N.J., James, A.K., Pickering, I.J., Krone, P.H., George, G.N. Effects of inorganic mercury on the olfactory pits of zebrafish larvae. *Metallomics* **2016**, *8*, 514-517.

(32) Korbas, M., Blechinger, S.R., Krone, P.H., Pickering, I.J., George, G.N. Localizing organomercury uptake and accumulation in zebrafish larvae at the tissue and cellular level. *Proc. Natl. Acad. Sci. USA*. **2008**, *105*, 12108–12112.

(33) Korbas, M., Krone, P.H., Pickering, I.J., George, G.N. Dynamic accumulation and redistribution of methylmercury in the lens of developing zebrafish embryos and larvae. *J. Biol. Inorg. Chem*. **2010**, *15*, 1137-1145.

(34) Korbas, M., MacDonald, T.C., Pickering, I.J., George, G.N., Krone, P.H. Chemical form matters: Differential accumulation of mercury following inorganic and organic mercury exposures in zebrafish larvae. *ACS Chem. Biol*. **2012**, *7*, 411-420.

(35) The zebrafish information network (ZFIN). https://www.zfin.org

(36) Liu, X., Guo, N., Zhang, Y., Chen, X.Q., Li, S., He, L., Li, Q. Strain dependent differential behavioral responses of zebrafish larvae to acute MK-801 treatment. *Pharmacol. Biochem. Behav*. **2014**, *27*, 82-89.

(37) Audira, G., Siregar, P., Strungaru, S.A., Huang, J.C., Hsiao, C.D. Which zebrafish strains are more suitable to perform behavioral studies? A comprehensive comparison by phenomic approach. *Biology-Basel* **2020**, *9*, article number 200.

(38) World Health Organization (WHO). Environmental Health Criteria 101: Methylmercury. International Programme on Chemical Safety, Geneva, Switzerland, 1990.

(39) World Health Organization (WHO). Environmental Health Criteria 1: Mercury. International Programme on Chemical Safety, Geneva, Switzerland, 1976.

(40) UN Environment. Global mercury assessment 2018. UN Environment Programme (UNEP) Chemicals and Health Branch, Geneva, Switzerland, 2019.

(41) SaskPower. Coal. Retrieved from: https://www.saskpower.com/Our-Power-Future/Our-Electricity/Electrical-System/Balancing-Supply-Options/Coal

(42) Minamata Convention on Mercury. UN Environment Programme (UNEP) Châtelaine, Switzerland. Retrieved from: https://www.mercuryconvention.org/

APPENDIX A

SUPPLEMENTARY INFORMATION FOR CHAPTER 2

Table A.2.1: Definitions of symbols from all numerical equations in Chapter 2.

Symbol	*Definition*	*Equation number*	*Page number*
A_t	Absorbance, measured by transmittance	2.1	33
μ	X-ray absorption coefficient	2.1	33
x	Sample depth	2.1	33
ln	Natural log	2.1	33
I_0	X-ray beam intensity incident on sample	2.1	33
I_1	X-ray beam intensity post-sample	2.1	33
A_f	Absorbance, measured by fluorescence	2.2	33
$\propto$	Proportional to	2.2	33
I_f	Intensity of fluorescence	2.2	33
$\chi(E)$	EXAFS oscillations	2.3	37
$\mu(E)$	X-ray absorption coefficient μ as a function of X-ray energy, E	2.3	37
$\mu_0(E)$	Non-oscillatory part of the X-ray absorption coefficient μ, specified as a function of X-ray energy, E	2.3	37
$\chi(k)$	EXAFS	2.4	38
N	Coordination number	2.4	38
$S_i(k)$	Amplitude reduction function, specific to shell i (and also $f_i(k)$, below)	2.4	38
$f_i(k)$	EXAFS amplitude function	2.4	38
k	Photoelectron wave vector	2.4	38
R	Path-length	2.4	38
S_0^2	Total amplitude reduction factor	2.4	38
$\lambda(k)$	Photoelectron mean free path function	2.4	38
σ^2	Mean-square deviation in R (Debye-Waller)	2.4	38
$\varphi_i(k)$	EXAFS backscatterer phase shift function	2.4	38
$\delta_c(k)$	EXAFS absorber phase shift function	2.4	38

APPENDIX B

SUPPLEMENTARY INFORMATION FOR CHAPTER 3

The publication of "Rethinking the Minamata tragedy: What mercury species was really responsible?" was received with some controversy in the scientific community. Below are two reply articles which have been published in *Environmental Science and Technology* in response to two comment articles which were also published in the same journal. Citations for comment articles are included before the text of each reply piece.

REPLY TO COMMENTS ON "RETHINKING THE MINAMATA TRAGEDY: WHAT MERCURY SPECIES WAS REALLY RESPONSIBLE?"[1]

Citation for comment: Tohyama, C. *Environ. Sci. Technol.* 2020, *54*, 8486-8487.

Supplementary text B.3.1

Professor Tohyama criticizes our recent ES&T paper,[2] which addressed the chemical species of mercury involved in the poisoning at Minamata. Pollution from a nearby chemical plant employing mercury catalysts resulted in mercury contents ranging from 10 to >100 ppm in seafood consumed by the local population.[3] Tohyama states that we ignored the old literature which, he contends, incontrovertibly proved that methylmercury was the sole cause of Minamata disease. Our scientific team has a long track record of published mercury research, and certainly was aware of the early ground-breaking Japanese work. Our recent research[2] began with the opportunity to examine a historically important sample; the brain of Cat 717. Analytical methods have recently advanced, but we nonetheless expected to confirm previous findings of predominant inorganic mercury.[4] Instead we found that the major mercury species was organometallic mercury, with a minor inorganic component of β-mercuric sulfide.[2] We next computationally examined the possible chemistry and by-products of the industrial process. Our calculations showed that generating methylmercury in the plant would be very difficult, and that more likely by-products were α-mercuri-acetaldehyde compounds. Our work[2] relates directly to the mercury species received by Cat 717. The chemical plant waste causing Minamata disease was likely a mixture of multiple mercury species, but the prominent presence of α-mercuri-acetaldehyde and related compounds seems probable. Prompted by our unexpected findings, and given that the evidence suggested that the plant waste already contained organometallic mercury,

we questioned whether biomethylation played any role. Because the organometallic mercury from the plant was likely a form other than methylmercury, we went still further and suggested that α-mercuri-acetaldehyde or related compounds and not methylmercury might have been responsible for Minamata disease.[2]

Tohyama disagrees with our suggestions since he feels that prior work provided definitive proof that methylmercury was responsible. He cites nine corroborating points as evidence, which fall into two categories – the clinical symptomatology and the extremely high degree of mercury exposure. These points are consistent with methylmercury as a cause, but do not constitute proof. Points (a) and (c) allude to symptoms, pathologies and signs, expected to be similar for related mercury chemical species. (b) and (f) reference elevated total mercury, but not a specific chemical form. His remaining points are subject to how reliably methylmercury was in fact determined – in tissues (d), (e), (g), (h), or in sludge and wastewater (i), and whether other mercury forms eluded detection.

We recognize the extraordinary efforts needed to isolate specific mercury compounds from complex samples such as tissues containing just traces of mercury. Tohyama cites studies of industrial wastes from the chemical factory,[5] and of shellfish,[6] which characterized isolated materials by standard chemical analysis methods following multiple solvent extractions and distillations. The species isolated from the complex mixture comprising the industrial waste distinctly resembled methylmercury chloride.[5] For shellfish, researchers concluded that the isolated material contained a mercury-carbon bond,[6] suggesting it was "most reasonable to assign the isolated crystals to methyl-methylmercuric sulfide" (CH_3HgSCH_3), but did not claim definitive identification. Indeed, the isolated compound was subsequently discussed as bis-methylmercury-sulfide $(CH_3Hg)_2S$,[7] or higher alkylmercury derivatives.[8] As a 1982 letter to ES&T discussed, the isolated compound was likely an alkylmercury derivative, rather than specifically methylmercury.[9] Whether the isolated compounds were major or minor components remains unclear. It is thus plausible that methylmercury was not the predominant form in the plant waste and that unequivocal proof of methylmercury as the sole cause of Minamata disease is lacking. –

When these early studies were conducted, methylmercury analytical methods were still being refined.[10–13] One issue with methods employing a mobile phase to estimate methylmercury is that an unsuspected organometallic mercury species might be missed altogether due to its

differing mobility.[2] The advantages (and disadvantages) of in-situ techniques are increasingly realized. X-ray absorption spectroscopy and its derivatives collectively referred to as advanced X-ray spectroscopy are especially well-suited to studies of tissues or environmental samples; essentially no sample pre-treatment is required and, since detection depends upon basic atomic physics, no mercury present is missed. The latter is an obvious strength, but also a weakness because minor components in complex mixtures might be obscured by the major species.

Professor Tohyama questions that biomethylation was considered as a source of methylmercury in Minamata disease, stating that the cause was direct release of methylmercury. Regardless, the biomethylation scenario was certainly postulated and debated.[14] One popular toxicology textbook, Casarett & Doull's Toxicology: The Basic Science of Poisons[15] states, "In the 1950s, industrial discharges of mercury into Minamata Bay in Japan became biomethylated to form methyl mercury, which then accumulated in the food chain and reached toxic concentrations in the fish and shellfish consumed in the surrounding communities." Additionally, A Textbook of Modern Toxicology[16] states, "In Japan in the 1950s and 1960s, wastes from a chemical and plastics plant containing mercury were drained into Minamata Bay. The mercury was converted to the readily absorbed methylmercury by bacteria in the aquatic sediments." Many journal articles also discuss this.[9,17–19]

Professor Tohyama suggests that the toxicological properties of α-mercuri-acetaldehyde and related compounds should be evaluated, and we are already preparing to do this. While methylmercury compounds are extensively studied as known species in the natural biogeochemical mercury cycle,[20] toxicological studies of other organometallic mercury compounds include just ethylmercury and phenylmercury species. Methylmercury and ethylmercury compounds show distinct but similar toxicological profiles,[21,22] and comparable localization patterns in exposed larval zebrafish.[23] Phenylmercury differs in apparently lacking teratogenicity and somewhat resembling inorganic mercury.[24,25] The mercury-phenyl carbon bond is more susceptible to protonolysis,[26] which could form inorganic mercury in vivo. We expect α-mercuri-acetaldehyde species to somewhat resemble ethylmercury in their toxicology, but further studies are needed. Moreover, as we discuss,[2] the environmental fate of these compounds is also unknown; evaluating this and the toxicology requires considerable work beyond our paper's scope.[2]

We recognize the toxic hazards posed by organometallic mercury compounds and the significant toxicity of methylmercury at sufficient exposure levels.[27] Although we cited over 50 papers,[2] Minamata disease literature is vast and we may have missed articles that others consider important. With all due respect we point out that much of the early work at Minamata was not completely conclusive, and contend that a scientific explanation of our findings is needed.

References B.3.2

(1) James, A.K., Nehzati, S., Dolgova, N.V., Sokaras, D., Kroll, T., O'Donoghue, J.L., Watson, J.E., Myers, G.J., Krone, P.H., Pickering, I.J., George, G.N. Reply to comments on "Rethinking the Minamata tragedy: What mercury species was really responsible?" *Environ. Sci. Technol.* **2020**, *54*, 8488-8490.

(2) James, A. K., Nehzati, S., Dolgova, N. V., Sokaras, D., Kroll, T., Eto, K., O'Donoghue, J. L., Watson, G. E., Myers, G. J., Krone, P. H., Pickering, I. J., George, G.N. Rethinking the Minamata tragedy: What mercury species was really responsible? *Environ. Sci. Technol*. **2020**, *54*, 2726–2733.

(3) Yokoyama, H. In *Mercury Pollution in Minamata*, Springer Briefs in Environmental Science, Springer Nature, Singapore, 2018.

(4) Eto, K., Yasutake, A., Nakano, A., Akagi, H., Tokunaga, H., Kojima, T. Reappraisal of the historic 1959 cat experiment in Minamata by the Chisso factory. *Tohoku J. Exp. Med*. **2001**, *194*, 197–203.

(5) Irukayama, K., Kai, F., Fujiki, M., Kondo, T. Studies on the origin of the causative agent of Minamata disease. III. Industrial wastes containing mercury compounds from Minamata factory. *Kumamoto Med. J.* **1962**, *15*, 57–68.

(6) Uchida, M., Hirakawa, K., Inoue, T. Biochemical studies on Minamata disease. IV. Isolation and chemical identification of the mercury compound in the toxic shellfish with special reference to the causal agent of the disease. *Kumamoto Med. J*. **1961**, *14*, 181–187.

(7) Uchida, M. Biochemical Studies on Minamata Disease. *Seikagaku* **1963**, 35, 430–439.

(8) Studies on the organic mercury compound in the fish and shellfish from Minamata Bay as the causative agent of Minamata Disease and the formation of the poison. *Nihon Eiseigaku Zasshi*, **1964**, *19*, 238–245.

(9) Taylor, D. Minamata disease. *Environ. Sci. Technol*. **1982**, *16*, 81A.

(10) Gage, J. C. The trace determination of phenyl- and methylmercury salts in biological material. *Analyst* **1961**, 457–459.

(11) Westöö, G. Determination of methylmercury compounds in foodstuffs II. Determination of methylmercury in fish, egg, meat and liver. *Acta Chem. Scand.* **1967**, *21*, 1790–1800.

(12) Akagi, H., Nishimura, H. Speciation of mercury in the environment. In: *Advances in Mercury Toxicology.* Suzuki, T., Imura, N., Clarkson, T. W. Eds. Plenum Press, New York, 1991, pp. 53–76.

(13) Puk, R., Weber, J. H. Critical review of analytical methods for determination of inorganic mercury and methylmercury compounds. *Appl. Organomet. Chem.* **1994**, *8*, 293–302.

(14) Kurzel, R. B., Cetrulo, C. L. The effect of environmental pollutants on human reproduction, including birth defects, *Environ. Sci. Technol*. **1981**, *15*, 626–640.

(15) Klaassen, C. D. Toxic responses of the cornea, retina, and central visual system. In *Casarett & Doull's Toxicology: The Basic Science of Poisons;* Fox, D.A., Boyes, W.K., Eds.; McGraw-Hill: New York, 2018, Ed. 9

(16) Cope, W. G., Hodgson, E. Classes of toxicants: Use classes. In *A Textbook of Modern Toxicology*. Ed. Hodgson, E., Wiley, Hoboken, 2010, Ed. 4. pp 52.

(17) Fujiki, M., Tajima, S. The pollution of Minamata Bay by mercury. *Water Sci. Technol.* **1992**, *11*, 133–140.

(18) Takizawa, Y. Understanding Minamata disease and strategies to prevent further environmental contamination by methylmercury. *Water Sci. Technol*., **2000**, *42*, 139–146.

(19) Eto, K. The pathology of methylmercury poisoning (Minamata disease). *Neuropathology*, **2010**, *30*, 417–419.

(20) Selin, N.E. Global biogeochemical cycling of mercury: A review. *Annu. Rev. Environ. Resour.* **2009**, *34*, 43–63.

(21) Clarkson, T. W. The three modern faces of mercury. *Environ. Health Perspect.* **2002**, *110 suppl.1*, 11–23.

(22) Burbacher, T. M., Shen, D. D., Liberato, N., Grant, K. S., Cernichiari, E., Clarkson, T. W. Comparison of blood and brain mercury levels in infant monkeys exposed to methylmercury or vaccines containing thimerosal. *Environ. Health Perspect.* **2005**, *113*, 1015–1021.

(23) Korbas, M., Blechinger, S. R., Krone, P. H., Pickering, I. J., George, G. N. Localizing organomercury uptake and accumulation in zebrafish larvae at the tissue and cellular level. *Proc. Natl. Acad. Sci. USA*, **2008**, *105*, 12108–12112.

(24) Hartke, G. T., Oehme, F. W., Leipold, H. W., Kruckenberg, S. M. Embryonic susceptibility of *Microtus ochrogaster* (Common Prairie Vole) to phenyl mercuric acetate *Toxicology* **1976**, *6*, 281–287.

(25) Bleyl, D. W., Klein, S., Woggon, H. Comparative studies of 2 organic mercury compounds alone or in combination with ethanol following pre- or postnatal application in mice. *Die Nahrung* **1985**, *29*, 93–103.

(26) Barbaro, P., Cecconi, F., Ghilardi, C. A., Midollini, S., Orlandini, A., Vacca, A. Metal coordination and Hg–C bond protonolysis in organomercury(II) compounds. Synthesis, characterization, and reactivity of the tetrahedral complexes $[(np_3)HgR] - [(CF_3)SO_3]$ {np_3 = $N(CH_2CH_2PPh_2)_3$; R = CH_3, C_2H_5, C_6H_5}. *Inorg. Chem.* **1994**, *33*, 6163–6170.

(27) Sokol, J. New mercury compound spotted in mass poisoning, *Science*, **2020**, *367*, 1415–1416.

REPLY TO COMMENTS ON "RETHINKING THE MINAMATA TRAGEDY: WHAT MERCURY SPECIES WAS REALLY RESPONSIBLE?"[1]

Citation for comment: Balogh, S.J., Tsui, M.T.K. *Environ. Sci. Technol.* 2020, *54*, 8482-8483.

Supplementary text B.3.3

Here we respond to correspondence by Balogh and Tsui who are critical of our recent ES&T publication which discussed the chemistry behind the Minamata tragedy.[2] Our study had two components, an advanced X-ray spectroscopy investigation of a historical brain tissue sample (Cat 717), and a computational chemistry study of the major chemical processes in the industrial plant. Previous chemical analyses of both the brain and of the chemical plant waste,[3] using the most advanced methodology then available, indicated that inorganic mercury forms were predominant in both. We found an unexpected and strikingly different result. The major mercury species in the brain of Cat 717 was found to be organometallic mercury, with a smaller inorganic component of β-mercuric sulfide. It seemed to us that this scientific finding deserved an explanation, and so we proceeded to investigate by rethinking the possible chemistry. Our findings led us to conclude that a different organometallic compound might have been important, α-mercuri-acetaldehyde, known chemically for decades, but having completely unexplored toxicology. We realized that this suggestion would be controversial.

Balogh and Tsui dismiss the experimental component of our work, asserting that the original speciation "is now unknowable". They support their contentions by citing a brief conference report[4] which suggests that methylmercury might be released into formalin preservative. More recent and comprehensive studies[5] suggest that this may not be true. Irrespective of this, possible losses and speciation changes of both mercury and selenium in the decades-old sample of Cat 717 preserved in formaldehyde (not paraffin embedded) are certainly a major concern. Indeed, our paper[2] provides an appropriately cautious discussion of this, but these deliberations are ignored by Balogh and Tsui. We refer the reader to our ES&T paper for more details.[2]

Balogh and Tsui review some of the older analytical evidence supporting methylmercury as a causative agent. We are aware of this prior work but do not agree that it constitutes incontrovertible proof of methylmercury as a cause for Minamata disease. Balogh and Tsui oversimplify analytical methodology and do not take into account the potential pitfalls that we discuss in our ES&T paper.[2] Conclusions of the early studies were subject to how reliably methylmercury was in fact determined in early studies of tissues, sludge and wastewater; using

the methods available at the time other mercury forms could have eluded detection. There are a number of analytical methods for quantitative methylmercury estimation,[6–9] but in the 1950's and 60's these were not yet well developed. The authors of the early reports are less emphatic in stating their conclusions than are Balogh and Tsui. While it is true that α-mercuri-acetaldehyde or related compounds were never "observed", it is also true that they might have easily been overlooked using the methods available at the time. Some methods employ a mobile phase to estimate methylmercury.[6–9] An unsuspected organometallic mercury species (such as α-mercuri-acetaldehyde) with differing mobility might easily be missed,[2] consistent with our finding of higher organometallic mercury levels than were shown by previous chemical analysis.[2,3] Other analytical methods determine organometallic mercury as the difference between total mercury and elemental mercury following selective reduction of any inorganic mercury present. They accurately determine total organometallic mercury but not which organometallic mercury species are present,[9] often assuming that all organometallic mercury is methylmercury. We disagree that methylmercury's predominant presence was unequivocally proven by the early work. Instead there was debate and uncertainty, compounded by substantial experimental and other challenges.

Balogh and Tsui dismiss our computational work, indicating that calculations fail to capture "real-world chemistry", but offer no evidence to support this statement. They also make an unsupported claim that methylmercury was generated in the factory. It seems likely that some methylmercury was generated, but what were the predominant forms? There is very strong evidence that Cat 717 was exposed to organometallic mercury, but conventional analysis of both Cat 717's brain and the chemical plant waste indicated a predominance of inorganic forms.[3] Our calculations necessarily focussed on the major chemical processes. They are valuable in showing what might or might not have occurred. Thus, methylmercury might have been formed via decomposition of α-mercuri-acetic acid:

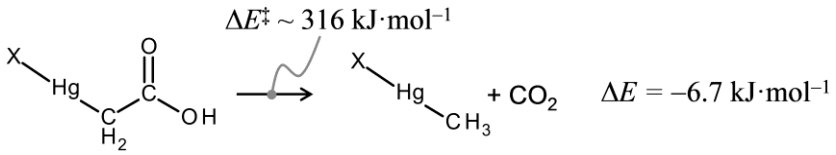

A second mechanism (not discussed in our paper) is the hydrolysis of α-mercuri-acetaldehyde to form methylmercury and formic acid:[10]

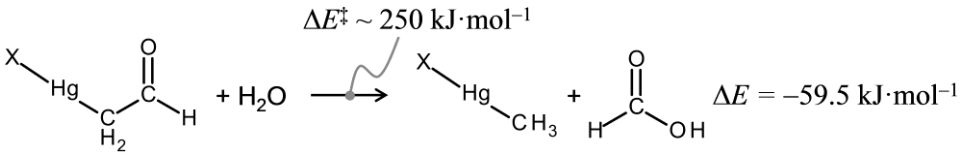

Although both reactions are exothermic, calculations show high activation barriers that make both unfavorable; these calculations are difficult to dismiss. Our conclusion was that it would be difficult for large quantities of methylmercury to form.

Balogh and Tsui are also critical that we did not cite many of the early Japanese-language publications. We regret any offenses of omission, but the volume of literature concerning Minamata is considerable and as a consequence it was not possible to cite everything. We did cite publications that reviewed the early work. In summary, having read their communication we see no reason to change our conclusions. Our work supports the hypothesis that compounds other than methylmercury might have been important in the Minamata mass poisoning. In our paper we went further, and conjectured that exposure to methylmercury compounds was not specifically involved in the Minamata tragedy. This was intended to provoke a thoughtful response in the reader, and indeed the idea that organometallic mercury compounds other than methylmercury might have been the cause of Minamata disease has been discussed previously.[11] In the 1980's such suggestions were not deemed inconsistent with evidence dating from the 1960's, but now appear controversial for some. Irrespective of this, a possible role of α-mercuri-acetaldehyde and related compounds should be considered.[2] Our work speaks only to the composition of the chemical plant waste, which is what Cat 717 received. How the compounds in question might be transformed in the environment remains unknown, and this together with their toxicology still needs to be investigated.

References B.3.4

(1) James, A.K., Nehzati, S., Dolgova, N.V., Sokaras, D., Kroll, T., O'Donoghue, J.L., Watson, J.E., Myers, G.J., Krone, P.H., Pickering, I.J., George, G.N. Reply to comments on "Rethinking the Minamata tragedy: What mercury species was really responsible*?" Environ. Sci. Technol*. **2020**, *54*, 8484-8485.

(2) James, A. K., Nehzati, S., Dolgova, N. V., Sokaras, D., Kroll, T., Eto, K., O'Donoghue, J. L., Watson, G. E., Myers, G. J., Krone, P. H., Pickering, I. J., George, G.N. Rethinking the Minamata tragedy: What mercury species was really responsible? *Environ. Sci. Technol.* **2020**, *54*, 2726–2733.

(3) Eto, K., Yasutake, A., Nakano, A., Akagi, H., Tokunaga, H., Kojima, T. Reappraisal of the historic 1959 cat experiment in Minamata by the Chisso factory. *Tohoku J. Exp. Med*. **2001**, *194*, 197–203.

(4) Akagi, H., Matsuo, N., Suzuki, T. Release of mercury from human tissues stored in formalin solution. *Eisei Kagaku* **1989**, *35*, 28.

(5) Mottet, K., Friberg, LO., Vahter, M., Body, R., Lind, B., Shen, D., Burbacher, T. Effects of perfusion, fixation, and freezing on the concentration and chemical form of mercury in the brain of rats exposed to methylmercury. *J. Trace Elem. Exp. Med*. **1993**, *6*, 23–30.

(6) Gage, J. C. The trace determination of phenyl- and methylmercury salts in biological material. *Analyst* **1961**, 457–459.

(7) Westöö, G. Determination of methylmercury compounds in foodstuffs II. Determination of methylmercury in fish, egg, meat and liver. *Acta Chem. Scand*. **1967**, *21*, 1790–1800.

(8) Akagi, H., Nishimura, H. Speciation of mercury in the environment. In: *Advances in Mercury Toxicology*. Suzuki, T., Imura, N., Clarkson, T. W. Eds. Plenum Press, New York, 1991, pp. 53–76.

(9) Puk, R., Weber, J. H. Critical review of analytical methods for determination of inorganic mercury and methylmercury compounds. *Appl. Organomet. Chem*. **1994**, *8*, 293–302.

(10) Sebe, E., Kitamura, S., Hayakawa, K., Sumino, K. Side reaction accompanied by catalytic hydration of acetylene. II. Evaluation of the mechanism of methylmercury compound synthesis. *Nihon Yakurigaku Zasshi* **1967**, *63*, 244–260.

(11) Taylor, D. Minamata Disease. *Environ. Sci. Technol*. **1982**, *16*, 81A.

APPENDIX C

SUPPLEMENTARY INFORMATION FOR CHAPTER 6

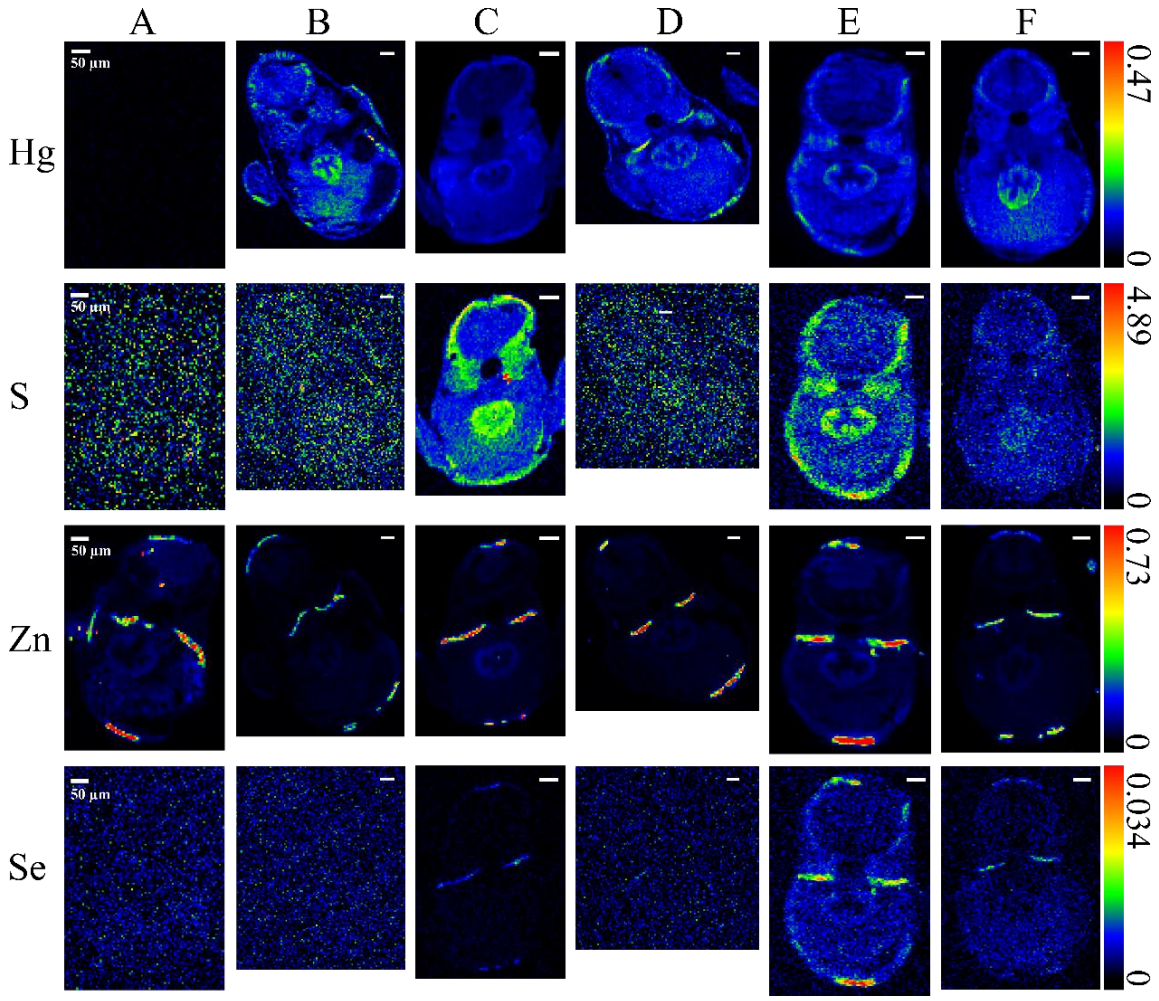

Figure C.6.1: X-ray fluorescence images of elemental distributions of mercury, sulfur, selenium and zinc in trunk sections 5 dpf larval zebrafish which have been cryopreserved and sectioned at 10 µm. Treatment groups are as follows: (A) control, (B) MeHg-L-Cys, (C) MeHg-D-Cys, (D) MeHg-L-Cys + BCH, (E) MeHg-L-Cys + L-phenylalanine, (F) MeHg-L-Cys + L-methionine. Color bar indicates maximum concentration (µg/cm2) of all images in each row. Mercury images are all scaled to MeHg-L-Cys treatment (B) for visual comparison of differences in uptake of mercury as a result of various treatment groups (C-F). Sulfur, selenium and zinc images are scaled to MeHg-L-Cys treatment (B) for observation on how mercury treatment affects other essential elements in larval zebrafish (A, C-F). Scale bar of 50 µm is denoted for reference.